PREDICTION AND EVALUATION OF HEPATIC BILE ACID TRANSPORTER-MEDIATED DRUG INTERACTIONS USING IN VITRO TOOLS AND PHARMACOKINETIC MODELING

Cen Guo

A dissertation submitted to the faculty of the University of North Carolina at Chapel Hill in partial fulfillment of the requirements for the degree of Doctor of Philosophy at the UNC Eshelman School of Pharmacy

Chapel Hill
2018

Approved by:

Kim L.R. Brouwer

Paul B. Watkins

Hugh A. Barton

Yanguang Cao

Daniel Gonzalez

ABSTRACT

Cen Guo: Prediction and Evaluation of Hepatic Bile Acid Transporter-Mediated Drug
Interactions Using In Vitro Tools and Pharmacokinetic Modeling
(Under the direction of Kim L.R. Brouwer)

The objective of this doctoral dissertation research was to develop novel strategies to predict and evaluate drug interactions with hepatic bile acid transporters. Sandwich-cultured hepatocytes (SCH) and mechanistic pharmacokinetic modeling were employed. Altered disposition of the model bile acid taurocholate (TCA) in human SCH due to inhibition of multiple transporters was predicted based on the potency of inhibitors [e.g., inhibition constant (K_i)] and kinetic parameters of TCA using pharmacokinetic modeling. The accuracy of predictions using total and unbound inhibitor concentrations was assessed. The effect of bosentan and telmisartan (model inhibitors) was predicted adequately by using intracellular unbound concentrations of the inhibitors. In subsequent studies, a simulation-based method was proposed to determine the relevant inhibitor concentration when predicting the effect of hepatic efflux transporter inhibition. For inhibitors with high plasma protein binding and/or high relative inhibition potency, using intracellular unbound rather than total inhibitor concentrations was optimal. The utility of this method was evaluated using experimental data from human SCH. To circumvent the limitations of individual transporter K_i data, a model-based approach was proposed to obtain overall K_i values against each efflux clearance pathway (i.e., biliary and basolateral efflux clearance) of TCA in rat SCH. The study design was optimized using modeling and simulation to estimate K_i values of troglitazone sulfate (the model inhibitor). Using this study design, K_i estimation in different hepatocyte lots, and limitations on the

iii

accuracy, were evaluated using simulated data. In addition to inhibition, transporter induction by Farnesoid X Receptor agonists was investigated in human SCH. Basolateral efflux and biliary clearance values for TCA, determined by pharmacokinetic modeling, were significantly increased by the Farnesoid X Receptor agonists, obeticholic acid and chenodeoxycholic acid. These studies provided direct functional evidence for transporter induction. Immunoblot analysis results suggested that organic solute transporter alpha/beta may be the primary transporter responsible for the increase in the basolateral efflux clearance of TCA.

This research leveraged pharmacokinetic modeling and simulation to integrate and interpret in vitro bile acid transport data. The approaches developed and the results detailed in this dissertation will improve the accuracy of predictions and mechanistic understanding of drug-bile acid interactions.

TABLE OF CONTENTS

LIST OF TABLES

LIST OF FIGURES

LIST OF ABBREVIATIONS

AIC   Akaike's Information Criteria

BEI   Biliary excretion index

BSA   Bovine serum albumin

BSEP or Bsep   Bile salt export pump

CDCA   Chenodeoxycholic acid

CL   Clearance

CL_{Uptake} or $CL_{int, uptake}$ Intrinsic uptake clearance

CL_{BL} or $CL_{int,BL}$ Intrinsic basolateral efflux clearance

CL_{Bile} or $CL_{int,Bile}$ Intrinsic biliary clearance

CYP   Cytochrome P450

DDI   Drug-drug interaction

d_8-TCA   Deuterium-labeled taurocholic acid

f_u Unbound fraction

$f_{u,cell,inhibitor}$ Intracellular unbound fraction of inhibitor

FXR   Farnesoid X receptor

HBSS   Hank's balanced salt solution

$[I]_{t,cell}$ or $[I]_{total,cell}$ Intracellular total inhibitor concentration

IC_{50}	Half-maximal inhibitory concentration
K_m	Michaelis-Menten constant
K_i	Inhibition constant
K_{Flux}	First-order rate constant for flux from bile networks into buffer
MDR or Mdr	Multidrug resistance protein
MRP or Mrp	Multidrug resistance-associated protein
NTCP or Ntcp	Sodium taurocholate co-transporting polypeptide
OATP or Oatp	Organic anion transporting polypeptide
OST or Ost	Organic solute transporter
OCA	Obeticholic acid
PK	Pharmacokinetics
SCH	Sandwich-cultured hepatocytes
TCA	Taurocholic acid
TS	Troglitazone sulfate
V_{max}	Maximum velocity

CHAPTER 1. Introduction [1]

1. General Introduction to the Dissertation

1.1 Importance of Drug Transporters in Clinical Pharmacology and Drug Development

Transport proteins (hereafter transporters) are membrane-bound proteins that move endogenous compounds (e.g., bile acids) and xenobiotics (e.g., drugs) across biological membranes. Transporters can have clinically relevant effects on the pharmacokinetics (PK) and pharmacodynamics of a drug in various organs by affecting the absorption, distribution, and elimination (Giacomini et al., 2010; Giacomini and Huang, 2013). Transporters are ubiquitously expressed in various tissues such as the liver, kidneys, intestine, and blood brain barrier and, therefore, play a key role in determining the efficacy and toxicity of drugs in different tissues. For example, hepatic uptake transporters determine the exposure of statins in the liver, which is the therapeutic target organ (Farmer, 2001). Conversely, drugs can modulate the expression and function of transporters through various mechanisms (e.g., inhibition and induction), resulting in altered disposition of transporter substrates (Farmer, 2001; Jackson et al., 2016; Zhang et al., 2017). Because of potential drug-drug interaction (DDI) liability mediated by transporters, regulatory agencies in the US (FDA), Europe (EMA), and Japan (PMDA) recommend performing in vitro transport assays and even running clinical DDI studies to evaluate interactions with transporters for investigational drugs acting as either a substrate or perpetrator.

---

[1]Section 4 of this chapter has been published as part of the review by Yang K, Guo C (contributed equally), Woodhead JL, St Claire RL 3rd, Watkins PB, Siler SQ, Howell BA, Brouwer KLR. Sandwich-cultured hepatocytes as a tool to study drug disposition and drug-induced liver injury. *J. Pharm. Sci.* 2016 Feb;105(2):443-59. DOI: 10.1016/j.xphs.2015.11.008. Reprinted by permission of Elsevier.

Accordingly, an increasing percentage of new drugs approved between 2003 and 2011 had transporter information in the package inserts (Agarwal et al., 2013).

1.2 Bile Acids and Hepatic Bile Acid Transporters

The liver is a major organ where transporters are expressed. The liver determines the homeostasis of many endogenous compounds, such as bile acids, by regulating their metabolism and transport. Bile acids are important components of the bile, and act as lipid solubilizers and cell signaling molecules that modulate bile acid homeostasis, hepatic inflammation (Allen et al., 2011), etc. Bile acids can be cytotoxic at high concentrations (Hofmann, 1999). The hydrophobic bile acids, such as lithocholic acid (LCA), chenodeoxycholic acid (CDCA), and deoxycholic acid are more cytotoxic than less hydrophobic bile acids, such as cholic acid and ursodeoxycholic acid. Bile acids are synthesized primarily in the liver from cholesterol by Cytochrome P450 cholesterol 7alpha-hydroxylase (CYP7A1), followed by hydroxylation by Cytochrome P450 sterol 12α-hydroxylase (CYP8B1) (Zhang and Chiang, 2001). Alternatively, bile acids can be synthesized in extrahepatic tissues by Cytochrome P450 oxysterol 7α-hydroxylase (CYP27A1) followed by hydroxylation by CYP7A1 in the liver (Norlin and Wikvall, 2007). Bile acids undergo further conjugation, primarily with taurine or glycine in human (Falany et al., 1994), and to a lesser extent, with glucuronide or sulfate moieties. Eventually, bile acids are secreted via the bile duct into the small intestine. The most abundant bile acids in serum are glycochenodeoxycholic acid, chenodeoxycholic acid (CDCA), and deoxycholic acid in humans (Trottier et al., 2011; Ferslew et al., 2015), while hyodeoxycholic acid, cholic acid, alpha or beta-muricholic acid, and CDCA are most abundant in rat serum(Garcia-Canaveras et al., 2012; Xie et al., 2013) Although taurocholic acid (TCA) is not the major bile acid, it is used most commonly as a substrate to study bile acid transporters.

Hepatic bile acid uptake transporters are expressed on the basolateral membrane transporting bile acids from the sinusoidal blood into hepatocytes. The clinically relevant hepatic uptake transporters are Solute Carrier (SLC) transporters, including sodium taurocholate cotransporting polypeptide (NTCP; encoded by *SLC10A1*) and organic anion-transporting polypeptides (OATPs; *SLCOs*). Although hepatic uptake usually is the predominating transport pathway under normal conditions, bile acids can be effluxed from the hepatocyte into the sinusoids through basolateral efflux transporters under cholestatic conditions. These transporters include multidrug resistance-associated protein 3 (MRP3; *ABCC3*) and MRP4 (*ABCC4*), as well as organic solute transporter α/β (OSTα/β; *SLC51*). Although OSTα/β was reported to be a bidirectional transporter in vitro (Ballatori et al., 2005), this transporter primarily acts as an efflux transporter in hepatocytes in vivo due to the extracellular and intracellular fluid sodium and potassium gradients in hepatocytes (Soroka et al., 2010). Biliary transporters expressed on the canalicular membrane of hepatocytes are responsible for bile acid excretion into the bile. The bile salt export pump (BSEP, *ABCB11*) excretes the majority of bile acid species, while MRP2 (*ABCC2*) is responsible for the excretion of sulfated bile acids (Dawson et al., 2009)(Figure 1.1). Novel bile acid transporters are still being identified.

Bile acid transporter-mediated drug interactions have important implications in drug safety. Inhibition of efflux transporters is acknowledged as a risk factor for drug-induced liver injury (DILI) (Kock et al., 2014). Inhibition of BSEP was one of the mechanisms for troglitazone- and bosentan-induced liver toxicity, which led to the withdrawal of troglitazone from the market (Yang et al., 2014b) and a black box warning for bosentan (Woodhead JL et al., 2014). Patients with mutations in the *ABCB11* gene that result in impaired BSEP function develop liver injury due to hepatic accumulation of toxic bile acids (Jansen and Muller, 2000). In

addition, an in vitro study involving more than 600 drugs provided direct evidence for an association between BSEP inhibition and hepatotoxicity (Morgan et al., 2013). Simultaneous inhibition of basolateral efflux transporters and BSEP is also a contributing factor for the development of DILI (Kock et al., 2014). In contrast, inhibition or downregulation of uptake transporters serves as a protective mechanism in response to cholestasis (Leslie et al., 2007; Meng et al., 2015). Due to the importance of hepatic bile acid transporters, scientific publications in this area have been constantly increasing over the past few decades (Figure 1.2).

1.3 Tools to Study Transporters: In Vitro and In Silico

Multiple in vitro tools with various levels of throughput and physical relevance can be used to study transport kinetics. They can be divided into two general categories: (i) expression systems, including inside-out membrane vesicles and cell lines transfected with specific uptake or efflux transporters; (ii) whole cells including polarized cell lines, such as Caco-2, and primary hepatocytes in suspension or in sandwich culture.

Transfected cell lines can be used to directly estimate kinetic/inhibition parameters for the overexpressed transporter. However, the results of these assays are confounded by the expression of endogenous transporters (Ahlin et al., 2009) and may not be suitable for compounds with low permeability. Inside-out membrane vesicles are used primarily to study efflux transporters, and are suitable for low-permeability compounds. The uptake buffer can represent the cytoplasm, and therefore uptake, rather than efflux, of the drug is measured. One caveat of this system is relatively high background noise for highly lipophilic compounds as a result of nonspecific binding to the membranes (Lai, 2013).

In contrast, cellular systems can be used to estimate kinetic parameters for specific clearance pathways, such as uptake, metabolism, or efflux, as well as the interplay of multiple

4

processes. Primary hepatocytes are more physiologically relevant than other systems for studying hepatic transporters. Suspended hepatocytes have been considered the "gold standard" for studying hepatic uptake, while sandwich-cultured primary hepatocytes are more suitable for studying vectorial transport due to the maintenance of in vivo polarity. A more detailed introduction regarding sandwich-cultured hepatocytes will be discussed in the following sections.

Some empirical methods have been developed to predict the role of transporters in the interplay with metabolism. The Biopharmaceutics Drug Disposition Classification System (BDDCS) are used to predict the role of transporters in PK and DDIs in the context of transport and metabolism interplay (Benet, 2009; Shugarts and Benet, 2009; Broccatelli et al., 2012). The Extended Clearance Classification System (ECCS) is used to identify major clearance pathways using in vitro and physicochemical properties (El-Kattan et al., 2016; Varma et al., 2016).

Computational models have been developed to predict putative inhibitors and substrates of transporters (Ekins et al., 2007; Ali et al., 2017). In general, two approaches have been used, including indirect ligand-based methods, such as pharmacophore and quantitative structure–activity relationship (QSAR) modeling, and direct structure-based approaches, which require crystallographic data of the transport protein (Chang et al., 2006). These models are useful in screening large numbers of compounds at an early stage.

PK modeling is a useful tool to analyze, interpret, and integrate transport data. Physiologically-based PK (PBPK) models may offer a platform to quantitatively evaluate the role of drug transporters and its interplay with metabolism and passive diffusion (Li et al., 2014a; Varma and El-Kattan, 2016). Although PBPK modeling and simulations have been successfully applied to predict metabolism-based DDIs, the confidence in predicting transporter-mediated

drug disposition and DDIs using PBPK models is considered low (Pan et al., 2016). The relatively poor model performance could be due to the uncertainty or ambiguity of in vitro transporter kinetic parameters, and limited knowledge concerning key factors, such as basic transport mechanisms (Pan et al., 2016). To improve the quality of in vitro data analysis, mechanistic PK modeling has unique advantages compared to empirical approaches and has gained lots of interest. Simcyp In Vitro Analysis Toolkit was developed to analyze in vitro transport data using modeling approaches. In addition, application of physiologically-relevant whole cell systems will be crucial for generating quality data that can be translated to in vivo.

2. Challenges in the Estimation of Transport Parameters using Expression Systems

2.1 Challenges in Estimating Inhibitory Potency

The inhibitory potency of a compound, which is represented by the half maximal inhibitory concentration (IC_{50}) or inhibition constant (K_i), is an important parameter for predicting DDIs. Large variability around this parameter has been reported, raising concerns about the predictability of clinical DDIs based on in vitro IC_{50} data. For example, the IC_{50} for digoxin transport showed up to ~800-fold difference across different labs (Lee et al., 2014).

A few factors have contributed to the large variability in IC_{50} data. First, substrate-dependent inhibition due to multiple binding sites has been reported for P-gp (Martin et al., 2000), BCRP (Giri et al., 2009), OATP1B1, OATP1B3, and OATP2B1 (Noe et al., 2007; Izumi et al., 2013; Shirasaka et al., 2014). In addition, IC_{50} or K_i values can be dependent on the experimental system (Bentz et al., 2013). False positive results have been reported due to cytotoxicity using transfected cell lines (Zheng et al., 2010). The actual concentration of the compound might be much lower than the nominal concentration due to non-specific binding to the incubation apparatus and/or lipid membranes, especially for highly lipophilic compounds. In

6

some cases, K_i values estimated from overexpression systems can be biased by the transporter expression level and the substrate affinity (Balakrishnan et al., 2007). In addition, the contribution of passive diffusion to the overall transport clearance of the substrate also makes it challenging to estimate the true IC_{50} related to the active uptake/efflux. Conventional methods to estimate IC_{50} using the efflux ratio in Caco-2 cells may introduce bias because the substrates inside the cell (intracellular concentrations) interact with efflux transporter while extracellular concentrations are measured. Therefore, the efflux ratio does not necessarily represent the efflux transporter function. In contrast, model-based approaches can directly reflect the efflux transporter function, and therefore provide more accurate estimations (Kishimoto et al., 2016).

2.2 Challenges in Estimating Transport Clearance Parameters

Transport kinetics can be described by the Michaelis-Menten equation below.

$$v= \frac{V_{max}\times[S]}{K_m+[S]} \quad (1)$$

where v, [S], and V_{max} represents the velocity of transport, the substrate concentration, and the maximal velocity, respectively. K_m represents the Michaelis-Menten constant, which is the substrate concentration at half V_{max}. High variability in V_{max} and K_m have been reported (Shirasaka et al., 2008), which may be attributed to the data analysis method and the limitation of experimental systems as described below.

When transfected cell lines are used to estimate kinetic parameters, flux rate across the monolayer reflects both uptake and efflux, and does not follow the principles of the Michaelis-Menten equation. However, traditional methods used the flux rate to estimate V_{max} and the concentration in the donor chamber (extracellular) to estimate K_m. In a study that used different monolayers, the K_m value for P-gp varied by > 25-fold based on extracellular concentrations (Shirasaka et al., 2008), but were within ~2-fold when this data set was analyzed using a

compartmental PK model and intracellular concentrations (Tachibana et al., 2010). In addition, since V_{max} is related to the expression level of the transporter, V_{max} generated from different experimental systems are not comparable (Harwood et al., 2016).

2.3 Mechanisms of Inhibition

Although most DDI predictions assume competitive inhibition, drugs may interact with transporters through other reversible mechanisms, such as noncompetitive inhibition, uncompetitive inhibition, and mixed inhibition. In addition, there are other types of interaction, such as induction (Williamson et al., 2013a), time-dependent inhibition (Shitara et al., 2009), and allosteric modulation (Sterz et al., 2009). Generally, the site of interaction is from the same side of the membrane domain (cis-inhibition). For example, efflux transporters are inhibited by drugs from the cytoplasmic side rather than the extracellular side of the membrane. In contrast, trans-inhibition has been reported where the transporters are inhibited by drugs from the opposite membrane domain. This effect could result from reversible or irreversible mechanisms (Vallejo et al., 2006). More details about reversible cis-inhibition are introduced below, and additional information about induction will be introduced later.

Competitive inhibition is most common due to the overlapping substrate and inhibitor specificity of transporters. The basic rule is that the binding of the substrate or the inhibitor is mutually exclusive. In the presence of inhibitor, the apparent K_m of the reaction increases while the V_{max} remains the same. The relationship can be described in Eq. 2, where [I] represents the inhibitor concentration and K_i (also known as the inhibition constant) represents the dissociation constant of free transporter and inhibitor from the transporter-inhibitor complex. Noncompetitive inhibitors do not affect the binding of substrate to the transporter, meaning K_m is not affected, but the overall effect is a decrease in the amount of functional transporter, shown as a reduction

of V_{max}. The relationship is described in Eq. 3. In mixed-type inhibition (Eq. 4), the inhibitor decreases V_{max} while it may increase or decrease K_m. When $\alpha=1$, mixed inhibition is the same as noncompetitive inhibition. Uncompetitive inhibitors only bind to transporter-substrate complexes, and are the least common mechanism of reversible inhibition. The overall effect is a decrease in V_{max} and K_m, as described in Eq. 5. (Ring et al., 2014)

$$v = \frac{V_{max} \times [S]}{K_m \times \left(1 + \frac{[I]}{K_i}\right) + [S]} \tag{2}$$

$$v = \frac{V_{max} \times [S]}{K_m \times \left(1 + \frac{[I]}{K_i}\right) + [S] \times \left(1 + \frac{[I]}{K_i}\right)} \tag{3}$$

$$v = \frac{V_{max} \times [S]}{K_m \times \left(1 + \frac{[I]}{K_i}\right) + [S] \times \left(1 + \frac{[I]}{\alpha \times K_i}\right)} \tag{4}$$

$$v = \frac{V_{max} \times [S]}{K_m + [S] \times \left(1 + \frac{[I]}{K_i}\right)} \tag{5}$$

In order to estimate K_i and identify the inhibition mechanism, the system will be incubated with at least five different substrate levels that bracket the K_m in the presence of at least five different inhibitor concentrations that cover the K_i. An incubation time within the linear range must be used. Traditionally, the inhibition mechanism is differentiated by visualizing the transformed data in a Lineweaver-Burk plot, with $1/[S]$ and $1/v$ on the x- and y-axis, respectively. Alternatively, models representing different inhibition mechanisms are fit to the data using nonlinear regression analysis. The best-fit model is selected based on the goodness-of-fit, represented by the lowest Akaike's Information Criteria (AIC) value.

2.4 Protein Binding and the Implications for Drug-Drug Interactions

Importance of Unbound Concentration

Based on the free drug hypothesis, it is generally assumed that only unbound drug molecules interact with their protein targets, including transporters (Schmidt et al., 2010).

Therefore, knowing the unbound concentration is important. An analysis of >180 drugs approved by FDA between 2003 and 2013 showed that the plasma protein binding of one-quarter of the drugs were > 99% (Liu et al., 2014). Usually, unbound concentration is calculated as the product of the unbound fraction (f_u) and the total drug concentration.

In the blood, drugs bind to various proteins including human serum albumin (HSA), alpha 1-acid glycoprotein (AAG), and lipoproteins. Lipophilic and acidic drugs tend to bind to HSA (with concentration around 670 µM); basic drugs tend to bind to AAG (with concentration around 16 µM). Measurement of plasma f_u is relatively straightforward and has been reviewed previously (Di et al., 2017). Inside the cell, drugs can partition into the plasma membrane or organelle membranes or bind to intracellular proteins including cytosolic fatty acid binding protein (Z-fraction), 3a-hydroxy-steroid dehydrogenase (Y-protein), and glutathione-S-transferase B (ligandin) (Levi and Arias, 1969; Burczynski et al., 1999). In addition, many drugs show preferential subcellular organelle sequestration, particularly in lysosomes and mitochondria (Zheng et al., 2011). The lysosomal pH is relatively low (~4-5), which is maintained by a Mg^{2+} ATP-dependent proton pump, so lysosomal trapping mostly affects compounds with a basic center (pKa>8) (Kaufmann and Krise, 2007). In mitochondria, the electrochemical gradient is the main driving force for sequestration as mitochondria exhibit a negative membrane potential of ~160mV, which attracts the accumulation of lipophilic cations. The accumulation of delocalized lipophilic cations in the mitochondria could be 1000-fold higher than that in cytosol (Duvvuri and Krise, 2005). In summary, the distribution of drugs in the cell is not homogenous.

Despite the free drug hypothesis, there is no consensus on which inhibitor concentration to use for comparison with IC_{50} in order to predict DDI potential. For example, with hepatic uptake transporters, the 2012 FDA draft guidance suggested using $10 \times [I]_{max,total}$ (FDA/CDER,

2012), instead of $10\times[I]_{max,unbound}$, which was proposed in the 2010 ITC whitepaper. $[I]_{max,total}$ and $[I]_{max,unbound}$ represent total and unbound maximum systemic plasma concentrations, respectively. The EMA guidance published in 2012 recommends using $25\times[I]_{u,inlet,max}$ (EMA, 21 June 2012); the FDA guidance published in 2017 recommends using $10\times[I]_{u,inlet,max}$ (FDA/CDER, 2017), where $[I]_{u,inlet,max}$ represents unbound maximum plasma concentration at the inlet to the liver. For hepatic efflux transporters, the unbound hepatocellular concentration is more relevant than the plasma concentration, but no regulatory recommendations are available yet.

Current Methods to Measure Intracellular Unbound Concentration

Intracellular unbound drug concentrations are critical determinants of drug interactions with therapeutic targets, enzymes, and efflux transporters. The measurement or estimation of intracellular unbound concentrations has been reviewed by the ITC (Chu et al., 2013). In general, the methods most commonly used to measure or model intracellular unbound concentration are: 1) homogenization method; 2) temperature method; 3) prediction based on physicochemical properties; 4) cytosol isolation method; and 5) compartmental PK modeling. In addition, a new technology based on mass spectrometry imaging techniques has been used to measure intracellular drug concentrations in vivo (Dollery, 2013), but this method is limited by equipment requirements and the high cost.

In Method 1, the compounds are mixed with homogenized hepatocytes or liver tissue followed by equilibrium dialysis, which is the most common practice to obtain f_u (Mateus et al., 2013). Although this method is high throughput and commonly used, it assumes homogenous intracellular distribution of drugs without considering subcellular sequestration. In Method 2, hepatocytes are incubated with compounds at 4°C for 60 min; intracellular f_u is calculated as the medium unbound concentration divided by total cellular concentration, assuming complete

inactivation of uptake transporters at 4°C and that concentration equilibrium of the unbound drug is reached between the medium and hepatocytes(Shitara et al., 2013). In Method 3, the empirical relationship between $logD_{7.4}$ and f_u in hepatocytes has been reported by different groups (Austin et al., 2005; Yabe et al., 2011). In Method 4, drugs are incubated with hepatocytes to mimic the drug distribution process. Then the cytosol is isolated by differential centrifugation of cell lysate that has been gently homogenized to avoid breaking subcellular organelles. Following that, the total amount and f_u of drugs in the cytosol are measured (Pfeifer et al., 2013b). In Method 5, compartmental PK models are used to describe the transport process and membrane partitioning of transporter substrates, and intracellular unbound concentrations are estimated. This PK modeling approach has been applied to analyze data obtained from isolated perfused rat livers and MDCK cell lines. Although this method might be more accurate due to its mechanistic nature, it is very time-consuming and laborious to generate time-course data for modeling.

Although Method 1 is high-throughput, a comparison of a data set consisting of 18 diverse compounds revealed that the f_u in human hepatocytes measured using Method 1 was generally lower and correlated poorly with that measured by Methods 2 and 3 (Riede et al., 2017). Although Method 2 and 4 consider subcellular distribution and possibly are more accurate, they are not widely utilized due to the resource-intensive nature of these methods.

To understand the importance of intracellular binding, the distribution of intracellular unbound fraction for 29 compounds measured using human or rat primary hepatocytes ($f_{u,hepatocyte}$) was obtained from the literature (Gardiner and Paine, 2011; Mateus et al., 2013; Pfeifer et al., 2013b; Treiber et al., 2014; Guo et al., 2016). All the $f_{u,hepatocyte}$ data were measured using Method 1 or 4. Measured $f_{u,hepatocyte}$ ranged from 0.00076 to 0.93. The distribution of $f_{u,hepatocyte}$ is presented as a histogram in Figure S3.1; 17% (5 out of 29) of the compounds had

$f_{u,hepatocyte}$ values smaller than 0.01, whereas 31% (9 out of 29) and 52% (15 out of 29) of the compounds had $f_{u,hepatocyte}$ values of 0.01-0.5 and 0.5-1, respectively.

3. Indirect Modulation of Hepatic Bile Acid Transporters

In addition to direct inhibition, transporter function could be modulated through indirect mechanisms, such as induction or alteration in localization. Hepatic bile acid transporters are regulated by various signaling pathways and nuclear receptors (NRs), with farnesoid X receptor (FXR) being the main NR for bile acids (Halilbasic et al., 2013).

NTCP transcription is regulated by bile acids, cytokines, liver injury/disease, and hormones. Although FXR does not bind with the NTCP promoter directly, it induces the expression of other factors that repress NTCP expression (Kosters and Karpen, 2008). Other NRs involved in NTCP regulation are small heterodimer partner, retinoic acid receptor alpha:retinoid X receptor alpha (RARα:RXRα), hepatocyte nuclear factor 4α, and glucocorticoid receptor. A FXR-responsive element in the BSEP promoter area has been identified (Ananthanarayanan et al., 2001). BSEP expression is upregulated by FXR agonists, and downregulated by inflammatory injury and estrogens [reviewed in (Stieger, 2011)]. In addition, RXR and membrane lipid composition also affect BSEP function (Paulusma et al., 2009). MRP3 is regulated by constitutive androstane receptor (CAR), pregnane X receptor (PXR), vitamin D receptor and peroxisome proliferator-activated receptor alpha (PPARα), while MRP4 is induced by CAR and PPARα (Wagner et al., 2010). The expression of heterodimeric transporters OSTα/OSTβ is induced via FXR and LXR (Dawson et al., 2009). Besides transcriptional regulation, transporter trafficking also plays a role in determining the amount of functional transporters expressed on the plasma membrane. Trafficking of transporters to and from the membrane may involve phosphoinositide 3-kinase, protein kinase C (PKC), and cyclic AMP

(Chandra et al., 2005; Stieger et al., 2007; Park et al., 2012). This short-term regulation enables hepatocytes to quickly adapt to increased cellular bile acids as a protective mechanism.

It is challenging to study the induction of transporters due to limited knowledge of quantitative relationships between function and mRNA expression. In fact, mRNA expression data are highly variable and poorly correlated with the protein expression and function of transporters (Ahlin et al., 2009; Thompson et al., 2017). Furthermore, in vivo evidence for induction of transporter function is limited, and further studies are warranted.

4. Sandwich-Cultured Hepatocytes as a Tool to Study Drug Disposition and Drug-Induced Liver Injury

4.1 Introduction of Sandwich-Cultured Hepatocytes (SCH)

Among many in vitro and in vivo model systems, primary hepatocytes remain the gold standard to assess hepatic drug metabolism and transport. Hepatocytes can be isolated from the species of interest, including humans, to address species differences in hepatic disposition of drugs. Primary hepatocytes express multiple metabolic enzymes and transporters, enabling assessment of overall hepatobiliary drug disposition. However, hepatocytes in suspension or under conventional culture conditions quickly lose cell polarity and viability, which limits their utility (Borlak and Klutcka, 2004; Swift et al., 2010). Culturing hepatocytes between two layers of gelled collagen (sandwich configuration) improves morphology and viability of hepatocytes, and maintains function for longer periods of time in culture (Dunn et al., 1991; Dunn et al., 1992). In addition, sandwich-cultured hepatocytes (SCH) regain polarity, allowing proper localization of basolateral and canalicular transporters as well as formation of functional bile networks (Figure 1.1) (LeCluyse et al., 1994; Liu et al., 1998).

When properly cultured, the expression and function of basolateral uptake transporters including NTCP and OATPs are maintained over time in human SCH (Hoffmaster et al., 2004; Kotani et al., 2011; Bi et al., 2012), whereas down-regulation of Ntcp and Oatp has been reported for rat SCH (Liu et al., 1998; Kotani et al., 2011). Upon isolation, hepatocytes lose biliary excretory function due to internalization of canalicular efflux transporters (Bow et al., 2008). However, canalicular transport proteins [e.g., BSEP/Bsep, P-glycoprotein (P-gp), breast cancer resistance protein (BCRP/Bcrp), and MRP/Mrp2] properly localize over time and regain excretory function in human and rat SCH (Liu et al., 1998). A schematic representation of hepatic transporters in SCH is shown in Figure 1.1. Phase I [e.g., cytochrome P450 (CYP)] and phase II [e.g., UDP-glucuronosyltransferase (UGT), sulfotransferase (SULT)] metabolizing enzymes also are expressed in SCH, although some enzymes exhibit decreased expression and/or function over time in SCH compared to freshly isolated hepatocytes, depending on the culture conditions and medium composition (Li et al., 2010; Jacobsen et al., 2011; Tchaparian et al., 2011). The influence of culture conditions and culture time on the expression and/or function of enzymes and transporters in the SCH system have been reviewed in detail elsewhere and is not the main focus of this chapter (Swift et al., 2010; De Bruyn et al., 2013; Godoy et al., 2013).

SCH provide a unique tool to estimate biliary excretion of compounds. Substances excreted into bile and accumulated in the canalicular network can be quantified by modulating tight junctions using buffer with and without calcium (Liu et al., 1999a; Liu et al., 1999b). Therefore, SCH have been used widely to assess hepatobiliary disposition of drugs and metabolites, and potential DDIs. Transcriptional and post-translational regulatory machinery are well-maintained in SCH, which makes it a suitable model for studying induction and feedback regulation of enzymes and transporters in response to compounds or other interventions (Dunn et

al., 1992; Jackson et al., 2009). Metabolically competent SCH also have been employed to study the pharmacology and toxicology of drugs and hepatically-generated metabolites. Because of the essential role of the liver in drug elimination, hepatocytes are often a target of drug-induced toxicity. SCH have been used in the assessment of direct cytotoxicity and in mechanistic studies to determine perturbations of biological processes and to better understand underlying mechanisms of DILI.

In this chapter, applications of SCH in studying hepatobiliary drug disposition are reviewed. First, use of the SCH system to characterize hepatic drug metabolism and transport is discussed. Predictions of in vivo drug disposition and clinical DDIs using SCH data combined with mechanistic and/or PBPK modeling also are reviewed.

4.2 Use of SCH in Studying Metabolism

During drug discovery and development, assessment of metabolism and transport of new chemical entities is important to predict clinical exposure and potential DDIs. In this section, the use of SCH to study drug disposition is reviewed with a focus on metabolism and hepatobiliary transport of compounds and DDIs, and enzyme-transporter interplay. This section also highlights the estimation of enzyme- and transporter-mediated intrinsic clearance values using mechanistic PK modeling in addition to empirical methods. In vitro-in vivo extrapolation of intrinsic clearance and incorporation into PBPK modeling is discussed.

Metabolism

SCH have been used to study drug disposition, including hepatic uptake, metabolism and biliary excretion. Although human liver microsomes (HLMs), S9 subcellular fractions, and primary hepatocytes cultured in monolayers (without extracellular matrix overlay) are used more commonly in metabolism studies, SCH are used often when extended incubation times (>24 hr)

16

are needed, after which the viability and function of primary hepatocytes cultured in monolayers begin to deteriorate (Swift et al., 2010). The metabolic clearance values of the low clearance drugs tolbutamide and warfarin, as well as the high clearance compound 7-ethoxycoumarin, were estimated using mathematical modeling after co-incubation with human SCH for 48 hr. (Treijtel et al., 2004) (Treijtel et al., 2005). The calculated intrinsic clearance was in accordance with literature reports. The advantage of using SCH was demonstrated in another study where DB829, the active metabolite of an antitrypanosomal prodrug, was detected only in trace amounts in HLMs at the end of the 180-min incubation, but was detected readily in human SCH throughout the 24-hr incubation (Generaux et al., 2013).

Metabolism-Mediated DDIs

Both inhibition- and induction-mediated DDIs have been studied using SCH. The CYP substrates used in these studies generally are selected to penetrate the hepatocytes via passive diffusion to eliminate the confounding effect of transporters. Although CYP inhibition has been studied primarily using HLMs, a few studies using SCH have been reported. The inhibitory effect of tritolide on CYP3A was evaluated by Shen et al (Shen et al., 2014). Both the expression and activity (measured by midazolam hydroxylation) of CYP3A in rat SCH were reduced after exposure to tritolide for up to 24 hr. Bi et al. reported that the intracellular accumulation of buprenorphine and midazolam in human SCH was increased by rifamycin SV due to inhibition of CYP3A4 and UGT1A1, which mediate the metabolism of these two victim substrates (Bi et al., 2012). SCH allow for longer exposure time, making them suitable for CYP induction studies. For example, the activity of CYP3A was assessed in human SCH after incubation with pregnancy-related hormones for 72 hr (Zhang et al., 2015).

4.3 Use of SCH in Studying Hepatobiliary Transport

Mechanisms of Hepatobiliary Disposition

Under appropriate culture conditions, SCH express key transporters that are properly localized, and therefore, SCH are uniquely advantageous to study the mechanisms of hepatobiliary transport of a compound as well as the effects of a compound on hepatobiliary transporters. SCH isolated from naturally occurring genetically deficient rodents [e.g., Mrp2-deficient Wistar rats (TR⁻ rats), Eisai-hyperbilirubinemic Sprague-Dawley rats (EHBR rats)] or genetically modified animals with loss-of-function of a specific transporter can be used to elucidate the role of that transporter in disposition of the compound (Yue et al., 2011; Zamek-Gliszczynski et al., 2012). Knockdown of Bcrp using RNA interference in SCH isolated from wild-type rats elucidated the role of Bcrp in drug hepatobiliary disposition (Yue et al., 2009; Yang et al., 2014a). With human SCH, the role of individual transporters may be evaluated by using "specific" transporter inhibitors if they are available, or by modifying the experimental conditions (e.g., uptake study in the absence and presence of sodium). However, highly specific transport inhibitors and substrates are often lacking. Furthermore, genetically modified animals are only available for a few transporters, and loss of function of one transporter may result in compensatory changes in other pathways. Therefore, a multi-experimental approach integrating SCH data, transfected systems and membrane vesicles can be used to characterize the involvement of multiple transporters (Lepist et al., 2014). Understanding the transport mechanism(s) could facilitate identification of potential DDIs involving uptake and efflux transporters. Previous reviews have discussed the utility of SCH for these types of studies (Swift et al., 2010; De Bruyn et al., 2013), and recent reports are discussed below.

Yanni et al. (Yanni et al., 2010) identified the hepatic transporters involved in micafungin disposition by co-incubation of micafungin with an NTCP inhibitor [taurocholic acid (TCA)], an OATP inhibitor (rifampin), BSEP inhibitors (TCA and nefazodone), a BCRP inhibitor (GF120918), as well as a P-gp and MRP2 inhibitor (cyclosporine A). Mohamed et al. (Mohamed and Kaddoumi, 2014) reported that the disposition of tacrine, which was approved for treatment of Alzheimer's disease, was mediated by Octs, Mrp2 and P-gp by using rat SCH and chemical inhibitors. A similar approach to elucidate the responsible hepatobiliary transporters for 17α-hydroxyprogesterone caproate and its effect on BA transporters has been reported (Sharma et al., 2013). One caveat with this type of approach is that these "specific" inhibitors may have other effects on metabolism and/or transport. To overcome this issue, transporter assays using transfected cells can be used to confirm findings from the SCH studies. For example, disposition of a natural product timosaponin b2 (TB2) was characterized using rat SCH and involvement of specific transporters was confirmed using human OATP1B1- and OATP1B3-expressing HEK-293 cells and membrane vesicles isolated from cells expressing human MRP2 and BCRP (Sheng et al., 2015).

In addition to drugs, the disposition of endogenous compounds has been studied using SCH. For example, amyloid-β (Aβ) hepatic disposition was studied in human SCH since Aβ accumulation contributes to Alzheimer's disease (Mohamed and Kaddoumi, 2013). Aβ was found to be taken up primarily by low-density lipoprotein receptor-related protein-1 (LRP), and effluxed by P-gp. This finding indicates that enhancement of Aβ hepatic clearance via LRP1 and P-gp induction could be a novel therapeutic approach for the prevention and treatment of Alzheimer's disease. Toxic compounds such as arsenic also have been studied in human SCH.

The results suggest that arsenic basolateral efflux prevails over biliary excretion, and is mediated at least in part by MRPs, most likely MRP4 (Roggenbeck et al., 2015).

Estimation of Transport Clearance

In the estimation of uptake clearance, hepatocytes in suspension generally are preferred due to the ease of use (De Bruyn et al., 2011; Williamson et al., 2013b) and concerns regarding down-regulation of uptake transporters in rat SCH (Kotani et al., 2011). Uptake transporter function in human SCH, however, appears to be well maintained under appropriate culture conditions (Kotani et al., 2011; Bi et al., 2012). Recent evidence suggests that cryopreserved hepatocytes cultured in sandwich configuration are a more feasible research tool to evaluate in vitro transport parameters than suspended hepatocytes, which may be affected by membrane leakage caused by cryopreservation (Kimoto et al., 2012). To distinguish active uptake from passive diffusion, hepatocytes can be co-incubated with an OATP inhibitor if the active uptake is mediated mainly by OATP. For example, rifampicin SV (100 µM) was reported to block OATP function in OATP-transfected cell lines and human SCH without affecting the passive diffusion (Vavricka et al., 2002; Bi et al., 2012). Alternatively, active uptake in SCH can be determined by the difference in uptake in the absence and presence of sodium if the active uptake is governed primarily by NTCP. Or uptake can be measured at low temperatures (e.g., 4°C compared to 37°C). However, reduced uptake at 4°C might be an artificial effect of a more rigid cell membrane, and thus, active uptake using this approach may be overestimated (Webborn et al., 2007).

In SCH, the biliary efflux clearance and biliary excretion index (BEI) can be calculated using B-CLEAR® technology and Equations 6-8 (Liu et al., 1999a). A detailed description of B-CLEAR® technology, including an overview of the advantages and limitations, has been

published by Swift et al (Swift et al., 2010). Essentially, the accumulation of compound in

cells+bile canaliculi and the accumulation of compound in cells can be differentiated by

modulating the tight junctions using Ca^{2+}-containing and Ca^{2+}-free Hank's balanced salt solution

(HBSS), respectively. The utility of SCH data for extrapolation from in vitro biliary clearance to

in vivo biliary clearance was reviewed previously by De Bruyn et al. (De Bruyn et al., 2013).

$$CL_{b,app,in\ vitro} = \frac{Amount_{cell+bile}-Amount_{cell}}{Time \times Concentration_{medium}} \quad (6)$$

$$CL_{b,int,\ in\ vitro} = \frac{Amount_{cell+bile}-Amount_{cell}}{Time \times Concentration_{cell}} \quad (7)$$

$$BEI = \frac{Amount_{cell+bile}-Amount_{cell}}{Amount_{cell+bile}} \times 100\% \quad (8)$$

$CL_{b,\ app,\ in\ vitro}$ and $CL_{b,\ int,\ in\ vitro}$ represent in vitro apparent biliary clearance and in vitro intrinsic

biliary clearance, respectively. BEI represents biliary excretion index, which is the fraction of

compound accumulated in the bile compartment relative to the total accumulation in cells plus

bile.

Use of the SCH assay to categorize compounds as low, intermediate or high biliary

clearance was first reported by Liu et al.(Liu et al., 1999b), and has been confirmed by numerous

investigators and reviewed by De Bruyn et al. and Swift et al.(Swift et al., 2010; De Bruyn et al.,

2013). Pan et al.(Pan et al., 2012) evaluated the biliary clearance of 110 compounds from

Novartis exhibiting different permeability properties using the rat SCH model. The predicted

biliary clearance from rat SCH correlated well with in vivo rat data, except for underestimation

of biliary clearance for compounds with extremely low passive permeability and metabolism.

The rank order of biliary clearance from human SCH data corresponded with clinical data for

compounds with low to high biliary clearance (Ghibellini et al., 2007), despite modest

underestimation of the absolute values (by 50-80%). The underestimation might be due to the

decreased activity of uptake transporters depending on the culture conditions, and use of

compound concentrations in the medium (Eq. 6) instead of the intracellular concentrations (Eq. 7) to predict biliary clearance. A more recent paper compared the human SCH estimated biliary clearance with clinical data and showed good agreement for drugs with no significant active hepatic uptake (absolute average fold error [AAFE] = 1.6). For drugs showing significant active uptake in human SCH, the predictability of biliary clearance was improved when scaled based on the extended clearance term (AAFE = 2.0), which incorporated sinusoidal uptake along with a global scaling factor for active uptake and the canalicular efflux clearance (Kimoto et al., 2017). More precise estimates of biliary clearance parameters for in vitro-in vivo scaling are discussed in greater detail in the "Mechanistic and PBPK Modeling" section.

To improve the precision of biliary clearance predictions using both rat and human SCH, the following approaches have been reported. The correlation between in vitro and in vivo biliary clearance is improved by using unbound plasma concentrations in the estimation of in vivo biliary clearance (Fukuda et al., 2008). Moreover, the difference between in vivo intrinsic biliary clearance and predicted intrinsic biliary clearance from the SCH data using Eq. 7 is smaller than the difference between in vivo apparent biliary clearance and predicted apparent biliary clearance from SCH data based on Eq. 6 (Nakakariya et al., 2012). Therefore, in vitro intrinsic biliary clearance (calculated based on intracellular concentrations instead of medium concentrations) is more reflective of in vivo biliary clearance (Nakakariya et al., 2012). In addition, quantitative proteomic approaches have been applied to improve biliary clearance predictions, as discussed in detail in the "Mechanistic and PBPK Modeling" section.

Basolateral efflux clearance can be estimated by preloading SCH with a substrate, and measuring the medium concentration at the end of the efflux phase. Ferslew et al. estimated basolateral efflux clearance of enalaprilat (generated in hepatocytes after incubation of rat SCH

with enalapril) based on the cumulative amount of enalaprilat effluxed into the medium and intracellular enalaprilat concentrations over the efflux period (Ferslew et al., 2014). The functional importance of MRP4 in the basolateral efflux of enalaprilat was demonstrated by using the pan-MRP inhibitor MK-571 in rat SCH, and confirmed in membrane vesicles prepared from HEK-293 cells overexpressing human MRP4. Of note, direct estimation of basolateral efflux clearance using this approach was possible because biliary excretion of enalaprilat is negligible. For compounds that undergo extensive biliary excretion, mechanistic modeling is necessary to deconvolute basolateral efflux, biliary excretion, and flux from the bile compartment to the medium, as discussed in the "Mechanistic and PBPK Modeling" section.

Transporter-Mediated DDIs

Transporter-based drug-drug and drug-bile acid interactions may have significant toxicological implications. SCH are a physiologically representative, organ-specific, whole-cell system that is well suited to elucidate the relative contribution of individual transporters to overall clearance, and to estimate the net effect of inhibition/induction at multiple sites. Both acute (direct and indirect) and long-term effects on transporters have been studied in SCH.

Pfeifer et al. elucidated the sites and mechanisms of DDIs between ritonavir (perpetrator) and ^{99m}Tc–mebrofenin (victim substrate) using human SCH coupled with modeling and simulation of clinical data (Bi et al., 2012; Pfeifer et al., 2013a). Ritonavir decreased ^{99m}Tc–mebrofenin uptake without changing the BEI of ^{99m}Tc–mebrofenin, despite the fact that ritonavir had been reported to inhibit MRP2, which mediates the biliary excretion of ^{99m}Tc–mebrofenin. These in vitro findings were consistent with the clinical observation that single or multiple doses of ritonavir increased ^{99m}Tc–mebrofenin systemic exposure without significantly changing biliary recovery of ^{99m}Tc–mebrofenin. SCH data revealed that intracellular ritonavir

concentrations after clinical doses were not high enough to inhibit MRP2 based on data generated in membrane vesicles for ^{99m}Tc–mebrofenin transport by MRP2.

Unlike direct inhibition of transporters, indirect modulation of transporters is under-appreciated and the relevant studies using SCH are still limited. Powell et al. reported post-translational regulation of OATP1B3 by the PKC activator, phorbol-12-myristate-13-acetate (PMA). This mechanism was revealed by the fact that pre-treatment of SCH with PMA inhibited OATP1B3 function while co-incubation with PMA did not (Powell et al., 2014). Kruglov et al. reported that the type II inositol 1,4,5-trisphosphate receptor modulates Bsep activity in rat SCH through post-translational regulation (Kruglov et al., 2011). The important role of N-glycosylation of ATP-binding cassette transporters on transport activity was established using rat SCH (Zhang et al., 2005; Draheim et al., 2010). The induction of transporters after long-term incubation (>24 hr) also was studied in SCH (Annaert et al., 2001; Turncliff et al., 2004; Lee et al., 2008), and has been reviewed in (Swift et al., 2010). More recent examples studied the effect of nuclear receptors on transporter induction. Up-regulation of transporter mRNA expression in response to prototypical activators of PXR, aryl hydrocarbon receptor, and CAR were reported in mouse SCH (Noel et al., 2013). It was reported that dexamethasone treatment induced the expression and function of Mrp2 in rat SCH. Studies using human SCH showed that FXR agonists up-regulated the mRNA expression of bile acid efflux transporters (Jackson et al., 2016; Zhang et al., 2017).

4.4 Use of SCH in Studying Enzyme-Transporter Interplay

The complexity of DDI predictions may be increased further by the interplay between enzymes and transporters. Many compounds interact with enzymes and transporters simultaneously. For example, cyclosporine inhibits CYP3A4, and multiple transporters including

P-gp and OATP1B1. Gemfibrozil and gemfibrozil glucuronide inhibit CYP2C8 and OATP1B1 (Neuvonen et al., 2006). Moreover, the parent compound and derived metabolites may have similar or opposite effects on transporters and enzymes. For drugs that are metabolized extensively, the presence of metabolic capacity in SCH enables the simultaneous evaluation of parent and metabolite effects without prior knowledge regarding the metabolites. This capability is very beneficial, especially in the early stages of drug discovery when metabolite identification has not been conducted and purified metabolites are not available. A few examples are discussed below.

For drugs that are rapidly metabolized and the metabolites are not transporter inhibitors, the intracellular concentration of the parent compound might not be high enough to inhibit efflux transporters. For example, cilexetil (CIL) exhibited potent BSEP inhibition based on membrane vesicle assays. However, BSEP inhibition by CIL was not observed in human SCH after 120-min exposure, which might be due to the metabolic elimination of CIL in SCH (Fukuda et al., 2014). In this case, the membrane vesicle data led to a false positive prediction of BSEP inhibition. Sometimes metabolites are more potent inhibitors of transporters, such as troglitazone sulfate compared to troglitazone. In this case, data from a metabolism-deficient system could lead to false-negative results (Yang et al., 2014b). The interplay between formation and excretion of troglitazone metabolites was studied in rat SCH lacking Bcrp and Mrp2 by Yang et al. using RNA interference techniques to knock down Bcrp in SCH prepared from TR$^-$ rats which are Mrp2 deficient (Yang et al., 2014a). In some cases, only the metabolites are transporter inhibitors. For example, although estradiol and bilirubin do not inhibit MRP2, pre-exposure of rat SCH to estradiol and bilirubin decreased the biliary excretion of 5-(and 6)-carboxy-2',7'-

dichlorofluorescein, a MRP2 substrate, which could be attributed to inhibition by the generated metabolites of estradiol and bilirubin (Nakanishi et al., 2012).

4.5 Use of SCH Data in Mechanistic and PBPK Modeling

PBPK modeling is a useful tool to predict the PK of novel compounds in the systemic circulation and target organs. Successful PBPK models depend on reliable estimates of compound-specific information (e.g., clearance, tissue partition coefficients, and the rate and extent of absorption). SCH have been used to estimate clearance values that are incorporated into PBPK models. The methods to estimate in vitro clearance using SCH, and to extrapolate from in vitro to in vivo clearance values are discussed below.

In vitro intrinsic uptake and efflux clearance values have been estimated using empirical methods, as described in the previous sections. The apparent clearance value determined from SCH data may be comprised of more than one clearance pathway. Despite this limitation, estimated clearance values generated by empirical/static approaches can represent useful prior information to guide the experimental design for mechanistic modeling and simulation, and generally requires a relatively small number of data points.

Mechanistic PK models have been developed to deconvolute apparent uptake and efflux clearance values and obtain more accurate estimates. Linear kinetics are assumed and the clearance terms (rather than V_{max} and K_m) are used because a single, low concentration of substrate typically is studied. To estimate the kinetic parameters, multiple time points during both the uptake and efflux phase are required. Depending on the permeability of the substrate, passive diffusion clearance could be estimated solely from 37°C data. The kinetic parameters estimated could be used to perform sensitivity analyses and Monte Carlo simulations, which can help identify key model input parameters. Depending on the model structure and complexity, the

published mechanistic PK models are classified into three categories. The model structures and exemplar experimental protocols are shown in Figure 1.3; the model output parameters, assumptions and applications of each model are summarized in Table 1.1.

Model I

This model is the simplest for the SCH system (Figure 1.3A). Three compartments represent the medium, cell, and bile, with passive diffusion, active uptake, biliary efflux, and metabolism processes included. Key kinetic parameters include intrinsic passive diffusion clearance ($CL_{int, pass}$); intrinsic uptake clearance ($CL_{int, uptake}$), and intrinsic biliary clearance ($CL_{int, bile}$). Basolateral efflux is assumed to be negligible. When significant metabolism is observed, intrinsic metabolic clearance ($CL_{int, met}$) is set to the unbound intrinsic clearance value determined in HLMs. To generate the experimental data, SCH are first pre-incubated with standard Hank's balanced salt solution (HBSS), Ca^{2+}-free HBSS, or standard HBSS containing rifamycin SV, followed by incubation with the substrate. Substrate uptake is terminated at different time points, and the intracellular and medium concentrations of the substrate are measured. This model has been applied to estimate the in vitro intrinsic clearance for OATP substrates (Jones et al., 2012; Jones et al., 2013; Li et al., 2014b).

Model II

Unlike Model I where $CL_{int, met}$ is fixed to a pre-determined value, $CL_{int, met}$ is fitted to metabolite(s) concentration-time data in Model II. In addition, intrinsic basolateral efflux clearance of metabolite ($CL_{int, BL, metabolite}$) is included rather than assuming passive diffusion. $K_{flux, metabolite}$, which accounts for the "flux" of metabolite from the canalicular compartment into the buffer, also is incorporated (Oshio and Phillips, 1981; Phillips et al., 1982; Boyer et al., 1988). In this model, it is assumed that only metabolites undergo efflux into bile or medium.

(Figure 1.3B). The experimental protocol is similar to that of Model I except that the pre-incubation phase only consists of two conditions (HBSS and Ca^{2+}-free HBSS), and both parent and metabolite(s) concentrations are measured. Lee et al. fitted this model to concentration-time data for troglitazone and metabolites [troglitazone sulfate, glucuronide, and quinone] in rat and human SCH (Lee et al., 2010). This model has been used to characterize the contribution of individual clearance pathways to the disposition of mycophenolic acid (MPA) and MPA glucuronide (MPAG) (Matsunaga et al., 2014), and the inhibitory potency of cyclosporine on each pathway in human SCH (Matsunaga et al., 2015). The modeling results suggest that cyclosporine A inhibits both basolateral uptake and biliary efflux clearance of MPAG without changing the conversion of MPA to MPAG. This mechanism explains the cyclosporine A-mediated decrease in enterohepatic circulation of MPAG and lower systemic exposure of MPA and MPAG in humans.

Model III

Model III is more suitable for compounds with minimal passive diffusion that are not extensively metabolized (Figure 1.3C), such as rosuvastatin (RSV) and TCA. To obtain an accurate estimate of basolateral efflux, a novel uptake and efflux protocol is used, which includes an uptake phase followed by an efflux phase where serial samples are obtained. Uptake, biliary, and basolateral efflux clearance values for RSV, ^{3}H-TCA, and d_8-TCA were estimated from rat and human SCH data (Pfeifer et al., 2013c; Yang et al., 2015; Guo et al., 2016). The impact of impaired clearance of RSV and ^{3}H-TCA were simulated, and predicted perpetrator effects on d_8-TCA disposition were compared with experimental observations.

In this experimental design, a few practical factors need to be considered for determining the maximum incubation time. Most of the time, the uptake phase is extended beyond the linear

range to attain steady-state intracellular conditions, which reduces the error in certain parameter estimates observed with shorter incubation times. However, exposure to Ca^{2+}-free HBSS for more than 30 min increases cytotoxicity (Swift et al., 2010). Therefore, after pre-incubation with Ca^{2+}-containing or Ca^{2+}-free HBSS for 10 min, SCH are incubated with Ca^{2+}-containing HBSS during the uptake phase. The uptake phase should be limited to 20 min in Ca^{2+}-containing HBSS to avoid resealing of tight junctions in SCH pre-incubated with Ca^{2+}-free HBSS (Pfeifer et al., 2013c).

Scaling Methods

In vivo intrinsic clearance is a key parameter for PBPK models that can be extrapolated from in vitro clearance using the following scaling methods. The simplest and most straightforward approach for scaling up is based on hepatocellularity and liver weight as described previously (Houston, 1994) and reviewed by Poulin and Haddad (Poulin and Haddad, 2013). Scaling with physiological parameters works well for metabolic clearance. However, this approach leads to an underprediction of $CL_{int, \, uptake}$ and an overprediction of $CL_{int, \, bile}$ using human SCH (Jones et al., 2012). Underprediction of uptake may occur when $CL_{int, \, BL}$ is disregarded in the model, or when uptake transporters are down-regulated in vitro compared to in vivo (Jacobsen et al., 2011). Overprediction of $CL_{int, \, bile}$ may occur due to the absence of enterohepatic recirculation, and/or ignoring K_{flux} in the mechanistic model (Jones et al., 2012). Clearly, over-simplification of the model structure can lead to over- or under-prediction of parameters. To address the misprediction of in vivo parameters, Jones et al. determined compound-specific scaling factors (SFs) by comparing in vivo clearance to in vitro clearance data from human SCH (Jones et al., 2012); geometric mean SFs for intrinsic unbound uptake clearance ($CL_{int, \, u, \, uptake}$), intrinsic unbound biliary clearance ($CL_{int, \, u, \, bile}$) and intrinsic unbound

passive diffusion clearance ($CL_{int, u, pass}$) of seven OATP substrates were reported as 58, 0.061, and 1, respectively (Jones et al., 2012). These SFs have been used in the in vitro-in vivo extrapolation of other OATP substrates such as telmisartan (Jones et al., 2012; Li et al., 2014b). A similar approach has been applied to estimate SFs for $CL_{int, uptake}$ of glyburide, pravastatin, and repaglinide (Varma et al., 2012; Varma et al., 2013b; Varma et al., 2014). Li et al. developed a single set of empirical SFs by simultaneously modeling data for the same seven OATP substrates; these authors reported SFs of 55 for $CL_{int, u, uptake}$, 0.019 for $CL_{int, u, bile}$, and 0.092 for $CL_{int, u, pass}$ (Li et al., 2014c). The difference in the estimated SF for $CL_{int, u, pass}$ between the two studies (1 vs. 0.092) could be due to different approaches for model fitting [the SF for intrinsic unbound metabolic clearance ($CL_{int, u, met}$) was not estimated by Jones et al. because $CL_{int, u, met}$ was not identifiable, but this SF was fitted in the work of Li et al.]

The approach described above relies on intravenous PK data to estimate empirical SFs. If intravenous data are not available, the in vitro-in vivo extrapolation could be facilitated by information regarding transporter abundance. Absolute quantification of transporter expression by mass spectrometry was first reported by Terasaki and colleagues based on the assumption that all expressed protein is localized on the membrane and, therefore, functional (Shawahna et al., 2011; Agarwal et al., 2012; Sakamoto et al., 2013; Uchida et al., 2013; Sakamoto et al., 2015). This technique has been advanced by the work of Lai et al.(Kimoto et al., 2012) (Li et al., 2009; Li et al., 2010; Bi et al., 2012), Unadkat et al. (Shawahna et al., 2011; Agarwal et al., 2012), and more recently by Artursson et al. (Vildhede et al., 2015), and Galetin et al. (Badee et al., 2015).

Intrinsic clearance values estimated using the approaches detailed above can be used directly in PBPK models (Jamei et al., 2009). Alternatively, the overall intrinsic clearance values can be combined with liver blood flow and protein binding data to estimate hepatic clearance

based on the well-stirred or parallel-tube models of hepatic disposition (Wilkinson, 1987). PK profiles have been predicted successfully for numerous compounds including statins, sartans, mebrofenin, pafuramidine, glyburide, and repaglinide using PBPK models that incorporated clearance values estimated from SCH (Bi et al., 2012; Jones et al., 2012; Varma et al., 2012; Pfeifer et al., 2013c; Jamei et al., 2014; Li et al., 2014a; Varma et al., 2014) (Yan et al., 2012) (Jones et al., 2013; Varma et al., 2013a; Li et al., 2014a).

5. Project Rationale and Specific Aims

The objective of this dissertation research was to develop in vitro and in silico approaches to increase our ability to predict and evaluate drug-bile acid interactions mediated by inhibition or induction of hepatic transporters. This work provided frameworks and innovative approaches to improve the prediction of transporter-mediated disposition of drugs and bile acids, which has important implications for safe and efficacious pharmacotherapy. To achieve this goal, mechanistic PK modeling combined with data generated in SCH were used.

5.1 Rationale for Aim #1

Transporter inhibition assays have been adopted by the pharmaceutical industry and included in regulatory guidelines to predict DDIs. However, many false negative or positive predictions have been reported using routine assay methods (Vaidyanathan et al., 2016). Explanations for inaccurate predictions include simultaneous inhibition of multiple transporters, inaccurate estimation of inhibitor concentrations at the site of action (due to protein binding and subcellular distribution), and uncertainty in K_i or IC_{50} measurements.

Many drugs are dual inhibitors of uptake and efflux transporters, such as telmisartan and bosentan (Morgan et al., 2013). The net effect of inhibition of multiple transporters depends on the relative contribution of each transporter to the overall clearance in addition to the inhibitory

potency. Mechanistic PK modeling of data from human SCH is useful in assessing the relative contribution of each clearance pathway to overall drug disposition (Pfeifer et al., 2013c; Matsunaga et al., 2014; Yang et al., 2015), and predicting transporter-mediated disposition and DDIs in vivo (Jones et al., 2012; Jones et al., 2013; Li et al., 2014b). However, none of these publications have combined inhibition data from transfected systems with kinetic data from human SCH to predict the net effects of an inhibitor.

Currently, there is no consensus on which inhibitor concentration is the most relevant and effective data input for predicting the interaction with hepatic efflux transporters. A comparison of prediction accuracy using various types of intracellular inhibitor concentrations, including total or unbound concentration in cell or cytosol, will be needed. In addition, a classification system would be helpful to determine a priori the benefit of measuring intracellular unbound fraction ($f_{u,cell,inhibitor}$) for accurate predictions. Therefore, **Aim #1 (Chapter 2 and 3)** focused on developing frameworks to predict altered bile acid disposition due to the inhibition of multiple transporters, and to assess the relevant inhibitor concentration for hepatic efflux transporters. TCA was chosen as the model bile acid since TCA is the standard substrate for most bile acid transporter inhibition assays.

5.2 Rationale for Aim #2

Inhibition constants (such as K_i or IC_{50}) for individual transporters are important parameters in predicting DDIs and DILI. Generally, inhibition constants are obtained from expression systems. Despite their ease of use, the quality of these data are limited by a few factors: transporter expression levels may not be physiologically relevant and membrane composition of these systems may not be ideal; the relative contribution of each transporter to the overall substrate clearance is often unknown for most substrates. These issues could be

avoided by using a physiologically-relevant holistic system, SCH, combined with PK modeling. Mechanistic PK modeling of SCH data allows for the assessment of inhibition potency against each clearance pathways (e.g., biliary and basolateral efflux), which represents the inhibition potency against multiple transporters in the same clearance pathway. The mechanism of inhibition is another critical factor that influences the impact of inhibition. Noncompetitive inhibition may lead to greater bile acid accumulation and an increased potential for toxicity compared to competitive inhibition, as shown by the troglitazone sulfate example (Woodhead JL et al., 2014). To identify the inhibition mechanism using expression systems, multiple substrate and inhibitor concentrations are needed, which is resource intensive. Since the intracellular concentrations of the substrate and inhibitor change over time in SCH, it is possible to identify the inhibition mechanism against the biliary clearance by using fewer concentrations of the substrate and inhibitor. To achieve this goal, sufficient data input is needed to allow for accurate parameter estimation. The purpose of **Aim #2 (Chapter 4)** was to provide an optimized study design for, and assess the practicality of, estimating the inhibition potency and identifying inhibition mechanism against multiple transport pathways using PK modeling and data from SCH. Troglitazone sulfate was chosen as the model inhibitor, which exhibits multiple inhibition mechanisms towards different bile acid efflux transporters. TCA was employed as the model substrate.

5.3 Rationale for Aim #3

Intracellular bile acids can bind with FXR, which increases gene transcription to enhance bile acid efflux and decrease bile acid uptake by the liver (Ananthanarayanan et al., 2001; Lee et al., 2006). FXR is a promising novel drug target to treat metabolic and chronic liver diseases because of its role in regulating bile acid homeostasis. Obeticholic acid (OCA), an analogue of

33

CDCA, is the first-in-class FXR agonist, and has been approved for the treatment of primary biliary cholangitis. Studies using human SCH showed that OCA and CDCA treatment for 72 hr increased mRNA expression of the basolateral efflux transporter OSTα/β and the canalicular transporter BSEP. Plasma bile acid concentrations in cholestatic patients are increased (Keppler, 2011; Chen et al., 2013), which may be due to increased hepatic basolateral efflux or decreased hepatic uptake and/or biliary excretion of bile acids. However, direct functional evidence for the induction of bile acid efflux transporters (i.e., OSTα/β and BSEP) by FXR agonists is lacking both in vitro and in vivo. This information will provide mechanistic rationale for FXR as a therapeutic target for the treatment of cholestatic diseases by reducing bile acid burden in hepatocytes. In addition, exploration of the molecular mechanism will corroborate the observed alterations in function. Studies outlined in **Aim #3 (Chapter 5)** were designed to evaluate the changes in the function and expression of hepatic bile acid transporters by FXR agonists, OCA and CDCA. TCA again was chosen as the substrate to study bile acid transporter function.

Aim #1. Develop an integrated approach to accurately predict the effect of hepatic transporter inhibition on the hepatobiliary disposition of bile acids.

Hypothesis: Altered bile acid disposition due to inhibition of multiple transporters can be predicted by integrating experimental and mechanistic PK modeling approaches. Total or unbound concentrations in the cell or cytosol may lead to different prediction results. For certain inhibitors, it is optimal to measure intracellular unbound fraction of inhibitor ($f_{u,cell,inhibitor}$) and use intracellular unbound inhibitor concentration rather than total concentration when predicting their inhibitory effects. This benefit can be determined a priori based on the PK characteristics of the inhibitor and victim substrate.

1.a. Characterize the hepatobiliary disposition (basolateral uptake and efflux, canalicular efflux) of taurocholate in protein-containing medium using human sandwich-cultured hepatocyte data and mechanistic PK modeling.

1.b. Predict the effect of bosentan and telmisartan on taurocholate disposition by integrating individual IC_{50} data and the relevant inhibitor concentrations into a mechanistic PK model.

1.c. Assess the impact of changes in $f_{u,cell,inhibitor}$ on the prediction of efflux transporter-mediated drug-bile acid interactions for various theoretical inhibitors using simulation; validate the simulation results with experimental data.

Aim #2. Estimate inhibition constants against bile acid efflux clearance values using PK modeling of data from sandwich-cultured hepatocytes.

Hypothesis: Using PK modeling of sandwich-cultured hepatocyte data and a single dose of inhibitor and substrate, K_i values of the inhibitor against the biliary and basolateral efflux clearance pathways of the substrate can be estimated simultaneously, and the inhibition mechanism can be identified. Modeling and simulation can assist the development of an optimal study design for this purpose.

2.a. Develop an optimal study design to estimate the K_i of the model inhibitor, troglitazone sulfate, against biliary and basolateral efflux clearance pathways of taurocholate in rat sandwich-cultured hepatocytes using mechanistic PK modeling and simulation. Distinguish the inhibition mechanism of troglitazone sulfate against the biliary clearance based on the best-fit model of the kinetic data.

2.b. Assess the practicality of using this optimal study design in different lots of rat hepatocytes.

Aim #3. Evaluate the induction of bile acid efflux transporters in human sandwich-cultured hepatocytes by FXR agonists.

Hypothesis: Treatment of FXR agonists, obeticholic acid and chenodeoxycholic acid, for 72 hr increases the function and protein expression of bile acid efflux transporters. The functional changes can be reflected by taurocholate clearance values estimated by mechanistic PK modeling.

3.a. Assess the hepatobiliary disposition (basolateral uptake and efflux, canalicular efflux) of taurocholate in human sandwich-cultured hepatocytes after 72-hr treatment with obeticholic acid and chenodeoxycholic acid using mechanistic PK modeling.

3.b. Quantify the protein expression of bile acid transporters in human sandwich-cultured hepatocytes after 72-hr treatment with obeticholic acid and chenodeoxycholic acid.

Chapters 2-5 focus on the use of mechanistic PK modeling and simulation as tools to elucidate and predict drug interactions mediated by the inhibition and induction of hepatic bile acid transporters using sandwich-cultured hepatocytes. Chapter 6 summarizes findings from this dissertation research and proposes a number of future directions for the projects. The outcomes of this dissertation research will facilitate the prediction of drug-drug interactions and drug-induced liver injury based on PK modeling and vitro data.

Table 1.1. Output parameters, assumptions, and applications of mechanistic PK modeling to assess clearance in SCH.

Type of Model	Output Parameters	Comments	Reference
Model I	$CL_{int, uptake}$ $CL_{int, pass}$ $CL_{int, bile}$	**Assumptions**: • No basolateral efflux • No K_{flux} • $CL_{int, met}$ same as estimated from HLMs **Applications:** • Substrates without basolateral efflux • $CL_{int, met}$ from other systems fixed in the model	(Jones et al., 2012; Jones et al., 2013; Li et al., 2014b)
Model II	$CL_{int, uptake, parent}$ $CL_{int, uptake, metabolite}$ $CL_{int, BL, metabolite}$ $CL_{int, bile, metabolite}$ $CL_{int, met}$ $K_{flux, metabolite}$	**Assumption:** • No passive diffusion • Only metabolites effluxed into bile and medium **Applications:** • Simultaneous estimation of transport clearance of parent and metabolite, as well as metabolic clearance	(Lee et al., 2010; Matsunaga et al., 2015)
Model III	$CL_{int, uptake}$ $CL_{int,BL}$ $CL_{int,bile}$ K_{flux}	**Assumptions:** • No passive diffusion • No metabolism **Applications:** • Accurate estimation of $CL_{int, BL}$ and K_{flux} by using a novel uptake and efflux protocol • Useful for substrates that undergo minimal metabolism	(Pfeifer et al., 2013c; Yang et al., 2015; Guo et al., 2016)

K_{flux}, first-order rate constant for flux from bile networks into buffer; $CL_{int, uptake}$, intrinsic uptake clearance; $CL_{int, pass}$, intrinsic passive diffusion clearance; $CL_{int,bile}$, intrinsic biliary clearance; $CL_{int,met}$, intrinsic metabolic clearance; $CL_{int, BL}$, intrinsic basolateral efflux clearance; $CL_{int, uptake, parent}$, intrinsic uptake clearance of parent; $CL_{int, uptake, metabolite}$, intrinsic uptake clearance of metabolite; $CL_{int,bile, metabolite}$, intrinsic biliary clearance of metabolite; $CL_{int, BL, metabolite}$, intrinsic

basolateral efflux clearance of metabolite; $K_{flux, metabolite}$, first-order rate constant for flux from bile networks into buffer of metabolite; HLMs, human liver microsomes

Figure 1.1. Scheme illustrating the polarized expression of transporters in human sandwich-cultured human hepatocytes.

Three adjacent hepatocytes with interconnecting canalicular spaces sealed by tight junctions (red rectangles) are shown. Important ATP-binding cassette (ABC) transport proteins are depicted by blue solid arrows denoting the direction of transport. Solute carrier (SLC) transporters are depicted with black double arrows. Uptake transporters in the basolateral (sinusoidal) membrane include sodium taurocholate co-transporting polypeptide (NTCP); organic anion transporter 2 (OAT2) and OAT7; organic cation transporter 1 (OCT1); and organic anion transporting polypeptide 1B1 (OATP1B1), OATP1B3 and OATP2B1. The heteromeric organic solute transporter (OSTα/β) is also depicted on the basolateral membrane. Efflux transporters expressed in the hepatocyte basolateral membrane include multidrug resistance-associated protein 3 (MRP3), MRP4 and MRP6. Canalicular (apical) efflux pumps include MRP2, breast cancer resistance protein (BCRP), bile-salt export pump (BSEP), MDR1 P-glycoprotein (P-gp), and multidrug and toxin extrusion protein 1 (MATE1).
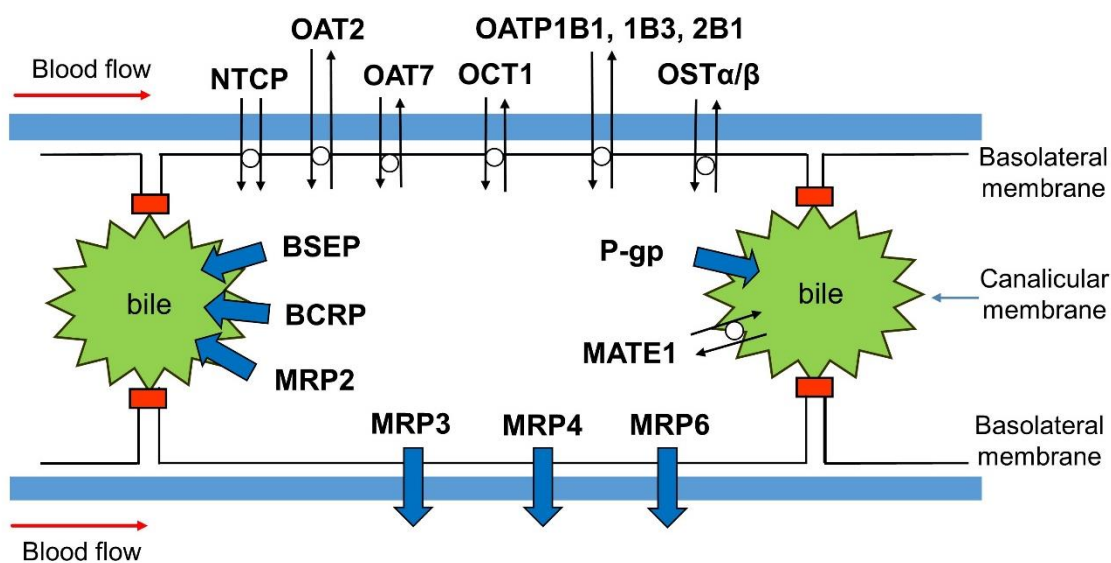
Figure 1.2. Number of PubMed publications with "hepatic" and "bile acid transporter" in the title or abstract from 1980 to 2017.
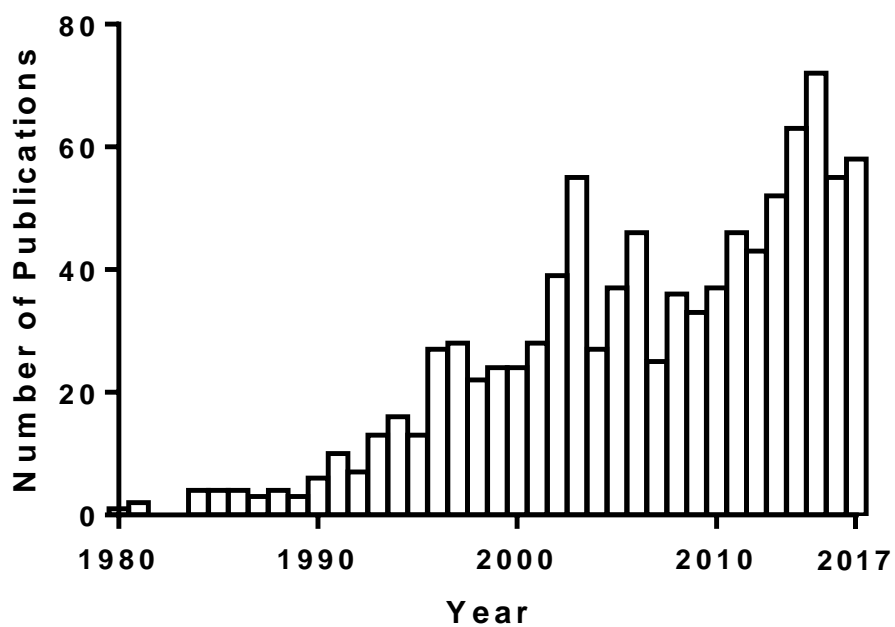
Figure 1.3. Schematic diagram depicting the mechanistic pharmacokinetic models (left) and experimental protocols (right) in sandwich-cultured hepatocytes. **(A)** *Model I*, uptake studies were conducted in the presence of standard HBSS, Ca^{2+}-free HBSS, or standard HBSS containing rifamycin SV. **(B)** *Model II*, uptake studies were conducted in the presence of standard HBSS or Ca^{2+}-free HBSS. **(C)** *Model III*, uptake and efflux studies were conducted in the presence of standard HBSS or Ca^{2+}-free HBSS.

In the model schemes (left), dashed boxes represent the sampling compartments. X, V, and C denote the mass of substrate, compartmental volume, and substrate concentration, respectively. Subscripts on mass, volume, and concentration terms denote the corresponding compartment in the model scheme, superscripts represent the presence or absence of Ca^{2+} in the pre-incubation and efflux buffer. X in parentheses represents experimental measurements. Output parameters include: intrinsic uptake clearance ($CL_{int, uptake}$), intrinsic passive diffusion clearance ($CL_{int, pass}$), intrinsic biliary clearance ($CL_{int, bile}$), intrinsic metabolic clearance ($CL_{int, met}$), intrinsic basolateral efflux clearance ($CL_{int, BL}$), first-order rate constant for flux from bile networks into buffer (K_{flux}), intrinsic uptake clearance of parent ($CL_{int, uptake, parent}$), intrinsic uptake clearance of metabolite ($CL_{int, uptake, metabolite}$), intrinsic biliary clearance of metabolite ($CL_{int,bile, metabolite}$), intrinsic basolateral efflux clearance of metabolite ($CL_{int, BL, metabolite}$), and first-order rate constant for flux from bile networks into buffer of metabolite ($K_{flux, metabolite}$).

In the experimental protocols diagram, the white boxes represent incubation with Ca^{2+}-free or standard HBSS. Grey shaded boxes represent inclusion of the substrate in standard HBSS during the uptake phase. Black boxes represent a 1-min wash with Ca^{2+}-free or standard HBSS. The sampling times and incubation length are shown in this diagram as an example, but need to be adjusted depending on the pharmacokinetic characteristics of the substrate.

a. Model I

Standard HBSS ($X_{Cell+Bile}$):
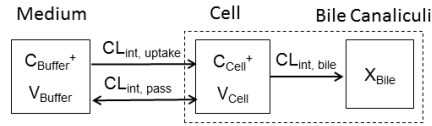
Medium   Cell   Bile Canaliculi

C_{Buffer}^{+} V_{Buffer} $CL_{int, uptake}$ $CL_{int, pass}$ C_{Cell}^{+} V_{Cell} $CL_{int, bile}$ X_{Bile}

Pre-incubation   Sampling (Cell lysate) 2, 5, 10, 20 min

Std HBSS 10 min   UPTAKE Std HBSS 20 min

Ca^{2+}-free HBSS (X_{Cell}):

Medium   Cell

C_{Buffer}^{-} V_{Buffer} $CL_{int, uptake}$ $CL_{int, pass}$ C_{Cell}^{-} V_{Cell} $CL_{int, bile}$
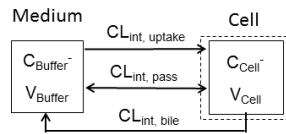
Ca^{2+}-Free HBSS, 10 min   UPTAKE Std HBSS 20 min

Standard HBSS containing Rif SV ($X_{cell+Bile}$):

Medium   Cell   Bile Canaliculi

C_{Buffer}^{+} V_{Buffer} $CL_{int, pass}$ C_{Cell}^{+} V_{Cell} $CL_{int, bile}$ X_{Bile}
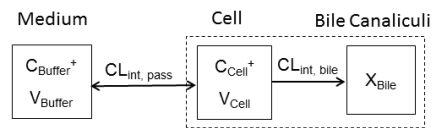
Std HBSS+Rif SV 10 min   UPTAKE Std HBSS+Rif SV 20 min

b. Model II

Standard HBSS ($X_{parent, Cell}$, $X_{parent, Buffer}^{+}$, $X_{metabolite, Cell+Bile}$, $X_{metabolite, Buffer}^{+}$):
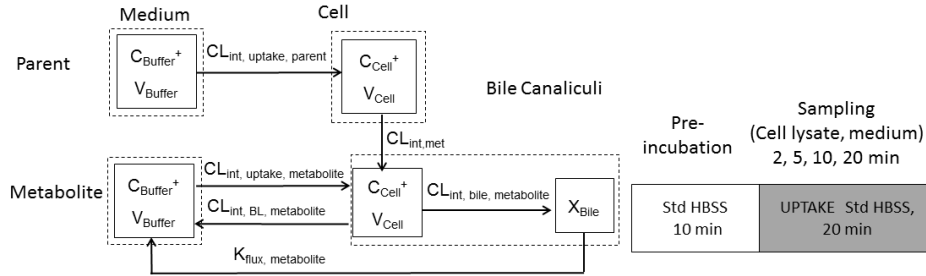
Medium   Cell

Parent

C_{Buffer}^{+} V_{Buffer} $CL_{int, uptake, parent}$ C_{Cell}^{+} V_{Cell}

Bile Canaliculi

$CL_{int,met}$

Metabolite

C_{Buffer}^{+} V_{Buffer} $CL_{int, uptake, metabolite}$ $CL_{int, BL, metabolite}$ C_{Cell}^{+} V_{Cell} $CL_{int, bile, metabolite}$ X_{Bile} $K_{flux, metabolite}$

Pre-incubation   Sampling (Cell lysate, medium) 2, 5, 10, 20 min

Std HBSS 10 min   UPTAKE Std HBSS, 20 min

Ca^{2+}-free HBSS ($X_{parent, Cell}$, $X_{parent, Buffer}^{-}$, $X_{metabolite, Cell}$, $X_{metabolite, Buffer}^{-}$):

Ca^{2+}-Free HBSS, 10 min   UPTAKE Std HBSS, 20 min

Medium   Cell

Parent

C_{Buffer}^{-} V_{Buffer} $CL_{int, uptake, parent}$ C_{Cell}^{-} V_{Cell}

$CL_{int, bile, metabolite}$ $CL_{int, met}$

Metabolite

C_{Buffer}^{-} V_{Buffer} $CL_{int, uptake, metabolite}$ $CL_{int, BL, metabolite}$ C_{Cell}^{-} V_{Cell}
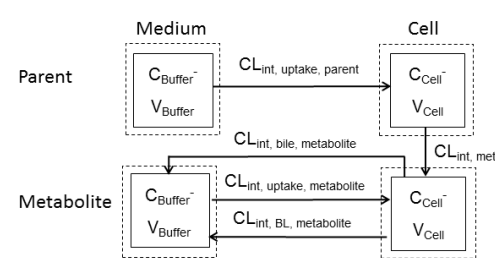
c. Model III

Standard HBSS ($X_{Cell+Bile}$, X_{Buffer}^{+}):
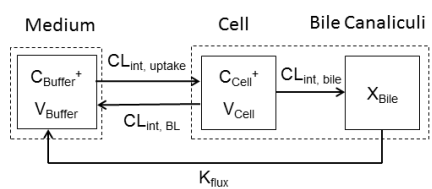
Medium   Cell   Bile Canaliculi

C_{Buffer}^{+} V_{Buffer} $CL_{int, uptake}$ $CL_{int, BL}$ C_{Cell}^{+} V_{Cell} $CL_{int, bile}$ X_{Bile} K_{flux}

Pre-Incubation   Sampling (Cell Lysate) 2, 5, 10,20 min   Sampling (Cell Lysate, medium) 2, 5, 10, 15 min

Std HBSS 10 min   UPTAKE Std HBSS, 20 min   EFFLUX Std HBSS, 15 min

Wash with Std HBSS (~1 min)

Ca^{2+}-free HBSS (X_{Cell}, X_{Buffer}^{-}):

C_{Buffer}^{-} V_{Buffer} $CL_{int, uptake}$ $CL_{int, BL}$ C_{Cell}^{-} V_{Cell} $CL_{int, bile}$
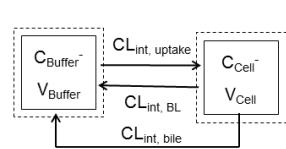
Ca^{2+}-Free HBSS, 10 min   UPTAKE Std HBSS, 20 min   EFFLUX Ca^{2+}-Free HBSS, 15 min

Wash with Ca^{2+}-Free HBSS (~1 min)

42

REFERENCES

Agarwal S, Chinn L and Zhang L (2013) An overview of transporter information in package inserts of recently approved new molecular entities. *Pharm Res* **30**:899-910.

Agarwal S, Uchida Y, Mittapalli RK, Sane R, Terasaki T and Elmquist WF (2012) Quantitative proteomics of transporter expression in brain capillary endothelial cells isolated from P-glycoprotein (P-gp), breast cancer resistance protein (Bcrp), and P-gp/Bcrp knockout mice. *Drug Metab Dispos* **40**:1164-1169.

Ahlin G, Hilgendorf C, Karlsson J, Szigyarto CA, Uhlen M and Artursson P (2009) Endogenous gene and protein expression of drug-transporting proteins in cell lines routinely used in drug discovery programs. *Drug Metab Dispos* **37**:2275-2283.

Ali I, Welch MA, Lu Y, Swaan PW and Brouwer KLR (2017) Identification of novel MRP3 inhibitors based on computational models and validation using an in vitro membrane vesicle assay. *Eur J Pharm Sci* **103**:52-59.

Allen K, Jaeschke H and Copple BL (2011) Bile acids induce inflammatory genes in hepatocytes: a novel mechanism of inflammation during obstructive cholestasis. *Am J Pathol* **178**:175-186.

Ananthanarayanan M, Balasubramanian N, Makishima M, Mangelsdorf DJ and Suchy FJ (2001) Human bile salt export pump promoter is transactivated by the farnesoid X receptor/bile acid receptor. *J Biol Chem* **276**:28857-28865.

Annaert PP, Turncliff RZ, Booth CL, Thakker DR and Brouwer KL (2001) P-glycoprotein-mediated in vitro biliary excretion in sandwich-cultured rat hepatocytes. *Drug Metab Dispos* **29**:1277-1283.

Austin RP, Barton P, Mohmed S and Riley RJ (2005) The binding of drugs to hepatocytes and its relationship to physicochemical properties. *Drug Metab Dispos* **33**:419-425.

Badee J, Achour B, Rostami-Hodjegan A and Galetin A (2015) Meta-analysis of expression of hepatic organic anion-transporting polypeptide (OATP) transporters in cellular systems relative to human liver tissue. *Drug Metab Dispos* **43**:424-432.

Balakrishnan A, Hussainzada N, Gonzalez P, Bermejo M, Swaan PW and Polli JE (2007) Bias in estimation of transporter kinetic parameters from overexpression systems: Interplay of transporter expression level and substrate affinity. *J Pharmacol Exp Ther* **320**:133-144.

Ballatori N, Christian WV, Lee JY, Dawson PA, Soroka CJ, Boyer JL, Madejczyk MS and Li N (2005) OSTalpha-OSTbeta: a major basolateral bile acid and steroid transporter in human intestinal, renal, and biliary epithelia. *Hepatology* **42**:1270-1279.

Benet LZ (2009) The drug transporter-metabolism alliance: uncovering and defining the interplay. *Mol Pharm* **6**:1631-1643.

Bentz J, O'Connor MP, Bednarczyk D, Coleman J, Lee C, Palm J, Pak YA, Perloff ES, Reyner E, Balimane P, Brannstrom M, Chu X, Funk C, Guo A, Hanna I, Heredi-Szabo K, Hillgren K, Li L, Hollnack-Pusch E, Jamei M, Lin X, Mason AK, Neuhoff S, Patel A, Podila L, Plise E, Rajaraman G, Salphati L, Sands E, Taub ME, Taur JS, Weitz D, Wortelboer HM, Xia CQ, Xiao G, Yabut J, Yamagata T, Zhang L and Ellens H (2013) Variability in P-glycoprotein inhibitory potency (IC50) using various in vitro experimental systems: implications for universal digoxin drug-drug interaction risk assessment decision criteria. *Drug Metab Dispos* **41**:1347-1366.

Bi YA, Kimoto E, Sevidal S, Jones HM, Barton HA, Kempshall S, Whalen KM, Zhang H, Ji C, Fenner KS, El-Kattan AF and Lai Y (2012) In vitro evaluation of hepatic transporter-mediated clinical drug-drug interactions: hepatocyte model optimization and retrospective investigation. *Drug Metab Dispos* **40**:1085-1092.

Borlak J and Klutcka T (2004) Expression of basolateral and canalicular transporters in rat liver and cultures of primary hepatocytes. *Xenobiotica* **34**:935-947.

Bow DA, Perry JL, Miller DS, Pritchard JB and Brouwer KL (2008) Localization of P-gp (Abcb1) and Mrp2 (Abcc2) in freshly isolated rat hepatocytes. *Drug Metab Dispos* **36**:198-202.

Boyer JL, Gautam A and Graf J (1988) Mechanisms of bile secretion: insights from the isolated rat hepatocyte couplet. *Semin Liver Dis* **8**:308-316.

Broccatelli F, Cruciani G, Benet LZ and Oprea TI (2012) BDDCS class prediction for new molecular entities. *Mol Pharm* **9**:570-580.

Burczynski FJ, Fandrey S, Wang G, Pavletic PA and Gong Y (1999) Cytosolic fatty acid binding protein enhances rat hepatocyte [3H]palmitate uptake. *Can J Physiol Pharmacol* **77**:896-901.

Chandra P, Zhang P and Brouwer KL (2005) Short-term regulation of multidrug resistance-associated protein 3 in rat and human hepatocytes. *Am J Physiol Gastrointest Liver Physiol* **288**:G1252-1258.

Chang C, Ekins S, Bahadduri P and Swaan PW (2006) Pharmacophore-based discovery of ligands for drug transporters. *Advanced drug delivery reviews* **58**:1431-1450.

Chen J, Deng W, Wang J, Shao Y, Ou M and Ding M (2013) Primary bile acids as potential biomarkers for the clinical grading of intrahepatic cholestasis of pregnancy. *Int J Gynaecol Obstet* **122**:5-8.

Chu X, Korzekwa K, Elsby R, Fenner K, Galetin A, Lai Y, Matsson P, Moss A, Nagar S, Rosania GR, Bai JP, Polli JW, Sugiyama Y and Brouwer KL (2013) Intracellular drug concentrations and transporters: measurement, modeling, and implications for the liver. *Clin Pharmacol Ther* **94**:126-141.

Dawson PA, Lan T and Rao A (2009) Bile acid transporters. *J Lipid Res* **50**:2340-2357.

De Bruyn T, Chatterjee S, Fattah S, Keemink J, Nicolai J, Augustijns P and Annaert P (2013) Sandwich-cultured hepatocytes: utility for in vitro exploration of hepatobiliary drug disposition and drug-induced hepatotoxicity. *Expert Opin Drug Metab Toxicol* **9**:589-616.

De Bruyn T, Ye ZW, Peeters A, Sahi J, Baes M, Augustijns PF and Annaert PP (2011) Determination of OATP-, NTCP- and OCT-mediated substrate uptake activities in individual and pooled batches of cryopreserved human hepatocytes. *Eur J Pharm Sci* **43**:297-307.

Di L, Breen C, Chambers R, Eckley ST, Fricke R, Ghosh A, Harradine P, Kalvass JC, Ho S, Lee CA, Marathe P, Perkins EJ, Qian M, Tse S, Yan Z and Zamek-Gliszczynski MJ (2017) Industry Perspective on Contemporary Protein-Binding Methodologies: Considerations for Regulatory Drug-Drug Interaction and Related Guidelines on Highly Bound Drugs. *J Pharm Sci* **106**:3442-3452.

Dollery CT (2013) Intracellular Drug Concentrations. *Clin Pharmacol & Ther*: 93: 263–266.

Draheim V, Reichel A, Weitschies W and Moenning U (2010) N-glycosylation of ABC transporters is associated with functional activity in sandwich-cultured rat hepatocytes. *Eur J Pharm Sci* **41**:201-209.

Dunn JC, Tompkins RG and Yarmush ML (1991) Long-term in vitro function of adult hepatocytes in a collagen sandwich configuration. *Biotechnol Prog* **7**:237-245.

Dunn JC, Tompkins RG and Yarmush ML (1992) Hepatocytes in collagen sandwich: evidence for transcriptional and translational regulation. *J Cell Biol* **116**:1043-1053.

Duvvuri M and Krise JP (2005) Intracellular drug sequestration events associated with the emergence of multidrug resistance: a mechanistic review. *Front Biosci* **10**:1499-1509.

Ekins S, Ecker GF, Chiba P and Swaan PW (2007) Future directions for drug transporter modelling. *Xenobiotica* **37**:1152-1170.

El-Kattan AF, Varma MV, Steyn SJ, Scott DO, Maurer TS and Bergman A (2016) Projecting ADME Behavior and Drug-Drug Interactions in Early Discovery and Development: Application of the Extended Clearance Classification System. *Pharm Res* **33**:3021-3030.

EMA (21 June 2012) Guideline on the investigation of drug interactions. .

Falany CN, Johnson MR, Barnes S and Diasio RB (1994) Glycine and taurine conjugation of bile acids by a single enzyme. Molecular cloning and expression of human liver bile acid CoA:amino acid N-acyltransferase. *J Biol Chem* **269**:19375-19379.

Farmer JA (2001) Learning from the cerivastatin experience. *Lancet* **358**:1383-1385.

FDA/CDER US (2012) Drug interaction studies - study design, data analysis, and implications for dosing and labeling recommendations, DRAFT GUIDANCE.

FDA/CDER US (2017) In Vitro Metabolism- and Transporter- Mediated Drug-Drug Interaction Studies Guidance for Industry DRAFT GUIDANCE.

Ferslew BC, Kock K, Bridges AS and Brouwer KL (2014) Role of multidrug resistance-associated protein 4 in the basolateral efflux of hepatically derived enalaprilat. *Drug Metab Dispos* **42**:1567-1574.

Ferslew BC, Xie G, Johnston CK, Su M, Stewart PW, Jia W, Brouwer KL and Barritt ASt (2015) Altered Bile Acid Metabolome in Patients with Nonalcoholic Steatohepatitis. *Dig Dis Sci* **60**:3318-3328.

Fukuda H, Nakanishi T and Tamai I (2014) More relevant prediction for in vivo drug interaction of candesartan cilexetil on hepatic bile acid transporter BSEP using sandwich-cultured hepatocytes. *Drug Metab Pharmacokinet* **29**:94-96.

Fukuda H, Ohashi R, Tsuda-Tsukimoto M and Tamai I (2008) Effect of plasma protein binding on in vitro-in vivo correlation of biliary excretion of drugs evaluated by sandwich-cultured rat hepatocytes. *Drug Metab Dispos* **36**:1275-1282.

Garcia-Canaveras JC, Donato MT, Castell JV and Lahoz A (2012) Targeted profiling of circulating and hepatic bile acids in human, mouse, and rat using a UPLC-MRM-MS-validated method. *J Lipid Res* **53**:2231-2241.

Gardiner P and Paine SW (2011) The impact of hepatic uptake on the pharmacokinetics of organic anions. *Drug Metab Dispos* **39**:1930-1938.

Generaux CN, Ainslie GR, Bridges AS, Ismail MA, Boykin DW, Tidwell RR, Thakker DR and Paine MF (2013) Compartmental and enzyme kinetic modeling to elucidate the biotransformation pathway of a centrally acting antitrypanosomal prodrug. *Drug Metab Dispos* **41**:518-528.

Ghibellini G, Vasist LS, Leslie EM, Heizer WD, Kowalsky RJ, Calvo BF and Brouwer KL (2007) In vitro-in vivo correlation of hepatobiliary drug clearance in humans. *Clin Pharmacol Ther* **81**:406-413.

Giacomini KM and Huang SM (2013) Transporters in drug development and clinical pharmacology. *Clin Pharmacol Ther* **94**:3-9.

Giacomini KM, Huang SM, Tweedie DJ, Benet LZ, Brouwer KL, Chu X, Dahlin A, Evers R, Fischer V, Hillgren KM, Hoffmaster KA, Ishikawa T, Keppler D, Kim RB, Lee CA, Niemi M, Polli JW, Sugiyama Y, Swaan PW, Ware JA, Wright SH, Yee SW, Zamek-Gliszczynski MJ and Zhang L (2010) Membrane transporters in drug development. *Nat Rev Drug Discov* **9**:215-236.

Giri N, Agarwal S, Shaik N, Pan G, Chen Y and Elmquist WF (2009) Substrate-dependent breast cancer resistance protein (Bcrp1/Abcg2)-mediated interactions: consideration of multiple binding sites in in vitro assay design. *Drug Metab Dispos* **37**:560-570.

Godoy P, Hewitt NJ, Albrecht U, Andersen ME, Ansari N, Bhattacharya S, Bode JG, Bolleyn J, Borner C, Bottger J, Braeuning A, Budinsky RA, Burkhardt B, Cameron NR, Camussi G, Cho CS, Choi YJ, Craig Rowlands J, Dahmen U, Damm G, Dirsch O, Donato MT, Dong J, Dooley S, Drasdo D, Eakins R, Ferreira KS, Fonsato V, Fraczek J, Gebhardt R, Gibson A, Glanemann M, Goldring CE, Gomez-Lechon MJ, Groothuis GM, Gustavsson L, Guyot C, Hallifax D, Hammad S, Hayward A, Haussinger D, Hellerbrand C, Hewitt P, Hoehme S, Holzhutter HG, Houston JB, Hrach J, Ito K, Jaeschke H, Keitel V, Kelm JM, Kevin Park B, Kordes C, Kullak-Ublick GA, LeCluyse EL, Lu P, Luebke-Wheeler J, Lutz A, Maltman DJ, Matz-Soja M, McMullen P, Merfort I, Messner S, Meyer C, Mwinyi J, Naisbitt DJ, Nussler AK, Olinga P, Pampaloni F, Pi J, Pluta L, Przyborski SA, Ramachandran A, Rogiers V, Rowe C, Schelcher C, Schmich K, Schwarz M, Singh B, Stelzer EH, Stieger B, Stober R, Sugiyama Y, Tetta C, Thasler WE, Vanhaecke T, Vinken M, Weiss TS, Widera A, Woods CG, Xu JJ, Yarborough KM and Hengstler JG (2013) Recent advances in 2D and 3D in vitro systems using primary hepatocytes, alternative hepatocyte sources and non-parenchymal liver cells and their use in investigating mechanisms of hepatotoxicity, cell signaling and ADME. *Arch Toxicol* **87**:1315-1530.

Guo C, Yang K, Brouwer KR, St Claire RL, 3rd and Brouwer KL (2016) Prediction of Altered Bile Acid Disposition Due to Inhibition of Multiple Transporters: An Integrated Approach Using Sandwich-Cultured Hepatocytes, Mechanistic Modeling, and Simulation. *J Pharmacol Exp Ther* **358**:324-333.

Guo C, Yang K, Liao M, Xia CQ, Brouwer KR and Brouwer KLR (2017) Prediction of Hepatic Efflux Transporter-Mediated Drug Interactions: When Is it Optimal to Measure Intracellular Unbound Fraction of Inhibitors? *J Pharm Sci* **106**:2401-2406.

Halilbasic E, Claudel T and Trauner M (2013) Bile acid transporters and regulatory nuclear receptors in the liver and beyond. *J Hepatol* **58**:155-168.

Harwood MD, Achour B, Neuhoff S, Russell MR, Carlson G, Warhurst G and Rostami-Hodjegan A (2016) In Vitro-In Vivo Extrapolation Scaling Factors for Intestinal P-glycoprotein and Breast Cancer Resistance Protein: Part II. The Impact of Cross-Laboratory Variations of Intestinal Transporter Relative Expression Factors on Predicted Drug Disposition. *Drug Metab Dispos* **44**:476-480.

Hoffmaster KA, Turncliff RZ, LeCluyse EL, Kim RB, Meier PJ and Brouwer KL (2004) P-glycoprotein expression, localization, and function in sandwich-cultured primary rat and human hepatocytes: relevance to the hepatobiliary disposition of a model opioid peptide. *Pharm Res* **21**:1294-1302.

Hofmann AF (1999) Bile Acids: The Good, the Bad, and the Ugly. *News Physiol Sci* **14**:24-29.

Houston JB (1994) Utility of in vitro drug metabolism data in predicting in vivo metabolic clearance. *Biochem Pharmacol* **47**:1469-1479.

Izumi S, Nozaki Y, Komori T, Maeda K, Takenaka O, Kusano K, Yoshimura T, Kusuhara H and Sugiyama Y (2013) Substrate-dependent inhibition of organic anion transporting polypeptide 1B1: comparative analysis with prototypical probe substrates estradiol-17beta-glucuronide, estrone-3-sulfate, and sulfobromophthalein. *Drug Metab Dispos* **41**:1859-1866.

Jackson JP, Freeman KM, Friley WW, St Claire RL, 3rd and Brouwer KR (2016) Basolateral Efflux Transporters: A Potentially Important Pathway for the Prevention of Cholestatic Hepatotoxicity. *Appl In Vitro Toxicol* **2**:207-216.

Jackson JP, Kabirov KK, Kapetanovic IM and Lyubimov A (2009) In vitro assessment of P450 induction potential of novel chemopreventive agents SR13668, 9-cis-UAB30, and pentamethychromanol in primary cultures of human hepatocytes. *Chem Biol Interact* **179**:263-272.

Jacobsen JK, Jensen B, Skonberg C, Hansen SH and Badolo L (2011) Time-course activities of Oct1, Mrp3, and cytochrome P450s in cultures of cryopreserved rat hepatocytes. *Eur J Pharm Sci* **44**:427-436.

Jamei M, Bajot F, Neuhoff S, Barter Z, Yang J, Rostami-Hodjegan A and Rowland-Yeo K (2014) A mechanistic framework for in vitro-in vivo extrapolation of liver membrane transporters: prediction of drug-drug interaction between rosuvastatin and cyclosporine. *Clin Pharmacokinet* **53**:73-87.

Jamei M, Marciniak S, Feng K, Barnett A, Tucker G and Rostami-Hodjegan A (2009) The Simcyp population-based ADME simulator. *Expert Opin Drug Metab Toxicol* **5**:211-223.

Jansen PL and Muller M (2000) Genetic cholestasis: lessons from the molecular physiology of bile formation. *Can J Gastroenterol* **14**:233-238.

Jones HM, Barton HA, Lai Y, Bi YA, Kimoto E, Kempshall S, Tate SC, El-Kattan A, Houston JB, Galetin A and Fenner KS (2012) Mechanistic pharmacokinetic modeling for the prediction of transporter-mediated disposition in humans from sandwich culture human hepatocyte data. *Drug Metab Dispos* **40**:1007-1017.

Jones HM, Mayawala K and Poulin P (2013) Dose selection based on physiologically based pharmacokinetic (PBPK) approaches. *The AAPS journal* **15**:377-387.

Kaufmann AM and Krise JP (2007) Lysosomal sequestration of amine-containing drugs: analysis and therapeutic implications. *J Pharm Sci* **96**:729-746.

Keppler D (2011) Cholestasis and the role of basolateral efflux pumps. *Z Gastroenterol* **49**:1553-1557.

Kimoto E, Bi YA, Kosa RE, Tremaine LM and Varma MVS (2017) Hepatobiliary Clearance Prediction: Species Scaling From Monkey, Dog, and Rat, and In Vitro-In Vivo Extrapolation of Sandwich-Cultured Human Hepatocytes Using 17 Drugs. *J Pharm Sci* **106**:2795-2804.

Kimoto E, Yoshida K, Balogh LM, Bi YA, Maeda K, El-Kattan A, Sugiyama Y and Lai Y (2012) Characterization of organic anion transporting polypeptide (OATP) expression and its functional contribution to the uptake of substrates in human hepatocytes. *Mol Pharm* **9**:3535-3542.

Kishimoto W, Ishiguro N, Ludwig-Schwellinger E, Ebner T, Maeda K and Sugiyama Y (2016) Usefulness of A Model-Based Approach for Estimating In Vitro P-Glycoprotein Inhibition Potency in a Transcellular Transport Assay. *J Pharm Sci* **105**:891-896.

Kock K, Ferslew BC, Netterberg I, Yang K, Urban TJ, Swaan PW, Stewart PW and Brouwer KL (2014) Risk factors for development of cholestatic drug-induced liver injury: inhibition of hepatic basolateral bile acid transporters multidrug resistance-associated proteins 3 and 4. *Drug Metab Dispos* **42**:665-674.

Kosters A and Karpen SJ (2008) Bile acid transporters in health and disease. *Xenobiotica* **38**:1043.

Kotani N, Maeda K, Watanabe T, Hiramatsu M, Gong LK, Bi YA, Takezawa T, Kusuhara H and Sugiyama Y (2011) Culture period-dependent changes in the uptake of transporter substrates in sandwich-cultured rat and human hepatocytes. *Drug Metab Dispos* **39**:1503-1510.

Kruglov EA, Gautam S, Guerra MT and Nathanson MH (2011) Type 2 inositol 1,4,5-trisphosphate receptor modulates bile salt export pump activity in rat hepatocytes. *Hepatology* **54**:1790-1799.

Lai Y (2013) 9 - Transporter study methodologies, in *Transporters in Drug Discovery and Development* pp 675-718, Woodhead Publishing.

LeCluyse EL, Audus KL and Hochman JH (1994) Formation of extensive canalicular networks by rat hepatocytes cultured in collagen-sandwich configuration. *Am J Physiol* **266**:C1764-1774.

Lee CA, Kalvass JC, Galetin A and Zamek-Gliszczynski MJ (2014) ITC commentary on the prediction of digoxin clinical drug-drug interactions from in vitro transporter assays. *Clin Pharmacol Ther* **96**:298-301.

Lee H, Zhang Y, Lee FY, Nelson SF, Gonzalez FJ and Edwards PA (2006) FXR regulates organic solute transporters alpha and beta in the adrenal gland, kidney, and intestine. *J Lipid Res* **47**:201-214.

Lee JK, Leslie EM, Zamek-Gliszczynski MJ and Brouwer KL (2008) Modulation of trabectedin (ET-743) hepatobiliary disposition by multidrug resistance-associated proteins (Mrps) may prevent hepatotoxicity. *Toxicol Appl Pharmacol* **228**:17-23.

Lee JK, Marion TL, Abe K, Lim C, Pollock GM and Brouwer KL (2010) Hepatobiliary disposition of troglitazone and metabolites in rat and human sandwich-cultured hepatocytes: use of Monte Carlo simulations to assess the impact of changes in biliary excretion on troglitazone sulfate accumulation. *J Pharmacol Exp Ther* **332**:26-34.

Lepist EI, Gillies H, Smith W, Hao J, Hubert C, St Claire RL, 3rd, Brouwer KR and Ray AS (2014) Evaluation of the endothelin receptor antagonists ambrisentan, bosentan, macitentan, and sitaxsentan as hepatobiliary transporter inhibitors and substrates in sandwich-cultured human hepatocytes. *PLoS One* **9**:e87548.

Leslie EM, Watkins PB, Kim RB and Brouwer KL (2007) Differential inhibition of rat and human Na+-dependent taurocholate cotransporting polypeptide (NTCP/SLC10A1)by bosentan: a mechanism for species differences in hepatotoxicity. *J Pharmacol Exp Ther* **321**:1170-1178.

Levi AJ and Arias IM (1969) Two hepatic cytoplasmic protein fractions, Y and Z, and their possible role in the hepatic uptake of bilirubin, sulfobromophthalein, and other anions. *J Clin Invest* **48**:2156-2167.

Li N, Bi YA, Duignan DB and Lai Y (2009) Quantitative expression profile of hepatobiliary transporters in sandwich cultured rat and human hepatocytes. *Mol Pharm* **6**:1180-1189.

Li N, Singh P, Mandrell KM and Lai Y (2010) Improved extrapolation of hepatobiliary clearance from in vitro sandwich cultured rat hepatocytes through absolute quantification of hepatobiliary transporters. *Mol Pharm* **7**:630-641.

Li R, Barton HA and Varma MV (2014a) Prediction of pharmacokinetics and drug-drug interactions when hepatic transporters are involved. *Clin Pharmacokinet* **53**:659-678.

Li R, Ghosh A, Maurer TS, Kimoto E and Barton HA (2014b) Physiologically based pharmacokinetic prediction of telmisartan in human. *Drug Metab Dispos* **42**:1646-1655.

Li R, Barton HA, Yates PD, Ghosh A, Wolford AC, Riccardi KA and Maurer TS (2014c) A "middle-out" approach to human pharmacokinetic predictions for OATP substrates using physiologically-based pharmacokinetic modeling. *J Pharmacokinet Pharmacodyn* **41**:197-209.

Liu X, Brouwer KL, Gan LS, Brouwer KR, Stieger B, Meier PJ, Audus KL and LeCluyse EL (1998) Partial maintenance of taurocholate uptake by adult rat hepatocytes cultured in a collagen sandwich configuration. *Pharm Res* **15**:1533-1539.

Liu X, Chism JP, LeCluyse EL, Brouwer KR and Brouwer KL (1999a) Correlation of biliary excretion in sandwich-cultured rat hepatocytes and in vivo in rats. *Drug Metab Dispos* **27**:637-644.

Liu X, LeCluyse EL, Brouwer KR, Lightfoot RM, Lee JI and Brouwer KL (1999b) Use of Ca2+ modulation to evaluate biliary excretion in sandwich-cultured rat hepatocytes. *J Pharmacol Exp Ther* **289**:1592-1599.

Liu X, Wright M and Hop CE (2014) Rational use of plasma protein and tissue binding data in drug design. *J Med Chem* **57**:8238-8248.

Martin C, Berridge G, Higgins CF, Mistry P, Charlton P and Callaghan R (2000) Communication between multiple drug binding sites on P-glycoprotein. *Mol Pharmacol* **58**:624-632.

Mateus A, Matsson P and Artursson P (2013) Rapid measurement of intracellular unbound drug concentrations. *Mol Pharm* **10**:2467-2478.

Matsunaga N, Suzuki K, Nakanishi T, Ogawa M, Imawaka H and Tamai I (2015) Modeling approach for multiple transporters-mediated drug-drug interactions in sandwich-cultured human hepatocytes: effect of cyclosporin A on hepatic disposition of mycophenolic acid phenyl-glucuronide. *Drug Metab Pharmacokinet* **30**:142-148.

Matsunaga N, Wada S, Nakanishi T, Ikenaga M, Ogawa M and Tamai I (2014) Mathematical modeling of the in vitro hepatic disposition of mycophenolic acid and its glucuronide in sandwich-cultured human hepatocytes. *Mol Pharm* **11**:568-579.

Meng Q, Chen X, Wang C, Liu Q, Sun H, Sun P, Huo X, Liu Z, Yao J and Liu K (2015) Protective Effects of Alisol B 23-Acetate Via Farnesoid X Receptor-Mediated Regulation of Transporters and Enzymes in Estrogen-Induced Cholestatic Liver Injury in Mice. *Pharm Res* **32**:3688-3698.

Mohamed LA and Kaddoumi A (2013) In vitro investigation of amyloid-beta hepatobiliary disposition in sandwich-cultured primary rat hepatocytes. *Drug Metab Dispos* **41**:1787-1796.

Mohamed LA and Kaddoumi A (2014) Tacrine sinusoidal uptake and biliary excretion in sandwich-cultured primary rat hepatocytes. *J Pharm Pharm Sci* **17**:427-438.

Morgan RE, van Staden CJ, Chen Y, Kalyanaraman N, Kalanzi J, Dunn RT, 2nd, Afshari CA and Hamadeh HK (2013) A multifactorial approach to hepatobiliary transporter assessment enables improved therapeutic compound development. *Toxicol Sci* **136**:216-241.

Nakakariya M, Ono M, Amano N, Moriwaki T, Maeda K and Sugiyama Y (2012) In vivo biliary clearance should be predicted by intrinsic biliary clearance in sandwich-cultured hepatocytes. *Drug Metab Dispos* **40**:602-609.

Nakanishi T, Ikenaga M, Fukuda H, Matsunaga N and Tamai I (2012) Application of quantitative time-lapse imaging (QTLI) for evaluation of Mrp2-based drug-drug interaction induced by liver metabolites. *Toxicol Appl Pharmacol* **263**:244-250.

Neuvonen PJ, Niemi M and Backman JT (2006) Drug interactions with lipid-lowering drugs: mechanisms and clinical relevance. *Clin Pharmacol Ther* **80**:565-581.

Noe J, Portmann R, Brun ME and Funk C (2007) Substrate-dependent drug-drug interactions between gemfibrozil, fluvastatin and other organic anion-transporting peptide (OATP) substrates on OATP1B1, OATP2B1, and OATP1B3. *Drug Metab Dispos* **35**:1308-1314.

Noel G, Le Vee M, Moreau A, Stieger B, Parmentier Y and Fardel O (2013) Functional expression and regulation of drug transporters in monolayer- and sandwich-cultured mouse hepatocytes. *Eur J Pharm Sci* **49**:39-50.

Norlin M and Wikvall K (2007) Enzymes in the conversion of cholesterol into bile acids. *Curr Mol Med* **7**:199-218.

Oshio C and Phillips MJ (1981) Contractility of bile canaliculi: implications for liver function. *Science* **212**:1041-1042.

Pan G, Boiselle C and Wang J (2012) Assessment of biliary clearance in early drug discovery using sandwich-cultured hepatocyte model. *J Pharm Sci* **101**:1898-1908.

Pan Y, Hsu V, Grimstein M, Zhang L, Arya V, Sinha V, Grillo JA and Zhao P (2016) The Application of Physiologically Based Pharmacokinetic Modeling to Predict the Role of Drug Transporters: Scientific and Regulatory Perspectives. *J Clin Pharmacol* **56 Suppl 7**:S122-131.

Park SW, Schonhoff CM, Webster CR and Anwer MS (2012) Protein kinase Cdelta differentially regulates cAMP-dependent translocation of NTCP and MRP2 to the plasma membrane. *Am J Physiol Gastrointest Liver Physiol* **303**:G657-665.

Paulusma CC, de Waart DR, Kunne C, Mok KS and Elferink RP (2009) Activity of the bile salt export pump (ABCB11) is critically dependent on canalicular membrane cholesterol content. *J Biol Chem* **284**:9947-9954.

Pfeifer ND, Goss SL, Swift B, Ghibellini G, Ivanovic M, Heizer WD, Gangarosa LM and Brouwer KL (2013a) Effect of Ritonavir on (99m)Technetium-Mebrofenin Disposition in Humans: A Semi-PBPK Modeling and In Vitro Approach to Predict Transporter-Mediated DDIs. *CPT: pharmacometrics & systems pharmacology* **2**:e20.

Pfeifer ND, Harris KB, Yan GZ and Brouwer KL (2013b) Determination of intracellular unbound concentrations and subcellular localization of drugs in rat sandwich-cultured hepatocytes compared with liver tissue. *Drug Metab Dispos* **41**:1949-1956.

Pfeifer ND, Yang K and Brouwer KL (2013c) Hepatic basolateral efflux contributes significantly to rosuvastatin disposition I: characterization of basolateral versus biliary clearance using a novel protocol in sandwich-cultured hepatocytes. *J Pharmacol Exp Ther* **347**:727-736.

Phillips MJ, Oshio C, Miyairi M, Katz H and Smith CR (1982) A study of bile canalicular contractions in isolated hepatocytes. *Hepatology* **2**:763-768.

Poulin P and Haddad S (2013) Toward a new paradigm for the efficient in vitro-in vivo extrapolation of metabolic clearance in humans from hepatocyte data. *J Pharm Sci* **102**:3239-3251.

Powell J, Farasyn T, Kock K, Meng X, Pahwa S, Brouwer KL and Yue W (2014) Novel mechanism of impaired function of organic anion-transporting polypeptide 1B3 in human hepatocytes: post-translational regulation of OATP1B3 by protein kinase C activation. *Drug Metab Dispos* **42**:1964-1970.

Riede J, Camenisch G, Huwyler J and Poller B (2017) Current in vitro Methods to Determine Hepatic Kpuu: a Comparison of Their Usefulness and Limitations. *J Pharm Sci*.

Ring B, Wrighton SA and Mohutsky M (2014) Reversible Mechanisms of Enzyme Inhibition and Resulting Clinical Significance, in Enzyme Kinetics in Drug Metabolism: Fundamentals and Applications (Nagar S, Argikar U, Tweedie D eds) *NY, Humana Press* **1113**:37-56.

Roggenbeck BA, Carew MW, Charrois GJ, Douglas DN, Kneteman NM, Lu X, Le XC and Leslie EM (2015) Characterization of arsenic hepatobiliary transport using sandwich-cultured human hepatocytes. *Toxicol Sci* **145**:307-320.

Sakamoto A, Matsumaru T, Yamamura N, Suzuki S, Uchida Y, Tachikawa M and Terasaki T (2015) Drug Transporter Protein Quantification of Immortalized Human Lung Cell Lines Derived from Tracheobronchial Epithelial Cells (Calu-3 and BEAS2-B), Bronchiolar-Alveolar Cells (NCI-H292 and NCI-H441), and Alveolar Type II-like Cells (A549) by Liquid Chromatography-Tandem Mass Spectrometry. *J Pharm Sci* **104**:3029-3038.

Sakamoto A, Matsumaru T, Yamamura N, Uchida Y, Tachikawa M, Ohtsuki S and Terasaki T (2013) Quantitative expression of human drug transporter proteins in lung tissues: analysis of regional, gender, and interindividual differences by liquid chromatography-tandem mass spectrometry. *J Pharm Sci* **102**:3395-3406.

Schmidt S, Gonzalez D and Derendorf H (2010) Significance of protein binding in pharmacokinetics and pharmacodynamics. *J Pharm Sci* **99**:1107-1122.

Sharma S, Ellis EC, Gramignoli R, Dorko K, Tahan V, Hansel M, Mattison DR, Caritis SN, Hines RN, Venkataramanan R and Strom SC (2013) Hepatobiliary disposition of 17-OHPC and taurocholate in fetal human hepatocytes: a comparison with adult human hepatocytes. *Drug Metab Dispos* **41**:296-304.

Shawahna R, Uchida Y, Decleves X, Ohtsuki S, Yousif S, Dauchy S, Jacob A, Chassoux F, Daumas-Duport C, Couraud PO, Terasaki T and Scherrmann JM (2011) Transcriptomic and quantitative proteomic analysis of transporters and drug metabolizing enzymes in freshly isolated human brain microvessels. *Mol Pharm* **8**:1332-1341.

Shen G, Zhuang X, Xiao W, Kong L, Tan Y and Li H (2014) Role of CYP3A in regulating hepatic clearance and hepatotoxicity of triptolide in rat liver microsomes and sandwich-cultured hepatocytes. *Food Chem Toxicol* **71**:90-96.

Sheng J, Tian X, Xu G, Wu Z, Chen C, Wang L, Pan L, Huang C and Pan G (2015) The hepatobiliary disposition of timosaponin b2 is highly dependent on influx/efflux transporters but not metabolism. *Drug Metab Dispos* **43**:63-72.

Shirasaka Y, Mori T, Murata Y, Nakanishi T and Tamai I (2014) Substrate- and dose-dependent drug interactions with grapefruit juice caused by multiple binding sites on OATP2B1. *Pharm Res* **31**:2035-2043.

Shirasaka Y, Sakane T and Yamashita S (2008) Effect of P-glycoprotein expression levels on the concentration-dependent permeability of drugs to the cell membrane. *J Pharm Sci* **97**:553-565.

Shitara Y, Maeda K, Ikejiri K, Yoshida K, Horie T and Sugiyama Y (2013) Clinical significance of organic anion transporting polypeptides (OATPs) in drug disposition: their roles in hepatic clearance and intestinal absorption. *Biopharm Drug Dispos* **34**:45-78.

Shitara Y, Nagamatsu Y, Wada S, Sugiyama Y and Horie T (2009) Long-lasting inhibition of the transporter-mediated hepatic uptake of sulfobromophthalein by cyclosporin a in rats. *Drug Metab Dispos* **37**:1172-1178.

Shugarts S and Benet LZ (2009) The role of transporters in the pharmacokinetics of orally administered drugs. *Pharm Res* **26**:2039-2054.

Soroka CJ, Ballatori N and Boyer JL (2010) Organic solute transporter, OSTalpha-OSTbeta: its role in bile acid transport and cholestasis. *Semin Liver Dis* **30**:178-185.

Sterz K, Mollmann L, Jacobs A, Baumert D and Wiese M (2009) Activators of P-glycoprotein: Structure-activity relationships and investigation of their mode of action. *ChemMedChem* **4**:1897-1911.

Stieger B (2011) The role of the sodium-taurocholate cotransporting polypeptide (NTCP) and of the bile salt export pump (BSEP) in physiology and pathophysiology of bile formation. *Handb Exp Pharmacol*:205-259.

Stieger B, Meier Y and Meier PJ (2007) The bile salt export pump. *Pflugers Arch* **453**:611-620.

Swift B, Pfeifer ND and Brouwer KL (2010) Sandwich-cultured hepatocytes: an in vitro model to evaluate hepatobiliary transporter-based drug interactions and hepatotoxicity. *Drug Metab Rev* **42**:446-471.

Tachibana T, Kitamura S, Kato M, Mitsui T, Shirasaka Y, Yamashita S and Sugiyama Y (2010) Model analysis of the concentration-dependent permeability of P-gp substrates. *Pharm Res* **27**:442-446.

Tchaparian EH, Houghton JS, Uyeda C, Grillo MP and Jin L (2011) Effect of culture time on the basal expression levels of drug transporters in sandwich-cultured primary rat hepatocytes. *Drug Metab Dispos* **39**:2387-2394.

Thompson CG, Fallon JK, Mathews M, Charlins P, Remling-Mulder L, Kovarova M, Adamson L, Srinivas N, Schauer A, Sykes C, Luciw P, Garcia JV, Akkina R, Smith PC and Kashuba ADM (2017) Multimodal analysis of drug transporter expression in gastrointestinal tissue. *AIDS* **31**:1669-1678.

Treiber A, Aanismaa P, de Kanter R, Delahaye S, Treher M, Hess P and Sidharta P (2014) Macitentan does not interfere with hepatic bile salt transport. *J Pharmacol Exp Ther* **350**:130-143.

Treijtel N, Barendregt A, Freidig AP, Blaauboer BJ and van Eijkeren JC (2004) Modeling the in vitro intrinsic clearance of the slowly metabolized compound tolbutamide determined in sandwich-cultured rat hepatocytes. *Drug Metab Dispos* **32**:884-891.

Treijtel N, van Helvoort H, Barendregt A, Blaauboer BJ and van Eijkeren JC (2005) The use of sandwich-cultured rat hepatocytes to determine the intrinsic clearance of compounds with different extraction ratios: 7-ethoxycoumarin and warfarin. *Drug Metab Dispos* **33**:1325-1332.

Trottier J, Caron P, Straka RJ and Barbier O (2011) Profile of serum bile acids in noncholestatic volunteers: gender-related differences in response to fenofibrate. *Clin Pharmacol Ther* **90**:279-286.

Turncliff RZ, Meier PJ and Brouwer KL (2004) Effect of dexamethasone treatment on the expression and function of transport proteins in sandwich-cultured rat hepatocytes. *Drug Metab Dispos* **32**:834-839.

Uchida Y, Tachikawa M, Obuchi W, Hoshi Y, Tomioka Y, Ohtsuki S and Terasaki T (2013) A study protocol for quantitative targeted absolute proteomics (QTAP) by LC-MS/MS: application for inter-strain differences in protein expression levels of transporters, receptors, claudin-5, and marker proteins at the blood-brain barrier in ddY, FVB, and C57BL/6J mice. *Fluids and barriers of the CNS* **10**:21.

Vaidyanathan J, Yoshida K, Arya V and Zhang L (2016) Comparing Various In Vitro Prediction Criteria to Assess the Potential of a New Molecular Entity to Inhibit Organic Anion Transporting Polypeptide 1B1. *J Clin Pharmacol* **56 Suppl 7**:S59-72.

Vallejo M, Briz O, Serrano MA, Monte MJ and Marin JJ (2006) Potential role of trans-inhibition of the bile salt export pump by progesterone metabolites in the etiopathogenesis of intrahepatic cholestasis of pregnancy. *J Hepatol* **44**:1150-1157.

Varma MV and El-Kattan AF (2016) Transporter-Enzyme Interplay: Deconvoluting Effects of Hepatic Transporters and Enzymes on Drug Disposition Using Static and Dynamic Mechanistic Models. *J Clin Pharmacol* **56 Suppl 7**:S99-s109.

Varma MV, El-Kattan AF, Feng B, Steyn SJ, Maurer TS, Scott DO, Rodrigues AD and Tremaine LM (2016) Extended Clearance Classification System (ECCS) informed approach for evaluating investigational drugs as substrates of drug transporters. *Clin Pharmacol Ther*.

Varma MV, Lai Y, Feng B, Litchfield J, Goosen TC and Bergman A (2012) Physiologically based modeling of pravastatin transporter-mediated hepatobiliary disposition and drug-drug interactions. *Pharm Res* **29**:2860-2873.

Varma MV, Lai Y, Kimoto E, Goosen TC, El-Kattan AF and Kumar V (2013a) Mechanistic modeling to predict the transporter- and enzyme-mediated drug-drug interactions of repaglinide. *Pharm Res* **30**:1188-1199.

Varma MV, Lin J, Bi YA, Rotter CJ, Fahmi OA, Lam J, El-Kattan AF, Goosen TC and Lai Y (2013b) Quantitative Prediction of Repaglinide-Rifampicin Complex Drug Interactions Using Dynamic and Static Mechanistic Models: Delineating Differential CYP3A4 Induction and OATP1B1 Inhibition Potential of Rifampicin. *Drug Metab Dispos*. **41**: 966-974

Varma MV, Scialis RJ, Lin J, Bi YA, Rotter CJ, Goosen TC and Yang X (2014) Mechanism-based pharmacokinetic modeling to evaluate transporter-enzyme interplay in drug interactions and pharmacogenetics of glyburide. *The AAPS journal* **16**:736-748.

Vavricka SR, Van Montfoort J, Ha HR, Meier PJ and Fattinger K (2002) Interactions of rifamycin SV and rifampicin with organic anion uptake systems of human liver. *Hepatology* **36**:164-172.

Vildhede A, Wisniewski JR, Noren A, Karlgren M and Artursson P (2015) Comparative Proteomic Analysis of Human Liver Tissue and Isolated Hepatocytes with a Focus on Proteins Determining Drug Exposure. *J Proteome Res* **14**:3305-3314.

Wagner M, Zollner G and Trauner M (2010) Nuclear receptor regulation of the adaptive response of bile acid transporters in cholestasis. *Semin Liver Dis* **30**:160-177.

Webborn PJ, Parker AJ, Denton RL and Riley RJ (2007) In vitro-in vivo extrapolation of hepatic clearance involving active uptake: theoretical and experimental aspects. *Xenobiotica* **37**:1090-1109.

Wilkinson GR (1987) Clearance approaches in pharmacology. *Pharmacol Rev* **39**:1-47.

Williamson B, Dooley KE, Zhang Y, Back DJ and Owen A (2013a) Induction of influx and efflux transporters and cytochrome P450 3A4 in primary human hepatocytes by rifampin, rifabutin, and rifapentine. *Antimicrob Agents Chemother* **57**:6366-6369.

Williamson B, Soars AC, Owen A, White P, Riley RJ and Soars MG (2013b) Dissecting the relative contribution of OATP1B1-mediated uptake of xenobiotics into human hepatocytes using siRNA. *Xenobiotica* **43**:920-931.

Woodhead JL, Yang K, Siler SQ, Watkins PB, Brouwer KLR, Barton HA and BA H (2014) Exploring BSEP inhibition-mediated toxicity with a mechanistic model of drug-induced liver injury. *Front Pharmacol* **5**.

Xie G, Zhong W, Li H, Li Q, Qiu Y, Zheng X, Chen H, Zhao X, Zhang S, Zhou Z, Zeisel SH and Jia W (2013) Alteration of bile acid metabolism in the rat induced by chronic ethanol consumption. *FASEB J* **27**:3583-3593.

Yabe Y, Galetin A and Houston JB (2011) Kinetic characterization of rat hepatic uptake of 16 actively transported drugs. *Drug Metab Dispos* **39**:1808-1814.

Yan GZ, Generaux CN, Yoon M, Goldsmith RB, Tidwell RR, Hall JE, Olson CA, Clewell HJ, Brouwer KL and Paine MF (2012) A semiphysiologically based pharmacokinetic modeling approach to predict the dose-exposure relationship of an antiparasitic prodrug/active metabolite pair. *Drug Metab Dispos* **40**:6-17.

Yang K, Pfeifer ND, Hardwick RN, Yue W, Stewart PW and Brouwer KL (2014a) An experimental approach to evaluate the impact of impaired transport function on hepatobiliary drug disposition using Mrp2-deficient TR- rat sandwich-cultured hepatocytes in combination with Bcrp knockdown. *Mol Pharm* **11**:766-775.

Yang K, Pfeifer ND, Kock K and Brouwer KL (2015) Species differences in hepatobiliary disposition of taurocholic acid in human and rat sandwich-cultured hepatocytes: implications for drug-induced liver injury. *The Journal of pharmacology and experimental therapeutics* **353**:415-423.

Yang K, Woodhead JL, Watkins PB, Howell BA and Brouwer KL (2014b) Systems pharmacology modeling predicts delayed presentation and species differences in bile acid-mediated troglitazone hepatotoxicity. *Clin Pharmacol Ther* **96**:589-598.

Yanni SB, Augustijns PF, Benjamin DK, Jr., Brouwer KL, Thakker DR and Annaert PP (2010) In vitro investigation of the hepatobiliary disposition mechanisms of the antifungal agent micafungin in humans and rats. *Drug Metab Dispos* **38**:1848-1856.

Yue W, Abe K and Brouwer KL (2009) Knocking down breast cancer resistance protein (Bcrp) by adenoviral vector-mediated RNA interference (RNAi) in sandwich-cultured rat hepatocytes: a novel tool to assess the contribution of Bcrp to drug biliary excretion. *Mol Pharm* **6**:134-143.

Yue W, Lee JK, Abe K, Sugiyama Y and Brouwer KL (2011) Decreased hepatic breast cancer resistance protein expression and function in multidrug resistance-associated protein 2-deficient (TR(-)) rats. *Drug Metab Dispos* **39**:441-447.

Zamek-Gliszczynski MJ, Bedwell DW, Bao JQ and Higgins JW (2012) Characterization of SAGE Mdr1a (P-gp), Bcrp, and Mrp2 knockout rats using loperamide, paclitaxel, sulfasalazine, and carboxydichlorofluorescein pharmacokinetics. *Drug Metab Dispos* **40**:1825-1833.

Zhang M and Chiang JY (2001) Transcriptional regulation of the human sterol 12alpha-hydroxylase gene (CYP8B1): roles of heaptocyte nuclear factor 4alpha in mediating bile acid repression. *J Biol Chem* **276**:41690-41699.

Zhang P, Tian X, Chandra P and Brouwer KL (2005) Role of glycosylation in trafficking of Mrp2 in sandwich-cultured rat hepatocytes. *Mol Pharmacol* **67**:1334-1341.

Zhang Y, Jackson JP, St Claire RL, 3rd, Freeman K, Brouwer KR and Edwards JE (2017) Obeticholic acid, a selective farnesoid X receptor agonist, regulates bile acid homeostasis in sandwich-cultured human hepatocytes. *Pharmacology research & perspectives* **5**: e00329.

Zhang Z, Farooq M, Prasad B, Grepper S and Unadkat JD (2015) Prediction of gestational age-dependent induction of in vivo hepatic CYP3A activity based on HepaRG cells and human hepatocytes. *Drug Metab Dispos* **43**:836-842.

Zheng N, Tsai HN, Zhang X, Shedden K and Rosania GR (2011) The subcellular distribution of small molecules: a meta-analysis. *Mol Pharm* **8**:1611-1618.

Zheng X, Diao L, Ekins S and Polli JE (2010) Why we should be vigilant: drug cytotoxicity observed with in vitro transporter inhibition studies. *Biochem Pharmacol* **80**:1087-1092.

CHAPTER 2. Prediction of Altered Bile Acid Disposition due to Inhibition of Multiple Transporters: An Integrated Approach using Sandwich-Cultured Hepatocytes, Mechanistic Modeling and Simulation [2]

Introduction

Transporters play a critical role in the absorption, distribution, and elimination of many drugs and endogenous compounds, such as bile acids. Transporter-mediated drug-bile acid interactions may have significant toxicological implications, such as troglitazone- and bosentan-induced hepatotoxicity due to inhibition of the bile salt export pump (BSEP) (Woodhead JL et al., 2014; Yang et al., 2014). Transporter inhibition assays have been adopted by the pharmaceutical industry or included in the recent regulatory guidelines to predict drug-drug interactions (FDA/CDER, 2012). However, the static method, based on the ratio of total plasma maximum concentration (C_{max}) and 50% inhibitory concentration (IC_{50}) or inhibition constant (K_i) of the inhibitor, may not accurately predict the hepatic disposition of victim substrates. Limitations associated with the static method may explain the lack of cholestatic liability of some MRP2 and BSEP inhibitors (Dawson et al., 2012; Pfeifer et al., 2013a). To accurately translate transporter inhibition data (i.e. IC_{50} or K_i) to the prediction of hepatocellular exposure of victim substrates, a number of factors should be considered.

First, hepatic bile acid exposure is regulated by hepatic uptake transporters [e.g. sodium taurocholate co-transporting polypeptide (NTCP) and organic anion-transporting polypeptides (OATPs)], as well as canalicular (e.g. BSEP) and basolateral efflux transporters [e.g. multidrug resistance-associated protein 3 (MRP3) and MRP4]. Often, inhibitors of efflux transporters also inhibit uptake transporters, which may exert protective effects (Leslie et al., 2007). However, the static model based on inhibition data from over-expression systems considers uptake and efflux as isolated processes. To overcome this limitation, mechanistic pharmacokinetic modeling coupled with data from sandwich-cultured hepatocytes have been used to deconvolute the relative contribution of various clearance pathways to the disposition of rosuvastatin, mycophenolic acid, and ^{3}H-TCA (Pfeifer et al., 2013c; Matsunaga et al., 2014; Yang et al., 2015). Transporters are expressed and properly localized in the sandwich-cultured hepatocyte system, which can be used to assess the function of multiple transporters (Yang et al., 2016). Thus, this cellular model is uniquely suited to evaluate the interplay of multiple transport pathways and predict the net effect due to inhibition of multiple transporters on the hepatic disposition of victim substrates.

Secondly, the presence of protein in plasma is an important physiological factor. However, albumin at physiological concentrations (e.g., 4% bovine serum albumin; BSA) (Doherty et al., 2006; Wolf et al., 2008) has not been added routinely into *in vitro* experimental systems, such as membrane vesicles, to study transporter-based interactions and assess IC_{50} or K_i values. In addition, according to the "free drug hypothesis", the inhibitory effect is driven by the local unbound concentration of inhibitor, which is the cytosolic unbound inhibitor concentration ($[I]_{u,cyt}$) for efflux transporters, and the medium unbound inhibitor concentration ($[I]_{u,med}$) for uptake transporters (Smith et al., 2010). Some high-throughput methods have been used to

measure cellular total and unbound inhibitor concentrations ($[I]_{t,cell}$ and $[I]_{u,cell}$, respectively) (Mateus et al., 2013). However, the isolation of cytosol and measurement of cytosolic total and unbound inhibitor concentrations ($[I]_{t,cyt}$ and $[I]_{u,cyt}$, respectively) adds complexity (Pfeifer et al., 2013b). Thus, $[I]_{t,cyt}$ or $[I]_{u,cyt}$ has not been adopted routinely into the prediction of efflux transporter-based drug interactions. The necessity of measuring the cellular unbound fraction of inhibitor ($f_{u,cell,inhibitor}$) and/or the cytosolic unbound fraction of inhibitor ($f_{u,cyt,inhibitor}$) needs to be assessed.

The purpose of this study was to develop an integrated approach to predict altered bile acid disposition mediated by inhibition of multiple transporters in sandwich-cultured human hepatocytes (SCHH), with a focus on taurocholic acid (TCA), a prototypical bile acid. TCA is generally not metabolized and is commonly used in BSEP and NTCP assays since its transport mechanism is well characterized. First, the hepatobiliary disposition of deuterium-labeled TCA (d_8-TCA) was characterized in the presence of 4% BSA and pharmacokinetic parameters were estimated using mechanistic pharmacokinetic modeling. Total hepatocellular concentrations ($C_{t,Cells}$) were identified as the most sensitive model output according to sensitivity analysis. The effect of model inhibitors, i.e. telmisartan and bosentan, on TCA $C_{t,Cells}$ was predicted based on medium and intracellular inhibitor concentrations (i.e., $[I]_{t,cell}$, $[I]_{u,cell}$, $[I]_{t,cyt}$ and $[I]_{u,cyt}$, separately) and bile acid transporter inhibition data. The predictive performance of the model was evaluated by comparing the simulation results with experimental data and calculating the average fold error (AFE). To determine the necessity of measuring $f_{u,cell,inhibitor}$ for future studies, sensitivity analyses of $f_{u,cell,inhibitor}$ values for the model inhibitors and a set of theoretical inhibitors were performed. Based on the simulation results, a framework was proposed to help guide future study design.

Materials and Methods

Materials

All chemicals were purchased from Sigma-Aldrich (St. Louis, MO) unless otherwise stated. BioCoat[TM] cell culture plates and Matrigel® were obtained from BD Biosciences (San Jose, CA). QualGro[TM] Seeding Medium and QualGro[TM] Hepatocyte Culture Medium were obtained from Qualyst Transporter Solutions (Durham, NC). d_8-TCA, d_4-TCA (internal standard for d_8-TCA), telmisartan, d_3-telmisartan (internal standard for telmisartan), bosentan, and ambrisentan (internal standard for bosentan) were obtained from Toronto Research Chemicals (ON, Canada). OmniPur® Bovine Serum Albumin (BSA; Fraction V, Heat Shock Isolation) was purchased from Thomas Scientific (Swedesboro, NJ). Pierce bicinchoninic acid Protein Assay was obtained from Thermo Fisher Scientific Inc. (Rockford, IL) and the LDH Cytotoxicity Detection Kit was purchased from Roche Diagnostics (Indianapolis, IN).

Sandwich-Cultured Human Hepatocytes (SCHH)

B-CLEAR®-HU Transporter Certified[TM] cryopreserved human hepatocytes (Lot numbers: HUM4045, HUM4061B, and HUM4059 purchased from Triangle Research Labs, Durham, NC) were seeded in QualGro[TM] Seeding Medium at a density of $0.4{\times}10^6$ cells/well in 24-well BioCoat[TM] plates and $1.75{\times}10^6$ cells/well in 6-well BioCoat[TM] plates, and cultured in a sandwich configuration (overlaid with Matrigel®) in QualGro[TM] Hepatocyte Culture Medium as previously reported (Swift et al., 2010). Donors included one Caucasian male, one Caucasian female and one Hispanic female ranging in age from 2 to 44 years old with a body mass index ranging from 18.3 to 30.

Uptake and Efflux Studies of d8-TCA in SCHH

Uptake and efflux studies of d8-TCA were performed in SCHH as reported previously with minor modifications (Pfeifer et al., 2013c). Briefly, on day 6 of culture, SCHH seeded in 24-well plates were pre-incubated with standard (Ca^{2+}-containing) or Ca^{2+}-free (Ca^{2+}/Mg^{2+}-free buffer containing EGTA) Hanks' balanced salt solution (HBSS) for 10 min. Incubation with standard HBSS maintains the integrity of the tight junctions, while incubation with Ca^{2+}-free HBSS disrupts the tight junctions, allowing the contents in the bile canaliculi to be washed into the medium (B-CLEAR® technology, Qualyst Transporter Solutions, Durham, NC). Following pre-incubation, the uptake phase was initiated by treating the SCHH with dosing solution (1 μM d8-TCA in 0.3 mL/well standard HBSS, with 4% BSA) for up to 20 min. At the end of the uptake phase, the dosing solution was removed, and the SCHH were washed twice with standard or Ca^{2+}-free HBSS at 37°C for 1 min, and incubated with the third application of buffer for a 15-min efflux. Accumulation of d8-TCA in Cells+Bile (standard HBSS) and Cells (Ca^{2+}-free HBSS) during uptake (2, 5, 10, and 20 min) and efflux (2, 5, 10, and 15 min) phases was determined by terminal sampling of triplicate wells at each time point. During the efflux phase, incubation buffer also was collected at 2, 5, 10, and 15 min. At the end of incubation, the hepatocytes were washed with ice-cold standard HBSS three times and the samples were stored at −80 °C for future analysis.

Determination of Kinetic Parameters for d8-TCA using Mechanistic Modeling

A model scheme incorporating linear uptake and efflux clearance was adopted (Pfeifer et al., 2013c; Yang et al., 2015) and was fit to d8-TCA Cells+Bile, Cells, and incubation medium total mass-time data from three individual SCHH experiments (Fig. 2.1A). The model fitting was performed with Phoenix WinNonlin, v6.3 (Certara, St. Louis, MO) using the stiff estimation

method and a power model to account for residual error. Differential Equations 1 to 5 describe the changes in the amount of TCA in the different compartments in this model.

Mass in standard HBSS:

$$\frac{dX^+_{t,Buffer}}{dt} = CL_{BL} \times C^+_{t,Cells} + K_{Flux} \times X_{t,Bile} - CL_{Uptake} \times C^+_{t,Buffer} - K_{Wash} \times X^+_{t,Buffer} \qquad X^+_{Buffer}{}^\circ = X_{dose}$$

(1)

Mass in Ca^{2+}-free HBSS:

$$\frac{dX^-_{t,Buffer}}{dt} = (CL_{BL} + CL_{Bile}) \times C^-_{t,Cells} - CL_{Uptake} \times C^-_{t,Buffer} - K_{Wash} \times X^-_{t,Buffer} \qquad X^-_{Buffer}{}^\circ = X_{dose}$$

(2)

Mass in Cells:

$$\frac{dX^{+or-}_{t,Cells}}{dt} = CL_{Uptake} \times C^{+or-}_{t,Buffer} - (CL_{BL} + CL_{Bile}) \times C^{+or-}_{t,Cells} \qquad X^{+or-}_{Cell}{}^\circ = 0 \quad (3)$$

Mass in Bile (standard HBSS):

$$\frac{dX_{t,Bile}}{dt} = CL_{Bile} \times C^+_{t,Cells} - K_{Flux} \times X_{t,Bile} \qquad X_{Bile}{}^\circ = 0 \quad (4)$$

Mass in Cells+Bile (standard HBSS):

$$\frac{dX_{t,Cells+Bile}}{dt} = \frac{dX_{t,Bile}}{dt} + \frac{dX^+_{t,Cells}}{dt} \qquad X^\circ_{Cells+Bile} = 0 \quad (5)$$

where $C_{t,Cells}$ represents the total intracellular concentration, and was calculated as X_{Cells}/V_{Cells}; V_{Cells} was calculated and fixed using the protein content of each preparation and a value of 7.4 µL/mg protein (Pfeifer et al., 2013c; Yang et al., 2015); "+" and "-" refer to Ca^{2+}-containing (standard HBSS) and Ca^{2+}-free HBSS, respectively; $X_{t,Cells}$ represents the total amount in Cells; $X_{t,Cells+Bile}$ represents the total amount in Cells+Bile; $X_{t,Bile}$ represents the total amount in Bile; $C_{t,Buffer}$ represents the total Buffer concentration; V_{Buffer} was set as a constant (0.3 mL); CL_{Uptake} represents total uptake clearance; CL_{BL} represents total basolateral efflux clearance; CL_{Bile} represents total biliary clearance; and K_{Flux} represents the first-order rate constant that describes

the flux from bile networks into the medium due to periodic contraction of the bile canalicular

networks (Pfeifer et al., 2013c)(Oshio and Phillips, 1981; Phillips et al., 1982; Lee et al., 2010).

Clearance units (μL/min/mg protein) were converted to mL/min/g liver based on the protein

content in liver tissue (90 mg protein/g liver) (Sohlenius-Sternbeck, 2006). To represent the 1-

min wash step, K_{wash} was activated for 1min at the end of the 20-min uptake phase using an if-

then statement. K_{wash} was fixed at 1×10^4 min^{-1}, which was sufficient to eliminate the d_8-TCA

from the buffer compartment based on simulations. Initial parameter estimates were obtained

from previous reports for ^{3}H-TCA (Yang et al., 2015).

Sensitivity Analyses of Model Output

Sensitivity analyses were conducted using Berkeley-Madonna v.8.3.11 to identify the

most sensitive SCHH model output with respect to changes in clearance (CL). Different model

outputs measured in the SCHH experiment, including the (A) total concentration of TCA in Cells

($C_{t,Cells}$), (B) total amount in Cells+Bile ($X_{t,Cells+Bile}$), (C) total amount in Bile ($X_{t,Bile}$), (D) ratio of

the total amount of TCA in Cells to the total amount of TCA in Cells+Bile ($X_{t,Cells}/X_{t,Cells+Bile}$),

(E) ratio of the total amount of TCA in Bile to the total amount of TCA in Cells ($X_{t,Bile}/X_{t,Cells}$),

and (F) ratio of the total amount in Bile to the total amount in Cells+Bile ($X_{t,Bile}/X_{t,Cells+Bile}$), were

simulated throughout the time course assuming CL_{Uptake} and CL_{Efflux} were inhibited by 0- to 0.99-

fold. CL_{Efflux} was defined as $CL_{Bile}+CL_{BL}$, assuming CL_{Bile} and CL_{BL} were impaired to the same

extent. The simulated fold-changes of the model output values at steady state (120 min) were

plotted against the fraction of inhibition of CL_{Uptake} and CL_{Efflux} in a 3-D fashion using SigmaPlot

v.11, Systat Software Inc (San Jose, California). The fraction of inhibition was calculated as

($CL-CL_{inhibitor}$)/CL, where CL and $CL_{inhibitor}$ represent the clearance in the absence and presence

of inhibitor, respectively. A higher fraction of inhibition means more potent inhibition.

Determination of Cellular and Cytosolic Total and Unbound Concentrations of Inhibitors ($[I]_{t,cell}$, $[I]_{t,cyt}$, $[I]_{u,cell}$, and $[I]_{u,cyt}$, respectively)

SCHH seeded in 6-well plates were pre-incubated with Ca^{2+}-free HBSS for 10 min, followed by a 20-min incubation with dosing solution of model inhibitors (1 and 10 μM of telmisartan, or 0.8 and 8 μM of bosentan in standard HBSS with 4% BSA). After the incubation, cells were washed with ice-cold HBSS three times and stored at −80°C for future analysis. All the incubations in this study were performed at 37°C.

Cells were fractionated as reported previously with minor modification (Pfeifer et al., 2013b). Briefly, hepatocytes from the same treatment group were pooled and homogenized by passing the cells in fractionation buffer through a 27g needle 20 times to disrupt the cell membranes. The resultant cell lysate was subject to 10,000g centrifugation for 10 min at 4°C to isolate cytosol (supernatant) from other cell debris. The protein content of cell lysate was determined by Pierce biocinchoninic acid Protein Assay. The LDH activity of each fraction (i.e. cell lysate, cytosol and suspended pellet) was measured using an LDH cytotoxicity detection kit to reflect LDH recovery from cytosol. Glucose-6-phosphatase, succinate dehydrogenase, and acid phosphatase activity of each fraction were measured to assess microsomal, mitochondrial, and lysosomal contamination, respectively. The percentage of the organelle-specific enzyme activity measured in each fraction was calculated in comparison to the whole lysate to assess recovery. The unbound fraction (f_u) was determined by equilibrium dialysis as previously reported (Pfeifer et al., 2013b). Briefly, triplicate aliquots of samples (dosing solution, cell lysate and cytosol) were loaded into a 96-well equilibrium dialysis apparatus (HTDialysis, LLC; Gales Ferry, CT) and incubated at 37°C for 8 hours with shaking, which was sufficient to achieve equilibrium for most compounds (Banker et al., 2003). The f_u was back-calculated based on

Equation 6 to account for dilution during the homogenization and fractionation process as described previously (Kalvass et al., 2007).

$$\text{Undiluted } f_u = \frac{1/D}{\left(\left(\frac{1}{fu_{measured}}\right)-1\right)+1/D} \qquad (6)$$

where D represents the dilution factor.

The total mass of inhibitors in cell lysate and cytosol samples was measured. Cellular concentrations were calculated by dividing the mass by the estimated cellular volume of 7.4 µL/mg protein (Pfeifer et al., 2013c; Yang et al., 2015); cytosolic concentrations were calculated by dividing the mass by the estimated cytosolic volume, assuming cytosolic volume represents 70% of cellular volume (Grunberg et al., 2009). Unbound inhibitor concentrations ($[I]_u$) were calculated as the product of total inhibitor concentration ($[I]_t$) and f_u.

Simulation of Inhibitor Effects on TCA Disposition and Comparison with Experimental Results

d_8-TCA $C_{t,Cells}$ were measured after the following treatments: a 10-min pre-incubation of SCHH with telmisartan (1 or 10 µM) or bosentan (0.8 or 8 µM) in Ca^{2+}-free HBSS with 4% BSA, followed by a 10-min co-incubation with d_8-TCA (1 µM) and telmisartan or bosentan in standard HBSS with 4% BSA. TCA $C_{t,Cells}$ after 10-min uptake were simulated using Equations 1-5 and $CL_{inhibitor}$ values, which were calculated using Equations 7-10.

$$CL_{Uptake,inhibitor} = 0.7 \times CL_{Uptake} \Big/ \left(1+\frac{[I]_{u,med}}{IC_{50,NTCP}}\right) + 0.3 \times CL_{Uptake} \Big/ \left(1+\frac{[I]_{u,med}}{IC_{50,OATP1B1}}\right) \qquad (7)$$

$$CL_{BL,inhibitor} = CL_{BL} \Big/ \left(1+\frac{[I]_{cell}}{IC_{50,\ MRP3}}\right) \qquad (8)$$

$$CL_{BL,inhibitor} = CL_{BL} \Big/ \left(1+\frac{[I]_{cell}}{IC_{50,\ MRP4}}\right) \qquad (9)$$

$$CL_{Bile,inhibitor} = CL_{Bile} \Big/ \left(1+\frac{[I]_{cell}}{IC_{50,\ BSEP}}\right) \qquad (10)$$

where $CL_{Uptake,Inhibitor}$, $CL_{BL,inhibitor}$, and $CL_{Bile,inhibitor}$ represent the CL_{Uptake}, CL_{BL}, and CL_{Bile} of TCA in the presence of inhibitors, respectively; $[I]_{u,med}$ represents the unbound concentration of inhibitor in the medium; $[I]_{cell}$ represents the cellular inhibitor concentration, and different types of cellular concentration were used in the simulation, including $[I]_{t,cell}$, $[I]_{u,cell}$, $[I]_{t,cyt}$, $[I]_{u,cyt}$ (obtained as described in the previous section; values are shown in Table 2.3). The mean IC_{50} values for each transporter in Table 2.1 were used with the assumptions that NTCP and OATPs contribute 70% and 30%, respectively, to CL_{Uptake} (Shitara et al., 2003; De Bruyn et al., 2014), BSEP mediates CL_{Bile} (Noe et al., 2002; Chandra and Brouwer, 2004; Hayashi et al., 2005), and CL_{BL} is governed by MRP3 (Zhang et al., 2003) or MRP4 (Rius et al., 2006). Since the relative contribution of MRP3 and MRP4 is unknown, two extremes were simulated assuming MRP3 (Equation 8) or MRP4 (Equation 9) contributes 100% to CL_{BL}. Monte Carlo simulations of 40 individuals were performed 10 times using parameter estimates and the associated variance (Table 2.2); clearance was assumed to be normally distributed. The fold changes in the TCA $C_{t,Cells}$ in the presence vs. the absence of inhibitors were calculated and compared between predicted and observed results. Arithmetic mean and 95% confidence intervals of the fold changes were reported. The precision of the prediction was evaluated using the average fold error (AFE) (Equation 11) (Vildhede et al., 2016).

$$AFE = 10^{\frac{\sum \log\left(\frac{\text{Predicted fold change}}{\text{Observed fold change}}\right)}{\text{Number of predictions}}} \qquad (11)$$

Sensitivity Analyses of Model Input

The sensitivity of $f_{u,cell,inhibitor}$, a compound-specific parameter for telmisartan and bosentan, on model output (TCA $C_{t,Cells}$) was evaluated. Monte Carlo simulations were performed to predict the fold changes in the TCA $C_{t,Cells}$ at steady state (120 min) using parameters and the associated variance in Table 2.2, and Equations 1-5 and 7, 8, 10, where

$[I]_{cell}=[I]_{t,cell}\times f_{u,cell,inhibitor}$. Different $f_{u,cell,inhibitor}$ values (0.02-1) were used in the simulations. $[I]_{t,cell}$ and $[I]_{u,med}$ in SCHH incubated with telmisartan (1 or 10 μM) and bosentan (0.8 or 8 μM) were obtained from Table 2.3, as described above.

Furthermore, to generalize the sensitivity analysis of $f_{u,cell,inhibitor}$ to a broader range of inhibitors, TCA $C_{t,Cells}$ at steady state (120 min) in the presence of theoretical inhibitors with different ($[I]_{t,cell}/IC_{50}$) values (ranging from 0.5 to 60) were simulated assuming $f_{u,cell,inhibitor}=1$ or 0.02, respectively. In these simulations, IC_{50} represented the inhibitory potency against efflux transporters, and CL_{BL} and CL_{Bile} were assumed to be inhibited to the same extent. All simulations were performed with and without 50% inhibition of CL_{Uptake}.

Bioanalysis

Lysis solution [500 μL of 70% methanol/30% water containing internal standard (25 nM d_4-TCA, d_3-telmisartan, or ambrisentan)] was added to each well of previously frozen 24-well or 6-well plates containing study samples. Plates were shaken for ~15 min and the cell lysate solution was filtered, evaporated to dryness and reconstituted. Medium samples (100 μL) were extracted with 300 μL of 100% methanol containing internal standard, filtered, evaporated, and reconstituted. Standards and quality control samples were prepared by adding a known amount of standards into a blank cell plate or medium followed by the same sample processing methods with test samples. d_8-TCA samples were reconstituted in 60% methanol/40% water containing 10 mM ammonium acetate and analysed by liquid chromatography with triple quadrupole mass spectrometry (LC-MS/MS) using a Shimadzu binary high performance liquid chromatography (HPLC) system (Columbia, MD) and Thermo Electron TSQ® Quantum Discovery MAX ™ (Waltham, MA) with an Ion Max ESI source using negative electrospray ionization mode. Samples (10 μL) were injected onto a 100×1.0mm Hypersil Gold™ C_{18} column (Thermo

Scientific, Bellefonte, PA). The mobile phase was methanol/water with 0.5 mM ammonium acetate at a flow rate of 50 μL/min. The transitions monitored (parent m/z > product m/z) were 522 > 128 and 518 > 124 for d_8-TCA and d_4-TCA. The calibration curve range was 0.5-100 pmol/well. Telmisartan samples were reconstituted in 70% methanol/30% water with 0.1% formic acid and analysed by the same LC-MS/MS system using positive electrospray ionization mode. The mobile phase was methanol/water with 0.1% formic acid at a flow rate of 50 μL/min. The transitions monitored were 515.2 > 276.2 and 518.2 > 279.2 for telmisartan and d_3-telmisartan, respectively. The calibration curve range was 0.01-10 pmol/well. Bosentan samples were reconstituted in 60% methanol/30% water with 0.1% formic acid and analysed by LC-MS/MS using a Shimadzu binary HPLC system (Columbia, MD) and Applied Biosystems API-3000 mass spectrometer operated in positive electrospray ionization mode. Samples (10 μL) were loaded onto a 100×1.0 mm Hypersil Gold^{TM} C_{18} column (Thermo Scientific, Bellefonte, PA). The mobile phase was acetonitrile/water with 0.2% formic acid. The transitions monitored were 522.3 > 202.2 for bosentan and 379.1 > 303.1 for ambrisentan. The calibration curve range was 0.05-50 pmol/well. Acceptance criteria for % accuracy of back calculated values was 15-20%. TCA accumulation in cell lysate was corrected for nonspecific binding to the BioCoat^{TM} plate without cells.

Results

Hepatobiliary Disposition of d_8-TCA in SCHH

The model scheme depicted in Fig 1A, and Equations 1-5, were used to describe SCHH data (TCA in Cells+Bile, Cells, and incubation medium) from three human livers. Data were analyzed as three independent data sets and were well described by the mechanistic model (individual fits are not shown). The mean (±S.E.M.) data and simulated mass-time profiles

generated using the mean of best-fit parameter estimates from the three SCHH data sets (Table 2.2) are presented in Fig. 2.1B. After 20-min uptake, TCA $C_{t,Cells}$ was 5.6 μM. The mean kinetic parameters and the associated variance estimated by fitting the differential Equations 1-5 to TCA mass-time data from three independent SCHH preparations are presented in Table 2.2. The estimated total CL_{Uptake} of TCA was approximately one order of magnitude greater than total CL_{Bile} and total CL_{BL} estimates; TCA CL_{Bile} was approximately 2-fold greater than CL_{BL}. These parameter estimates were used in the subsequent simulations.

Sensitivity Analyses of Model Output

To identify a model output that was sensitive to impairment in both CL_{Uptake} and CL_{Efflux}, the simulated fold changes in different endpoints of the SCHH assay (at steady state) were plotted against the fraction of inhibition of CL_{Uptake} and CL_{Efflux} in Fig. 2.2, where $CL_{Efflux} = CL_{BL} + CL_{Bile}$. The most sensitive model output to both CL_{Uptake} and CL_{Efflux} of TCA was $C_{t,Cells}$. $C_{t,Cells}$ decreased to 0.01-fold of baseline when CL_{Uptake} was inhibited by 99% and CL_{Efflux} was not inhibited, and increased to approximately15-fold of baseline when CL_{Efflux} was inhibited by 99% and CL_{Uptake} was not inhibited. Other endpoints were only sensitive to either CL_{Uptake} (e.g., $X_{t,Cells+Bile}$) or CL_{Efflux} (e.g., $X_{t,Bile}$, $X_{t,Bile}/X_{t,Cells}$ and $X_{t,Bile}/X_{t,Cells+Bile}$) and the fold changes were less pronounced. Therefore, the TCA $C_{t,Cells}$ was chosen as the model output in the subsequent simulations to reflect the altered hepatobiliary disposition of TCA in the presence of inhibitors.

Determination of Cellular and Cytosolic Total and Unbound Concentrations of Inhibitors

After 20-min incubation with SCHH, the total and unbound concentrations of telmisartan and bosentan in medium, whole cell lysates, and cytosol were measured; the results are reported in Table 2.3. The cytosol was isolated with ~100% recovery (based on the LDH assay; data not shown) and low contamination of subcellular organelles (3% recovery of the enzyme marker for

71

microsomal contamination; 5% recovery of the enzyme marker for mitochondrial

contamination). As shown in Table 2.3, telmisartan was highly bound in the whole cell lysate

and cytosol ($f_{u,cell,inhibitor}$=0.09-0.13 and $f_{u,cyt,inhibitor}$=0.05-0.08); the cytosolic unbound telmisartan

concentrations were only 5.3-7% of the total concentrations in the cell. The unbound fraction of

bosentan was higher than telmisartan ($f_{u,cell,inhibitor}$=0.22-0.41 and $f_{u,cyt,inhibitor}$=0.12); the cytosolic

unbound bosentan concentration was 11% of the total concentration in the whole cell. More than

one-half of the amount of telmisartan (62%-70%) and bosentan (58%-63%) in the whole cell

lysate was recovered in the cytosol. Considering that cytosolic volume represents ~70% of the

cellular volume (Grunberg et al., 2009), the cytosolic and cellular total concentrations were

similar.

Comparison of Simulated and Observed TCA Disposition in the Presence of Inhibitors

The fold changes in the TCA $C_{t,Cells}$ in the presence of inhibitors (telmisartan and

bosentan) vs. in the absence of inhibitors were simulated and compared to experimental results

(Table 2.4). Monte Carlo simulations were performed for 40 individuals and repeated 10 times

using either Equation 8 or Equation 9 assuming either MRP3 or MRP4 mediated the basolateral

efflux of TCA. The simulation results were similar and therefore, only the simulations based on

MRP3 inhibition were presented, since MRP3 expression was reported to be higher than MRP4

expression in human liver and hepatocytes (Vildhede et al., 2015; Wisniewski et al., 2016). In

the prediction of telmisartan's effect on TCA $C_{t,Cells}$, the AFE of simulations using $[I]_{u,cell}$ and

$[I]_{u,cyt}$ was 1.0 and 0.99, respectively. The 95% confidence interval of the simulation results

overlapped with the range of observed data. When $[I]_{t,cell}$ and $[I]_{t,cyt}$ were used in the simulation,

TCA $C_{t,Cells}$ was over-predicted and the AFE was 1.4 and 1.3, respectively. In the prediction of

bosentan's effect, the mechanistic model slightly over-predicted the fold change for TCA $C_{t,Cells}$,

with an AFE of 1.2-1.3, no matter which inhibitor concentration was used. According to the simulations (Figure S2.1), telmisartan-induced changes in TCA $C_{t,Cells}$ increased as the uptake phase was extended. After a 30-min uptake phase, the simulated TCA $C_{t,Cells}$ for telmisartan based on $[I]_{t,cell}$ was 3-fold of the simulation based on $[I]_{u,cyt}$.

Sensitivity Analyses of Model Inputs

Since the use of $[I]_u$ or $[I]_t$ affected the simulation of TCA $C_{t,Cells}$ differently for telmisartan and bosentan, sensitivity analysis of $f_{u,cell,inhibitor}$ for telmisartan and bosentan was performed by simulating TCA $C_{t,Cells}$ using $[I]_{t,cell}$ of telmisartan and bosentan and various $f_{u,cell,inhibitor}$ values (0.02-1) (Table 2.3). Simulated TCA $C_{t,Cells}$ at steady state were expressed as the mean and standard deviation of fold changes over baseline (without inhibitors) (shown in Fig. 2.3). The TCA $C_{t,Cells}$ was sensitive to changes in $f_{u,cell,inhibitor}$ for telmisartan but not for bosentan at both the low and high dosing concentrations. At the low dosing concentration, the mean fold change in the TCA $C_{t,Cells}$ increased from 0.8 to 2.5 when the $f_{u,cell,inhibitor}$ for telmisartan changed from 0.02 to 1; the mean fold change in the TCA $C_{t,Cells}$ increased from 0.8 to 1 when the $f_{u,cell,inhibitor}$ for bosentan changed from 0.02 to 1. At the high dosing concentration, the mean fold change in the TCA $C_{t,Cells}$ ranged from 0.9 to 4 when the $f_{u,cell,inhibitor}$ for telmisartan changed from 0.02 to 1; the mean fold change ranged from 0.8 to 1.5 when the $f_{u,cell,inhibitor}$ for bosentan changed from 0.02 to 1. (Fig. 2.3).

To explore the differential sensitivity of TCA $C_{t,Cells}$ to $f_{u,cell,inhibitor}$ for different inhibitors, the TCA $C_{t,Cells}$ in the presence of a set of theoretical inhibitors with various ($[I]_{t,cell}/IC_{50}$) values were simulated using $f_{u,cell,inhibitor}=1$ and 0.02 (Fig. 2.4). For inhibitors with the same ($[I]_{t,cell}/IC_{50}$) value, if the inhibitor exhibited no intracellular binding (i.e., $f_{u,cell,inhibitor}=1$), the simulated fold change in the TCA $C_{t,Cells}$ was greater than when the inhibitor exhibited extensive intracellular

73

binding (i.e., $f_{u,cell,inhibitor}=0.02$). As the ($[I]_{t,cell}/IC_{50}$) value increased, the difference in simulated

TCA $C_{t,Cells}$ between $f_{u,cell,inhibitor}=1$ and 0.02 increased. For inhibitors with ($[I]_{t,cell}/IC_{50}$) >1, the

predicted TCA $C_{t,Cells}$ when $f_{u,cell,inhibitor}=1$ was more than twice of the predicted TCA $C_{t,Cells}$

when $f_{u,cell,inhibitor}=0.02$. These relationships were the same with or without 50% inhibition of

CL_{Uptake} (data not shown).

Discussion

In this study, an integrated approach was developed to predict the net effect of inhibition

of multiple transporters on the hepatocellular disposition of the model bile acid TCA based on

inhibition constants and SCHH data using mechanistic modeling. Importantly, the intracellular

binding of inhibitors was considered in the simulations, and a strategy was proposed to

determine whether it is necessary to measure the intracellular binding *a priori*.

The following assumptions were made for the mechanistic modeling. Linear kinetics was

assumed because the unbound concentration of TCA in the medium ($f_{u,med}\times1$ µM, where $f_{u,med}$

refers to the unbound fraction of TCA in the medium equivalent to 0.15 in 4% BSA)(Wolf et al.,

2008) was below the K_m of TCA for the uptake transporter NTCP (5-20 µM) and OATPs (5.8-

71.8 µM) (Shitara et al., 2003; Nozawa et al., 2004; Mita et al., 2006; De Bruyn et al., 2014). In

addition, the cellular total concentration of TCA (5.6 µM) after 20-min uptake was below the K_m

for the efflux transporters BSEP (6.2 µM) (Hayashi et al., 2005), MRP3 (30 µM) and MRP4 (7.7

µM); if intracellular binding is taken into account, the cellular unbound concentration of TCA

would be even lower. Passive diffusion was not included in the model because active uptake

plays a major role in the hepatocellular accumulation of TCA (Shitara et al., 2003; Mita et al.,

2006).

To simulate the effects of inhibitors on TCA disposition, Equations 7-10 were used. Due to low TCA concentrations, Equations 7-10 held true regardless of the mechanisms of inhibition and the IC_{50} value was substituted for K_i. The inhibitory effects of metabolites of telmisartan and bosentan were assumed to be negligible. There are no literature reports about inhibitory effects of telmisartan metabolites on human bile acid transporters. Although a bosentan metabolite, Ro 47-8634, was reported to be an inhibitor of rat Bsep (K_i=8.5 µM) (Fattinger et al., 2001), the intracellular concentration of this metabolite in human SCHH is less than 5% of bosentan (Matsunaga et al., 2015). In addition, the concentration of this metabolite in human plasma (Dingemanse et al., 2002) and feces (Weber et al., 1999) is much lower than bosentan. Both MRP3 and MRP4 have been reported to contribute to the basolateral efflux of TCA without consensus on the relative contribution. The expression of MRP3 is higher than MRP4 in human liver and hepatocytes; while the affinity of TCA towards MRP4 (K_m=7.7 µM) (Rius et al., 2006) is higher than MRP3 (K_m=30 µM) (Zhang et al., 2003). Akita and colleagues reported that TCA was not transported to a significant degree by MRP3 (Akita et al., 2002). Therefore, two extreme scenarios were simulated assuming 100% contribution of either MRP3 or MRP4; the simulation results were similar so MRP3 was selected as the main basolateral efflux transporter for subsequent simulations.

In the current study, a physiologic concentration of protein (4% BSA) was added to mimic the *in vivo* scenario. Using the mechanistic model, the estimated total CL_{Uptake} of TCA was 0.63 mL/min/g liver (Table 2.2) and the unbound CL_{Uptake} of TCA was 4.2 mL/min/g liver (calculated as total $CL_{Uptake}/f_{u,med}$). This value is close to the reported unbound CL_{Uptake} (2.2 mL/min/g liver) (Yang et al., 2015). CL_{BL} and CL_{Bile} were similar to values reported previously (CL_{BL}=0.042 mL/min/g liver and CL_{Bile}=0.14 mL/min/g liver) (Yang et al., 2015).

In this study, we leveraged SCHH and a mechanistic model to evaluate the net effect of uptake and efflux. The comparison between simulated and experimental results for telmisartan and bosentan provided an example of the applicability of this approach to predict the net effect of inhibition at multiple sites on the disposition of a model bile acid (Table 2.4). This applicability is important because the interplay of multiple transporters is common. Examples of dual inhibitors of BSEP and NTCP include the non-hepatotoxic drugs pioglitazone, telmisartan, and reserpine (Morgan et al., 2010; Dong et al., 2014) as well as the hepatotoxic compound troglitazone (Yang et al., 2014) (Morgan et al., 2010). Some compounds are dual inhibitors of both uptake and basolateral efflux of TCA, such as alpha-naphthylisothiocyanate (Guo et al., 2014).

The slight differences between model predicted and experimental results observed for bosentan's effect on TCA $C_{t,Cells}$ could be attributed to the model assumptions discussed earlier. It should be noted that inhibitor-mediated alterations in TCA $C_{t,Cells}$ was not extensive due to the short 10-min uptake phase in this study and simultaneous inhibition of uptake and efflux. A more pronounced alteration in TCA $C_{t,Cells}$ could be achieved by extending the uptake phase (Figure S2.1). However, accurate measurement of the TCA $C_{t,Cells}$ after an uptake phase >30 min is technically challenging in sandwich-cultured hepatocytes. When Ca^{2+} is present during an extended uptake phase, the tight junctions reseal yielding a measured $X_{t,Cells+Bile}$ instead of $X_{t,Cells}$ (Pfeifer et al., 2013c).

This is the first study to evaluate the impact of using different cellular inhibitor concentrations to predict transporter-mediated interactions in SCHH. Use of cytosolic concentrations marginally improved the prediction of telmisartan's effects; the AFE dropped by ≤ 0.1 when $[I]_{cyt}$ instead of $[I]_{cell}$ was used. This difference was minor because telmisartan was

recovered primarily in the cytosol (62-70% of the total mass) and the cytosolic concentration approximated the cellular concentration. The impact of using $[I]_{cyt}$ instead of $[I]_{cell}$ would likely be greater for drugs that are trapped in subcellular organelles, such as furamidine (Pfeifer et al., 2013b). Different enzymatic markers were used to evaluate the purity and recovery of cytosol. However, membrane-anchored proteins (e.g., the endoplasmic reticulum marker glucose-6-phosphatase) would not be able to detect whether content in the endoplasmic reticulum lumen had been released into the cytosol. Lumen protein markers [e.g., ERp57 (Coe et al., 2010) or Glucosidase II (Zuber et al., 2000)] could be measured in future studies to exclude this possibility.

In DDI evaluations, $[I]_{t,cell}$ is used commonly to avoid false-negative predictions by assessing the "worst-case scenario", but this value can lead to false-positive predictions. Pfeifer et al. reported that using $[I]_{u,cell}$ of ritonavir correctly predicted no clinical MRP2-mediated DDI between ritonavir and ^{99m}Tc-mebrofenin, while predictions based on $[I]_{t,cell}$ of ritonavir led to a false positive prediction of DDI liability (Pfeifer et al., 2013a). In the case of telmisartan, simulations using $[I]_{t,cell}$ and $[I]_{t,cyt}$ slightly overpredicted TCA $C_{t,Cells}$ compared to simulations using $[I]_{u,cell}$ and $[I]_{u,cyt}$. Unlike telmisartan, simulations for bosentan's effect on TCA $C_{t,Cells}$ were similar regardless of whether total or unbound, cellular or cytosol, concentrations of bosentan were employed (Table 2.4). Sensitivity analysis revealed the differential sensitivity of TCA $C_{t,Cells}$ to $f_{u,cell,inhibitor}$ for telmisartan and bosentan (Fig. 2.3). This difference suggested that although it is ideal to use $[I]_u$, it is not necessary to measure $f_{u,cell,inhibitor}$ and use $[I]_{u,cell}$ for every inhibitor. Simulations of a set of theoretical inhibitors showed that inhibitors with high $([I]_{t,cell}/IC_{50})$ values were more sensitive to changes in $f_{u,cell,inhibitor}$ (Fig. 2.4). For example, when $([I]_{t,cell}/IC_{50})$ was >1, the simulation assuming no protein binding over-predicted TCA $C_{t,Cells}$ by

twice or more. Inhibitors with large ($[I]_{t,cell}/IC_{50}$) values either tend to accumulate in the cells or serve as strong inhibitors of efflux transporters. In these cases, ignoring protein binding would greatly impact the prediction, and thus, $f_{u,cell,inhibitor}$ needs to be measured. The ($[I]_{t,cell}/IC_{50}$) value of telmisartan was 3.6 at the 10 µM dose level and the ($[I]_{t,cell}/IC_{50}$) value of bosentan was 0.8 at the 8 µM dose level. This difference could explain the greater sensitivity of predicted TCA $C_{t,Cells}$ to changes in $f_{u,cell,inhibitor}$ of telmisartan compared to bosentan.

Based on the results of these studies, a framework was proposed to predict the net effect of drug-bile acid interactions mediated by inhibition of multiple transporters (Fig. 2.5). The kinetic parameters (CL_{Uptake}, CL_{Bile}, and CL_{BL}) of the victim bile acid (e.g. TCA) are estimated by mechanistic modeling; in the presence of inhibitors, the clearance values are affected by $[I]_{u,med}$ or $[I]_{cell}$ and IC_{50} or K_i values. The choice of which $[I]_{cell}$ value to use (e.g., $[I]_{t,cell}$, $[I]_{t,cyt}$, $[I]_{u,cell}$, $[I]_{u,cyt}$) depends on the sensitivity of the model output to $f_{u,cell,inhibitor}$, which is determined by the ($[I]_{t,cell}/IC_{50}$) value of the inhibitor. If this value is high, the model output, $C_{t,Cells}$, is sensitive to changes in $f_{u,cell,inhibitor}$. In these cases, it is critical to measure $f_{u,cell,inhibitor}$, as demonstrated in this study. For inhibitors that sequester in subcellular organelles, it may be necessary to isolate cytosol and measure $[I]_{u,cyt}$. Finally, the altered hepatocellular disposition of the victim bile acid, namely $C_{t,Cells}$, can be simulated using $CL_{inhibitor}$ (calculated using Equations 7-10). This approach could be applied to evaluate transporter-mediated interactions involving other victim substrates (e.g. hepatotoxic bile acids), which would have significant toxicological implications.

Table 2.1. Inhibition constants (µM) of telmisartan and bosentan against transporters involved in the hepatic uptake and efflux of TCA.

Clearance	Transporter	Telmisartan	Reference	Bosentan	Reference
CL_{Uptake}	NTCP	60 (K_i)	(Dong et al., 2014)	18 (K_i) 36 (IC_{50})	(Leslie et al., 2007) (Lepist et al., 2014)
	OATP1B1	0.44 (K_i)	(Hirano et al., 2006)	18 [a]	
CL_{Bile}	BSEP	16-16.2 (IC_{50})	(Lai, 2014), (Morgan et al., 2013)	23-42 (IC_{50})	(Morgan et al., 2013) (Lepist et al., 2014)
CL_{BL}	MRP4	11-36 (IC_{50})	(Sato et al., 2008) (Morgan et al., 2013)	22 (IC_{50})	(Morgan et al., 2013)
	MRP3	60 (IC_{50})	(Morgan et al., 2013)	42 (IC_{50})	(Morgan et al., 2013)

[a] *not available and therefore assumed to be the same as NTCP*

Table 2.2. Recovered estimates of d_8-TCA total uptake clearance (CL_{Uptake}), basolateral efflux clearance (CL_{BL}), biliary clearance (CL_{Bile}) and K_{Flux} in the presence of 4% BSA. Estimates were based on the model scheme and time-course data depicted in Fig. 2.1. The model was fit to data generated from n=3 independent SCHH preparations (triplicate measurements) separately.

Parameter Estimate	Mean	SD	CV%
CL_{Uptake} (*mL/min/g liver*)	0.63	0.12	20
CL_{BL} (*mL/min/g liver*)	0.034	0.011	32
CL_{Bile} (*mL/min/g liver*)	0.074	0.030	36
K_{Flux} (*min^{-1}*)	0.018	0.0015	8

Table 2.3. Measured total and unbound concentrations of inhibitors ($[I]_t$ and $[I]_u$, µM) in the medium ($[I]_{med}$), whole cell lysate ($[I]_{cell}$), and cytosol ($[I]_{cyt}$). SCHH were treated with telmisartan (1 or 10 µM) and bosentan (0.8 or 8 µM) for 20 min in the presence of 4% BSA. Data were generated from n=1 SCHH preparation. Unbound concentration and f_u data were expressed as mean values obtained from triplicate measurements (cell lysate and cytosol) and duplicate measurements (medium) and values in parentheses represent ranges. Total concentrations were from single measurements.

Inhibitor	Medium			Cell lysate			Cytosol		
	$[I]_{t,med}$	$[I]_{u,med}$	$f_{u,med}$	$[I]_{t,cell}$	$[I]_{u,cell}$	$f_{u,cell,inhibitor}$	$[I]_{t,cyt}$	$[I]_{u,cyt}$	$f_{u,cyt,inhibitor}$
Telmisartan	1	0.012 (0.0098-0.014)	0.012 (0.0098-0.014)	16	2.1 (1.6-2.5)	0.13 (0.099-0.16)	16	0.85 (0.8-0.9)	0.053 (0.050-0.056)
	10	0.20 (0.18-0.22)	0.02 (0.018-0.022)	40	3.7 (2.7-4.8)	0.094 (0.068-0.12)	35	2.8 (1.8-3.4)	0.080 (0.052-0.098)
Bosentan	0.8	0.031 (0.023-0.039)	0.039 (0.029-0.048)	1.9	0.79 (0.66-0.93)	0.41 (0.34-0.48)	1.7	0.21 (0.21-0.21)	0.12 (0.12-0.12)
	8	0.45 (0.44-0.47)	0.057 (0.055-0.058)	17	3.8 (3.1-4.5)	0.22 (0.18-0.26)	14	N/A[a]	N/A[a]

[a] N/A: not available

Table 2.4. Experimentally observed and simulated alteration of TCA total concentration in Cells ($C_{t,Cells}$) due to telmisartan and bosentan. Observed data are presented as fold change in the presence compared to the absence of inhibitors. SCHH were pre-treated with telmisartan (1 and 10 µM) or bosentan (0.8 and 8 µM) for 10 min, followed by co-incubation with d_8-TCA and telmisartan or bosentan for 10 min. Observed data represented arithmetic mean (range) measured in n=1 SCHH preparation in duplicate. Monte Carlo simulations for 40 individuals were performed 10 times using parameter estimates and associated variance (Table 2.2), different inhibitor concentrations (Table 2.3), and IC_{50} data (Table 2.1) assuming CL_{Uptake} was mediated by NTCP (70%) and OATPs (30%), CL_{Bile} was mediated by BSEP, and CL_{BL} was governed by MRP3. Simulation data are presented as arithmetic mean of 10 simulations (95% confidence interval). Average fold errors were calculated based on Equation 11.

Inhibitor	Dosing conc.	Observation	Fold Change in TCA $C_{t,Cells}$ Simulation			
			$[I]_{t,cell}$	$[I]_{u,cell}$	$[I]_{t,cyt}$	$[I]_{u,cyt}$
Telmisartan	1 µM	0.91 (0.87-0.95)	1.3 (1.3-1.4)	1.0 (0.99-1.1)	1.3 (1.3-1.3)	1.0 (0.94-1.1)
	10 µM	1.1 (1.0-1.1)	1.4 (1.3-1.4)	1.0 (0.98-1.0)	1.3 (1.3-1.3)	0.96 (0.95-0.98)
	Average fold error		1.4	1.0	1.3	0.99
Bosentan	0.8 µM	0.88 (0.83-0.92)	1.0 (0.99-1.0)	0.99 (0.96-1.0)	1.0 (0.99-1.0)	0.99 (0.97-1.0)
	8 µM	0.81 (0.80-0.82)	1.2 (1.2-1.3)	1.0 (1.0-1.1)	1.1 (1.1-1.2)	N/A[a]
	Average fold error		1.3	1.2	1.3	N/A[a]

[a] N/A: not available

Figure 2.1. (A) Model schemes depicting disposition of d_8-TCA in sandwich-cultured human hepatocytes (SCHH) using standard (Cells+Bile) Hanks' balanced salt solution (HBSS) (left) and Ca^{2+}-free (Cells) HBSS (right). (B) d_8-TCA mass vs. time data in SCHH lysate (left) and incubation buffer (right). Closed symbols/solid lines represent d_8-TCA in Cells + Bile or standard HBSS, and open symbols/dashed lines represent d_8-TCA in Cells or Ca^{2+}-free HBSS. Experimental data (circles) represent the mean $\pm$ S.E.M. (n = 3 SCHH preparations in triplicate per group). The simulated profiles (lines) were generated from Equations 1-5 using the mean of best-fit parameter estimates from 3 SCHH datasets (Table 2.2).
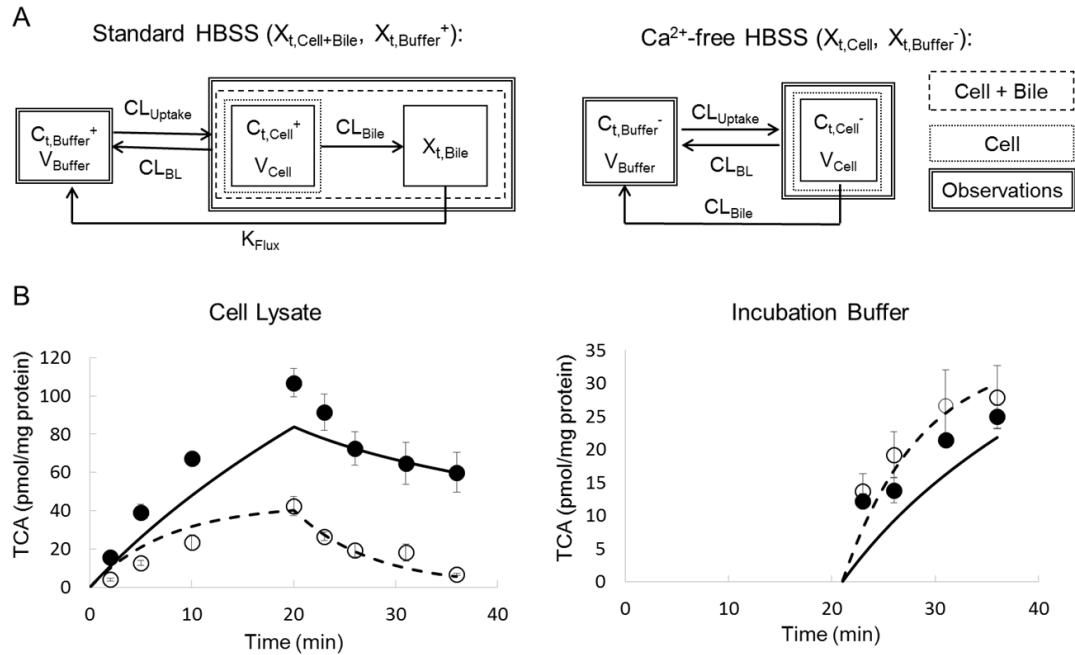
Figure 2.2. Impact of impaired CL_{Uptake} and CL_{Efflux} ($CL_{Efflux} = CL_{BL} + CL_{Bile}$) of TCA on different model outputs: (A) TCA total concentration in Cells ($C_{t,Cells}$), (B) TCA total amount in Cells+Bile ($X_{t,Cells+Bile}$), (C) TCA total amount in Bile ($X_{t,Bile}$), (D) Ratio of the total amount of TCA in Cells to the total amount of TCA in Cells+Bile ($X_{t,Cells}/X_{t,Cells+Bile}$), (E) Ratio of the total amount of TCA in Bile to the total amount of TCA in Cells ($X_{t,Bile}/X_{t,Cells}$), and (F) Ratio of the total amount of TCA in Bile to the total amount of TCA in Cells+Bile ($X_{t,Bile}/X_{t,Cells+Bile}$) in SCHH. The Z-axis represents the fold change compared to baseline (shown in the color map on the right), based on simulations of TCA accumulation at steady state. Figures C, E, and F have been rotated to improve visibility of the 3-D surface.
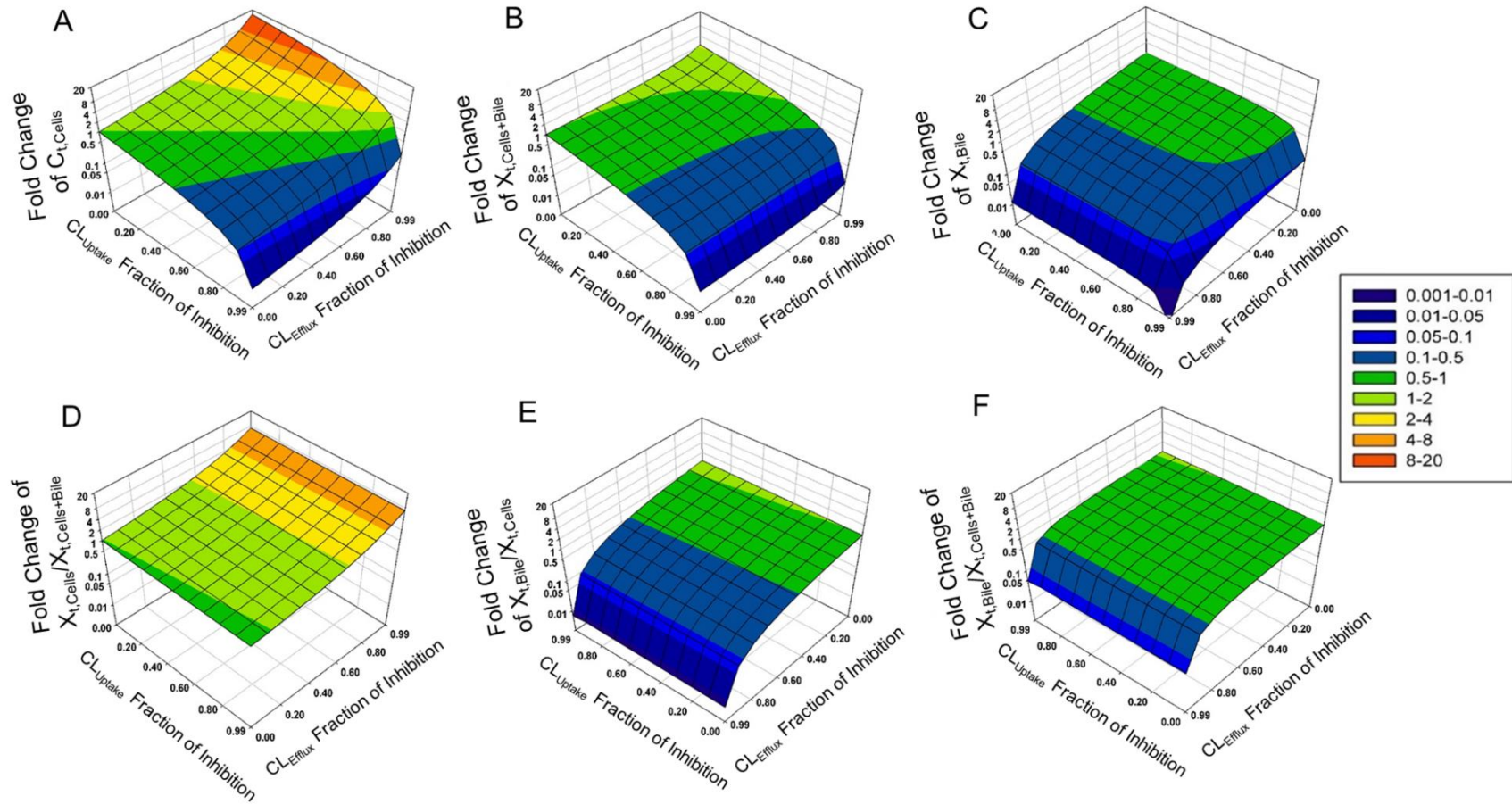
Figure 2.3. Sensitivity analysis of cellular unbound fraction of inhibitor ($f_{u,cell,inhibitor}$) for telmisartan and bosentan. Fold changes in the TCA $C_{t,Cells}$ at steady state compared to baseline (without inhibitors), in the presence of telmisartan and bosentan were simulated based on the average IC_{50} values (Table 2.1), cellular total inhibitor concentration (Table 2.3), and different $f_{u,cell,inhibitor}$ values using a Monte Carlo simulation approach. Data were expressed as mean and S.D. of 40 simulated individuals.
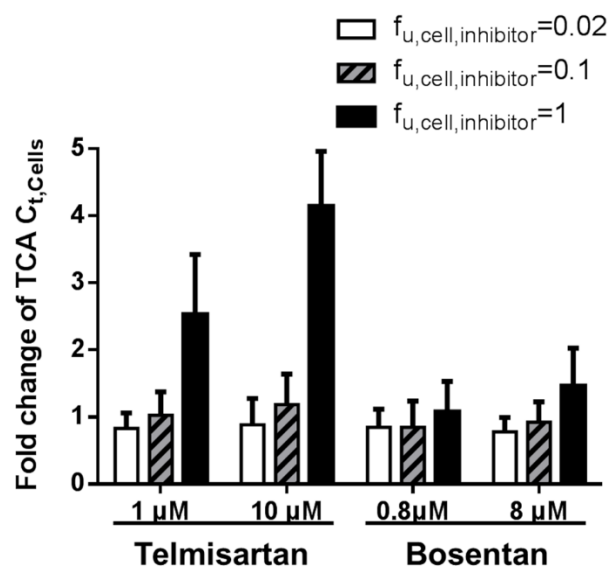
Figure 2.4. The sensitivity of the predicted TCA $C_{t,Cells}$ to changes in $f_{u,cell,inhibitor}$ as a function of ($[I]_{t,cell}/IC_{50}$) values for a set of theoretical inhibitors. TCA $C_{t,Cells}$ in the presence of theoretical inhibitors with different ($[I]_{t,cell}/IC_{50}$) values were simulated assuming $f_{u,cell,inhibitor} = 1$ (black bar) and $f_{u,cell,inhibitor} = 0.02$ (white bar). The fold changes of TCA $C_{t,Cells}$ compared to baseline (without inhibitors) are plotted on the y-axis.
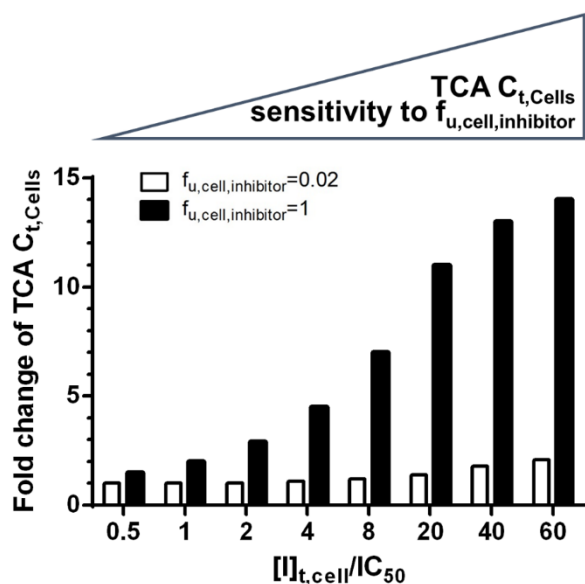
Figure 2.5. Proposed framework to predict altered bile acid disposition in sandwich-cultured human hepatocytes (SCHH) mediated by inhibition of multiple transporters. Black solid boxes represent experimental observations, and black double-lines depict the simulation output, as detailed in the Discussion. The kinetic parameters, including uptake clearance (CL_{Uptake}), biliary clearance (CL_{Bile}), and basolateral efflux clearance (CL_{BL}), of the victim bile acid (e.g. taurocholic acid) are estimated by using mechanistic modeling; in the presence of inhibitors, the clearance values ($CL_{inhibitor}$) are estimated using Equations 7-10 based on inhibitor concentrations in the medium or cells ($[I]_{cell}$) and IC_{50} or K_i values. The choice of which $[I]_{cell}$ to use depends on the ($[I]_{t,cell}/IC_{50}$) value of the inhibitor, where $[I]_{t,cell}$ represents cellular total concentration of inhibitor. If this value is high, the cellular unbound fraction of inhibitor ($f_{u,cell,inhibitor}$) should be measured to estimate $[I]_{u,cell}$, where $[I]_{u,cell}$ represents the cellular unbound concentration of inhibitor. Otherwise, $[I]_{t,cell}$ can be used. Finally, the altered cellular total concentrations ($C_{t,Cells}$) of the victim bile acid are simulated using $CL_{inhibitor}$.
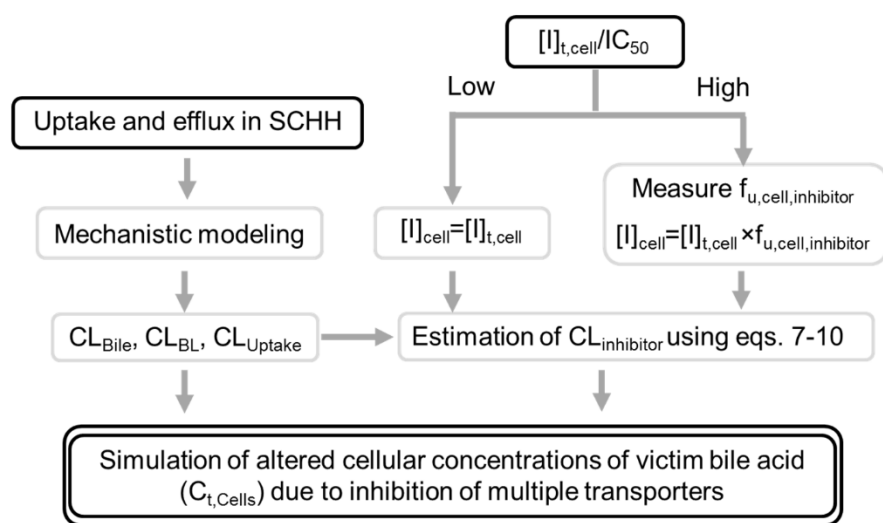
REFERENCES

Akita H, Suzuki H, Hirohashi T, Takikawa H and Sugiyama Y (2002) Transport activity of human MRP3 expressed in Sf9 cells: comparative studies with rat MRP3. *Pharm Res* **19**:34-41.

Banker MJ, Clark TH and Williams JA (2003) Development and validation of a 96-well equilibrium dialysis apparatus for measuring plasma protein binding. *J pharm Sci* **92**:967-974.

Chandra P and Brouwer KLR (2004) The complexities of hepatic drug transport: current knowledge and emerging concepts. *Pharml Res* **21**:719-735.

Coe H, Jung J, Groenendyk J, Prins D and Michalak M (2010) ERp57 modulates STAT3 signaling from the lumen of the endoplasmic reticulum. *J Biol Chem* **285**:6725-6738.

Dawson S, Stahl S, Paul N, Barber J and Kenna JG (2012) In vitro inhibition of the bile salt export pump correlates with risk of cholestatic drug-induced liver injury in humans. *Drug Metab Dispos* **40**:130-138.

De Bruyn T, Sempels W, Snoeys J, Holmstock N, Chatterjee S, Stieger B, Augustijns P, Hofkens J, Mizuno H and Annaert P (2014) Confocal imaging with a fluorescent bile acid analogue closely mimicking hepatic taurocholate disposition. *J pharm Sci* **103**:1872-1881.

Dingemanse J, Bodin F, Weidekamm E, Kutz K, and van Giersbergen P (2002) Influence of food intake and formulation on the pharmacokinetics and metabolism of bosentan, a dual endothelin receptor antagonist. J Clin Pharmacol 42:283-289.

Doherty MM, Poon K, Tsang C and Pang KS (2006) Transport is not rate-limiting in morphine glucuronidation in the single-pass perfused rat liver preparation. *J Pharmacol Exp Ther* **317**:890-900.

Dong Z, Ekins S and Polli JE (2014) Quantitative NTCP pharmacophore and lack of association between DILI and NTCP Inhibition. *Eur J Pharm Sci* **66c**:1-9.

Fattinger K, Funk C, Pantze M, Weber C, Reichen J, Stieger B and Meier PJ (2001) The endothelin antagonist bosentan inhibits the canalicular bile salt export pump: a potential mechanism for hepatic adverse reactions. *Clin Pharmacol Ther* **69**:223-231.

US FDA/CDER (2012) Guidance for Industry. Drug Interaction Studies — Study Design, Data Analysis, and Implications for Dosing and Labeling Recommendations. US FDA websitev[online],http://www.fda.gov/downloads/Drugs/GuidanceComplianceRegulatoryInformation/Guidances/UCM292362.pdf

Grunberg W, Staufenbiel R, Constable PD, Dann HM, Morin DE and Drackley JK (2009) Liver phosphorus content in Holstein-Friesian cows during the transition period. *J Dairy Sci* **92**:2106-2117.

Guo C, He L, Yao D, A J, Cao B, Ren J, Wang G and Pan G (2014) Alpha-naphthylisothiocyanate modulates hepatobiliary transporters in sandwich-cultured rat hepatocytes. *Toxicol Lett* **224**:93-100.

Hayashi H, Takada T, Suzuki H, Onuki R, Hofmann AF and Sugiyama Y (2005) Transport by vesicles of glycine- and taurine-conjugated bile salts and taurolithocholate 3-sulfate: a comparison of human BSEP with rat Bsep. *Biochim Biophys Acta* **1738**:54-62.

Hirano M, Maeda K, Shitara Y and Sugiyama Y (2006) Drug-drug interaction between pitavastatin and various drugs via OATP1B1. *Drug Metab Dispos* **34**:1229-1236.

Kalvass JC, Maurer TS and Pollack GM (2007) Use of plasma and brain unbound fractions to assess the extent of brain distribution of 34 drugs: comparison of unbound concentration ratios to in vivo p-glycoprotein efflux ratios. *Drug Metab Dispos* **35**:660-666.

Lai Y (2014) Transporters in Drug Discovery and Development: Detailed Concepts and Best Practice. Woodhead Publishing. Sawston, UK

Lee JK, Marion TL, Abe K, Lim C, Pollock GM and Brouwer KLR (2010) Hepatobiliary disposition of troglitazone and metabolites in rat and human sandwich-cultured hepatocytes: use of Monte Carlo simulations to assess the impact of changes in biliary excretion on troglitazone sulfate accumulation. *J Pharmacol Exp Ther* **332**:26-34.

Lepist EI, Gillies H, Smith W, Hao J, Hubert C, St Claire RL, 3rd, Brouwer KR and Ray AS (2014) Evaluation of the endothelin receptor antagonists ambrisentan, bosentan, macitentan, and sitaxsentan as hepatobiliary transporter inhibitors and substrates in sandwich-cultured human hepatocytes. *PloS One* **9**:e87548.

Leslie EM, Watkins PB, Kim RB and Brouwer KLR (2007) Differential inhibition of rat and human Na$^+$-dependent taurocholate cotransporting polypeptide (NTCP/SLC10A1)by bosentan: a mechanism for species differences in hepatotoxicity. *J Pharmacol Exp Ther* 321:1170-1178.

Mateus A, Matsson P and Artursson P (2013) Rapid measurement of intracellular unbound drug concentrations. *Mol Pharm* **10**:2467-2478.

Matsunaga N, Kaneko N, Staub AY, Nakanishi T, Nunoya KI, Imawaka H and Tamai I (2016) Analysis of metabolic pathway of bosentan and cytotoxicity of bosentan metabolites based on a quantitative modeling of metabolism and transport in sandwich-cultured human hepatocytes. *Drug Metab Dispos* **44**:16-27.

Matsunaga N, Wada S, Nakanishi T, Ikenaga M, Ogawa M and Tamai I (2014) Mathematical modeling of the in vitro hepatic disposition of mycophenolic acid and its glucuronide in sandwich-cultured human hepatocytes. *Mol Pharm* **11**:568-579.

Mita S, Suzuki H, Akita H, Hayashi H, Onuki R, Hofmann AF and Sugiyama Y (2006) Vectorial transport of unconjugated and conjugated bile salts by monolayers of LLC-PK1 cells doubly transfected with human NTCP and BSEP or with rat Ntcp and Bsep. *Am J Physiol Gastrointest Liver Physiol* **290**:G550-556.

Morgan RE, Trauner M, van Staden CJ, Lee PH, Ramachandran B, Eschenberg M, Afshari CA, Qualls CW, Jr., Lightfoot-Dunn R and Hamadeh HK (2010) Interference with bile salt export pump function is a susceptibility factor for human liver injury in drug development. *Toxicol Sci* **118**:485-500.

Morgan RE, van Staden CJ, Chen Y, Kalyanaraman N, Kalanzi J, Dunn RT, 2nd, Afshari CA and Hamadeh HK (2013) A multifactorial approach to hepatobiliary transporter assessment enables improved therapeutic compound development. *Toxicol Sci* **136**:216-241.

Noe J, Stieger B and Meier PJ (2002) Functional expression of the canalicular bile salt export pump of human liver. *Gastroenterology* **123**:1659-1666.

Nozawa T, Imai K, Nezu J, Tsuji A and Tamai I (2004) Functional characterization of pH-sensitive organic anion transporting polypeptide OATP-B in human. *J Pharmacol Exp Ther* **308**:438-445.

Oshio C and Phillips MJ (1981) Contractility of bile canaliculi: implications for liver function. *Science (New York, NY)* **212**:1041-1042.

Pfeifer ND, Goss SL, Swift B, Ghibellini G, Ivanovic M, Heizer WD, Gangarosa LM and Brouwer KLR (2013a) Effect of Ritonavir on (99m)Technetium-Mebrofenin Disposition in Humans: A Semi-PBPK Modeling and In Vitro Approach to Predict Transporter-Mediated DDIs. *CPT Pharmacometrics Syst Pharmacol* **2**:e20.

Pfeifer ND, Harris KB, Yan GZ and Brouwer KLR (2013b) Determination of intracellular unbound concentrations and subcellular localization of drugs in rat sandwich-cultured hepatocytes compared with liver tissue. *Drug Metab Dispos* **41**:1949-1956.

Pfeifer ND, Yang K and Brouwer KLR (2013c) Hepatic basolateral efflux contributes significantly to rosuvastatin disposition I: characterization of basolateral versus biliary clearance using a novel protocol in sandwich-cultured hepatocytes. *J Pharmacol Exp Ther* **347**:727-736.

Phillips MJ, Oshio C, Miyairi M, Katz H and Smith CR (1982) A study of bile canalicular contractions in isolated hepatocytes. *Hepatology* **2**:763-768.

Rius M, Hummel-Eisenbeiss J, Hofmann AF and Keppler D (2006) Substrate specificity of human ABCC4 (MRP4)-mediated cotransport of bile acids and reduced glutathione. *Am J Physiol Gastrointest Liver Physiol* **290**:G640-649.

Sato M, Iwanaga T, Mamada H, Ogihara T, Yabuuchi H, Maeda T and Tamai I (2008) Involvement of uric acid transporters in alteration of serum uric acid level by angiotensin II receptor blockers. *Pharm Res* **25**:639-646.

Shitara Y, Li AP, Kato Y, Lu C, Ito K, Itoh T and Sugiyama Y (2003) Function of uptake transporters for taurocholate and estradiol 17beta-D-glucuronide in cryopreserved human hepatocytes. *Drug Metab Pharmacokinet* **18**:33-41.

Smith DA, Di L and Kerns EH (2010) The effect of plasma protein binding on in vivo efficacy: misconceptions in drug discovery. *Nat Rev Drug Discov* **9**:929-939.

Sohlenius-Sternbeck AK (2006) Determination of the hepatocellularity number for human, dog, rabbit, rat and mouse livers from protein concentration measurements. *Toxicol In Vitro* **20**:1582-1586.

Swift B, Pfeifer ND and Brouwer KLR (2010) Sandwich-cultured hepatocytes: an in vitro model to evaluate hepatobiliary transporter-based drug interactions and hepatotoxicity. *Drug Metab Rev* **42**:446-471.

Vildhede A, Mateus A, Khan EK, Lai Y, Karlgren M, Artursson P and Kjellsson MC (2016) Mechanistic Modeling of Pitavastatin Disposition in Sandwich-Cultured Human Hepatocytes: A Proteomics-Informed Bottom-Up Approach. *Drug Metab Dispos* **44**:505-516.

Vildhede A, Wisniewski JR, Noren A, Karlgren M and Artursson P (2015) Comparative Proteomic Analysis of Human Liver Tissue and Isolated Hepatocytes with a Focus on Proteins Determining Drug Exposure. *J Proteome Res* **14**:3305-3314.

Weber C, Gasser R and Hopfgartner G (1999) Absorption, excretion, and metabolism of the endothelin receptor antagonist bosentan in healthy male subjects. *Drug Metab Dispos* **27**:810-815.

Wisniewski JR, Vildhede A, Noren A and Artursson P (2016) In-depth quantitative analysis and comparison of the human hepatocyte and hepatoma cell line HepG2 proteomes. *J Proteomics* **16**:136:234-47.

Wolf KK, Brouwer KR, Pollack GM and Brouwer KLR (2008) Effect of albumin on the biliary clearance of compounds in sandwich-cultured rat hepatocytes. *Drug Metab Dispos* **36**:2086-2092.

Woodhead JL, Yang K, Siler SQ, Watkins PB, Brouwer KLR, Barton HA and Howell BA (2014) Exploring BSEP inhibition-mediated toxicity with a mechanistic model of drug-induced liver injury. *Front Pharmacol* **5**: 240.

Yang K, Guo C, Woodhead JL, St Claire RL, 3rd, Watkins PB, Siler SQ, Howell BA and Brouwer KLR (2016) Sandwich-Cultured Hepatocytes as a Tool to Study Drug Disposition and Drug-Induced Liver Injury. *J pharm Sci* **105**:443-459.

Yang K, Pfeifer ND, Kock K and Brouwer KLR (2015) Species Differences in Hepatobiliary Disposition of Taurocholic Acid in Human and Rat Sandwich-Cultured Hepatocytes: Implications for Drug-Induced Liver Injury. *J Pharmacol Exp Ther* **353**:415-23.

Yang K, Woodhead JL, Watkins PB, Howell BA and Brouwer KLR (2014) Systems pharmacology modeling predicts delayed presentation and species differences in bile acid-mediated troglitazone hepatotoxicity. *Clin Pharmacol Ther* **96**:589-598.

Zhang DW, Gu HM, Vasa M, Muredda M, Cole SP and Deeley RG (2003) Characterization of the role of polar amino acid residues within predicted transmembrane helix 17 in determining the substrate specificity of multidrug resistance protein 3. *Biochemistry* **42**:9989-10000.

Zuber C, Spiro MJ, Guhl B, Spiro RG and Roth J (2000) Golgi apparatus immunolocalization of endomannosidase suggests post-endoplasmic reticulum glucose trimming: implications for quality control. *Mol Biol Cell* **11**:4227-4240.

Supplement

Figure S2.1. Simulated effect of telmisartan at (A) 1 μM and (B) 10 μM on TCA $C_{t,Cells}$ after a 120-min uptake. Simulations were based on cellular total concentration ($[I]_{t,cell}$), cellular unbound concentration ($[I]_{u,cell}$), and cytosolic unbound concentration ($[I]_{u,cyt}$) measured in this study (Table 2.3), and telmisartan inhibition constants (Table 2.1).
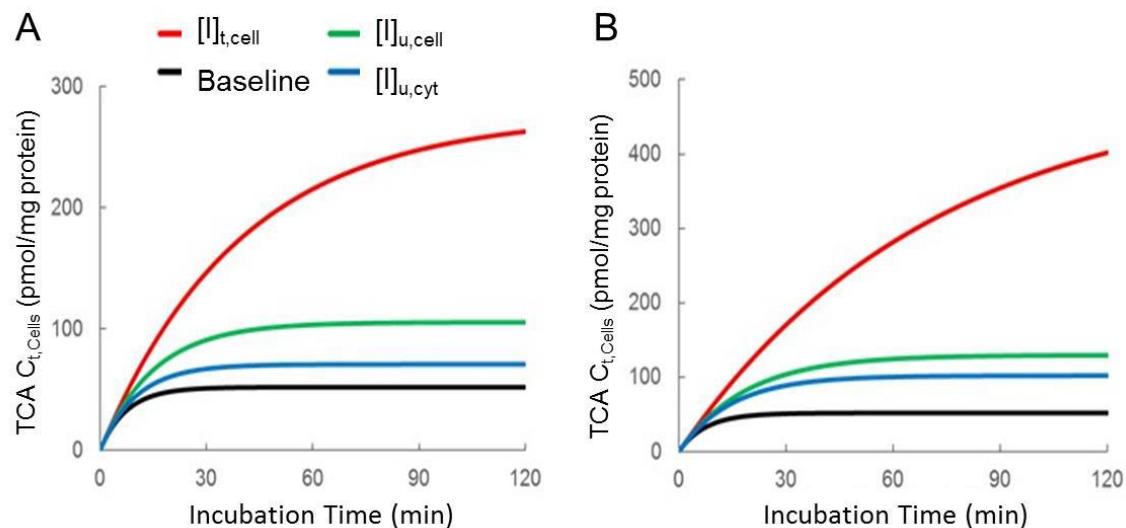
CHAPTER 3. Prediction of Hepatic Efflux Transporter-mediated Drug Interactions: When is it Optimal to Measure Intracellular Unbound Fraction of Inhibitors?[3]

Introduction

Drug interactions (DIs) due to inhibition of hepatic efflux transporters may result in increased hepatic exposure to drugs and endogenous compounds, which may lead to hepatotoxicity. According to regulatory guidance, the prediction of efflux transporter-mediated DIs is based on the half maximal inhibitory concentration (IC_{50}) or inhibition constant, and the concentration of the inhibitor(EMA, 21 June 2012; FDA/CDER, 2012). There is no consensus on which type of inhibitor concentration (total or unbound; plasma or intracellular) is optimal to use in the prediction. Theoretically, the intracellular unbound inhibitor concentration ($[I]_{unbound,cell}$) would be the most relevant concentration for assessing the inhibition of efflux transporters. However, there is no widely accepted method to measure the intracellular unbound fraction of inhibitor in hepatocytes ($f_{u,cell,inhibitor}$). The $f_{u,cell,inhibitor}$ values obtained from the higher-throughput method using hepatocyte or liver homogenate correlated poorly with those obtained from other methods that require incubation with hepatocytes(Riede et al., 2017).

If the benefit of using $[I]_{unbound,cell}$ instead of intracellular total inhibitor concentration ($[I]_{total,cell}$) to predict the inhibitory effect could be determined *a priori*, resources necessary for the measurement of $f_{u,cell,inhibitor}$ could be better allocated. Our previous study suggested that this benefit may vary depending on the characteristics of the inhibitor, such as the ($[I]_{total,cell}$/IC_{50}) value(Guo et al., 2016). In addition,

---

this benefit may depend on other factors, such as the extent of intracellular binding of the inhibitor, simultaneous inhibition of uptake and efflux transporters, and the experimental conditions under which the data were generated. For example, in most *in vitro* inhibition experiments, the dosing solution is protein-free. However, in some studies, the dosing solution contains 4% bovine serum albumin (BSA) to mimic protein binding in plasma (Wolf et al., 2008; Guo et al., 2016). To our knowledge, the impact of using $[I]_{unbound,cell}$ on the prediction results by considering these factors has not been evaluated systematically.

To fill this knowledge gap, we simulated the effect of various theoretical inhibitors on the disposition of a model substrate including the abovementioned factors. Taurocholate (TCA), a prototypical bile acid used for transporter studies, was the model substrate. Based on the simulation results, a framework was developed to categorize "risk" inhibitors for which $[I]_{unbound,cell}$ led to a substantially better prediction of the inhibitory effect than $[I]_{total,cell}$. For these inhibitors, the measurement of $f_{u,cell,inhibitor}$ was optimal. To demonstrate the utility of this framework, 15 experimental compounds were categorized. Experimental data for the inhibitory effect of five compounds (bosentan, ambrisentan, rosuvastatin, ritonavir, troglitazone-sulfate) were compared to the simulation results.

Materials and Methods

Simulation of TCA Intracellular Concentrations

Pharmacokinetic parameters describing TCA disposition in sandwich-cultured human hepatocytes (SCHH) were obtained by mechanistic pharmacokinetic modeling using Phoenix WinNonlin, v6.3 (Certara, Princeton, NJ) (Guo et al., 2016). These kinetic parameters were used to simulate total cellular concentrations of TCA ($[TCA]_{total,cell}$) over time using Berkeley-Madonna v.8.3.11 (University of California at Berkeley, CA).

Simulation of [TCA]$_{total,cell}$ in the Presence of Transporter Inhibitors with Various Degrees of Intracellular Binding

The steady-state [TCA]$_{total,cell}$ in the presence of inhibitors was simulated by using biliary clearance (CL$_{Bile}$) and basolateral efflux clearance (CL$_{BL}$) in the presence of inhibitors, which were estimated using Eq. 1, and assuming the IC$_{50}$ against CL$_{Bile}$ (biliary IC$_{50}$) and IC$_{50}$ against CL$_{BL}$ (basolateral IC$_{50}$) were the same. Uptake clearance (CL$_{Uptake}$) was assumed to be inhibited by 10%, 50% or 90%. Experimental conditions both in the presence and absence of 4% BSA were simulated, consistent with the two different approaches that are used routinely for *in vitro* studies.

The effect of various theoretical inhibitors was simulated by varying the ([I]$_{total,cell}$/IC$_{50}$) value from 0.5 to 60. The effect of considering intracellular binding of inhibitors on the prediction of [TCA]$_{total,cell}$ was assessed by changing f$_{u,cell,inhibitor}$ from 1 to 0.5, 0.2, 0.1, 0.02, or 0.01. The fold change in simulated [TCA]$_{total,cell}$ when f$_{u,cell,inhibitor}$=1 divided by the simulated [TCA]$_{total,cell}$ when f$_{u,cell,inhibitor}$=0.5, 0.2, 0.1, 0.02, or 0.01 was calculated (Equation 2). The corresponding f$_{u,plasma,inhibitor}$ values for the assumed f$_{u,cell,inhibitor}$ values used in the simulations were calculated using the relationship reported by Jones et al. (Jones et al., 2012). This conversion was performed in order to create reference values that the experimental f$_{u,plasma,inhibitor}$ values could be compared with in the following sections. The original equation was rearranged to calculate f$_{u,plasma,inhibitor}$ from f$_{u,cell,inhibitor}$, and it was assumed that the concentration of binding proteins in hepatocytes was one-half of that in plasma (Poulin and Theil, 2000). The parameter values and simulation assumptions are summarized in Table S3.1.

CL$_{Bile}$ or CL$_{BL}$ in the presence of inhibitors = (CL$_{Bile}$ or CL$_{BL}$) / [1+ f$_{u,cell,inhibitor}$ × ([I]$_{total,cell}$/IC$_{50}$)]

(1)

Fold change = ([TCA]$_{total,cell}$ when f$_{u,cell,inhibitor}$=1) / ([TCA]$_{total,cell}$ when f$_{u,cell,inhibitor}$=0.5, 0.2, 0.1, 0.02, or 0.01) (2)

Determination of the "Risk" Inhibitors Based on the ($[I]_{total,cell}/IC_{50}$) Value and Unbound Fraction in Plasma

If the fold change of $[TCA]_{total,cell}$ was > 2, $[I]_{unbound,cell}$ was considered superior to $[I]_{total,cell}$ when predicting inhibitory effects. In this case, the inhibitors were categorized as "risk" inhibitors for which measurement of $f_{u,cell,inhibitor}$ was optimal. This criterion was chosen based on the criterion used in the assessment of clinical DIs. Inhibitors that result in AUCi/AUC > 2 generally are considered as "high risk" for clinically relevant DIs, where $(AUC)_i$ represents area under the plasma drug concentration-time curve (AUC) of the substrate in the presence of inhibitors (Bachmann K and Ekins S, 2012). The lowest ($[I]_{total,cell}/IC_{50}$) value that led to a fold change of $[TCA]_{total,cell}$ >2 was chosen as the cut-off value. A framework based on the ($[I]_{total,cell}/IC_{50}$) and $f_{u,plasma,inhibitor}$ values was proposed.

To demonstrate the utility of this framework, 15 experimental compounds (salicylic acid, doxorubicin, diclofenac, telmisartan, troglitazone-sulfate, rosuvastatin, rifampicin, tolvaptan, DM-4103, DM-4107, sitaxentan, macitentan, ambrisentan, ritonavir, and troglitazone) were classified based on their ($[I]_{total,cell}/IC_{50}$) and $f_{u,plasma,inhibitor}$ values. $[I]_{total,cell}$ of these compounds were measured after 10- to 30-min incubation with SCHH at various dosing concentrations following a 10-min pre-incubation with Ca^{2+}-free Hanks' balanced salt solution, which disrupted the tight junctions for quantification of cellular content (Liu et al., 1999). The IC_{50} and $f_{u,plasma,inhibitor}$ values were obtained from the literature (Table S3.2.). The lowest IC_{50} against efflux transporters was used in the calculation of ($[I]_{total,cell}/IC_{50}$) values in order to be conservative.

Simulation of the Effect of Model Inhibitors on $[TCA]_{total,cell}$ and Comparison with Experimental Results

To verify the simulation results, the effect of five model inhibitors (bosentan, ambrisentan, rosuvastatin, ritonavir, troglitazone-sulfate) on TCA disposition in SCHH was measured and compared

with the simulation results. SCHH were pre-incubated with Hanks' balanced salt solution in the presence or absence of inhibitors for 10- to 30-min, followed by incubation with TCA for 10 min in the presence or absence of inhibitors. $[TCA]_{total,cell}$ at the end of incubation was measured. In addition, the $f_{u,cell,inhibitor}$ values of these inhibitors were measured as described earlier(Pfeifer et al., 2013b; Riede et al., 2017). Simulations of $[TCA]_{total,cell}$ after 10-min uptake were performed using both $[I]_{total,cell}$ and $[I]_{unbound,cell}$ and clearance values in the presence of inhibitors, as described previously (Guo et al., 2016). The average fold error (AFE) comparing the simulation with experimentally observed results was calculated to provide a measure of prediction accuracy, as reported previously (Guo et al., 2016).

Results and Discussion

Simulation of TCA Intracellular Concentrations

Kinetic parameters describing TCA disposition in the presence or absence of 4% BSA are shown in Table S3.3. Simulated $[TCA]_{total,cell}$ reached steady state after 120-min uptake, either in the absence or presence of inhibitors (Yang et al., 2015).

Simulation of $[TCA]_{total,cell}$ in the Presence of Transporter Inhibitors with Various Degrees of Intracellular Binding

Based on a literature review of the unbound fraction measured in hepatocyte homogenate (Figure S3.1.), $f_{u,cell,inhibitor}$ =0.5 to 0.01 were selected to represent various degrees of intracellular binding of inhibitors. $[TCA]_{total,cell}$ was over-predicted using $[I]_{total,cell}$ compared to simulations using $[I]_{unbound,cell}$. The extent of over-prediction was represented as the fold change calculated by Eq. 2, which was always ≥1, as shown in Figure 3.1. The fold change increased at first and then decreased as the ($[I]_{total,cell}/IC_{50}$) value increased from 0.5 to 60. For example, in Figure 3.1D, when ($[I]_{total,cell}/IC_{50}$) was >1.5, the fold change was >2. In this case, $[I]_{unbound,cell}$ was the preferred measure of inhibitor concentration instead of $[I]_{total,cell}$. These inhibitors either accumulate extensively in hepatocytes or are potent inhibitors of efflux

transporters. In addition, the fold change increased as the actual $f_{u,cell,inhibitor}$ decreased (from Figure 3.1A to 1E), indicating that the benefit of using $[I]_{unbound,cell}$ was bigger for inhibitors with greater intracellular binding. The fold change also was affected by the presence of BSA in the medium, shown as the difference between the open squares and solid circles, as well as the inhibition of uptake, which was assumed to be 50% in Fig. 3.1 vs. 10% and 90% in Figure S3.2 and Figure S3.3, respectively.

Determination of the "Risk" Inhibitors Based on the ($[I]_{total,cell}/IC_{50}$) Value and Unbound Fraction in Plasma

The cut-off value of ($[I]_{total,cell}/IC_{50}$) for classifying compounds as "risk" inhibitors was related to several factors, including $f_{u,plasma,inhibitor}$, the inhibition of uptake transporters, and the presence of 4% BSA in the medium (Table 3.1). For inhibitors with $f_{u,plasma,inhibitor}$ >0.33, the fold change calculated by Eq. 2 was always <2. Therefore, there is no benefit in using $[I]_{unbound,cell}$ instead of $[I]_{total,cell}$, regardless of the ($[I]_{total,cell}/IC_{50}$) value. For inhibitors with greater plasma protein binding, the cut-off value of ($[I]_{total,cell}/IC_{50}$) ranged from 1 to 4, assuming the biliary and basolateral IC_{50} values were the same.

The framework to determine the "risk" inhibitors was based on the $f_{u,plasma,inhibitor}$ and ($[I]_{total,cell}/IC_{50}$) values of the inhibitors (Figure 3.2). To be conservative, the lowest ($[I]_{total,cell}/IC_{50}$) cut-off value for inhibitors within the same $f_{u,plasma,inhibitor}$ group in Table 3.1 was used in the framework. The cut-off value of ($[I]_{total,cell}/IC_{50}$) was higher for compounds with a larger $f_{u,plasma,inhibitor}$ value. Out of the fifteen experimental compounds, seven compounds (salicylic acid, doxorubicin, rosuvastatin, ambrisentan, 0.28 µM ritonavir, DM-4103, and DM-4107) were classified as "low-risk" inhibitors, due to the low ($[I]_{total,cell}/IC_{50}$) or high $f_{u,plasma,inhibitor}$ values. For these compounds, the resources necessary for the measurement of $f_{u,cell,inhibitor}$ could be better allocated. Other inhibitors fell into the "risk" category.

This framework is limited by the assumption that biliary IC_{50} and basolateral IC_{50} were the same and the lowest IC_{50} of all efflux transporters was used to calculate the ($[I]_{total,cell}/IC_{50}$) value of the

inhibitor. To assess the impact of differential inhibition of basolateral and biliary efflux clearance, additional simulations were performed by varying the biliary IC_{50} or the basolateral IC_{50} up to 5-fold higher than the other IC_{50} value; in all cases, the lowest IC_{50} was used in the calculation of $([I]_{total,cell}/IC_{50})$. As shown in Table S3.4, when the basolateral IC_{50} was 5-fold higher than the biliary IC_{50}, the simulated fold change in $[TCA]_{total,cell}$ was similar (<2-fold difference) to the original assumption that the IC_{50} values were equal. When the biliary IC_{50} was 5-fold higher than the basolateral IC_{50}, the difference in $[TCA]_{total,cell}$ fold change was more obvious (>2-fold in some cases) compared to the original assumption. These simulations are consistent with expected changes because CL_{Bile} was the primary route of excretion of TCA, and therefore $[TCA]_{total,cell}$ was more sensitive to changes in CL_{Bile}. In this case, the cut-off value of $([I]_{total,cell}/IC_{50})$ should be adjusted, as shown in Table S3.5.

Simulation of the Effect of Model Inhibitors on [TCA]$_{total,cell}$ and Comparison with Experimental Results

The $[I]_{total,cell}$ and experimentally observed fold change in $[TCA]_{total,cell}$ in the presence vs. absence of inhibitors after 10-min uptake are shown in Table S3.6. The simulated and experimentally observed $[TCA]_{total,cell}$ were compared (Table 3.2). For "low-risk" inhibitors, the AFE of the simulations based on $[I]_{total,cell}$ and $[I]_{unbound,cell}$ were both close to 1, indicating both simulations had good prediction accuracy. In contrast, for "risk inhibitors", the AFEs of the simulations based on $[I]_{unbound,cell}$ were much closer to 1 compared to simulations based on $[I]_{total,cell}$. This difference in AFEs suggests that use of $[I]_{unbound,cell}$ results in better prediction accuracy. The difference would be more pronounced at steady state after a longer uptake phase (Guo et al., 2016). These experimental results, albeit for a limited number of compounds, demonstrated the validity of the simulation results and the framework.

Future Work

To evaluate the accuracy of the simulation results, experimental data with more inhibitors are needed. Ideally, $[I]_{total,cell}$ should be measured under the condition that the unbound medium concentration is similar to the clinically relevant unbound plasma concentration. By comparing the prediction results with the experimental data, the specificity and sensitivity of the approach could be calculated. In this study, a fold change of $[TCA]_{total,cell} > 2$ was chosen as the criterion to select the cut-off value of $([I]_{total,cell}/IC_{50})$. This criterion could be adjusted based on the therapeutic window of the substrate and a cut-off value that gives the best specificity and sensitivity. In addition, more data are needed to support the relationship between $f_{u,cell,inhibitor}$ and $f_{u,plasma,inhibitor}$.

Conclusions

In this study, a framework was developed to determine when it is optimal to measure $f_{u,cell,inhibitor}$ to accurately predict the effect of efflux transporter inhibitors on the disposition of TCA, a prototypical bile acid. When the $([I]_{total,cell}/IC_{50})$ value of the inhibitor was > 1 to 2, depending on the extent of plasma protein binding, the follow-up measurement of $f_{u,cell,inhibitor}$ was optimal. The framework was developed based on simulation results and was validated with experimental data.

In addition to bile acids such as TCA, this method could be applied to predict the disposition of other hepatic transporter substrates such as statins, whose therapeutic target is in the liver, or hepatotoxic compounds. Accurate prediction of the hepatocellular concentration of these compounds is important in determining their efficacy and safety.

Professor Sugiyama's research has contributed significantly to the field of pharmacokinetic modeling and simulation, including the role of transporters in drug disposition and transporter-mediated drug interactions. Advances in this field have laid the foundation for this work and will guide the refinement and application of tools to more precisely predict transporter-mediated DIs.

Table 3.1. Cut-off value of ($[I]_{total,cell}/IC_{50}$) to categorize "risk" inhibitors for compounds with various degrees of plasma protein binding. Compounds were categorized as "risk" inhibitors" when ($[I]_{total,cell}/IC_{50}$) was equal to or greater than the cut-off value.

Inhibition of uptake transporters (%)	Presence of 4% BSA in medium	$f_{u,plasma,inhibitor} =$				
		>0.33	0.33-0.11	0.11-0.053	0.053-0.01	0.01-0.005
10	Yes	Low-risk		1.5	1	1
	No		Low-risk	2	1.5	1.5
50	Yes		2	1.5	1	1
	No		4	2	1.5	1.5
90	Yes		2	1.5	1	1
	No		2	1.5	1	1

Table 3.2. Experimentally observed and simulated alteration of $[TCA]_{total,cell}$ due to inhibitors. Sandwich-cultured human hepatocytes were pre-incubated with Hanks' balanced salt solution in the presence or absence of inhibitors [bosentan (0.8 µM), ambrisentan (100 µM), rosuvastatin (2 µM), ritonavir (0.28, 2.8, and 28 µM), or troglitazone-sulfate (0.1 and 0.5 µM)], followed by co-incubation with TCA in the presence or absence of inhibitors for 10 min without BSA (except bosentan). The categorization of the inhibitors was based on the classification system in Fig. 3.2. Simulations of $[TCA]_{total,cell}$ in the presence of inhibitors were performed using $[I]_{total,cell}$ or $[I]_{unbound,cell}$. Average fold error (AFE) of the simulation results compared to experimental observations (shown in Table S3.6) were calculated as described previously (Guo et al., 2016).

Inhibitor	Dosing Concentration (µM)	Classification	$f_{u,cell,inhibitor}$	AFE Compared With Observation Simulations based on:	
				$[I]_{total,cell}$	$[I]_{unbound,cell}$
Bosentan[a]	0.8	Low-risk	0.1	1.3	1.2
Ambrisentan	100	Low-risk	0.067 [b]	1.1	0.97
Rosuvastatin	2	Low-risk	0.13 [c]	0.98	0.95
Ritonavir	0.28	Low-risk	0.006[d]	1.1	0.93
	2.8 and 28	Risk	0.006 [d]	1.7	1.0
Troglitazone-sulfate	0.1 and 0.5	Risk	0.0032 [b]	2.9	1.1

[a]experimental and simulated data were obtained from a previous study with 4% BSA in the dosing solution (Guo et al., 2016)

[b] obtained by incubating SCHH with the compounds, followed by isolating the cytosol and measuring unbound fraction in cytosol using equilibrium dialysis, as reported earlier (Pfeifer et al., 2013b)

[c] obtained from a previous study, where rosuvastatin was incubated with suspended human hepatocytes at 4 °C. The $f_{u,cell,inhibitor}$ was calculated as the medium unbound concentration divided by the total cellular concentration, assuming uptake transporters were not active at 4°C and concentration equilibrium of the unbound drug was achieved between the medium and hepatocytes (Riede et al., 2017).

[d] obtained from a previous study, where ritonavir was incubated with suspended human hepatocytes at a high concentration that blocked the active transport and metabolism. The $f_{u,cell,inhibitor}$ was calculated as the medium unbound concentration divided by the total cellular concentration, assuming the medium unbound concentration was equal to the intracellular unbound concentration (Keemink et al., 2015).

Figure 3.1. Fold change in simulated $[TCA]_{total,cell}$ when $f_{u,cell,inhibitor}=1$ vs. 0.5, 0.2, 0.1, 0.02, or 0.01, assuming the uptake was inhibited by 50%, and biliary IC_{50} and basolateral IC_{50} were the same. Open squares: in the absence of 4% BSA; solid circles: in the presence of 4% BSA. The red horizontal line represents the fold change of 2. The inset table shows the corresponding $f_{u,plasma,inhibitor}$ for each $f_{u,cell,inhibitor}$ calculated as described in Materials and Methods.
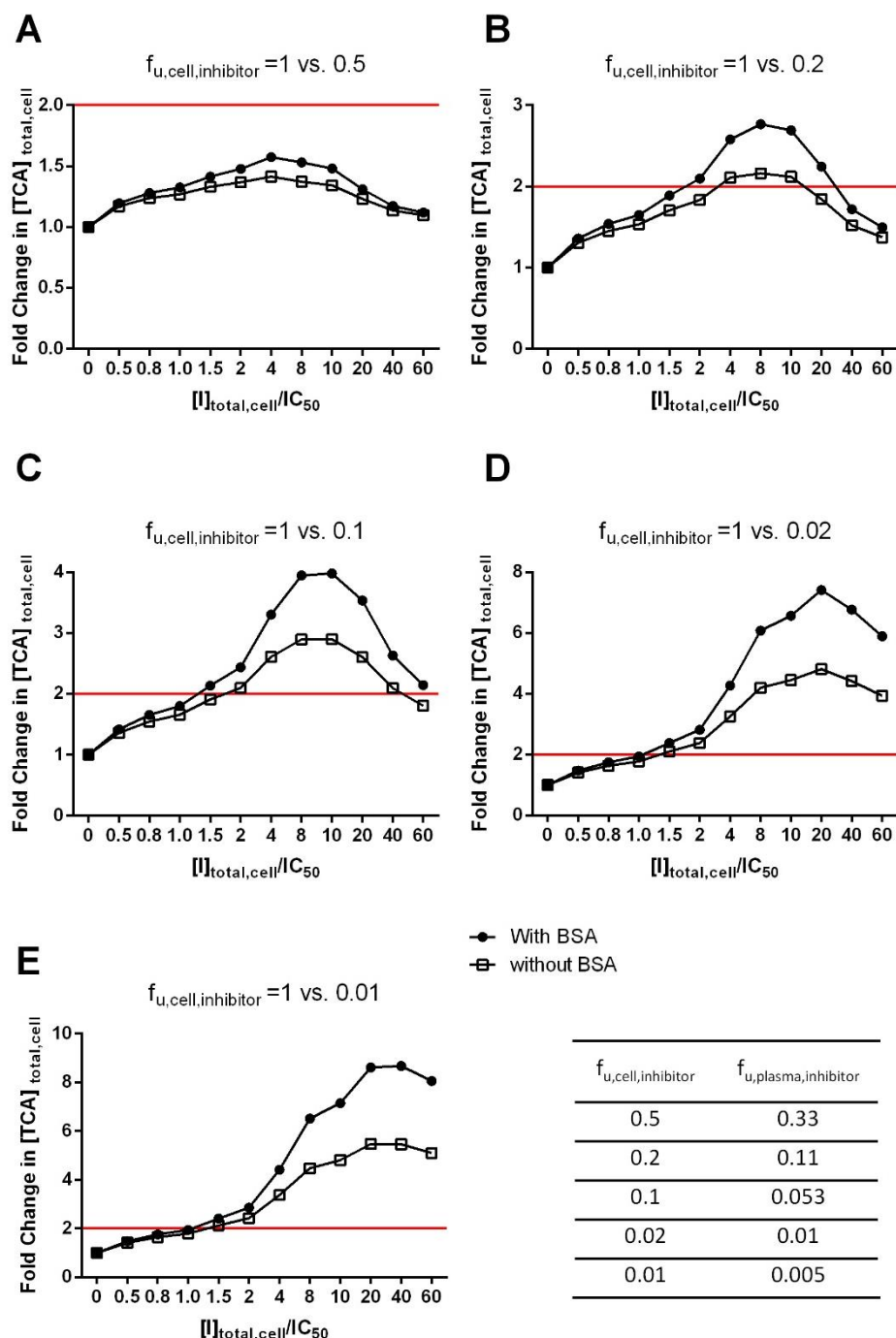
Figure 3.2. A framework to categorize "risk" inhibitors for which the measurement of $f_{u,cell,inhibitor}$ is optimal. The black solid line represents cut-off values of ($[I]_{total,cell}/IC_{50}$) for inhibitors with different $f_{u,plasma,inhibitor}$ values shown in Table 3.1; the lowest ($[I]_{total,cell}/IC_{50}$) cut-off value for inhibitors within the same $f_{u,plasma,inhibitor}$ group was used. Drugs that fall into the upper left quadrant above the solid line (grey shaded area) are classified as "low-risk" inhibitors. Drugs that fall into the lower right quadrant (white area) are considered as "risk" inhibitors and $f_{u,cell,inhibitor}$ should be measured. The color codes represent data from Takeda Pharmaceuticals (red), unpublished in-house data (brown), and publications by Life Technologies (Kimberly Freeman et al., 2009) (green), Qualyst Transporter Solutions (Lepist et al., 2014)(blue), and the Brouwer laboratory(Pfeifer et al., 2013a; Lu et al., 2016) (purple).

- ● salicylic acid 1µM
- ■ doxorubicin 1µM
- ▼ diclofenac 1µM
- ● telmisartan1µM
- ▲ troglitazone-sulfate 0.1µM
- ▼ troglitazone-sulfate 0.5µM
- ■ rosuvastatin 2µM
- ● rifampicin 10µM
- ● tolvaptan 50µM
- □ DM-4103
- ▲ DM-4107
- ▼ sitaxentan 10µM
- ◆ macitentan 10µM
- ○ ambrisentan 100µM
- ● ritonavir 0.28µM
- ▲ ritonavir 2.8µM
- ▼ ritonavir 28µM
- ■ troglitazone 5µM
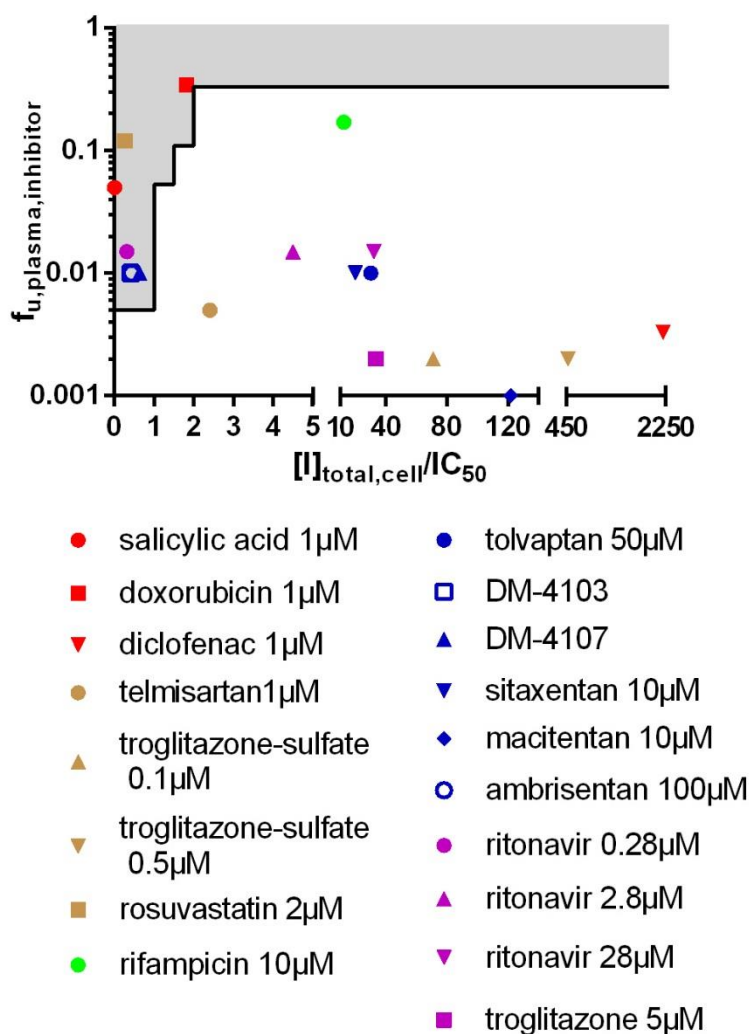
REFERENCES

Bachmann K, Ekins S. The potential of in silico and in vitro approaches to predict in vivo drug-drug interactions and ADMET/TOX properties. In: Williams JA, Lalonde R, Koup JR, Christ DD, eds. Predictive Approaches in Drug Discovery and Development: Biomarkers and In Vitro/In Vivo Correlations. Hoboken, NJ: John Wiley & Sons; 2012:307-331.

EMA (21 June 2012) Guideline on the investigation of drug interactions.

FDA/CDER US (2012) Drug interaction studies - study design, data analysis, and implications for dosing and labeling recommendations, DRAFT GUIDANCE.

Guo C, Yang K, Brouwer KR, St Claire RL, 3rd and Brouwer KL (2016) Prediction of Altered Bile Acid Disposition Due to Inhibition of Multiple Transporters: An Integrated Approach Using Sandwich-Cultured Hepatocytes, Mechanistic Modeling, and Simulation. *J Pharmacol Exp Ther* **358**:324-333.

Jones HM, Barton HA, Lai Y, Bi YA, Kimoto E, Kempshall S, Tate SC, El-Kattan A, Houston JB, Galetin A and Fenner KS (2012) Mechanistic pharmacokinetic modeling for the prediction of transporter-mediated disposition in humans from sandwich culture human hepatocyte data. *Drug Metab Dispos* **40**:1007-1017.

Keemink J, Augustijns P and Annaert P (2015) Unbound ritonavir concentrations in rat and human hepatocytes. *J Pharm Sci* **104**:2378-2387.

Kimberly Freeman , Jonathan Jackson and Ferguson SS (2009) Time-Course Disposition of Ritonavir and Prototypical Hepatic Inducers in Cultures of Primary Human Hepatocytes: Context for Induction & Inhibition Concentration Responses. *16th North American International Society for the Study of Xenobiotics (ISSX) Meeting*:P231, Baltimore, MD.

Lepist EI, Gillies H, Smith W, Hao J, Hubert C, St Claire RL, 3rd, Brouwer KR and Ray AS (2014) Evaluation of the endothelin receptor antagonists ambrisentan, bosentan, macitentan, and sitaxsentan as hepatobiliary transporter inhibitors and substrates in sandwich-cultured human hepatocytes. *PLoS One* **9**:e87548.

Liu X, LeCluyse EL, Brouwer KR, Lightfoot RM, Lee JI and Brouwer KL (1999) Use of Ca^{2+} modulation to evaluate biliary excretion in sandwich-cultured rat hepatocytes. *J Pharmacol Exp Ther* **289**:1592-1599.

Lu Y, Slizgi JR, Brouwer KR, St. Claire RL, Freeman KM, Pan M, Brock WJ and Brouwer KLR (2016) Hepatocellular Disposition and Transporter Interactions with Tolvaptan and Metabolites in Sandwich-Cultured Human Hepatocytes. *Drug Metab Dispos*. 44:867-870.

Pfeifer ND, Goss SL, Swift B, Ghibellini G, Ivanovic M, Heizer WD, Gangarosa LM and Brouwer KL (2013a) Effect of Ritonavir on (99m)Technetium-Mebrofenin Disposition in Humans: A Semi-PBPK Modeling and In Vitro Approach to Predict Transporter-Mediated DDIs. *CPT Pharmacometrics Syst Pharmacol* **2**:e20.

Pfeifer ND, Harris KB, Yan GZ and Brouwer KL (2013b) Determination of intracellular unbound concentrations and subcellular localization of drugs in rat sandwich-cultured hepatocytes compared with liver tissue. *Drug Metab Dispos* **41**:1949-1956.

Poulin P and Theil FP (2000) A priori prediction of tissue:plasma partition coefficients of drugs to facilitate the use of physiologically-based pharmacokinetic models in drug discovery. *J Pharm Sci* **89**:16-35.

Riede J, Camenisch G, Huwyler J and Poller B (2017) Current in vitro Methods to Determine Hepatic Kpuu: a Comparison of Their Usefulness and Limitations. *J Pharm Sci* **106**:2805-2814.

Wolf KK, Brouwer KR, Pollack GM and Brouwer KL (2008) Effect of albumin on the biliary clearance of compounds in sandwich-cultured rat hepatocytes. *Drug Metab Dispos* **36**:2086-2092.

Yang K, Pfeifer ND, Kock K and Brouwer KL (2015) Species differences in hepatobiliary disposition of taurocholic acid in human and rat sandwich-cultured hepatocytes: implications for drug-induced liver injury. *J Pharmacol Exp Ther* **353**:415-423.

Supplement

Table S3.1. Assumptions or parameter values used to simulate $[TCA]_{total,cell}$ in the presence of theoretical inhibitors with various degrees of intracellular binding.

Assumptions and Parameters	Values
Concentration of BSA in uptake buffer (%)	0, 4
Inhibition of uptake transporters (%)	10, 50, 90
$f_{u,cell,inhibitor}$	1, 0.5, 0.2, 0.1, 0.02, 0.01
Theoretical $[I]_{total,cell}/IC_{50}$	0.5-60

Table S3.2. Inhibition constants against TCA efflux transporters and unbound fraction in human plasma of inhibitors ($f_{u,plasma,inhibitor}$) for 15 experimental compounds. The lowest IC_{50} against efflux transporters was used in the calculation of ($[I]_{total,cell}/IC_{50}$) values.

Compound	BSEP IC_{50} (μM)	MRP3 IC_{50} (μM)	MRP4 IC_{50} (μM)	$f_{u,plasma,inhibitor}$	Reference
Salicylic acid	N/A	N/A	1500	0.05	(Johnson and Livingston, 1997)
Doxorubicin	133	N/A	19	0.344	(Terasaki et al., 1984; Morgan et al., 2013)
Diclofenac	N/A	N/A	0.006	0.0033	(El-Sheikh et al., 2007; Obach et al., 2008)
Telmisartan	16	60	11	0.004	(Obach et al., 2008; Morgan et al., 2013; Guo et al., 2016)
Rosuvastatin	133	27	N/A	0.12	(Obach et al., 2008; Morgan et al., 2013)
Troglitazone-sulfate	0.23	N/A	8	0.002 [a]	(Funk et al., 2001)
Ritonavir	1.74	11.1	34	0.015	(Morgan et al., 2013; Patterson et al., 2013)
Troglitazone	1.3	31	61	0.002	(Izumi et al., 1996; Morgan et al., 2013; Yang et al., 2014)
Rifampicin	10.5	69	42	0.2	(Izumi et al., 1996; Obach et al., 2008; Morgan et al., 2013)
Tolvaptan	31	>50	>50	0.01	(Shoaf et al., 2014; Slizgi et al., 2016)
DM-4103	4.15	45	4.3	0.01 [a]	(Slizgi et al., 2016)
DM-4107	119	61	38	0.01 [a]	(Slizgi et al., 2016)
Sitaxentan	25	N/A	N/A	0.01	(Ray et al., 2009; Dhaun et al., 2007)
Macitentan	11.9	N/A	N/A	0.001	(Lepist et al., 2014; Sidharta et al., 2015)
Ambrisentan	288	N/A	N/A	0.01	(Kenna et al., 2015)

BSEP: bile salt export pump; MRP: multidrug resistance-associated protein

IC_{50} values determined using inside-out membrane vesicles were obtained from the literature.

[a] assumed to be the same as the parent compound.

Table S3.3. Kinetic parameters of TCA in sandwich-cultured human hepatocytes in the presence and absence of 4% BSA. Estimates were based on the model scheme published previously (Guo et al., 2016). The model was fit to data generated from n = 3 independent sandwich-cultured human hepatocyte (SCHH) preparations (triplicate measurements) separately. The mean and CV% of estimated parameters from the three SCHH preparations are shown.

Parameters	With 4% BSA		Without 4% BSA	
	Mean [a]	CV%	Mean	CV%
CL_{Uptake} (mL/min/g liver)	0.63	20	8.1	25
CL_{BL} (mL/min/g liver)	0.034	32	0.042	45
CL_{Bile} (mL/min/g liver)	0.074	36	0.094	37
K_{Flux} (min^{-1})	0.018	8	0.049	12

Uptake clearance (CL_{Uptake}); basolateral efflux clearance (CL_{BL}); biliary clearance (CL_{Bile}); rate constant that describes the flux from bile networks into the medium (K_{Flux})

[a] obtained from previous study(Guo et al., 2016)

Table S3.4. Fold change in simulated $[TCA]_{total,cell}$ when $f_{u,cell,inhibitor} = 1$ vs. 0.5, 0.2, 0.1, 0.02, or 0.01, assuming the uptake was inhibited by 50%. Simulations were performed for three scenarios: A) the basolateral IC_{50} was 5-fold higher than the biliary IC_{50}, which was used to calculate the $([I]_{total,cell}/IC_{50})$; B) the basolateral and biliary IC_{50} were the same; C) the biliary IC_{50} was 5-fold higher than basolateral IC_{50}, which was used to calculate $([I]_{total,cell}/IC_{50})$.

$f_{u,cell,inhibitor} = 1$ vs. 0.5						
	With 4% BSA			Without 4% BSA		
$([I]_{total,cell}/IC_{50})$	5-fold higher basolateral IC_{50}	Equal IC_{50}	5-fold higher biliary IC_{50}	5-fold higher basolateral IC_{50}	Equal IC_{50}	5-fold higher biliary IC_{50}
0	1.00	1.00	1.00	1.00	1.00	1.00
0.5	1.14	1.20	1.09	1.12	1.17	1.07
0.8	1.19	1.28	1.12	1.17	1.24	1.10
1	1.22	1.33	1.14	1.19	1.27	1.12
1.5	1.28	1.41	1.19	1.24	1.33	1.16
2	1.33	1.48	1.22	1.27	1.37	1.18
4	1.43	1.57	1.33	1.33	1.41	1.27
8	1.50	1.53	1.46	1.36	1.37	1.35
10	1.51	1.48	1.49	1.36	1.34	1.37
20	1.45	1.31	1.54	1.31	1.23	1.38
40	1.31	1.17	1.44	1.23	1.14	1.32
60	1.23	1.12	1.35	1.17	1.10	1.26
$f_{u,cell,inhibitor} = 1$ vs. 0.2						
	With 4% BSA			Without 4% BSA		
$([I]_{total,cell}/IC_{50})$	5-fold higher basolateral IC_{50}	Equal IC_{50}	5-fold higher biliary IC_{50}	5-fold higher basolateral IC_{50}	Equal IC_{50}	5-fold higher biliary IC_{50}
0	1.00	1.00	1.00	1.00	1.00	1.00
0.5	1.25	1.36	1.15	1.22	1.31	1.13
0.8	1.37	1.54	1.22	1.32	1.45	1.19
1	1.44	1.65	1.26	1.38	1.53	1.23
1.5	1.58	1.89	1.35	1.49	1.71	1.30
2	1.70	2.10	1.44	1.58	1.83	1.37
4	2.04	2.58	1.70	1.80	2.11	1.57

8	2.37	2.77	2.08	1.97	2.16	1.81
10	2.44	2.69	2.22	2.00	2.12	1.89
20	2.47	2.24	2.57	1.97	1.84	2.07
40	2.16	1.72	2.54	1.78	1.52	2.02
60	1.90	1.50	2.32	1.62	1.37	2.16

$f_{u,cell,inhibitor} = 1$ vs. 0.1

	With 4% BSA			Without 4% BSA		
($[I]_{total,cell}/IC_{50}$)	5-fold higher basolateral IC_{50}	Equal IC_{50}	5-fold higher biliary IC_{50}	5-fold higher basolateral IC_{50}	Equal IC_{50}	5-fold higher biliary IC_{50}
0	1.00	1.00	1.00	1.00	1.00	1.00
0.5	1.29	1.42	1.17	1.26	1.36	1.15
0.8	1.44	1.66	1.26	1.39	1.55	1.22
1	1.53	1.80	1.31	1.46	1.66	1.27
1.5	1.73	2.14	1.43	1.62	1.91	1.36
2	1.90	2.44	1.54	1.75	2.10	1.45
4	2.43	3.30	1.91	2.11	2.61	1.73
8	3.06	3.95	2.48	2.45	2.89	2.11
10	3.24	3.98	2.71	2.53	2.90	2.24
20	3.53	3.53	3.41	2.62	2.60	2.62
40	3.23	2.63	3.71	2.42	2.09	2.73
60	2.85	2.15	3.52	2.19	1.80	2.62

$f_{u,cell,inhibitor} = 1$ vs. 0.02

	With 4% BSA			Without 4% BSA		
($[I]_{total,cell}/IC_{50}$)	5-fold higher basolateral IC_{50}	Equal IC_{50}	5-fold higher biliary IC_{50}	5-fold higher basolateral IC_{50}	Equal IC_{50}	5-fold higher biliary IC_{50}
0	1.00	1.00	1.00	1.00	1.00	1.00
0.5	1.33	1.48	1.19	1.30	1.41	1.17
0.8	1.50	1.75	1.29	1.44	1.64	1.25
1	1.62	1.94	1.35	1.53	1.77	1.31
1.5	1.87	2.38	1.50	1.74	2.10	1.42
2	2.11	2.81	1.64	1.92	2.38	1.53

4	2.93	4.27	2.14	2.49	3.26	1.91
8	4.18	6.08	3.02	3.23	4.20	2.50
10	4.65	6.56	3.42	3.49	4.45	2.74
20	6.01	7.41	4.90	4.15	4.81	3.57
40	6.59	6.76	6.31	4.35	4.41	4.27
60	6.38	5.89	6.74	4.20	3.94	4.47
$f_{u,cell,inhibitor} = 1$ vs. 0.01						
	With 4% BSA			Without 4% BSA		
($[I]_{total,cell}/IC_{50}$)	5-fold higher basolateral IC_{50}	Equal IC_{50}	5-fold higher biliary IC_{50}	5-fold higher basolateral IC_{50}	Equal IC_{50}	5-fold higher biliary IC_{50}
0	1.00	1.00	1.00	1.00	1.00	1.00
0.5	1.33	1.48	1.19	1.30	1.42	1.17
0.8	1.51	1.77	1.30	1.45	1.65	1.26
1	1.63	1.95	1.36	1.55	1.79	1.31
1.5	1.90	2.41	1.51	1.76	2.13	1.43
2	2.14	2.86	1.65	1.95	2.43	1.54
4	3.02	4.42	2.18	2.56	3.38	1.94
8	4.40	6.52	3.12	3.39	4.48	2.57
10	4.95	7.16	3.55	3.70	4.81	2.84
20	6.71	8.62	5.25	4.59	5.47	3.79
40	7.87	8.68	7.08	5.09	5.46	4.71
60	7.98	8.06	7.82	5.09	5.11	5.08

Table S3.5. Adjusted cut-off values of ($[I]_{total,cell}/IC_{50}$) to categorize "risk" inhibitors when the biliary IC_{50} was 5-fold higher than the basolateral IC_{50}, assuming the uptake was inhibited by 50%. Compounds were categorized as "risk" inhibitors" when ($[I]_{total,cell}/IC_{50}$) was equal to or greater than the cut-off value.

Presence of 4% BSA in medium	$f_{u,plasma,inhibitor} =$				
	>0.33	0.33-0.11	0.11-0.053	0.053-0.01	0.1-0.005
Yes	Low-risk	8	4	4	4
No		20	8	4	4

The cut-off values were chosen based on the simulated fold changes in $[TCA]_{total,cell}$ that was closest to 2 (Table S3.4). Scenario C (5-fold higher biliary IC_{50}) was the primary focus since the simulated fold changes in $[TCA]_{total,cell}$ in Scenario A and B (Table S3.4) were similar.

Table S3.6. Experimentally measured $[I]_{total,cell}$ and fold change in $[TCA]_{total,cell}$ in the presence of inhibitors. Sandwich-cultured human hepatocytes were pre-incubated with Hanks' balanced salt solution in the presence or absence of the inhibitors [ambrisentan (100 µM), rosuvastatin (2 µM), ritonavir (0.28, 2.8, and 28 µM), or troglitazone-sulfate (0.1 and 0.5 µM)] for 10-30 min, followed by incubation with TCA for 10 min in the presence or absence of inhibitors for 10 min without BSA. $[I]_{total,cell}$ and $[TCA]_{total,cell}$ were measured. Fold changes in the measured $[TCA]_{total,cell}$ in the presence vs. absence of inhibitors are reported.

Inhibitor	Dosing conc. (µM)	$[I]_{total,cell}$ (µM)	Fold change in $[TCA]_{total,cell}$
Ambrisentan	100	125 [a]	0.5 [a]
Rosuvastatin	2	7.1	0.92
Ritonavir	0.28	1.54 [c]	1.0 [b]
	2.8	22.4 [c]	0.76 [b]
	28	158 [c]	0.35 [b]
Troglitazone-sulfate	0.1	16	1.0
	0.5	113	0.65

[a] data obtained from (Lepist et al., 2014)

[b] data obtained from (McRae et al., 2006)

[c] data obtained from (Pfeifer et al., 2013a)

Figure S3.1. Distribution of unbound fraction measured in hepatocyte homogenate ($f_{u,hepatocytes}$). Hepatocellular binding data for 30 compounds were obtained from the literature. Data were included if the unbound fraction was measured in human or rat hepatocyte homogenate using equilibrium dialysis; hepatocytes were incubated with compounds before (Guo et al., 2016; Pfeifer et al., 2013b) or after (Austin et al., 2005; Treiber et al., 2014) homogenization.
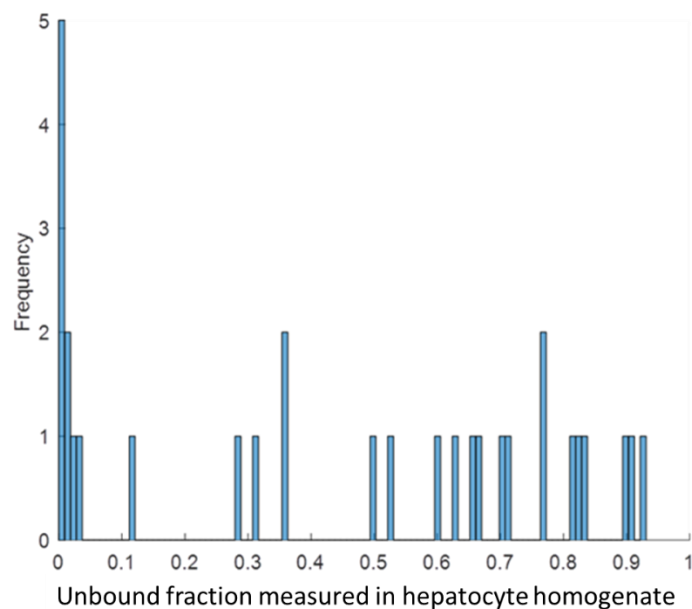
Figure S3.2. Fold change in simulated $[TCA]_{total,cell}$ when $f_{u,cell,inhibitor} = 1$ vs. 0.5 (A), 0.2 (B), 0.1 (C) 0.02 (D), 0.01 (E), assuming the uptake was inhibited by 10%, and CL_{Bile} and CL_{BL} were inhibited to the same extent. The red horizontal line represents the fold change of 2. Open squares: in the absence of 4% BSA; solid circles: in the presence of 4% BSA.
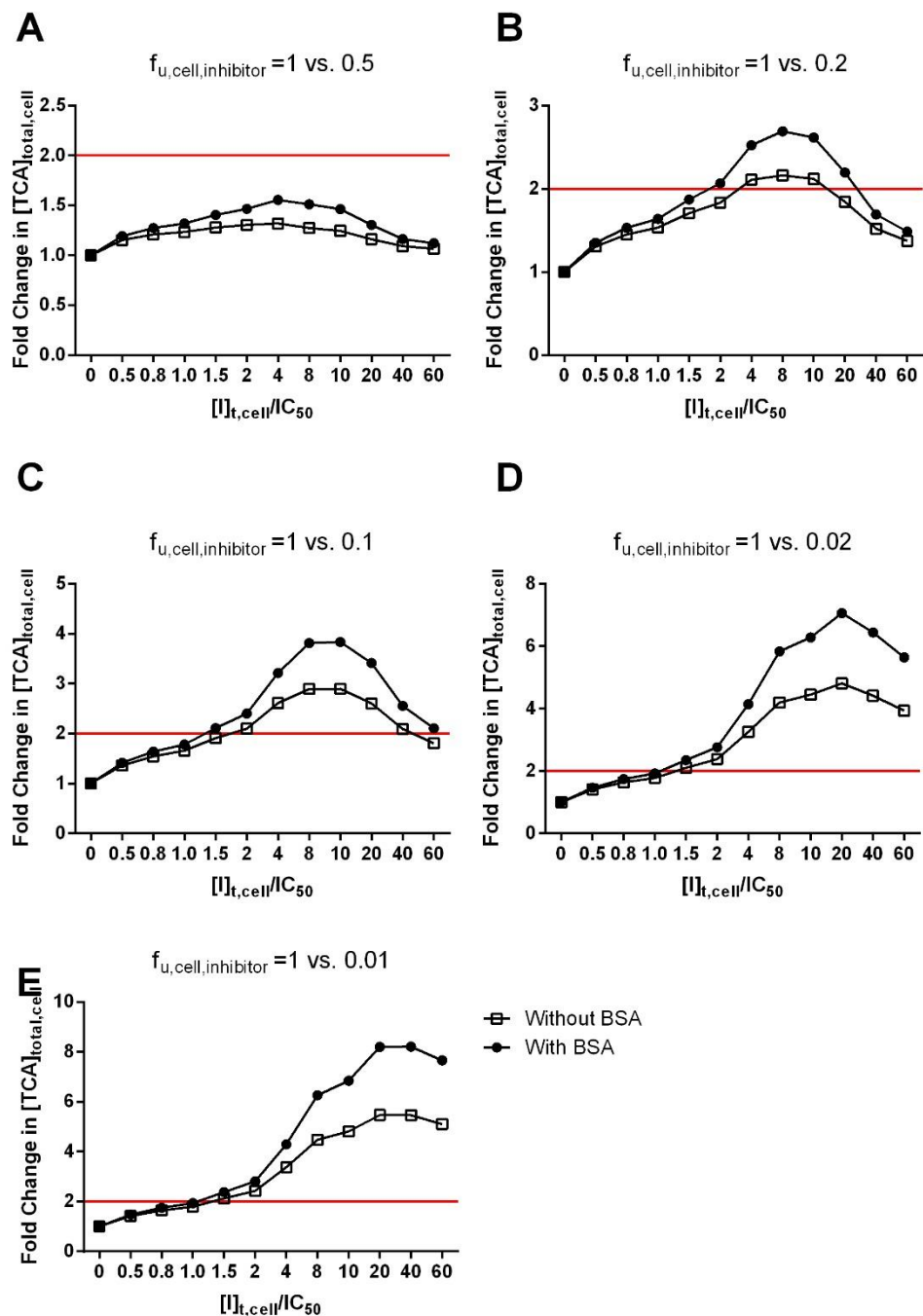
Figure S3.3. Fold change in simulated $[TCA]_{total,cell}$ when $f_{u,cell,inhibitor} = 1$ vs. 0.5 (A), 0.2 (B), 0.1 (C) 0.02 (D), 0.01 (E), assuming the uptake was inhibited by 90%, and CL_{Bile} and CL_{BL} were inhibited to the same extent. The red horizontal line represents the fold change of 2. Open squares: in the absence of 4% BSA; solid circles: in the presence of 4% BSA.
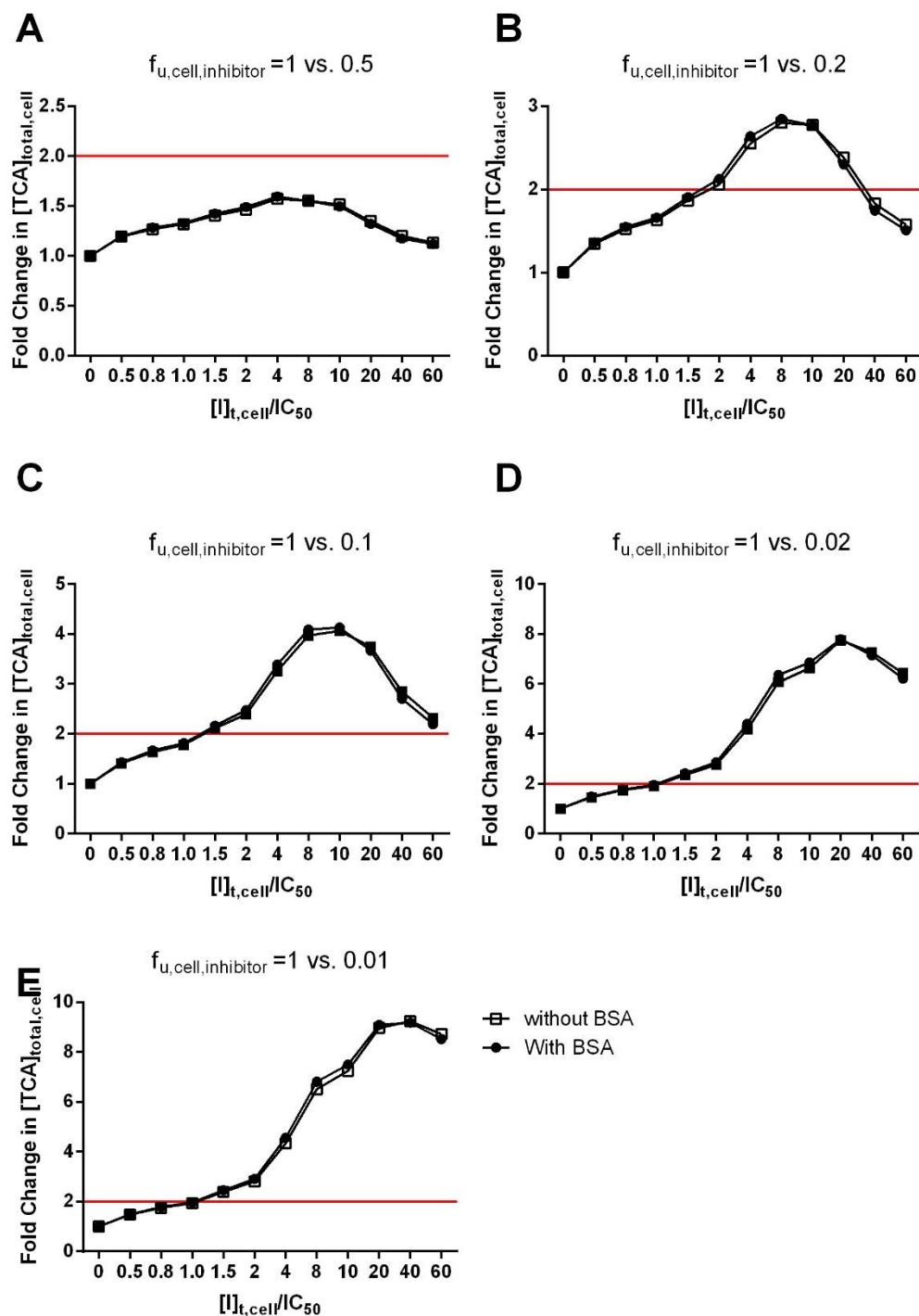
REFERENCES

Austin RP, Barton P, Mohmed S and Riley RJ (2005) The binding of drugs to hepatocytes and its relationship to physicochemical properties. *Drug Metab Dispos* **33**:419-425.

Dhaun N, Melville V, Kramer W, Stavros F, Coyne T, Swan S, Goddard J and Webb DJ (2007) The pharmacokinetic profile of sitaxsentan, a selective endothelin receptor antagonist, in varying degrees of renal impairment. *Br J Clin Pharmacol* **64**:733-737.

El-Sheikh AA, van den Heuvel JJ, Koenderink JB and Russel FG (2007) Interaction of nonsteroidal anti-inflammatory drugs with multidrug resistance protein (MRP) 2/ABCC2- and MRP4/ABCC4-mediated methotrexate transport. *J Pharmacol Exp Ther* **320**:229-235.

Funk C, Ponelle C, Scheuermann G and Pantze M (2001) Cholestatic potential of troglitazone as a possible factor contributing to troglitazone-induced hepatotoxicity: in vivo and in vitro interaction at the canalicular bile salt export pump (Bsep) in the rat. *Mol Pharmacol* **59**:627-635.

Guo C, Yang K, Brouwer KR, St Claire RL, 3rd and Brouwer KL (2016) Prediction of Altered Bile Acid Disposition Due to Inhibition of Multiple Transporters: An Integrated Approach Using Sandwich-Cultured Hepatocytes, Mechanistic Modeling, and Simulation. *J Pharmacol Exp Ther* **358**:324-333.

Izumi T, Enomoto S, Hosiyama K, Sasahara K, Shibukawa A, Nakagawa T and Sugiyama Y (1996) Prediction of the human pharmacokinetics of troglitazone, a new and extensively metabolized antidiabetic agent, after oral administration, with an animal scale-up approach. *J Pharmacol Exp Ther* **277**:1630-1641.

Johnson JA and Livingston TN (1997) Differences between blacks and whites in plasma protein binding of drugs. *Eur J Clin Pharmacol* **51**:485-488.

Kenna JG, Stahl SH, Eakins JA, Foster AJ, Andersson LC, Bergare J, Billger M, Elebring M, Elmore CS and Thompson RA (2015) Multiple compound-related adverse properties contribute to liver injury caused by endothelin receptor antagonists. *J Pharmacol Exp Ther* **352**:281-290.

Lepist EI, Gillies H, Smith W, Hao J, Hubert C, St Claire RL, 3rd, Brouwer KR and Ray AS (2014) Evaluation of the endothelin receptor antagonists ambrisentan, bosentan, macitentan, and sitaxsentan as hepatobiliary transporter inhibitors and substrates in sandwich-cultured human hepatocytes. *PloS one* **9**:e87548.

McRae MP, Lowe CM, Tian X, Bourdet DL, Ho RH, Leake BF, Kim RB, Brouwer KL and Kashuba AD (2006) Ritonavir, saquinavir, and efavirenz, but not nevirapine, inhibit bile acid transport in human and rat hepatocytes. *J Pharmacol Exp Ther* **318**:1068-1075.

Morgan RE, van Staden CJ, Chen Y, Kalyanaraman N, Kalanzi J, Dunn RT, 2nd, Afshari CA and Hamadeh HK (2013) A multifactorial approach to hepatobiliary transporter assessment enables improved therapeutic compound development. *Toxicol Sci* **136**:216-241.

Obach RS, Lombardo F and Waters NJ (2008) Trend analysis of a database of intravenous pharmacokinetic parameters in humans for 670 drug compounds. *Drug Metab Dispos* **36**:1385-1405.

Patterson KB, Dumond JB, Prince HA, Jenkins AJ, Scarsi KK, Wang R, Malone S, Hudgens MG and Kashuba AD (2013) Protein binding of lopinavir and ritonavir during 4 phases of pregnancy: implications for treatment guidelines. *J Acquir Immune Defic Syndr (1999)* **63**:51-58.

Pfeifer ND, Goss SL, Swift B, Ghibellini G, Ivanovic M, Heizer WD, Gangarosa LM and Brouwer KL (2013a) Effect of Ritonavir on (99m)Technetium-Mebrofenin Disposition in Humans: A Semi-PBPK Modeling and In Vitro Approach to Predict Transporter-Mediated DDIs. *CPT Pharmacometrics Syst Pharmacol* **2**:e20.

Pfeifer ND, Harris KB, Yan GZ and Brouwer KL (2013b) Determination of intracellular unbound concentrations and subcellular localization of drugs in rat sandwich-cultured hepatocytes compared with liver tissue. *Drug Metab Dispos* **41**:1949-1956.

Ray A, Tong L, Brouwer K, Melvin L, Hartman JC. Inhibitory effects of ERAs on human and rat hepatic transporters. ET-11: APS International Conference on Endothelin September 9–12, 2009, Montre´al, Canada

Shoaf SE, Bricmont P and Mallikaarjun S (2014) Pharmacokinetics and pharmacodynamics of oral tolvaptan in patients with varying degrees of renal function. *Kidney Int* **85**:953-961.

Sidharta PN, Treiber A and Dingemanse J (2015) Clinical pharmacokinetics and pharmacodynamics of the endothelin receptor antagonist macitentan. *Clin Pharmacokinet* **54**:457-471.

Slizgi JR, Lu Y, Brouwer KR, St Claire RL, Freeman KM, Pan M, Brock WJ and Brouwer KL (2016) Inhibition of Human Hepatic Bile Acid Transporters by Tolvaptan and Metabolites: Contributing Factors to Drug-Induced Liver Injury? *Toxicol Sci* **149**:237-250.

Terasaki T, Iga T, Sugiyama Y and Hanano M (1984) Pharmacokinetic study on the mechanism of tissue distribution of doxorubicin: interorgan and interspecies variation of tissue-to-plasma partition coefficients in rats, rabbits, and guinea pigs. *J Pharm Sci* **73**:1359-1363.

Treiber A, Aanismaa P, de Kanter R, Delahaye S, Treher M, Hess P and Sidharta P (2014) Macitentan does not interfere with hepatic bile salt transport. *J Pharmacol Exp Ther* **350**:130-143.

Yang K, Woodhead JL, Watkins PB, Howell BA and Brouwer KL (2014) Systems pharmacology modeling predicts delayed presentation and species differences in bile acid-mediated troglitazone hepatotoxicity. *Clin Pharmacol Ther* **96**:589-598.

CHAPTER 4. Modeling and Simulation-Guided Study Design for K_i Estimations against Bile Acid Efflux Clearance Values in Hepatocytes

Introduction

Transporter-mediated drug interactions have important implications for drug efficacy and safety. Inhibition of bile acid efflux transporters has contributed to the hepatotoxicity of many drugs such as troglitazone (TGZ) and bosentan (Smith, 2003; Chojkier, 2005). Clinical drug interaction liabilities depend on the potency and the mechanism of inhibition as well as substrate (victim) and inhibitor (perpetrator) concentrations at the site of inhibition (FDA/CDER, 2012). The inhibition potency is represented by the inhibition constant (K_i) or half-maximal inhibition concentration (IC_{50}) values, which are typically obtained from in vitro systems such as transfected cell lines or inside-out membrane vesicles derived from cells that express the protein of interest at high levels. Currently, robust predictions of transporter-mediated drug interactions remain challenging (Pan et al., 2016). Relatively poor model performance could be due to high uncertainty or variability in IC_{50} estimates, biased information generated from overexpressed transporter systems (Balakrishnan et al., 2007), a default assumption of competitive inhibition, and/or incomplete characterization of the transport mechanism of victim compounds, as discussed below. In addition, ambiguity in the relevant inhibitor concentration also contributes to poor model predictions.

Large inter-laboratory variability in K_i or IC_{50} values has been reported for efflux transporters such as, P-glycoprotein (P-gp) (Bentz et al., 2013) (Ellens et al., 2013) (Lee et al., 2014) and bile salt export pump (BSEP) (Kis et al., 2009; Morgan et al., 2013). The variability may be associated with the experimental protocol, the data analysis method, the in vitro systems that express transporters at non-

physiologically relevant levels, and inter-individual differences in the conduct of the experiment (Kis et al., 2009). In an effort to reduce the variability in P-gp IC_{50} estimates using different methods, a modeling-based approach was reported that showed the potential for pharmacokinetic (PK) modeling to improve the estimation of in vitro inhibition potency (Kishimoto et al., 2016). In addition, whole cell systems with physiologically-relevant transporter expression levels are important for generating quality data that can be translated to in vivo.

The inhibition mechanism (e.g., competitive vs. non-competitive) also affects the impact of transporter inhibition. Simulations revealed that noncompetitive inhibition of BSEP resulted in greater bile acid accumulation and potential hepatotoxicity (Woodhead JL et al., 2014). Conventionally, in order to identify the inhibition mechanism and estimate K_i of the inhibitor, in vitro systems are incubated with at least five different substrate concentrations in the presence of at least five different inhibitor concentrations (Ring et al., 2014). These experiments are resource- and labor-intensive. Therefore, it is highly desirable to develop a more efficient method that requires fewer inhibitor and substrate concentrations to identify the inhibition mechanism.

Another prerequisite for accurate model prediction is the complete understanding of transport mechanisms of victim substrates, including which transporters are involved in the disposition and their relative contribution to the overall clearance. These details may not be fully characterized for many compounds. For example, the basolateral efflux of taurocholic acid (TCA) may be mediated by multidrug resistance-associated protein 3 (MRP3), MRP4 (Zhang et al., 2003; Rius et al., 2006) and organic solute transporter α/β (OSTα/β) (Ballatori et al., 2008; Soroka et al., 2010). The relative contribution of each of these transporters is unknown in healthy or diseased hepatocytes. Therefore, it may be more useful to derive the K_i for a clearance pathway (e.g., biliary or basolateral efflux), which

represents a composite K_i for multiple transporters in the same clearance pathway, rather than the K_i for individual transporters.

In light of these knowledge gaps, a novel approach to estimate K_i values combining model-based analysis and data from sandwich-cultured hepatocytes (SCH) was developed in this study. SCH represent a physiologically-relevant whole-cell system that maintains the functionality of multiple transporters and biliary networks (LeCluyse et al., 2000; Yang et al., 2016). In vitro studies using SCH can be resource-intensive, especially considering the limited availability of high quality, transporter competent human hepatocytes. Therefore, a framework was developed to assist the experimentalist in planning the studies in such a way as to obtain robust identification of model parameters, minimize the number of required experiments, and optimize the use of resources. Although modeling and simulation have been used to minimize the experimentation for determining K_i and the inhibition mechanism for CYP enzymes (Kakkar et al., 2000), this approach has not been reported for transporter studies, which oftentimes require a whole-cell system and are more complicated.

In this study, the objective was to provide an optimized study design for, and assess the practicality of, the following hypotheses using modeling and simulation techniques: (1) K_i values for a model inhibitor against the biliary and basolateral efflux clearance values of a model bile acid substrate can be estimated simultaneously using data from rat sandwich-cultured hepatocytes and PK modeling. (2) The inhibition mechanism against the biliary clearance value of the model bile acid can be identified using a single dose of the inhibitor and substrate. TCA was used as the model bile acid because it is a commonly used substrate for in vitro bile acid transport studies and is thought to be metabolically stable (Hofmann and Hagey, 2008). Troglitazone sulfate (TS), the major metabolite of TGZ, was chosen as the model inhibitor because TS is a metabolically stable compound and a strong inhibitor of multiple bile acid transporters (Funk et al., 2001; Nozawa et al., 2004b; Marion et al., 2007; Yang et al., 2015).

Methods

The overall workflow of methods is shown in **Figure 4.1** and **Table 4.1**.

Estimation of TCA Kinetic Parameters

In Step #1, individual mass-time data for TCA disposition in rat SCH from a previous study was used to estimate TCA kinetic parameters (Yang et al., 2015). In the study by Yang et al., rat SCH from three hepatocyte lots were cultured in 6-well plates, pre-incubated for 10 min in Ca^{2+}-containing (standard) or Ca^{2+}-free Hanks' balanced salt solution (HBSS), and the uptake of ^{3}H-TCA (1 µM) in standard HBSS and efflux of ^{3}H-TCA in standard and Ca^{2+}-free HBSS in rat SCH were quantified. The total amount of TCA in Cells+Bile, Cells, and the efflux buffers (standard HBSS and Ca^{2+}-free HBSS) were measured. A mechanistic PK model (scheme depicted in **Figure 4.2**) was fit to the data from individual hepatocyte lots using Phoenix WinNonlin 7.0 (Certara USA, Inc., Princeton, NJ). Differential Equations 1 to 9 described changes in TCA amount over time. Kinetic parameters for TCA in control rat SCH were estimated, including $CL_{Uptake,TCA}$, $V_{max,BL,TCA}$, $V_{max,Bile,TCA}$, and $K_{Flux,TCA}$. The definition and fixed values of variables and parameters are listed in **Table 4.2**. The Michaelis-Menten constants for TCA are shown in **Table 4.3**.

$$\frac{dX^+_{t,Buffer,TCA}}{dt} = CL_{int,BL,TCA} \cdot C^+_{t,Cells,TCA} + K_{Flux,TCA} \cdot X_{t,Bile,TCA} - CL_{Uptake,TCA} \cdot C^+_{t,Buffer,TCA} - K_{Wash} \cdot X^+_{t,Buffer,TCA}$$

$$X^{+\ \circ}_{Buffer,TCA} = X_{dose,TCA} \tag{1}$$

$$\frac{dX^-_{t,Buffer,TCA}}{dt} = \left(CL_{int,BL,TCA} + CL_{int,Bile,TCA}\right) \cdot C^-_{t,Cells,TCA} - CL_{Uptake,TCA} \cdot C^-_{t,Buffer,TCA} - K_{Wash} \cdot X^-_{t,Buffer,TCA}$$

$$X^{-\ \circ}_{Buffer,TCA} = X_{dose,TCA} \tag{2}$$

$$\frac{dX^{+or-}_{t,Cells,TCA}}{dt} = CL_{Uptake,TCA} \cdot C^{+or-}_{t,Buffer,TCA} - \left(CL_{int,BL,TCA} + CL_{int,Bile,TCA}\right) \cdot C^{+or-}_{t,Cells,TCA}$$

$$X^{+or-\ \circ}_{Cells,TCA} = 0 \tag{3}$$

$$\frac{dX_{t,Bile,TCA}}{dt} = CL_{int,Bile,TCA} \cdot C^+_{t,Cells,TCA} - K_{Flux,TCA} \cdot X_{t,Bile,TCA}$$

$$X_{Bile,TCA}^{\circ}=0 \tag{4}$$

$$\frac{dX_{t,Cells+Bile,TCA}}{dt} = \frac{dX_{t,Bile,TCA}}{dt} + \frac{dX_{t,Cells,TCA}^{+}}{dt}$$

$$X_{Cells+Bile,TCA}^{\circ}=0 \tag{5}$$

$$CL_{int,BL,TCA}=\frac{V_{max,BL,TCA}}{K_{m,BL,TCA}+C_{t,Cells,TCA}^{+or-}} \tag{6}$$

$$CL_{int,Bile,TCA}=\frac{V_{max,Bile,TCA}}{K_{m,Bile,TCA}+C_{t,Cells,TCA}^{+or-}} \tag{7}$$

$$C_{t,Cells,TCA}=\frac{X_{t,Cells,TCA}}{V_{Cells}} \tag{8}$$

$$C_{t,Buffer,TCA}=\frac{X_{t,Buffer,TCA}}{V_{Buffer}} \tag{9}$$

Establishment of the TS-TCA Interaction Model

  To simulate the TS-TCA interaction, the disposition and interaction of TS and TCA were described by a PK model shown in **Figure 4.2**. The disposition of TS in rat SCH was simulated using differential equations and mean kinetic parameters of TS described in a previous study (Lee et al., 2010). The rate constants of TS were converted to clearance values and summarized in **Table 4.4**. In the presence of TS, $CL_{int,BL,TCA}^{TS}$, $CL_{int,Bile,TCA}^{TS}$, and $CL_{Uptake,TCA}^{TS}$ were estimated by Equations 10-12 to reflect noncompetitive inhibition of $CL_{int,BL,TCA}^{TS}$ and competitive inhibition of $CL_{int,Bile,TCA}^{TS}$ and $CL_{Uptake,TCA}^{TS}$ based on the current understanding of inhibition mechanisms shown in **Table 4.3**. This PK model was defined as **Model #1**. The definition and fixed values of variables and parameters used in Equations 10-12 are shown in **Table 4.2**. $V_{max,BL,TCA}$, $V_{max,Bile,TCA}$, and $CL_{Uptake,TCA}$ values were fixed at values estimated in Step #1**.** Simulations were performed using Phoenix WinNonlin 7.0 (Certara USA, Inc., Princeton, NJ).

$$CL_{int,BL,TCA}^{TS}=\frac{V_{max,BL,TCA}}{K_{m,BL,TCA}\cdot\left(1+\frac{C_{u,Cells,TS}}{K_{i,BL}}\right)+C_{t,Cells,TCA}^{+or-}\cdot\left(1+\frac{C_{u,Cells,TS}}{K_{i,BL}}\right)} \tag{10}$$

$$CL_{int,Bile,TCA}^{TS}=\frac{V_{max,Bile,TCA}}{K_{m,Bile,TCA}\cdot\left(1+\frac{C_{u,Cells,TS}}{K_{i,Bile}}\right)+C_{t,Cells,TCA}^{+or-}} \tag{11}$$

$$\mathrm{CL}_{\mathrm{Uptake,TCA}}^{\mathrm{TS}} = \frac{\mathrm{CL}_{\mathrm{Uptake,TCA}}}{\left(1+\frac{\mathrm{C_{u,med,TS}}}{\mathrm{K_{i,Uptake}}}\right)} \tag{12}$$

Evaluation of the TS-TCA Interaction Model

To evaluate the predictive performance of the TS-TCA interaction model, TCA disposition in individual rat SCH pre-incubated with TGZ from the study by Yang et al. (Yang et al., 2015) was compared with the corresponding simulation results. Briefly, rat SCH (n=3 hepatocyte lots) were pre-incubated with TGZ (10 µM) for 30 min in standard HBSS; then, rat SCH were incubated for 10 min in standard or Ca^{2+}-free HBSS, followed by uptake of ^{3}H-TCA (1 µM) in standard HBSS and efflux of ^{3}H-TCA in standard and Ca^{2+}-free HBSS, all in the absence of TGZ (**Figure S4.1**). Simulations were performed as described in Step #2 using TCA parameters for each hepatocyte lot (**Table 4.6**). Since the $\mathrm{CL}_{\mathrm{Uptake,TCA}}^{\mathrm{TS}}$ value in these hepatocytes could not be explained by Equation 12 (Yang et al., 2015) and $\mathrm{K}_{\mathrm{Flux,TCA}}^{\mathrm{TS}}$ was unknown, they were fixed to the estimates in the published study (Yang et al., 2015) for the simulations. Most intracellular TGZ was converted to TS during the pre-incubation phase **(Figure S4.1)**, and therefore, the inhibitory effect of TGZ was not considered in the simulations.

Optimization of Study Design

Simulations using PK Model #1 were conducted using various dosing schemes (**Table 4.5**) to assess whether data could be generated for reliable estimation of K_i values (within 2-fold of reference value) and to identify the inhibition mechanism for $\mathrm{CL_{int,Bile,TCA}}$, as described below. The various dosing schemes were selected to include different doses and timing of TS and TCA co-incubation. Restrictions on the dosing schemes were described in the Discussion section. Under each dosing scheme, the amount of TCA and TS in the Cells+Bile (standard HBSS) and Cells (Ca^{2+}-free HBSS) during the uptake and efflux phases, and the amount of TCA and TS in the incubation buffer during the efflux phase were simulated, using mean values of TCA and TS kinetic parameters (**Table 4.4** and **Table 4.6**). The sampling scheme was optimized so that the number of samples was sufficient for parameter estimation,

but ≤ 10 from a practical perspective. Sampling points that were critical for the estimation of $K_{i,BL}$ and $K_{i,Bile}$ were identified based on the partial derivative of a predicted function ($X_{t,Cells,TCA}$, $X_{t,Cells+Bile,TCA}$, $X_{t,Buffer,TCA}$) with respect to each parameter plotted against time. The model was most sensitive to changes in a particular parameter when the derivative was near a maximum or minimum value (Gabrielsson and Weiner, 2007). Simulated data taken at the critical sampling time points were used for subsequent model fitting to estimate K_i values in Step #5 using PK Model #1.

In order to test if the competitive inhibition mechanism of TS against $CL_{int,Bile,TCA}$ could be statistically distinguished from noncompetitive inhibition, the data set simulated by using PK Model #1 (described by Equations 10-12, competitive inhibition of $CL_{int,Bile,TCA}^{TS}$) was fit by both Model #1 and Model #2 (the same as Model #1 except that inhibition of $CL_{int,Bile,TCA}^{TS}$ was assumed to be noncompetitive, as described by Equation 13).

$$CL_{int,Bile,TCA}^{TS}=\frac{V_{max,Bile,TCA}}{K_{m,Bile,TCA} \cdot \left(1+\frac{C_{u,Cells,TS}}{K_{i,Bile}}\right) + C_{t,Cells,TCA}^{+or-} \cdot \left(1+\frac{C_{u,Cells,TS}}{K_{i,Bile}}\right)} \tag{13}$$

If Model #1 described the data better than Model #2, it indicated that the correct inhibition mechanism could be identified. The best-fit model was identified by the Akaike's Information Criterion (AIC) value, CV% for the $K_{i,Bile}$ estimate, and visual inspection of the predictions relative to the observations.

Assessment of the Optimized Study Design in Different Hepatocyte Lots

The best identified study design (i.e., dosing and sampling scheme) was developed based on simulated data using mean parameter values. The utility of this study design was assessed when inter-individual variability was incorporated into the kinetic profiles of TCA and TS. First, using the selected study design, the TS-TCA interaction was simulated using TCA kinetic parameters for three different hepatocyte lots shown in **Table 4.6**. These simulated data were used for model fitting to estimate K_i values and compare the fitting results using Model #1 and Model #2. In addition, each of the seven

kinetic parameters describing TCA and TS disposition (shown in Figure 4.2) was varied by 2-fold (0.5X and 2X) around the mean value, while all other parameters were held constant. Fourteen different sets of data were simulated using these theoretical parameter values and PK Model #1. These simulated data were used for model fitting to estimate K_i values. The study design was selected if $K_{i,BL}$ and $K_{i,Bile}$ estimates were within 2-fold (i.e., <100% difference) of the reference values.

To assess the impact of 2-fold variability in K_i on the simulation results, sensitivity analysis of $K_{i,Bile}$ and $K_{i,BL}$ was performed by varying each of these parameters by 2-fold while all other kinetic parameters were held constant, using the optimal dosing scheme.

Results

Estimation of TCA Kinetic Parameters

The PK model of TCA adequately described the data from the three individual rat SCH lots, with modest but consistent over-prediction of the amount in the cells **(Figure 4.3)**. $V_{max,BL,TCA}$ and $V_{max,Bile,TCA}$ values for the individual data sets were precisely estimated (CV% values were $\leq 21\%$). The CV% for the mean kinetic parameters of TCA varied from 19% and 70% **(Table 4.6)**.

Evaluation of the TS-TCA Interaction Model

Predictions based on the TS-TCA interaction model were generally in accordance with the observed TCA disposition in TGZ pre-treated rat SCH from three different rat hepatocyte donors **(Figure 4.4)**. There was modest but consistent over-prediction of the amount of TCA in the Cells and some under-prediction of the amount of TCA in Standard HBSS for Lot=1.

Optimization of Study Design and Assessment in Different Hepatocyte Lots

Among the dosing schemes shown in **Table 4.5**, only dosing scheme 4 and its corresponding optimal sampling schemes could generate data for reliable K_i estimates in different hepatocyte lots. When the number of samples was constrained to ≤ 10, other dosing schemes failed to provide reliable K_i

estimates in some of the hepatocyte lots assessed. In dosing scheme #4, Cells are pre-incubated with standard or Ca^{2+}-free HBSS for 10 min. Following pre-incubation, cells are dosed with 2 µM of TCA in standard HBSS (uptake phase). After a 20-min TCA uptake phase, 50 µM of TS is added into the TCA-containing incubation buffer for an additional 10-min TCA uptake phase. After the uptake phase, cells are washed for 1 min and then incubated with fresh standard or Ca^{2+}-free HBSS containing 50 µM of TS for 20 min (efflux phase) (**Figure 4.5**). For dosing scheme 4, important sampling times based on **Figure 4.6** included the amount of TCA and TS in cell lysate during the uptake (20, 25, 30 min) and efflux (1, 3, 5, 7, 9, 17, and 19 min) phases, and the amount of TCA and TS in the incubation buffer during the efflux phase (1, 3, 5, 7, 9, 17, and 19 min).

The model fitting results using Model #2 were compared with the results using the correct inhibition mechanism (Model #1). Although AIC values generated by Model #1 were lower than those from Model #2 **(Table 4.7)**, both models were able to describe the data equally well based on visual inspection of the generated curves (**Figure 4.7**). Therefore, data generated using this current study design cannot distinguish the correct inhibition mechanism from other mechanisms.

The variation in both TCA and TS clearance values may affect the identifiability of K_i using the current study design. This is because for different TCA PK profiles, the sensitive regions shown in **Figure 4.6** may differ, or may even be beyond the end of the experiment. In that case, this study design may not be suitable for some hepatocyte lots. This question was addressed in Step #5 and shown in **Table 4.7** and **Figure 4.8**. For the three hepatocyte lots, the differences between the K_i estimates and reference values were within 100% when the correct inhibition mechanism was assumed (Model #1). The CV% for all the parameter estimates in **Table 4.7** were very small, although the parameters estimated using the two models were substantially different. For the 14 hypothetical hepatocyte lots, which were generated when the seven kinetic parameters describing the disposition of TCA and TS were

varied by 2-fold, the differences between the estimated K_i values and reference values were within 100% (**Figure 4.8**). In all cases, the estimated $K_{i,Bile}$ values were greater than the reference values. In general, the estimated $K_{i,BL}$ values were also greater than the $K_{i,BL}$ reference values.

Based on **Figure 4.9**, a 2-fold change in K_i around the reference values (i.e. 0.11-0.46 µM for $K_{i,Bile}$ and 4-16 µM for $K_{i,BL}$) had minimal impact on the predicted $C_{t,Cells,TCA}$ and $C_{t,Cells+Bile,TCA}$.

Discussion

This study generated options for an optimal study design for collecting mass-time data in rat SCH to estimate K_i of TS against biliary and basolateral efflux clearance values of TCA. Through modeling the interaction between TS and TCA, both K_i values in different hepatocyte lots were estimated simultaneously and limitations on accuracy were evaluated. This study highlighted how existing bile acid kinetic data could be leveraged by using modeling and simulation to try to develop efficient experimental protocols for the quantitative analysis of bile acid PK data in SCH.

The optimization and assessment of the study design were based on simulated data using preexisting knowledge of the kinetic parameters of TCA and TS, and the inhibition potency. Assumptions that were made for the modeling and simulation are listed in **Table 4.1**. The justification for, and limitations of, these assumptions are discussed below.

Assumptions about K_m and K_i values were based on the current knowledge of TCA transport mechanisms shown in **Table 4.3**. K_m values were fixed to literature values obtained from membrane vesicles expressing human or rat transporters. K_m values may be affected by the expression level of the transporters (Shirasaka et al., 2008). Transporters other than BSEP and MRP4 may be involved in TCA biliary excretion and basolateral efflux, respectively. Therefore, the K_m values fixed in this study may not represent the true K_m value in rat SCH. In addition, the uptake and basolateral efflux mechanisms of TCA were assumed to be the same for rat and human because data generated with the rodent proteins

were not available. Michaelis-Menten equations were used to describe efflux clearance values in order to estimate K_i and identify inhibition mechanisms for efflux clearance pathways. Linear uptake of TCA was assumed because $C_{t,Buffer,TCA}$ was much lower than the K_m for NTCP, and the estimation of K_i and identifying the inhibition mechanism for $CL_{Uptake, TCA}$ were not the objective of this study.

It was assumed that TCA did not affect the disposition of TS. Based on current knowledge **(Table 4.3)**, the dosing concentration of TCA proposed in this study (2 µM) would not affect the uptake of TS. The inhibitory effect of TCA on Bcrp and basolateral efflux transporters of TS is unknown.

Noncompetitive inhibition of TS against $CL_{int,BL,TCA}$ was assumed based on previously published MRP4 membrane vesicle studies with [^{3}H]-dehydroepiandrosterone sulfate as the substrate (Yang et al., 2014). It is not clear if a substrate-dependent inhibition mechanism exists and if the potential involvement of other hepatic basolateral efflux transporters could affect the inhibition mechanism. In the study by Yang et al., the maximum $C_{t,Cells,TCA}$ for hepatocyte Lots #1-3 was <1 µM (**Figure 4.4**); these concentrations are much lower than $K_{m,BL,TCA}$ (7.7 µM). Thus, $CL_{int,BL,TCA}$ would be expected to be in the linear range and the mechanism of inhibition should have a minimal effect on the prediction results. With higher $C_{t,Cells,TCA}$, it might be possible to differentiate the inhibition mechanisms.

Despite the uncertainty in the assumptions mentioned above, this TS-TCA interaction model could be parameterized to give good agreement between predicted and experimental data in the presence of TGZ (**Figure 4.4**).

As shown in **Figure 4.8**, using the current study design, the accuracy in K_i estimates was modestly sensitive to the variability in TCA and TS kinetics. In all cases, estimated $K_{i,Bile}$ values were higher than the reference value. This may have occurred because $C_{u,Cells,TS}$ was much higher than the reference value for $K_{i,Bile}$, (0.23 µM) when samples were taken. As shown in Figure 4.10, using the optimized dosing scheme (#4), $C_{u,Cells,TS}$ was 0.6 µM at the first sampling point (25 min of uptake

phase). As shown in **Figure 4.9**, $C_{t,Cells,TCA}$ and $C_{t,Cells+Bile,TCA}$ were relatively insensitive to changes in $K_{i,Bile}$ (0.11-0.46 µM) and $K_{i,BL}$ (4-16 µM), indicating the potential challenge in accurately assessing the K_i values in the proposed experiment. Adding additional inhibitor doses should be considered to improve the accuracy of K_i estimation.

There was ambiguity in determining the mechanism of inhibition using the current protocol. None of the dosing schemes assessed in this study were able to clearly differentiate competitive and noncompetitive inhibition against $CL_{int,Bile,TCA}$. As shown in **Figure 4.7**, the optimal study design could not identify the inhibition mechanism in three hepatocyte lots. Therefore, in subsequent studies, only Model #1 was considered. One possible explanation for the challenge in distinguishing the inhibition mechanism is that the intracellular concentrations of TCA and TS did not span a broad enough range, or there was no/minimal overlap when the inhibitor and substrate were both within the critical concentration range. For reliable estimation of K_i values, generally $C_{u,Cells,TS}$ needs to range from 0 to the K_i value (0.23 µM and 8 µM) or higher. Conventionally, $C_{u,Cells,TS}$ that generates approximately 50-80% inhibition is considered the most informative region to determine K_i (Murphy, 2004). A later study showed that K_i estimates based on five inhibitor concentrations that ranged from 0 to the K_i value were sufficient (Zheng and Polli, 2010). To distinguish the inhibition mechanism for $CL_{int,Bile,TCA}$, it is desirable that $C_{t,Cells,TCA}$ spans from $1/5^{th}$ to 5-fold of the $K_{m,Bile,TCA}$ (9.7 µM)(Ring et al., 2014). The timeframe when these criteria were met is shaded in blue and red in **Figure 4.10**. In dosing scheme 2 and 3, there was sufficient overlap between the blue and red shaded areas for an average hepatocyte lot. When experimental and inter-donor variabilities are considered, this overlap might be difficult to achieve. Another possible explanation for the inability to distinguish the inhibition mechanism is that for each substrate concentration, there was only one inhibitor concentration present at that time point, since the intracellular concentrations of TCA and TS were dynamic. This is different from the traditional

approach to determining the mechanism of inhibition in which the inhibitor and substrate concentration at the site of interaction are static, and for each substrate concentration, there are 5 inhibitor concentrations. For future studies, two additional inhibitor and substrate dose levels should be included to obtain information about the inhibition mechanism.

The best currently available study design was identified after examining multiple dosing schemes, as shown in **Table 4.5**. Only dosing scheme 4 was able to generate data that met the following criteria: moderate accuracy of K_i estimates (<2-fold difference) with a reasonable number of sampling points ($\leq$ 10) in hepatocyte lots with variable kinetic profiles of TCA and TS. The dosing schemes were designed based on the following considerations. The length of the efflux phase in standard and Ca^{2+}-free HBSS is limited by 25 min because cell viability begins to decrease after prolonged exposure to Ca^{2+}-free HBSS (Swift et al., 2010). TS is a potent inhibitor of Ntcp and shows high intracellular binding. Thus, obtaining sufficient $C_{u,Cells,TS}$ without diminishing TCA uptake is challenging. To address that issue, in dosing scheme 4, TS was added into the system in the middle of the TCA uptake phase to allow for TCA accumulation in the Cells, which is important for measuring efflux clearance values.

In conclusion, using the best study design identified, K_i values of TS against TCA biliary and basolateral efflux clearance values in rat SCH could be estimated moderately accurately using a single dose of TS and TCA. This optimal study design could not distinguish competitive and noncompetitive inhibition mechanisms; this may require additional dose levels of TS and TCA. Modeling and simulation were helpful in utilizing known PK information for TCA and TS to facilitate the design of effective and efficient studies, which can be applied in future work to generate experimental data from SCH.

Table 4.1. Summary of each step in the Methods and Results. The definition of kinetic parameters are shown in **Table 4.2.**

Step	Data Input	Assumptions	Modeling & Simulation
1. Estimate TCA kinetic parameters	• TCA PK profile in control rat SCH (n=3 hepatocyte lots) [a] • $K_{m,Bile,TCA}$ and $K_{m,BL,TCA}$ [c]	• $K_{m,Bile,TCA}$=K_m of TCA for rat Bsep • $K_{m,BL,TCA}$=K_m of TCA for human MRP4 • Linear uptake and nonlinear efflux clearances	Estimate $CL_{Uptake,TCA}$, $V_{max.BL,TCA}$ and $V_{max,Bile,TCA}$ in each control rat SCH (Table 4.6, Fig. 4.3)
2. Establish TS-TCA interaction model	• TS PK parameters in rat SCH [b] • TCA PK parameters estimated in Step #1 • $K_{i,Bile}$, $K_{i,BL}$, and $K_{i,Uptake}$ [c]	• $K_{i,Bile}$=K_i of TS against Bsep; $K_{i,BL}$=K_i of TS against MRP4; $K_{i,Uptake}$=K_i of TS against Ntcp • Competitive inhibition of $CL_{Uptake,TCA}^{TS}$ and $CL_{int,Bile,TCA}^{TS}$, and noncompetitive inhibition of $CL_{int,BL,TCA}^{TS}$ • No effect of TCA on TS disposition	Simulate the effect of TS on TCA disposition using TCA clearance values calculated by Eqs. 10-12 and model structure in Fig. 4.2.
3. Evaluate TS-TCA interaction model	TCA PK profile in rat SCH pre-incubated with TGZ, and corresponding $CL_{Uptake,TCA}^{TS}$ and $K_{Flux,TCA}^{TS}$ values (n=3 hepatocyte lots) [a]	• During pre-incubation, all the TGZ was converted to its metabolites, mainly TS • $CL_{Uptake,TCA}^{TS}$ and $K_{Flux,TCA}^{TS}$ values in SCH pre-incubated with TGZ cannot be described by Eq. 12; therefore, literature values were used [a]	• Simulate the effect of TGZ pre-incubation on TCA disposition using Eqs. 10-11, and $CL_{Uptake,TCA}^{TS}$ and $K_{Flux,TCA}^{TS}$ values reported [a] • Compare simulated data with experimental observations [a] (Fig. 4.4)
4. Optimize the study design	• Mean values of TCA (Step #1) and TS parameters in control rat SCH [b] • Various dosing schemes	The study design is considered to be "optimal" if it can generate data for reliable estimation of K_i values (within 2-fold of reference value) in an average hepatocyte lot	• Simulate TS effect on TCA disposition using various dosing schemes (Table 4.5) • Fit the TS-TCA interaction model to the simulated PK profiles • Optimize the sampling scheme (Fig. 4.6)

			• Select the optimal study design (Fig. 4.5)
5. Assess the utility of the optimized protocol in individuals with variable TCA and/or TS PK profiles	• TCA PK parameters from 3 different lots of control rat SCH estimated in Step #1 • Mean values of TCA (Step #1) and TS PK parameters [b]	The study design is optimal if it can generate data for reliable estimation of K_i values (within 2-fold of reference value) in different lots of SCH with variable TCA and TS PK profiles	• Simulate TCA PK profiles using the optimized study design in 3 different lots of rat SCH • Simulate TCA PK profiles when TCA and TS PK parameters are varied by 2-fold around the mean value • Fit the TS-TCA interaction model to each of the simulated PK profiles (Fig. 4.7, 4.8, Table 4.7) • Assess whether the optimized protocol remains optimal in these individual lots of rat SCH

[a] (Yang et al., 2015)

[b] (Lee et al., 2010)

[c] Table 4.3

Table 4.2. Definition of variables and parameters in Equations 1-12.

Category	Name	Definition
Dependent variables	$C_{t,Cells,TCA}$	Total concentration of TCA in the Cells
	$C_{t,Buffer,TCA}$	Total concentration of TCA in the Buffer
	$X_{t,Cells,TCA}$	Total amount of TCA in Cells
	$X_{Cells+Bile,TCA}$	Total amount of TCA in Cells+Bile
	$X_{t,Bile,TCA}$	Total amount of TCA in Bile
	$C_{u,Cells,TS}$	Unbound intracellular concentration of TS, which equals the product of the total intracellular concentration and the intracellular unbound fraction [a]
	$C_{u,med,TS}$	Unbound medium concentration of TS, which is equivalent to the total concentration due to the absence of protein in the medium
Superscripts	"+" and "-"	Ca^{2+}-containing (standard) HBSS and Ca^{2+}-free HBSS, respectively
	"TS"	Parameter values in the presence of TS
Kinetic parameters	$CL_{Uptake,TCA}$	Uptake clearance of TCA, assumed to be linear
	$CL_{int,BL,TCA}$	Intrinsic basolateral efflux clearance of TCA, assumed to be nonlinear (Michaelis-Menten)
	$CL_{int,Bile,TCA}$	Intrinsic biliary clearance of TCA, assumed to be nonlinear (Michaelis-Menten)
	$K_{Flux,TCA}$	First-order rate constant that describes the flux of TCA from bile networks into the medium [b]
	$V_{max,BL,TCA}$	Maximum velocity for $CL_{int,BL,TCA}$
	$V_{max,Bile,TCA}$	Maximum velocity for $CL_{int,Bile,TCA}$
	$K_{m,BL,TCA}$	TCA concentration at one-half $V_{max,BL,TCA}$, fixed at 7.7 μM [c]
	$K_{m,Bile,TCA}$	TCA concentration at one-half $V_{max,Bile,TCA}$, fixed at 9.7 μM [d]
	$CL_{Uptake,TS}$	Uptake clearance of TS, assumed to be linear
	$CL_{int,BL,TS}$	Intrinsic basolateral efflux clearance of TS, assumed to be linear
	$CL_{int,Bile,TS}$	Intrinsic biliary clearance of TS, assumed to be linear
System-specific parameters	V_{Cells}	Volume of cellular compartment, fixed depending on the protein content of each preparation [e]
	V_{Buffer}	Volume of buffer compartment, fixed at 1.5 mL/well
	K_{wash}	Wash term to remove TCA at the end of the uptake phase, activated for 1 min and fixed at 5×10^4 min^{-1}
	$X_{dose,TCA}$	Total amount of TCA added in the incubation buffer, which is the product of dosing concentration of TCA and V_{Buffer}
	$K_{i,Uptake}$	Inhibition constant (K_i) of TS on $CL_{Uptake,TCA}$, fixed at 2.3 μM [f]

Inhibition constants	$K_{i,BL}$	K_i of TS on $CL_{int,BL,TCA}$, fixed at 8 µM [g]
	$K_{i,Bile}$	K_i of TS on $CL_{int,Bile,TCA}$, fixed at 0.23 µM [h]

[a] set at 0.003, assumed to be the same as the intracellular unbound fraction of TS in human hepatocytes (Guo et al., 2017; Riccardi et al., 2018)

[b] (Lee et al., 2010; Pfeifer et al., 2013; Yang et al., 2015)

[c] assumed to be the same as the K_m for human MRP4 determined in membrane vesicles (Table 4.3)

[d] assumed to be the same as the K_m for rat Bsep determined in membrane vesicles (Table 4.3)

[e] ranged from 5.5-7.6 µL/well for hepatocyte Lot#1-3 cultured in 6-well plates. An average value of 6.4 µL/well was used for simulation.

[f] assumed to be the same as the IC_{50} of TGZ for rat Ntcp (Table 4.3)

[g] assumed to be the same as the K_i of TS for human MRP4 determined in membrane vesicles (Table 4.3)

[h] assumed to be the same as the K_i of TS for rat Bsep determined in membrane vesicles (Table 4.3)

Table 4.3. Parameter values describing the interaction of TCA and TS with human or rat bile acid and TS transporters. The inhibition mechanism was assumed to be competitive for all parameters unless indicated otherwise.

Compound	Role	Uptake	Basolateral Efflux	Biliary
TCA	Substrate	NTCP (K_m=5-20 µM, 70% of total clearance) OATP1B (K_m=5.8-72 µM, 30% of total clearance) [a]	MRP3 (K_m=30 µM), MRP4 (K_m=7.7 µM) [e]	Bsep (K_m=9.7 µM) [g]
	Inhibitor	OATP1B1 (K_i=11.4 µM)[b]		
TS	Inhibitor	Ntcp (IC_{50}=2.3 µM) [c], OATP1B1 and OATP1B3 (IC_{50}<10 µM) [d]	MRP4 (K_i=8 µM, noncompetitive) [f]	Bsep (K_i=0.23 µM) [h]
	Substrate	OATP1B1 and OATP1B3 [d]		Bcrp [i]

[a] (Shitara et al., 2003; Nozawa et al., 2004a; Mita et al., 2006)

[b] (Gui et al., 2009)

[c] Assumed to be the same as TGZ (Marion et al., 2007)

[d] (Nozawa et al., 2004b)

[e] (Rius et al., 2006)

[f] (Yang et al., 2015)

[g] (Hayashi et al., 2005)

[h] (Funk et al., 2001)

[i] (Enokizono et al., 2007)

Table 4.4. Kinetic parameters of TS in rat SCH cultured in 6-well plates.

Kinetic Process	Rate constant (min^{-1})[a]	Clearance (µL/min/6 well)[b]	CV (%)
$CL_{Uptake,TS}$	0.004	6	36
$CL_{int,BL,TS}$	0.018	0.11	39
$CL_{int,Bile,TS}$	0.035	0.21	21

[a] published by (Lee et al., 2010)

[b] Efflux clearance values were calculated as the product of the rate constant and 6.4 (µL/well), which is V_{Cells}; Uptake clearance values were calculated as the product of the rate constant and 1500 (µL/well), which was V_{Buffer}.

Table 4.5. Different dosing schemes assessed in this study. The time period that each compound was present in the incubation system is noted in parentheses. A 1-min wash phase was included between the uptake and efflux phases.

Dosing Scheme	Compound	Dose (time)	
		Uptake	Efflux
1	TCA	5 µM (0-20min)	
	TS	10 µM (10-20min)	10 µM (21-41min)
2	TCA	5 µM (0-20 min)	
	TS		50 µM (21-41 min)
3	TCA	5 µM (0-30min)	
	TS	50 µM (20-30 min)	50 µM (31-51min)
4	TCA	2 µM (0-30min)	
	TS	50 µM (20-30 min)	50 µM (31-51min)

Table 4.6. Parameter estimates (CV%) of TCA obtained by fitting PK Model #1 to the published data from control rat SCH (Yang et al., 2015). Data from three different rat hepatocyte donors are designated as Lots 1-3.

Parameter	Unit	Lot=1	Lot=2	Lot=3	Mean	CV (%)
$CL_{Uptake,TCA}$	μL/min/well	15 (14%)	11 (6.5%)	6.4 (10%)	11	41
$V_{max,BL,TCA}$	pmol/min/well	34 (2.9%)	15 (2.7%)	8.1 (9.3)	19	70
$K_{m,BL,TCA}$	μM	7.0 (FIXED)			7.0	N/A[a]
$V_{max,Bile,TCA}$	pmol/min/well	17 (21%)	12 (9.3%)	16 (9.5%)	15	19
$K_{m,Bile,TCA}$	μM	9.7 (FIXED)			9.7	0
$K_{Flux,TCA}$	min^{-1}	0.071 (15%)	0.057 (10%)	0.057 (14%)	0.053	N/A[a]

[a]N/A, not available

Table 4.7. Best-fit parameters (µM) for TS and associated AIC values for competitive (Model #1) or noncompetitive (Model #2) inhibition of $CL_{int,Bile,TCA}$ using the simulated TCA profile from three different lots of hepatocytes.

Inhibition of $CL_{int,Bile,TCA}^{TS}$		Lot=1		Lot=2		Lot=3		Reference Value
		Model #1	Model #2	Model #1	Model #2	Model #1	Model #2	
$K_{i,BL}$	Estimate	6.7	5.9	13.0	14.4	13.6	15.3	8
	CV (%)	0.63	0.67	2.9	5.4	6.6	7.9	
$K_{i,Bile}$	Estimate	0.46	0.59	0.40	0.65	0.41	0.58	0.23
	CV (%)	0.70	0.73	2.4	4.1	3.7	5.6	
AIC		-169	-156	11	38	-0.01	12	

Figure 4.1. Workflow of the methods. The definition of kinetic parameters are shown in Table 4.2. Green and blue boxes represent data input and modeling & simulations, respectively. If Step #5 shows that the optimized study design is not useful different hepatocyte lots, Step #4 will be repeated for a different dosing scheme.
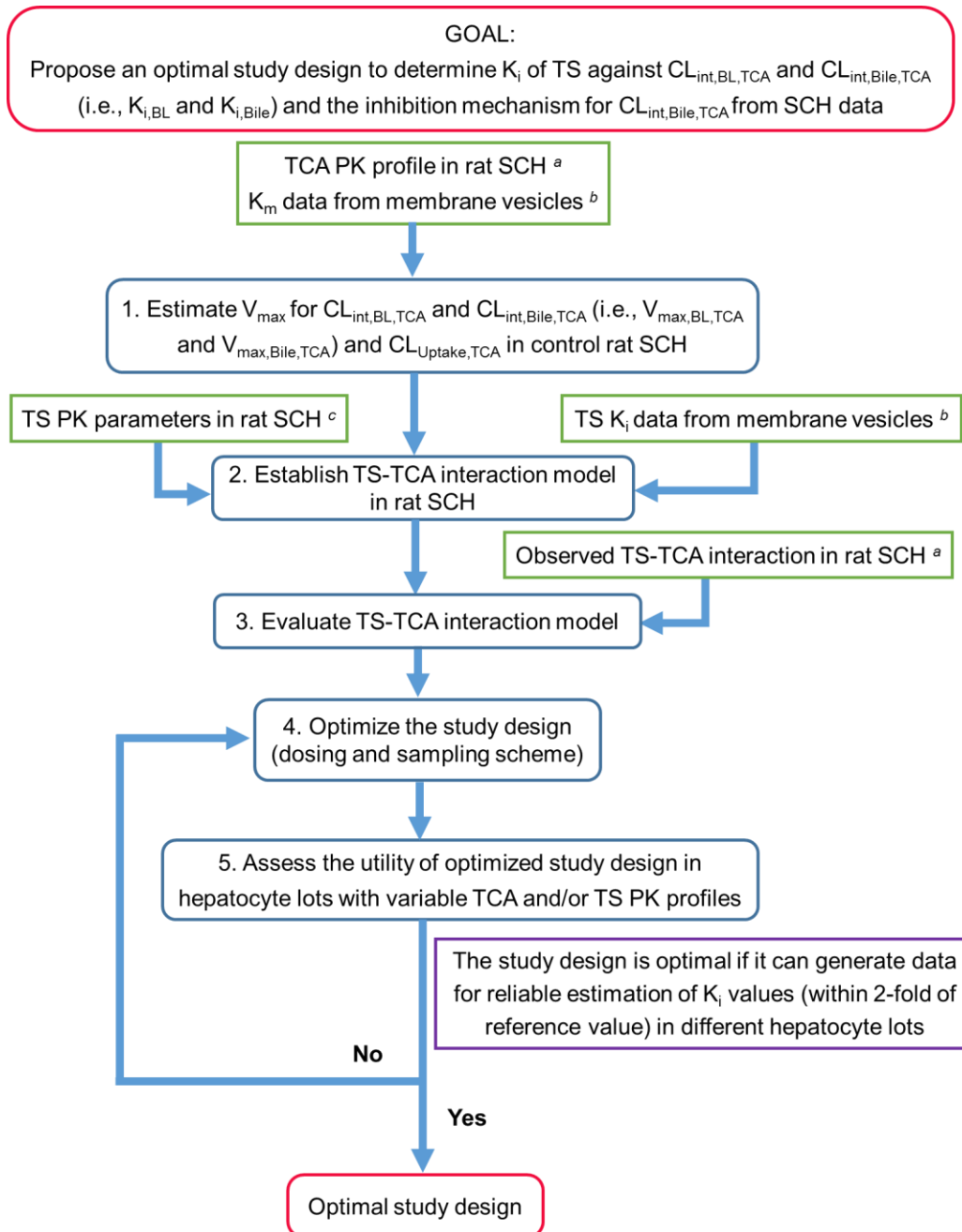
[a] (Yang et al., 2015)

[b] Published data as shown in Table 4.3

[c] (Lee et al., 2010)

Figure 4.2. Model schemes depicting the disposition of TCA and interaction of TS and TCA in rat SCH. The model structure for TCA in standard HBSS and Ca^{2+}-free HBSS was adapted from a previous study (Guo et al., 2016). The model structure for TS in Ca^{2+}-free HBSS was adapted from a previous study (Lee et al., 2010). CL_{Uptake}, $CL_{int,BL}$, and $CL_{int,Bile}$ represent the uptake clearance, intrinsic basolateral efflux clearance, and intrinsic biliary clearance, respectively. K_{Flux} represents the flux from bile networks into the medium. $CL_{int,BL,TCA}$ and $CL_{int,Bile,TCA}$ are inhibited by TS in the cell, shown in red; $CL_{Uptake,TCA}$ is inhibited by TS in the medium, shown in blue.
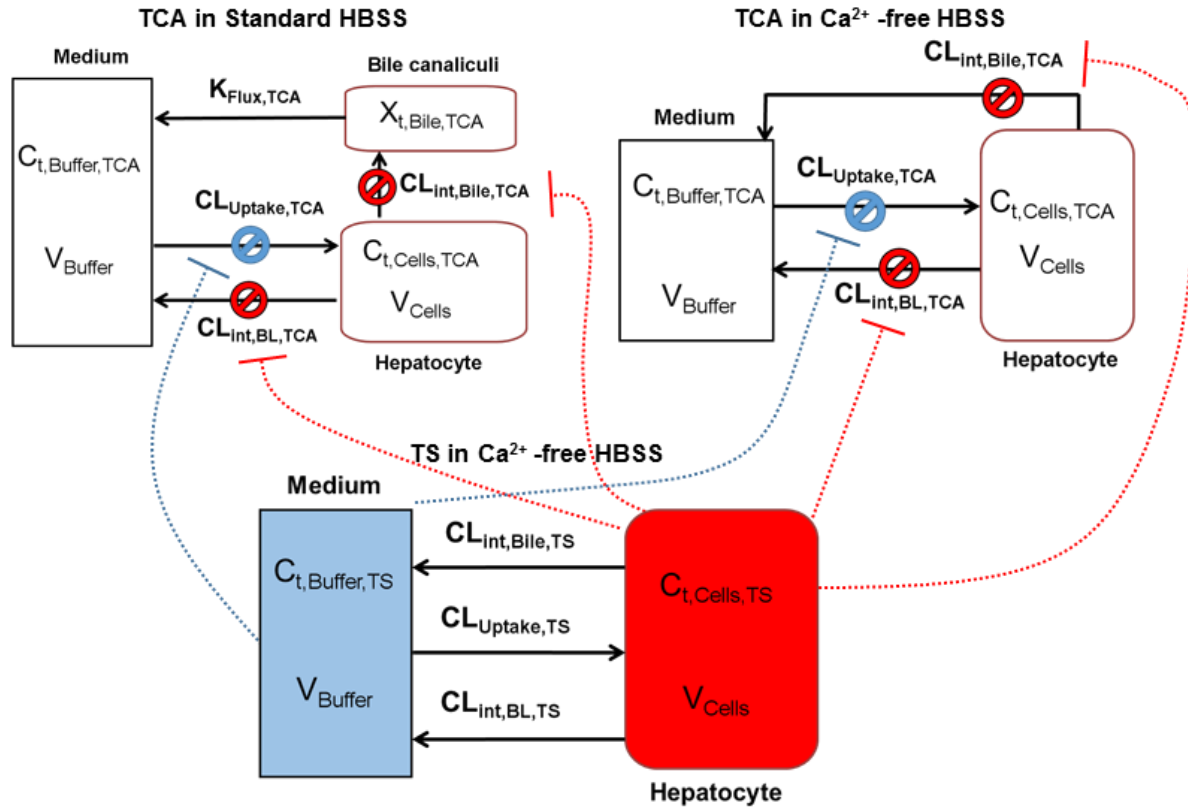
Figure 4.3. Observed (symbols) and model-fitted (solid lines) TCA amount vs. time in control rat SCH. Data from three different rat hepatocyte donors (Lots=1-3) are presented in black, blue, and orange.
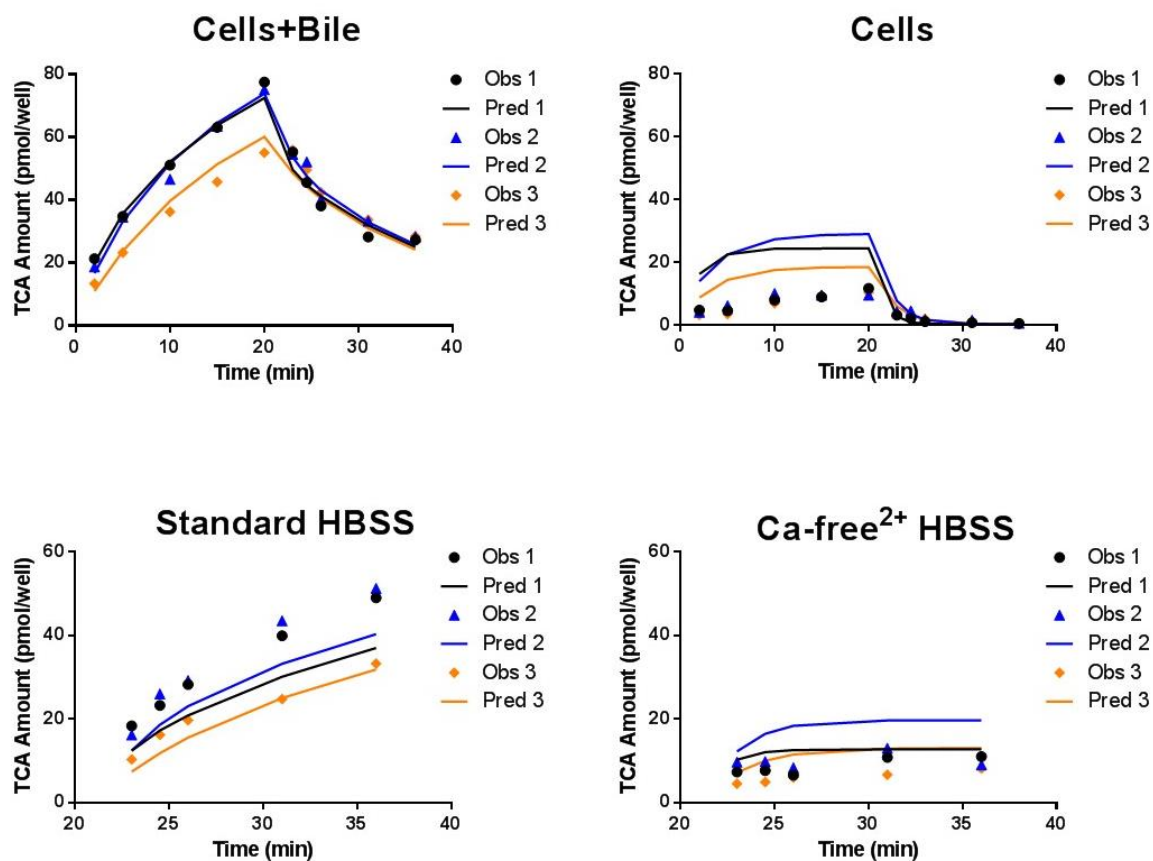
Figure 4.4. Observed (symbols) and model-simulated (solid lines) TCA amount vs. time in rat SCH after 30-min pre-incubation with TGZ. Data from three different rat hepatocyte donors (Lot=1-3) are presented in black, blue, and orange.
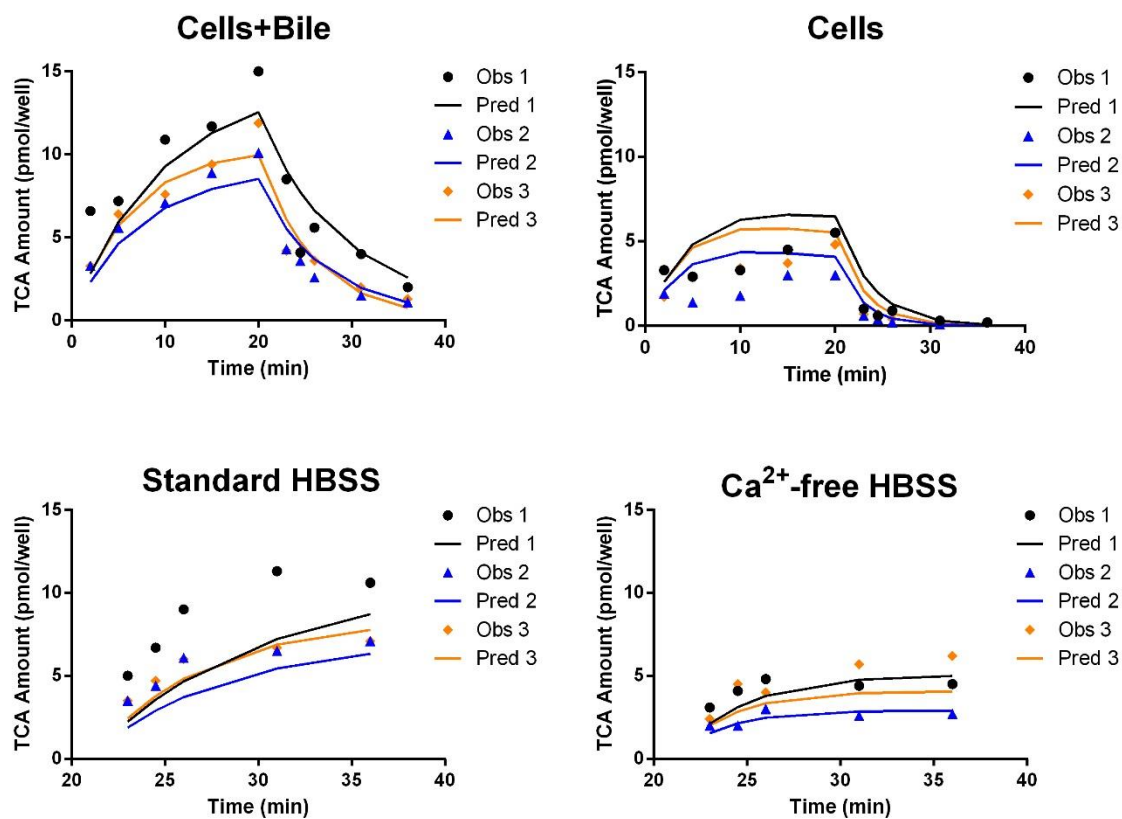
Figure 4.5. Optimal dosing and sampling scheme to generate data for the estimation of $K_{i,BL}$ and $K_{i,Bile}$ for TS using TCA as the substrate in rat SCH. Sampling time points include 20, 25, and 30 min in the uptake phase and 1, 3, 5, 7, 9, 17, and 19 min in the efflux phase.
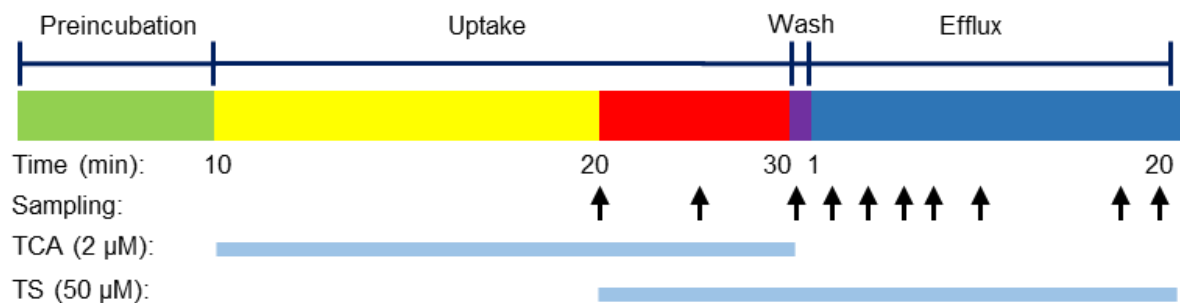
Figure 4.6. Model-predicted partial derivative plots of TCA amount in different compartments with respect to $K_{i,Bile}$ (red line, left y-axis) and $K_{i,BL}$ (black line, right y-axis) vs. time for TS-TCA interaction model using the mean kinetic parameters and the optimal dosing scheme (#4). Yellow circles indicate where sampling is critical for reliable estimation of the parameters.
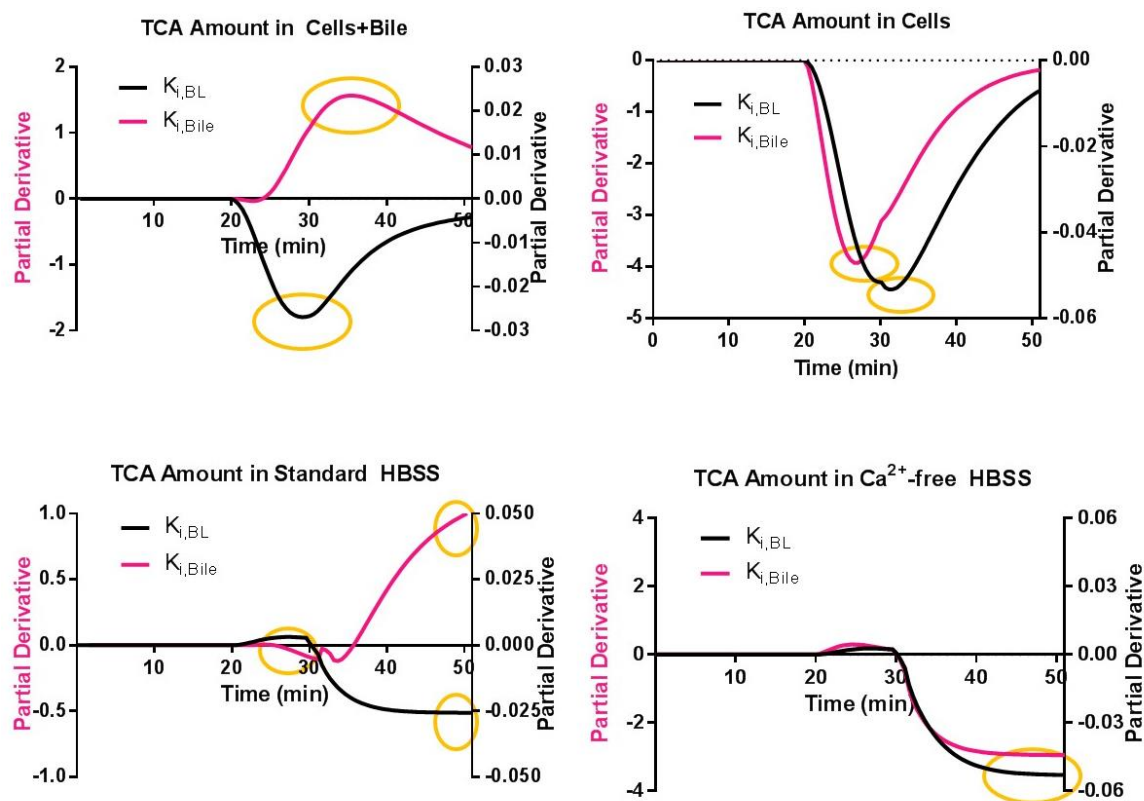
Figure 4.7. Observed (symbols) vs. model-fitted (solid lines) amount of TCA in different compartments. (A) Modeling fitting using PK Model #1 (noncompetitive inhibition against $CL_{int,BL,TCA}^{TS}$ and competitive inhibition against $CL_{int,Bile,TCA}^{TS}$); (B) Model fitting using PK Model #2 (noncompetitive inhibition against $CL_{int,BL,TCA}^{TS}$ and $CL_{int,Bile,TCA}^{TS}$)The optimal study design was used to generate the data. The yellow, red and blue bars at the top represent the uptake phase without inhibitor, the uptake phase with inhibitor, and the efflux phase, respectively.
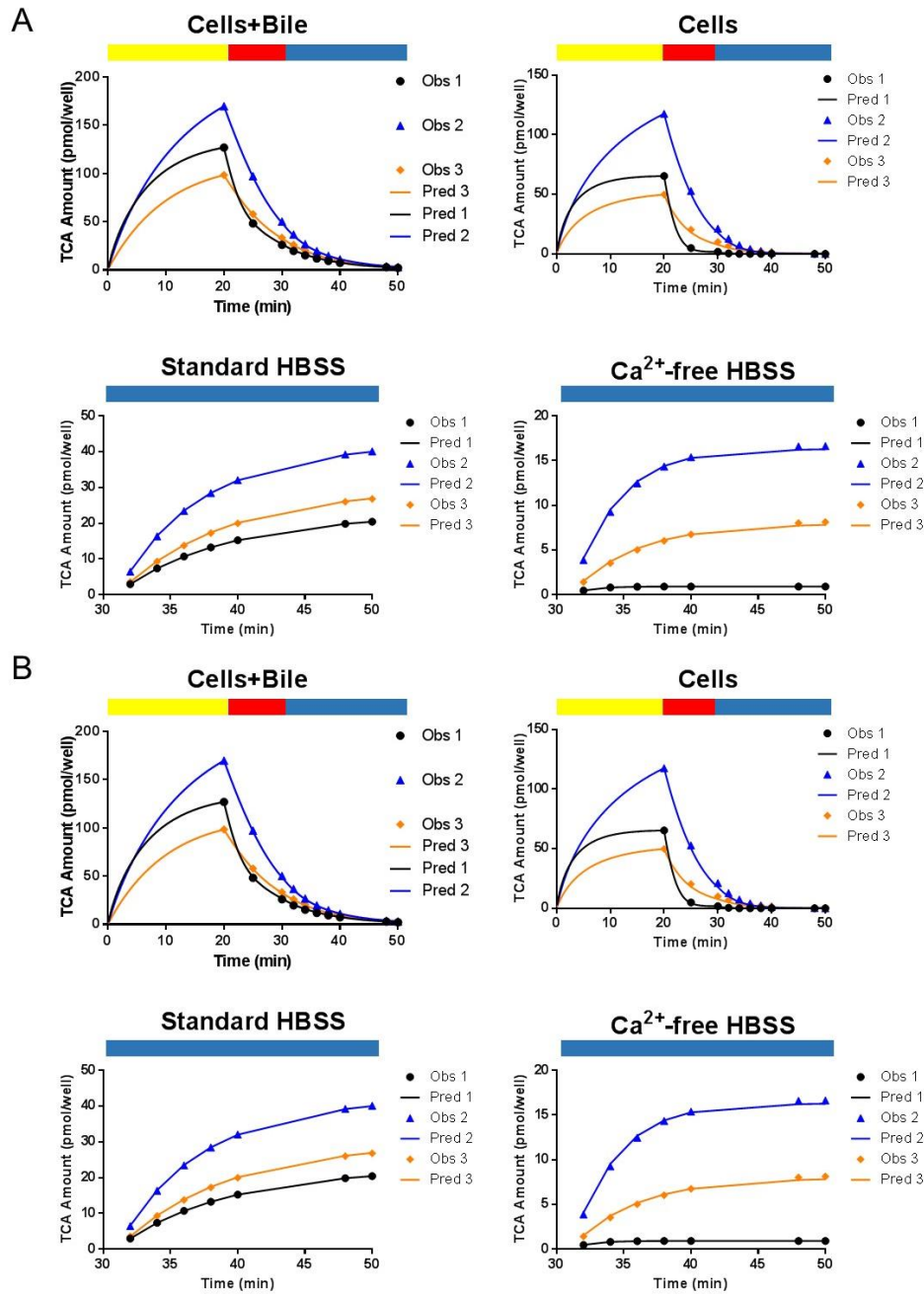
Figure 4.8. Sensitivity of $K_{i,BL}$ and $K_{i,Bile}$ estimates to changes in TCA and TS kinetic parameters. Each of TCA and TS kinetic parameter was varied by 2-fold (0.5X, gray bars; 2X, black bars) of the mean value while all other kinetic parameters were held constant. The difference between the estimated K_i values using PK Model #1 and the reference values (8 μM for $K_{i,BL}$ and 0.23 μM for $K_{i,Bile}$) are expressed as % of the reference values.
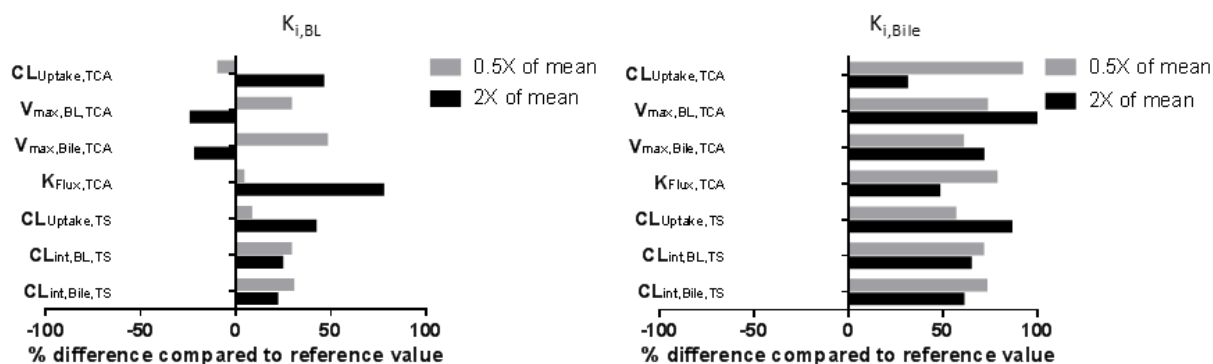
Figure 4.9. Sensitivity of TCA profiles to changes in $K_{i,Bile}$ (blue) and $K_{i,BL}$ (orange). Simulations were performed using the optimal study design and PK Model #1; $K_{i,Bile}$ and $K_{i,BL}$ were changed to 2-fold higher (solid lines) or 2-fold lower (dashed lines), separately.
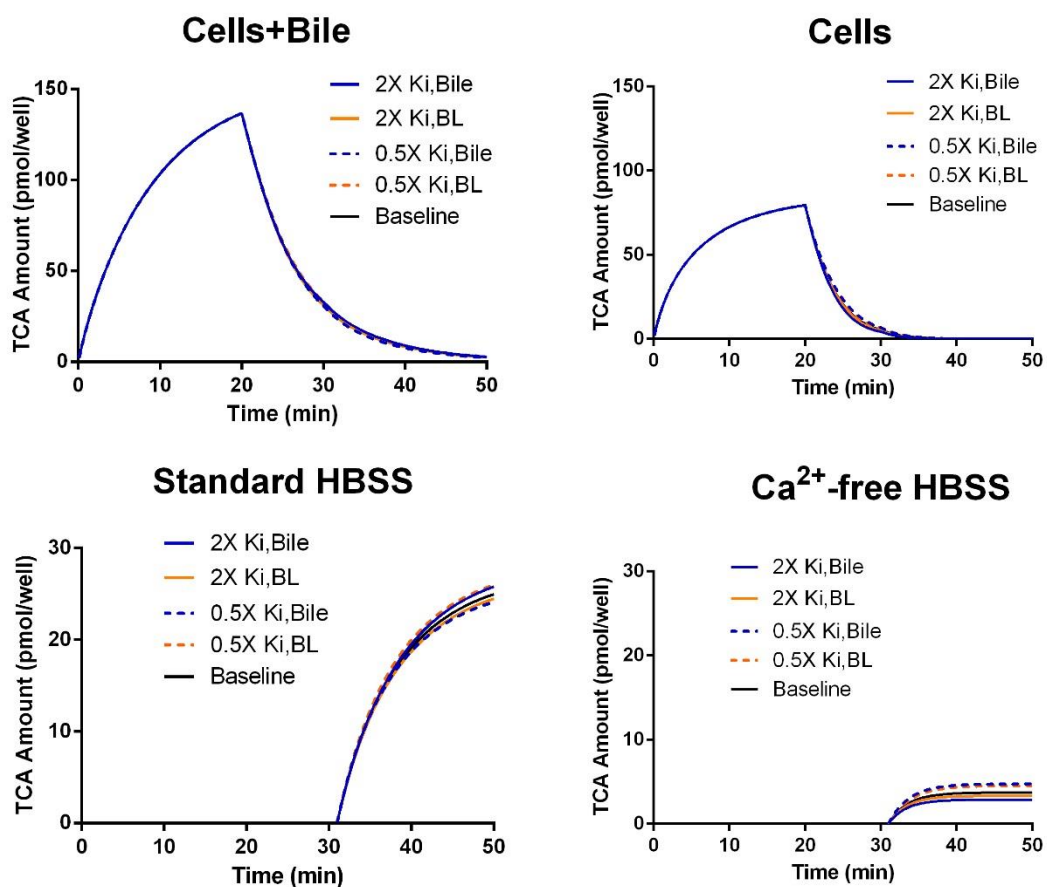
Figure 4.10. Intracellular concentrations of total TCA (red lines) and unbound TS (blue lines) vs. time simulated using the four different dosing schemes presented in **Table 4.5** based on PK Model #1. Mean kinetic parameters of TCA and TS were used for the simulation. The red shaded area represents the timeframe when TCA concentrations was greater than 5-fold of $K_{m,Bile,TCA}$ (9.7 μM). The blue shaded area represents the timeframe when TS concentrations were greater than $K_{i,Bile}$ (0.23 μM).
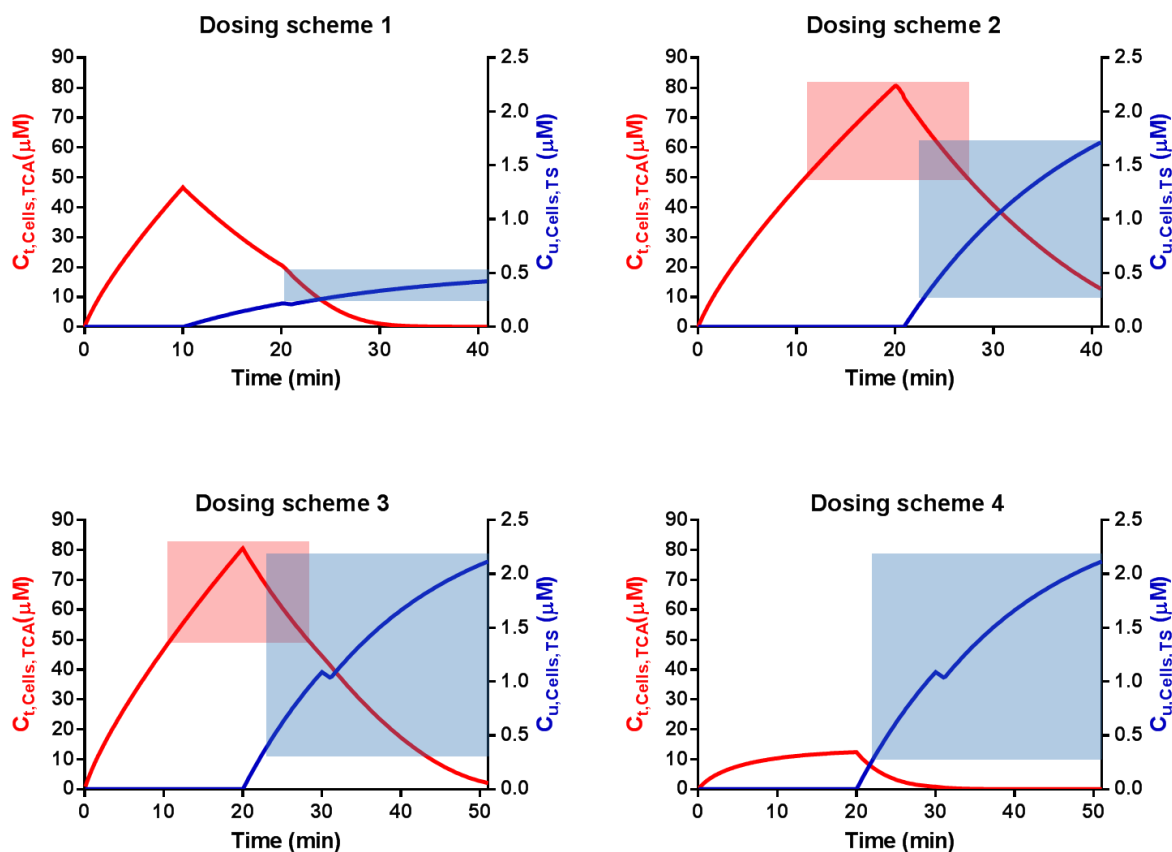
Figure 4.11. Workflow showing how to integrate the prior information and modify the proposed study design to estimate K_i values of inhibitors.

Inhibitor Information

- The rate and extent of uptake in SCH (measured at 3 time points and 2 dose levels)
- The range of IC_{50} against BSEP and MRP3/4 (using membrane vesicles, 3 dose levels)
- Intracellular unbound fraction of inhibitor

Substrate Information

- TCA (5 μM) uptake and efflux in SCH to estimate $CL_{Uptake,TCA}$, $V_{max,Bile,TCA}$ and $V_{max,BL,TCA}$

- Conduct the study using the current protocol; adjust the inhibitor dose level to ensure that intracellular unbound inhibitor concentration brackets the IC_{50} value and both compounds are measurable
- Measure TCA and inhibitor concentration over time
- Estimate $K_{i,Bile}$ and $K_{i,BL}$ while fixing other TCA parameters

REFERENCES

Balakrishnan A, Hussainzada N, Gonzalez P, Bermejo M, Swaan PW and Polli JE (2007) Bias in estimation of transporter kinetic parameters from overexpression systems: Interplay of transporter expression level and substrate affinity. *J Pharmacol Exp Ther* **320**:133-144.

Ballatori N, Fang F, Christian WV, Li N and Hammond CL (2008) Ostalpha-Ostbeta is required for bile acid and conjugated steroid disposition in the intestine, kidney, and liver. *Am J Physiol Gastrointest Liver Physiol* **295**:G179-g186.

Bentz J, O'Connor MP, Bednarczyk D, Coleman J, Lee C, Palm J, Pak YA, Perloff ES, Reyner E, Balimane P, Brannstrom M, Chu X, Funk C, Guo A, Hanna I, Heredi-Szabo K, Hillgren K, Li L, Hollnack-Pusch E, Jamei M, Lin X, Mason AK, Neuhoff S, Patel A, Podila L, Plise E, Rajaraman G, Salphati L, Sands E, Taub ME, Taur JS, Weitz D, Wortelboer HM, Xia CQ, Xiao G, Yabut J, Yamagata T, Zhang L and Ellens H (2013) Variability in P-glycoprotein inhibitory potency (IC(5)(0)) using various in vitro experimental systems: implications for universal digoxin drug-drug interaction risk assessment decision criteria. *Drug Metab Dispos* **41**:1347-1366.

Chojkier M (2005) Troglitazone and liver injury: in search of answers. *Hepatology* **41**:237-246.

Ellens H, Deng S, Coleman J, Bentz J, Taub ME, Ragueneau-Majlessi I, Chung SP, Heredi-Szabo K, Neuhoff S, Palm J, Balimane P, Zhang L, Jamei M, Hanna I, O'Connor M, Bednarczyk D, Forsgard M, Chu X, Funk C, Guo A, Hillgren KM, Li L, Pak AY, Perloff ES, Rajaraman G, Salphati L, Taur JS, Weitz D, Wortelboer HM, Xia CQ, Xiao G, Yamagata T and Lee CA (2013) Application of receiver operating characteristic analysis to refine the prediction of potential digoxin drug interactions. *Drug Metab Dispos* **41**:1367-1374.

Enokizono J, Kusuhara H and Sugiyama Y (2007) Involvement of breast cancer resistance protein (BCRP/ABCG2) in the biliary excretion and intestinal efflux of troglitazone sulfate, the major metabolite of troglitazone with a cholestatic effect. *Drug Metab Dispos* **35**:209-214.

FDA/CDER US (2012) Drug interaction studies - study design, data analysis, and implications for dosing and labeling recommendations, DRAFT GUIDANCE.

Funk C, Ponelle C, Scheuermann G and Pantze M (2001) Cholestatic potential of troglitazone as a possible factor contributing to troglitazone-induced hepatotoxicity: in vivo and in vitro interaction at the canalicular bile salt export pump (Bsep) in the rat. *Mol Pharmacol* **59**:627-635.

Gabrielsson J and Weiner D (2007) Design Elements, in Pharmacokinetic and Pharmacodynamic Data Analysis -Concepts and Applications, Fourth Edition. *Stockholm, Sweden, Swedish Pharmaceutical Press* **4**:464-490.

Gui C, Wahlgren B, Lushington GH and Hagenbuch B (2009) Identification, Ki determination and CoMFA analysis of nuclear receptor ligands as competitive inhibitors of OATP1B1-mediated estradiol-17beta-glucuronide transport. *Pharmacol Res* **60**:50-56.

Guo C, Yang K, Brouwer KR, St Claire RL, 3rd and Brouwer KL (2016) Prediction of Altered Bile Acid Disposition Due to Inhibition of Multiple Transporters: An Integrated Approach Using Sandwich-Cultured Hepatocytes, Mechanistic Modeling, and Simulation. *J Pharmacol Exp Ther* **358**:324-333.

Guo C, Yang K, Liao M, Xia CQ, Brouwer KR and Brouwer KLR (2017) Prediction of Hepatic Efflux Transporter-Mediated Drug Interactions: When Is it Optimal to Measure Intracellular Unbound Fraction of Inhibitors? *J Pharm Sci* **106**:2401-2406.

Hayashi H, Takada T, Suzuki H, Onuki R, Hofmann AF and Sugiyama Y (2005) Transport by vesicles of glycine- and taurine-conjugated bile salts and taurolithocholate 3-sulfate: a comparison of human BSEP with rat Bsep. *Biochim Biophys Acta* **1738**:54-62.

Hofmann AF and Hagey LR (2008) Bile acids: chemistry, pathochemistry, biology, pathobiology, and therapeutics. *Cell Mol Life Sci* **65**:2461-2483.

Kakkar T, Pak Y and Mayersohn M (2000) Evaluation of a minimal experimental design for determination of enzyme kinetic parameters and inhibition mechanism. *J Pharmacol Exp Ther* **293**:861-869.

Kis E, Ioja E, Nagy T, Szente L, Heredi-Szabo K and Krajcsi P (2009) Effect of membrane cholesterol on BSEP/Bsep activity: species specificity studies for substrates and inhibitors. *Drug Metab Dispos* **37**:1878-1886.

Kishimoto W, Ishiguro N, Ludwig-Schwellinger E, Ebner T, Maeda K and Sugiyama Y (2016) Usefulness of A Model-Based Approach for Estimating In Vitro P-Glycoprotein Inhibition Potency in a Transcellular Transport Assay. *J Pharm Sci* **105**:891-896.

LeCluyse E, Madan A, Hamilton G, Carroll K, DeHaan R and Parkinson A (2000) Expression and regulation of cytochrome P450 enzymes in primary cultures of human hepatocytes. *J Biochem Mol Toxicol* **14**:177-188.

Lee CA, Kalvass JC, Galetin A and Zamek-Gliszczynski MJ (2014) ITC commentary on the prediction of digoxin clinical drug-drug interactions from in vitro transporter assays. *Clin Pharmacol Ther* **96**:298-301.

Lee JK, Marion TL, Abe K, Lim C, Pollock GM and Brouwer KL (2010) Hepatobiliary disposition of troglitazone and metabolites in rat and human sandwich-cultured hepatocytes: use of Monte Carlo simulations to assess the impact of changes in biliary excretion on troglitazone sulfate accumulation. *J Pharmacol Exp Ther* **332**:26-34.

Marion TL, Leslie EM and Brouwer KL (2007) Use of sandwich-cultured hepatocytes to evaluate impaired bile acid transport as a mechanism of drug-induced hepatotoxicity. *Mol Pharm* **4**:911-918.

Mita S, Suzuki H, Akita H, Hayashi H, Onuki R, Hofmann AF and Sugiyama Y (2006) Vectorial transport of unconjugated and conjugated bile salts by monolayers of LLC-PK1 cells doubly transfected with human NTCP and BSEP or with rat Ntcp and Bsep. *Am J Physiol Gastrointest Liver Physiol* **290**:G550-556.

Morgan RE, van Staden CJ, Chen Y, Kalyanaraman N, Kalanzi J, Dunn RT, 2nd, Afshari CA and Hamadeh HK (2013) A multifactorial approach to hepatobiliary transporter assessment enables improved therapeutic compound development. *Toxicol Sci* **136**:216-241.

Murphy DJ (2004) Determination of accurate KI values for tight-binding enzyme inhibitors: an in silico study of experimental error and assay design. *Anal Biochem* **327**:61-67.

Nozawa T, Imai K, Nezu J, Tsuji A and Tamai I (2004a) Functional characterization of pH-sensitive organic anion transporting polypeptide OATP-B in human. *J Pharmacol Exp Ther* **308**:438-445.

Nozawa T, Sugiura S, Nakajima M, Goto A, Yokoi T, Nezu J, Tsuji A and Tamai I (2004b) Involvement of organic anion transporting polypeptides in the transport of troglitazone sulfate: implications for understanding troglitazone hepatotoxicity. *Drug Metab Dispos* **32**:291-294.

Pan Y, Hsu V, Grimstein M, Zhang L, Arya V, Sinha V, Grillo JA and Zhao P (2016) The Application of Physiologically Based Pharmacokinetic Modeling to Predict the Role of Drug Transporters: Scientific and Regulatory Perspectives. *J Clin Pharmacol* **56 Suppl 7**:S122-131.

Pfeifer ND, Yang K and Brouwer KL (2013) Hepatic basolateral efflux contributes significantly to rosuvastatin disposition I: characterization of basolateral versus biliary clearance using a novel protocol in sandwich-cultured hepatocytes. *J Pharmacol Exp Ther* **347**:727-736.

Riccardi KA, Ryu S, Lin J, Yates P, Tess DA, Li R, Singh D, Holder BR, Kapinos B, Chang G and Di L (2018) Comparison of Species and Cell-Type Differences in Fraction Unbound of Liver Tissues, Hepatocytes and Cell-Lines. *Drug Metab Dispos*.

Ring B, Wrighton SA and Mohutsky M (2014) Reversible Mechanisms of Enzyme Inhibition and Resulting Clinical Significance, in Enzyme Kinetics in Drug Metabolism: Fundamentals and Applications (Nagar S, Argikar U, Tweedie D eds) *NY, Humana Press* **1113**:37-56.

Rius M, Hummel-Eisenbeiss J, Hofmann AF and Keppler D (2006) Substrate specificity of human ABCC4 (MRP4)-mediated cotransport of bile acids and reduced glutathione. *Am J Physiol Gastrointest Liver Physiol* **290**:G640-649.

Shirasaka Y, Masaoka Y, Kataoka M, Sakuma S and Yamashita S (2008) Scaling of in vitro membrane permeability to predict P-glycoprotein-mediated drug absorption in vivo. *Drug Metab Dispos* **36**:916-922.

Shitara Y, Li AP, Kato Y, Lu C, Ito K, Itoh T and Sugiyama Y (2003) Function of uptake transporters for taurocholate and estradiol 17beta-D-glucuronide in cryopreserved human hepatocytes. *Drug Metab Pharmacokinet* **18**:33-41.

Smith MT (2003) Mechanisms of troglitazone hepatotoxicity. *Chem Res Toxicol* **16**:679-687.

Soroka CJ, Ballatori N and Boyer JL (2010) Organic solute transporter, OSTalpha-OSTbeta: its role in bile acid transport and cholestasis. *Semin Liver Dis* **30**:178-185.

Swift B, Pfeifer ND and Brouwer KL (2010) Sandwich-cultured hepatocytes: an in vitro model to evaluate hepatobiliary transporter-based drug interactions and hepatotoxicity. *Drug Metab Rev* **42**:446-471.

Woodhead JL, Yang K, Siler SQ, Watkins PB, Brouwer KLR, Barton HA and BA H (2014) Exploring BSEP inhibition-mediated toxicity with a mechanistic model of drug-induced liver injury. *Front Pharmacol* **5**.

Yang K, Guo C, Woodhead JL, St Claire RL, 3rd, Watkins PB, Siler SQ, Howell BA and Brouwer KLR (2016) Sandwich-Cultured Hepatocytes as a Tool to Study Drug Disposition and Drug-Induced Liver Injury. *J Pharm Sci* **105**:443-459.

Yang K, Pfeifer ND, Kock K and Brouwer KL (2015) Species differences in hepatobiliary disposition of taurocholic acid in human and rat sandwich-cultured hepatocytes: implications for drug-induced liver injury. *J Pharmacol Exp Ther* **353**:415-423.

Yang K, Woodhead JL, Watkins PB, Howell BA and Brouwer KL (2014) Systems pharmacology modeling predicts delayed presentation and species differences in bile acid-mediated troglitazone hepatotoxicity. *Clin Pharmacol Ther* **96**:589-598.

Zhang DW, Gu HM, Vasa M, Muredda M, Cole SP and Deeley RG (2003) Characterization of the role of polar amino acid residues within predicted transmembrane helix 17 in determining the substrate specificity of multidrug resistance protein 3. *Biochemistry* **42**:9989-10000.

Zheng X and Polli J (2010) Identification of inhibitor concentrations to efficiently screen and measure inhibition Ki values against solute carrier transporters. *Eur J Pharm Sci* **41**:43-52.

Supplement

Figure S4.1. Simulated unbound concentration of TGZ and TS in Cells over time using the protocol published by Yang et al (Yang et al., 2015). Briefly, rat SCH (n=3 hepatocyte lots) were pre-incubated with TGZ (10 µM) for 30 min in standard HBSS; then, rat SCH were incubated for 10 min in standard or Ca^{2+}-free HBSS, followed by uptake of ^{3}H-TCA (1 µM) in standard HBSS and efflux of ^{3}H-TCA in standard and Ca^{2+}-free HBSS, all in the absence of TGZ. Kinetic parameters of TGZ and TS used for the simulation were published previously (Lee et al., 2010).
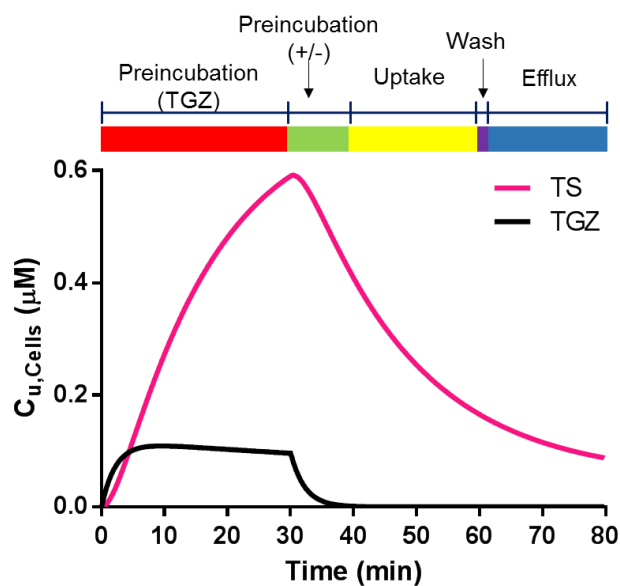
CHAPTER 5. FXR Agonists Obeticholic Acid and Chenodeoxycholic Acid Increase Bile Acid Efflux in Sandwich-Cultured Human Hepatocytes: Functional Evidence and Mechanisms[4]

Introduction

Farnesoid X Receptor (FXR) is a nuclear receptor that regulates genes involved in the homeostasis of bile acids (Lefebvre et al., 2009). Bile acids are signaling molecules that modulate hepatic metabolic and transporter function (Dawson et al., 2009), inflammation (Allen et al., 2011) as well as lipid, glucose and energy homeostasis (Staels and Kuipers, 2007; Thomas et al., 2008; Lefebvre et al., 2009). Therefore, FXR is a promising novel drug target to treat metabolic and chronic liver diseases, such as non-alcoholic steatohepatitis (NASH) and primary sclerosing cholangitis (Wagner et al., 2011; Trivedi et al., 2016; Fiorucci et al., 2007; Jiang et al., 2007). The first-in-class FXR agonist, obeticholic acid (OCA), has been approved for the treatment of primary biliary cholangitis (PBC). FXR is activated by various bile acids; chenodeoxycholic acid (CDCA) and conjugated CDCA species are the most potent natural agonists. OCA is an analog of CDCA, with 100-fold higher FXR activation potency (median effective concentration is 99 nM for OCA vs. 8.3 µM for CDCA) (Soisson et al., 2008; Markham and Keam, 2016).

Activation of FXR protects against the toxic accumulation of bile acids by decreasing bile acid synthesis and regulating bile acid transport (Adorini et al., 2012). For example, FXR activation by CDCA increased mRNA expression of bile acid efflux transporters including the bile salt export pump (BSEP) (Yu et al., 2002; Modica et al., 2010), multidrug resistance-associated protein 2 (MRP2) (Liu et al., 2014; Modica et al., 2010), and organic solute transporter (OSTα/β) (Liu et al., 2014; Modica et al., 2010; Boyer et al., 2006) in hepatic cell lines and primary human hepatocytes. Sandwich-cultured human hepatocytes (SCHH) are a physiologically-relevant model that maintains transporter function, morphology and regulatory machinery (LeCluyse et al., 2000; Yang et al., 2016), and therefore is an ideal system to study the regulation of bile acid transporters after non-acute (>24 hr) treatment of hepatocytes with FXR agonists. Recent studies revealed that OCA and CDCA treatment of SCHH for 72 hr increased mRNA expression of OSTα/β and BSEP with minor changes in MRP3, MRP4, and sodium taurocholate cotransporting polypeptide (NTCP) (Jackson et al., 2016; Zhang et al., 2017).

Unlike drug metabolizing enzymes, changes in gene expression of transporters do not always translate to changes in protein expression (Ahlin et al., 2009; Thompson et al., 2017) and/or function (Ohtsuki et al., 2012). This discrepancy may be explained by the prominent role of post-transcriptional regulation of hepatic transporters and the importance of transporter localization in determining transporter function (Gu and Manautou, 2010; Schonhoff et al., 2013; Wang et al., 2002; Chandra et al., 2005; Zhang et al., 2005).

Due to discrepancies between gene expression and transporter function, direct functional evidence for FXR agonist-mediated induction of bile acid efflux transporters (*i.e.,* OSTα/β and BSEP) is lacking. One of the challenges in quantitative assessment of hepatic transporter

161

function is the multiplicity of transporters expressed on the basolateral and canalicular membranes of hepatocytes, and the concurrent uptake and efflux of bile acids. Studies showed reduced intracellular accumulation of deuterium-labeled taurocholic acid (d_8-TCA), a prototypical bile acid, after treatment of SCHH with OCA and CDCA (Jackson et al., 2016; Zhang et al., 2017). Since d_8-TCA was added exogenously and the synthesis rate of TCA does not play a role, this change could be due to increased efflux or decreased uptake of d_8-TCA. On the basolateral membrane of human hepatocytes, NTCP, and to a much lesser extent the organic anion-transporting polypeptides (OATPs), contribute to TCA uptake. MRP3, MRP4, and OSTα/β are responsible for the basolateral efflux of TCA from human hepatocytes to the sinusoidal blood (Seward et al., 2003; Zhang et al., 2003; Rius et al., 2006; Ballatori et al., 2008; Soroka et al., 2010). To deconvolute these processes, a more sophisticated method, such as pharmacokinetic (PK) modeling is needed. To assess the function of the canalicular transporter BSEP, TCA biliary excretion can be quantified in SCHH using B-CLEAR® technology.

In the present study, mechanistic PK modeling of data obtained from SCHH using B-CLEAR® technology and our previously published basolateral efflux protocol (Pfeifer et al., 2013; Yang et al., 2015; Guo et al., 2016) was utilized to characterize the functional changes in bile acid transporters that occur with FXR activation. Changes in the basolateral uptake clearance, intrinsic basolateral efflux clearance, and intrinsic biliary clearance of an exogenously administered model bile acid, d_8-TCA, were evaluated in SCHH after 72-hr treatment with OCA and CDCA to reflect the transporter function. In order to identify the transporters that might be responsible for alterations in the overall clearance, the protein expression of TCA uptake and efflux transporters was assessed by immunoblot analysis.

162

Materials and Methods

Materials

BioCoat^{TM} cell culture plates and Matrigel$^{®}$ were obtained from BD Biosciences (San Jose, CA). QualGro^{TM} medium was obtained from Qualyst Transporter Solutions (Durham, NC). d_8-TCA was obtained from Toronto Research Chemicals (ON, Canada). Pierce bicinchoninic acid protein assay was obtained from Thermo Fisher Scientific (Waltham, MA).

Primary antibodies for OSTα, OSTβ, BSEP, and NTCP were purchased from Abcam (Cambridge, MA). Primary antibodies for MRP3 and MRP4 were obtained from Cell Signaling Technology (Danvers, MA) and Everest Biotech (Ramona, CA), respectively. The primary antibody for ATPase and all the secondary antibodies were purchased from Santa Cruz Biotechnology (Dallas, TX). Other reagents for immunoblot were obtained from Bio-Rad (Hercules, CA) or Thermo Fisher Scientific unless stated otherwise.

Hepatocyte Culture and FXR Agonists Treatment

Transporter Certified^{TM} cryopreserved human hepatocytes [HC3-26, HUM4122C/D, HUM4119C, and HUM8246 purchased from Xenotech (Kansas City, KS), Lonza (Basel, Switzerland), and Thermo Fisher Scientific, respectively] were obtained from two Caucasian females, one Asian male, and one African American female donor, respectively (age range: 30-43 years; body mass index range: 22-39). Hepatocytes were seeded at a density of 0.4-0.5×10^6 cells/well in 24-well BioCoat^{TM} plates and cultured in a sandwich configuration (overlaid with Matrigel$^{®}$) in QualGro^{TM} Induction Medium as previously reported (Swift et al., 2010). On Day 2 of culture, SCHH were treated with OCA (1 μM), CDCA (100 μM), or vehicle control for 72 hr. The dose of OCA was selected based on the maximum plasma concentration of OCA at steady state (~0.7-1 μM) (Edwards et al., 2016). In addition, based on the dose-gene expression

163

relationships published previously, the maximal effect on the induction of downstream genes was achieved at 1 µM OCA and 100 µM CDCA (Jackson et al., 2016; Zhang et al., 2017). Previous studies using the same lots of human hepatocytes (Jackson et al., 2016; Zhang et al., 2017), and a study using different lots of human hepatocytes (Yang et al., 2016), demonstrated that neither OCA (1 µM) nor CDCA (100 µM) affected the viability of SCHH. The medium was changed every 24 hr.

d_8-TCA Uptake and Efflux in SCHH

On Day 5 of culture (at the end of 72-hr treatment), uptake of d_8-TCA in Ca^{2+}-containing (standard) Hanks' balanced salt solution (HBSS) and efflux of d_8-TCA in standard and Ca^{2+}-free HBSS were performed (n=3 donors, HC3-26, HUM4122C, and HUM4119C, measured in triplicate), as described previously (Guo et al., 2016; Yang et al., 2015). Briefly, SCHH were pre-incubated with standard or Ca^{2+}-free HBSS for 10 min. Incubation with Ca^{2+}-free HBSS disrupts the tight junctions which seal the canalicular networks, allowing the contents in the bile canaliculi to be released into the medium (B-CLEAR$^®$ technology)(Liu et al., 1999). Following pre-incubation, SCHH were dosed with 2.5 µM of d_8-TCA in standard HBSS containing 4% bovine serum albumin (BSA) for 20 min (uptake phase). The presence of BSA (Fraction V, Thomas Scientific, NJ) during the uptake phase mimics the effect of protein binding in vivo. After the uptake phase, the cells were washed for 1 min and incubated with fresh protein-free standard or Ca^{2+}-free HBSS for 15 min (efflux phase). The total amount of d_8-TCA in Cells+Bile (standard HBSS) and Cells (Ca^{2+}-free HBSS) during the uptake phase (2, 5, 10, and 20 min) and the efflux phase (2, 5, 10, and 15 min), and the total amount of d_8-TCA in the incubation buffer during the efflux phase (2, 5, 10, and 15 min), were determined by liquid chromatography–mass spectrometry as reported previously (Guo et al., 2016).

Model-independent parameters describing the overall hepatobiliary disposition of TCA in SCHH were calculated using eqs 1 and 2 (Yang et al., 2016; Liu et al., 1999) as well as Equation 3.

$$CL_{app,Bile} = \frac{Amount_{Cells+Bile} - Amount_{Cells}}{Time \times Concentration_{Buffer}}$$
(1)

$$BEI = \frac{Amount_{Cells+Bile} - Amount_{Cells}}{Amount_{Cells+Bile}} \times 100\%$$
(2)

$$BRI = \frac{Amount_{Buffer} \text{ during efflux phase}}{Amount_{Cells} \text{ at end of 20-min uptake}} \times 100\%$$
(3)

$CL_{app,Bile}$ represents the in vitro apparent biliary clearance calculated at 10 min during the uptake phase. The biliary excretion index (BEI), determined at 10 min during the uptake phase, represents the fraction of compound accumulated in the bile compartment relative to the total accumulation of compound in Cells+Bile. The Buffer Recovery Index (BRI), determined at 2 min during the efflux phase, represents the fraction of compound effluxed from Cells and fluxed from bile canaliculi into the buffer relative to the total accumulation in Cells at the end of the 20-min uptake phase.

PK Modeling of TCA Disposition in SCHH

A mechanistic PK model (scheme depicted in Fig. 5.1) incorporating linear clearance processes (Guo et al., 2016; Yang et al., 2015) was modified and fit to the TCA total mass-time data in Cells+Bile, Cells, standard HBSS, and Ca^{2+}-free HBSS using Phoenix WinNonlin 7.0 (Certara USA, Inc., Princeton, NJ). A mixed proportional and additive error model was used to account for residual error. Parameter estimates from a previous report were used as initial estimates for the control group (Guo et al., 2016). Data from the same hepatocyte donor exposed to different treatments were modeled together. Various model structures were tested. The best-fit

model was selected based on Akaike's Information Criterion, the precision of parameter estimates, the degree of bias in the residual error, and visual inspection of the predicted curves relative to the observed data. The following kinetic parameters were estimated: total uptake clearance (CL_{Uptake}), total intrinsic basolateral efflux clearance ($CL_{int,BL}$), total intrinsic biliary clearance ($CL_{int,Bile}$), and the rate constant describing flux from bile networks into the medium (K_{Flux}) due to periodic contraction of bile canalicular networks (Oshio and Phillips, 1981; Lee et al., 2010). The mean values and coefficient of variation (CV%) of parameter estimates from the three donors were calculated. Differential eqs 4 to 8 were used to describe the changes in the amount of TCA with respect to time in different compartments in this model.

Mass in standard HBSS:

$$\frac{dX_{t,Buffer}^{+}}{dt} = CL_{u,int,BL} \times C_{t,Cells}^{+} \times f_{u,cell} + K_{Flux} \times X_{t,Bile} - CL_{u,Uptake} \times C_{t,Buffer}^{+} \times f_{u,buffer} - K_{Wash} \times X_{t,Buffer}^{+}$$

$$X_{Buffer}^{+}{}^{\circ} = X_{dose} \qquad (4)$$

Mass in Ca^{2+}-free HBSS:

$$\frac{dX_{t,Buffer}^{-}}{dt} = \left(CL_{u,int,BL} + CL_{u,int,Bile}\right) \times C_{t,Cells}^{-} \times f_{u,cell} - CL_{u,Uptake} \times C_{t,Buffer}^{-} \times f_{u,buffer} - K_{Wash} \times X_{t,Buffer}^{-}$$

$$X_{Buffer}^{-}{}^{\circ} = X_{dose} \qquad (5)$$

Mass in Cells:

$$\frac{dX_{t,Cells}^{+or-}}{dt} = CL_{u,Uptake} \times C_{t,Buffer}^{+or-} \times f_{u,buffer} - \left(CL_{u,int,BL} + \right.$$

$$\left. CL_{u,int,Bile}\right) \times C_{t,Cells}^{+or-} \times f_{u,cell}$$

$$X_{Cells}^{+or-}{}^{\circ} = 0 \qquad (6)$$

Mass in Bile (standard HBSS):

$$\frac{dX_{t,Bile}}{dt} = CL_{u,int,Bile} \times C_{t,Cells}^{+} \times f_{u,cell} - K_{Flux} \times X_{t,Bile}$$

$$X_{Bile}{}^{\circ} = 0 \qquad (7)$$

Mass in Cells+Bile (standard HBSS):

$$\frac{dX_{t,Cells+Bile}}{dt} = \frac{dX_{t,Bile}}{dt} + \frac{dX_{t,Cells}^+}{dt}$$

$$X_{Cells+Bile}^\circ = 0 \qquad\qquad (8)$$

where $C_{t,Cells}$ represents the total intracellular concentration, and was calculated as $X_{t,Cells}/V_{Cells}$; V_{Cells} represents cellular volume and was calculated and fixed using the protein content of each hepatocyte preparation and a value of 7.4 µL/mg protein (Pfeifer et al., 2013; Yang et al., 2015); "+" and "-" refer to Ca^{2+}-containing (standard HBSS) and Ca^{2+}-free HBSS, respectively; $X_{t,Cells}$, $X_{t,Cells+Bile}$, and $X_{t,Bile}$ represents total amount in Cells, Cells+Bile, and Bile, respectively; $C_{t,Buffer}$ represents the total concentration in Buffer; V_{Buffer} was set as a constant (0.3 mL); $CL_{u,Uptake}$ represents unbound uptake clearance; $CL_{u,int,BL}$ represents unbound intrinsic basolateral efflux clearance; $CL_{u,int,Bile}$ represents unbound intrinsic biliary clearance. The $f_{u,buffer}$ represents unbound fraction in buffer containing 4% BSA; $f_{u,buffer}$ was set at 0.15 (Wolf et al., 2008) during the 20-min uptake phase, and set at 1 during the 15-min efflux phase because BSA was present only in the uptake phase. The $f_{u,cell}$ represents unbound fraction in hepatocytes, and was assumed to be 0.15. CL_{Uptake} was calculated as $f_{u,buffer} \times CL_{u,Uptake}$; $CL_{int,BL}$ and $CL_{int,Bile}$ were calculated as $f_{u,cell} \times CL_{u,int,BL}$ and $f_{u,cell} \times CL_{u,int,Bile}$, respectively. To mimic the 1-min wash between the uptake and efflux phase, K_{Wash} was activated for 1 min using an if-then statement. K_{Wash} was fixed at 5×10^4 min^{-1}, which was sufficient to eliminate the d_8-TCA from the buffer compartment. Protein concentrations were measured by the bicinchoninic acid assay.

Immunoblots

At the end of 72-hr treatment (Day 5 cultures), SCHH (n=3 hepatocyte donors, HUM4122D, HC3-26, and HU8246) were washed with PBS, and the membrane protein was extracted using ProteoExtract® Native Membrane Protein Extraction Kit (Millipore Sigma,

Burlington, MA). Membrane proteins (12 µg, without boiling) were mixed with loading buffer containing 50 mM dithiothreitol and resolved on NuPAGE 4 to 12% Bis-Tris gel or 7% Tris-Acetate gel and the proteins were transferred to polyvinylidene fluoride membranes. After blocking in 5% nonfat milk in Tris-buffered saline with Tween 20 (TBST) for 1 hr, blots were incubated with the following primary antibodies diluted in 5% BSA (Sigma-Aldrich, St. Louis, MO): OSTα, (1:500), OSTβ (1:500), MRP3 (1:1000), MRP4 (1:200), BSEP (1:1000), NTCP (1:1500) overnight at 4 °C or with primary antibody for ATPase (1:500) for 3 hr at room temperature. Then the blots were probed with horseradish peroxidase-conjugated anti-rabbit (OSTs, BSEP, MRP3, NTCP, ATPase) or anti-goat IgG secondary antibody (MRP4) for 1 hr at room temperature (1:7000). Signals were detected by using the Amersham ECL Select Western Blotting Detection Reagent (GE Healthcare Bio-Sciences, Pittsburgh, PA) or Clarity Max ECL Substrate (Bio-Rad, Hercules, CA) with a BioRad ChemiDoc XRS+ system. Densitrometric analysis was performed using Image-J 1.6.0 (NIH, MD, US).

Data Analysis

Statistical analysis was performed on the clearance values and immunoblot results using GraphPad Prism (V6.01, La Jolla, CA). One-way ANOVA with Bonferroni's test was used to correct for multiple comparisons with the control group.

Results

Uptake and Efflux of d$_8$-TCA in SCHH

OCA and CDCA treatment markedly decreased the total amount of TCA in hepatocytes, the hepatocyte plus bile compartment, and the efflux buffer (Fig. 5.2). The BRI (%), representing the fraction of accumulated TCA in hepatocytes that undergoes efflux into buffer, was increased

from 27-36% in control to 50-53% and 47-78% in OCA- and CDCA-treated SCHH, respectively. The $CL_{app,Bile}$ of TCA ranged from 0.62-1.2 µL/min per milligram protein in control SCHH, but was decreased to 0.35-0.81 and 0.097-0.41 µL/min per milligram protein by OCA and CDCA treatment, respectively. However, the BEI (%) in control SCHH (63-71%) was similar to values after OCA (63-74%) and CDCA (46-71%) treatment.

PK Modeling of d_8-TCA Disposition in SCHH

Observed mass-time profiles of TCA from individual donors were plotted against the predicted mass-time profiles generated by using the best-fit parameters based on the mechanistic model (Fig. 5.2). The estimated clearance values of TCA in individual hepatocyte donors and the mean values calculated from the individual donors are presented in Table 5.1. The mechanistic model revealed that $CL_{int,Bile}$ was approximately 3-fold higher than $CL_{int,BL}$ in the control hepatocytes, consistent with previous report (Guo et al., 2016). The CV% of the estimated parameters from model fitting were acceptable ($< 65\%$, Table 5.1), indicating good precision of the model fitting. The fold change in each parameter in treated hepatocytes compared to control hepatocytes is shown in Fig 5.3. OCA and CDCA treatment significantly increased $CL_{int,BL}$ by $>$ 6-fold, and $CL_{int,Bile}$ by ~2-fold. Changes in CL_{Uptake} were not statistically significant.

Protein Expression of TCA Transporters

To investigate which transporters might have contributed to the changes in TCA disposition, immunoblot analysis of major bile acid transporters was performed using SCHH from three hepatocyte donors. As shown in Fig. 5.4, OCA treatment increased the average expression of OSTα and OSTβ to 260% and 1100% of control, respectively. CDCA treatment increased the average expression of OSTα and OSTβ to 280% and 1300% of control, respectively. The average BSEP expression was modestly upregulated to 185% and 165% of

169

control by OCA and CDCA. Changes in MRP3, MRP4, and NTCP protein expression were negligible (<25% changes). The changes in OSTα and OSTβ expression were statistically significant while the changes in other proteins were inconclusive.

Discussion

To our knowledge, this study is the first direct demonstration of functional induction of bile acid efflux transporters in response to FXR agonists, revealed by mechanistic PK modeling results. The combination of mechanistic PK modeling and molecular analysis provided a comprehensive data set for understanding the mechanisms of OCA- and CDCA-mediated alterations in hepatic bile acid transporters. Increases in the basolateral efflux clearance and biliary clearance were consistent with a pronounced upregulation of OSTβ protein expression, and a smaller increase in BSEP protein expression, respectively (Figure 5.5).

This study demonstrated the advantages of PK modeling in assessing changes in concurrent clearance pathways in a whole cell system. Quantitative assessment of basolateral bile acid efflux transporter function is challenging since plasma/medium bile acid concentrations reflect the net effect of synthesis and metabolism, as well as uptake and efflux. A recent report quantified the transport kinetics of a bile acid tracer [N-methyl-^{11}C] cholylsarcosine (^{11}C-CSar), which is similar to glycocholic acid, in human blood and liver using positron emission tomography (PET) (Orntoft et al., 2017). Based on a kinetic model, the rate constant for basolateral efflux of ^{11}C-CSar was higher in cholestatic patients compared to healthy subjects. Similarly, in this mechanistic PK modeling study, concurrent clearance pathways of TCA in hepatocytes were de-convoluted; $CL_{int,BL}$ and $CL_{int,Bile}$ of TCA were increased by FXR agonist treatment. This information may have been overlooked by merely calculating model-independent

parameters. Although BRI showed a 2-fold increase, indicating increased basolateral efflux, it underestimated the magnitude of change compared to the model-estimated 6-fold increase in $CL_{int,BL}$. After FXR agonist treatment, BEI remained the same and $CL_{app,Bile}$ decreased, while model-estimated $CL_{int,Bile}$ increased by 2-fold. In this case, BEI and $CL_{app,Bile}$ measured at a single time point failed to reflect the modest changes in biliary excretion because these model-independent parameters are also affected by basolateral uptake and efflux.

The FXR agonist-induced changes in transporter protein expression (greater induction of OSTβ and OSTα than BSEP) were consistent with the increases in TCA clearance (greater increase in $CL_{int,BL}$ than $CL_{int,Bile}$), which would be expected for plasma membrane-localized proteins. In addition, alterations in protein expression agreed with previously published gene expression data in SCHH. OCA treatment (1 µM, 72 hr) increased OSTα, OSTβ, and BSEP mRNA in SCHH by 6.4-, 43-, and 4.6-fold, respectively (Zhang et al., 2017), while CDCA treatment (100 µM, 72 hr) increased OSTα, OSTβ, and BSEP mRNA by 3.1-, 21-, and 2.2-fold, respectively (Jackson et al., 2016). No marked changes in the mRNA expression of MRP3, MRP4, or NTCP were observed in previous studies (Jackson et al., 2016; Zhang et al., 2017), consistent with the present protein expression data. Therefore, the increase in bile acid efflux was likely due to the induction of OSTβ and to a lesser extent to OSTα induction. Protein expression of NTCP remained unchanged in FXR agonist-treated SCHH, consistent with no statistically significant changes in CL_{Uptake} in CDCA-treated SCHH.

OSTα/β is expressed in many other organs including the intestine, kidneys, and testis, and it can transport a variety of endogenous compounds in addition to bile acids, such as estrone 3-sulfate, prostaglandin E, dehydroepiandrosterone 3-sulfate, and drugs like digoxin (Soroka et al., 2010). Therefore, up-regulation of OSTα and OSTβ may affect the disposition of various

endogenous and exogenous compounds, and may have significant physiological implications and affect pharmacotherapy. The heterodimeric OSTα/β is a facilitated transporter that can translocate organic solutes across the basolateral membrane in either direction in vitro (Ballatori et al., 2005). In vivo, it is the primary bile acid efflux transporter in the intestine (Soroka et al., 2010). Lower expression of OSTα and OSTβ in transfected COS cells decreased OSTα/β-mediated transport (Sultan et al., 2017). OSTβ is required for the maturation and stability of OSTα (Dawson et al., 2010). The baseline gene expression level of OSTα is 3-7-fold higher than OSTβ in human liver tissue (Ballatori et al., 2005; Ballatori et al., 2009). Since heterodimerization of the two subunits is required for transport function, greater induction of OSTβ might be needed for maximal function of OSTα/β. Like other basolateral efflux transporters, OSTα/β is expressed at much lower levels in healthy human hepatocytes. Under cholestatic conditions, basolateral efflux transporters are often up-regulated to serve as alternate excretory pathways for bile acids (Zollner et al., 2003; Chai et al., 2012). In the present study, OCA and CDCA treatment both increased the $CL_{int,BL}$ of TCA more than 6-fold relative to control, resulting in clearance values that were slightly greater than the $CL_{int,Bile}$. An increase in $CL_{int,BL}$ may exert a hepatoprotective effect by decreasing the hepatocellular accumulation of bile acids.

The marked induction of OSTα, OSTβ, and to a lesser extent BSEP, but not MRP3, MRP4, or NTCP, as shown by immunoblotting, could be explained by the differential regulatory mechanisms of these transporters. *SLC51A, SLC51B* (genes encoding OSTα and OSTβ, respectively) and *ABCB11* (gene encoding BSEP) are direct target genes for FXR (Ananthanarayanan et al., 2001; Yu et al., 2002; Landrier et al., 2006; Lee et al., 2006; Lefebvre et al., 2009). The FXR pathway was functional in SCHH and activated by OCA (1 µM) and

CDCA (100 µM) treatment, as shown by the following changes in other FXR target genes: decreased gene expression of CYP7A1, the synthesizing enzyme for bile acids, and increased gene expression of small heterodimer partner (SHP) (Zhang et al., 2017) (Jackson et al., 2016), similar to findings reported by Liu et al. (2014). However, MRP3 is regulated by retinoic acid receptor, pregnane X receptor, constitutive androstane receptor (CAR), and liver receptor homolog-1 (Inokuchi et al., 2001; Teng et al., 2003; Chen et al., 2007; Geier et al., 2007). MRP4 is regulated primarily by CAR (Geier et al., 2007; Assem et al., 2004). Although rat Ntcp is a target gene of FXR (Denson et al., 2001), gene expression of human NTCP was minimally affected by FXR agonists. Gene expression of NTCP remained unchanged in human liver slices after CDCA treatment (100 µM, 24 hr) (Jung et al., 2007) and in SCHH after CDCA (100 µM, 72 hr) and OCA treatment (1 µM, 72 hr) (Jackson et al., 2016; Zhang et al., 2017). A slight decrease (30%) in NTCP mRNA was reported in human hepatocytes after CDCA treatment (100 µM, 48 hr) (Liu et al., 2014). Our results, together with these literature reports, showed that NTCP protein expression and function do not appear to be markedly affected by OCA and CDCA treatment of SCHH at the concentrations utilized in the present study.

One assumption of the current PK model was that K_{Flux} was the same across different treatment groups. K_{Flux} is dependent on the contraction of bile canaliculi driven by the actin network (Watanabe et al., 1985). Since there is no evidence that FXR regulates actin function, K_{Flux} was fixed to control values to avoid over-parameterization.

In conclusion, FXR agonists OCA and CDCA increased bile acid efflux in SCHH, which contributed to reduced hepatocellular concentrations of d_8-TCA. OSTα/β appeared to be the major transporter responsible for the increase in intrinsic basolateral efflux clearance of d_8-TCA. These cellular effects, together with the suppression of bile acid synthesis (Jackson et al., 2016;

173

Zhang et al., 2017), provide the mechanistic rationale for FXR as a therapeutic target for the treatment of cholestatic diseases by reducing bile acid burden in hepatocytes. These results will enhance our understanding of the FXR-dependent mechanisms of OCA, and its impact on bile acid homeostasis.

Table 5.1. Parameter estimates of TCA $CL_{int,BL}$, $CL_{int,Bile}$, CL_{Uptake}, and K_{Flux}. Estimates and the corresponding CV% were obtained by fitting the model to the time-course data from individual SCHH preparations (Figure 5.2) based on the model scheme depicted in Figure 5.1. Mean values of these three individual estimates were calculated. Donor 1, 2 and 3 represent HUM4119C, HUM4122C, and HC3-26, respectively.

| | | $CL_{int,BL}$ | | $CL_{int,Bile}$ | | CL_{Uptake} | | K_{Flux} | |
| | | (µL/min per milligram protein) | | | | | | (min^{-1}) | |
Treatment	Donor	Estimate	CV%	Estimate	CV%	Estimate	CV%	Estimate	CV%
	1	0.29	33	0.80	14	1.6	6.4	0.048	7.3
	2	0.25	52	0.80	15	0.95	5.8	0.046	12
	3	0.19	58	0.70	16	1.4	4	0.037	11
Control	Mean	**0.24**	N/A [b]	**0.77**	N/A	**1.3**	N/A	**0.044**	N/A
	1	1.7	32	1.3	12	1.9	18	0.048 [a]	N/A
	2	1.6	41	1.3	14	1.04	24	0.046 [a]	N/A
	3	1.4	38	1.5	12	1.54	17	0.037 [a]	N/A
OCA	Mean	**1.6**	N/A	**1.4**	N/A	**1.5**	N/A	**0.044** [a]	N/A
	1	1.7	40	1.1	16	1.03	25	0.048 [a]	N/A
	2	1.6	64	1.4	24	0.54	36	0.046 [a]	N/A
	3	1.3	56	1.5	24	0.79	24	0.037 [a]	N/A
CDCA	Mean	**1.6**	N/A	**1.3**	N/A	**0.78**	N/A	**0.044** [a]	N/A

[a] K_{Flux} values in treated SCHH were fixed to the values in control SCHH from the same hepatocyte donor.

[b] N/A: not applicable

Figure 5.1. Model structure depicting TCA disposition in SCHH in standard HBSS and Ca^{2+}-free HBSS. $C_{u,Cells}$ and $C_{u,Buffer}$ represent unbound concentration in the cells and buffer, respectively. X_{Bile} represents the amount in the bile canalicular compartment.
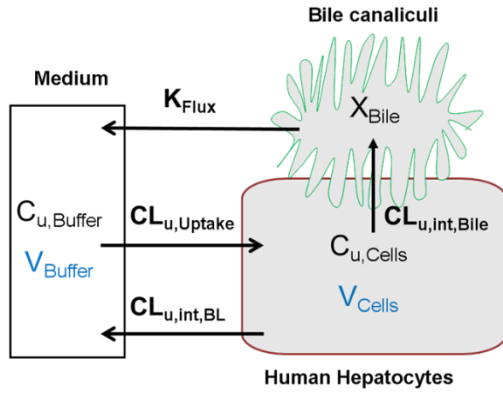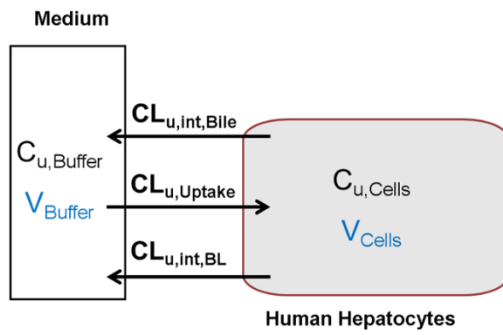
Figure 5.2. Predicted and observed amount of TCA in different matrices from three different SCHH donors. Black, orange, and blue colors represent control-, OCA-, and CDCA-treated groups, respectively, for observed (circles) and predicted (solid lines) data. Experimental data represent the mean ± S.D. (triplicate measurements). The fitted mass vs. time profiles were generated from eqs. 4-8, and the parameter estimates are reported in Table 5.1.
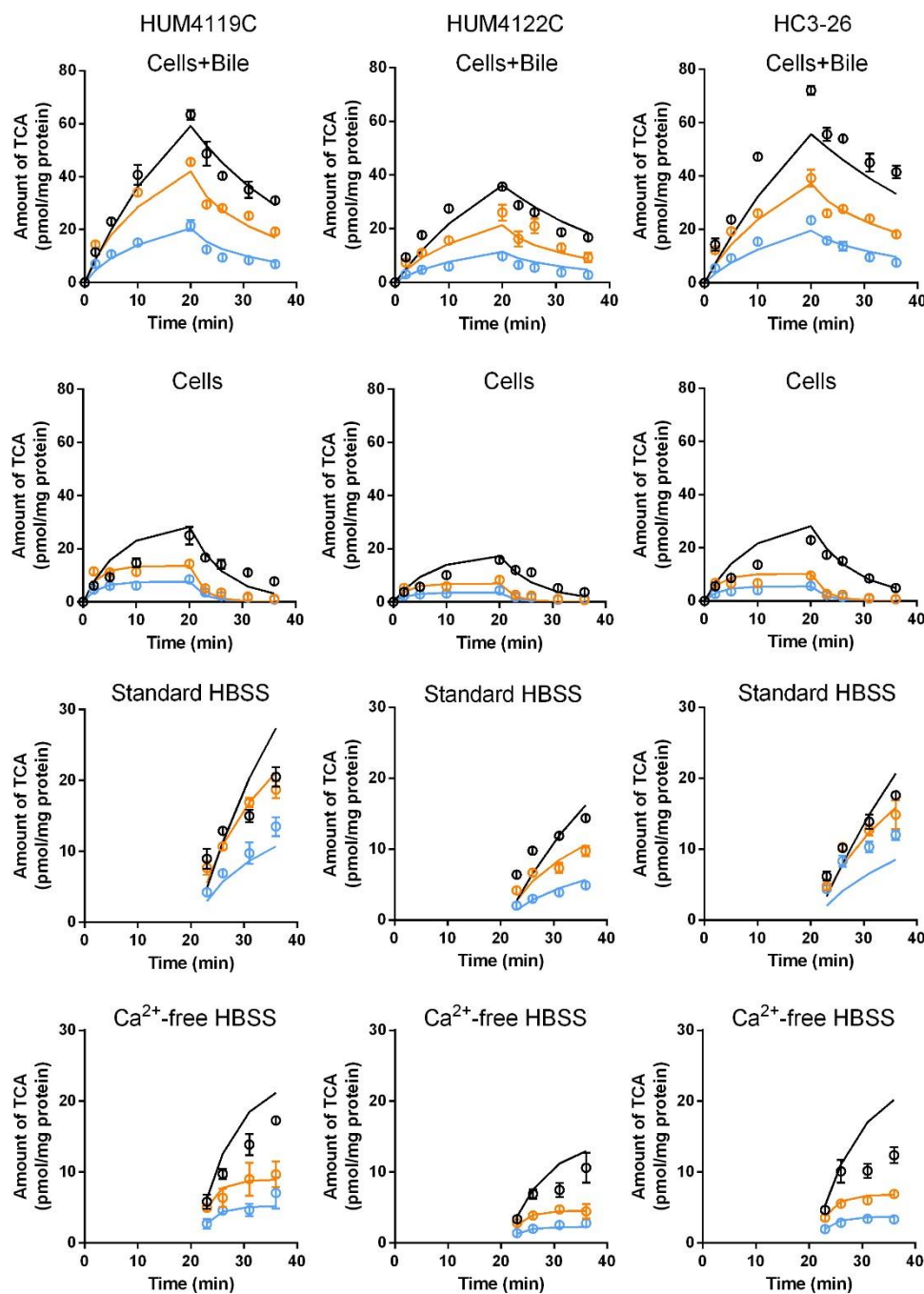
Figure 5.3. Fold change in $CL_{int,BL}$, $CL_{int,Bile}$ and CL_{Uptake} in OCA- and CDCA-treated SCHH compared to control. Data represent mean $\pm$ S.D. (n = 3 hepatocyte donors, as detailed in Table 5.1). **p<0.01; ***p<0.001 (treated vs. control).
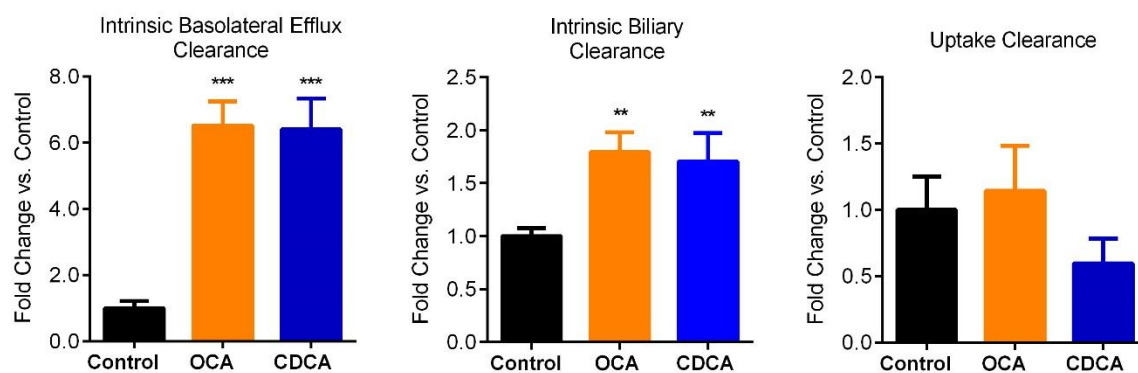
Figure 5.4. Effect of OCA and CDCA treatment of SCHH on the protein expression of OSTα, OSTβ, MRP3, MRP4, BSEP, and NTCP. (A) Immunoblots from three independent studies using three hepatocyte donors are shown. ATPase was used as the loading control for each blot. Donor 1, 2, and 3 represent HU8246, HUM4122D, and HC3-26, respectively. Each protein was analyzed on a separate membrane except that BSEP and NTCP shared the same membrane and the same ATPase bands. (B) Quantitative analyses conducted by calculating the relative densities of each protein normalized by the density of ATPase (mean and S.D. expressed as % of control; n = 3 hepatocyte donors). **p<0.01;***p<0.001 (treated vs. control).
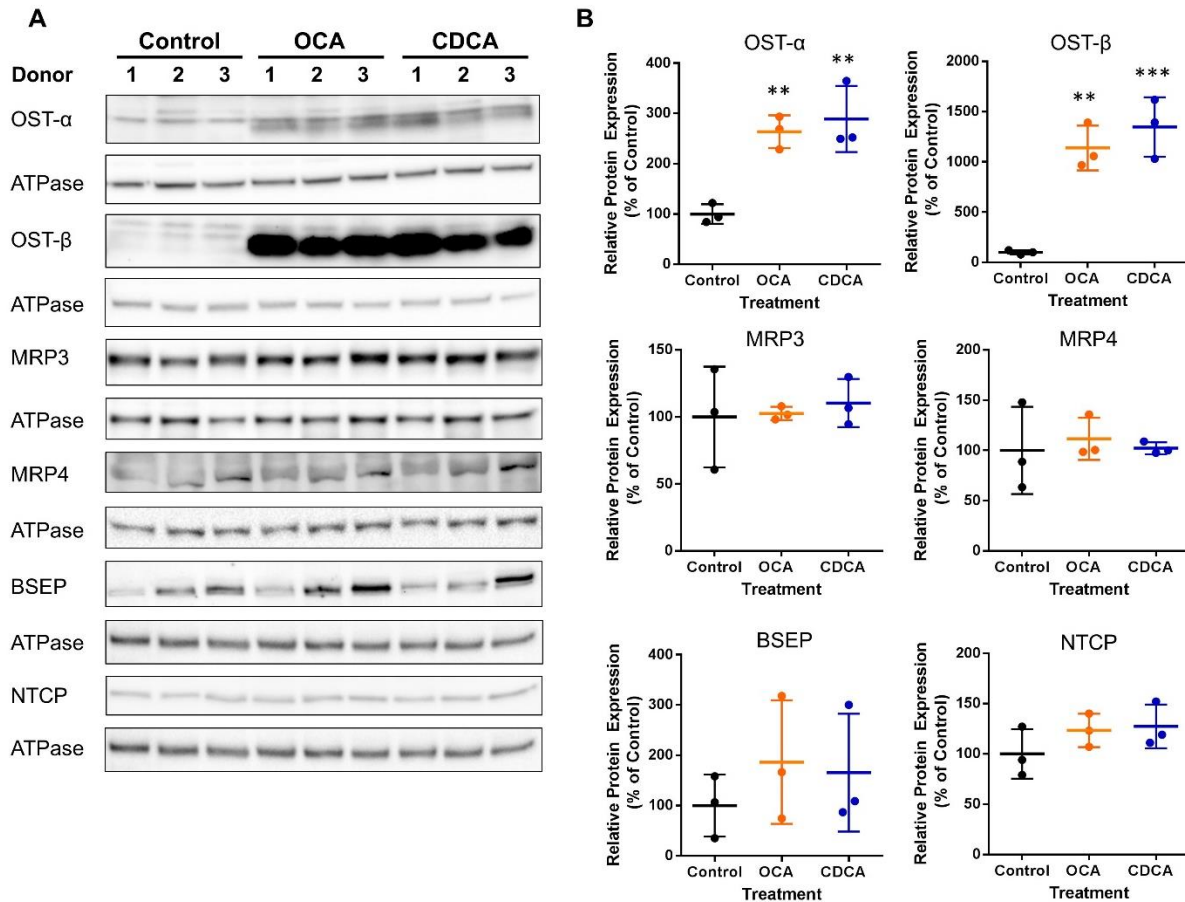
Figure 5.5. The effect of FXR agonists on bile acid clearance and protein expression of bile acid transporters in SCHH. Different colors represent the fold change in clearance values (arrowheads; CL_{Uptake}, $CL_{int,BL}$, $CL_{int,Bile}$) and protein levels of transporters (circles; OSTα/β, MRP3, MRP4, BSEP, NTCP).
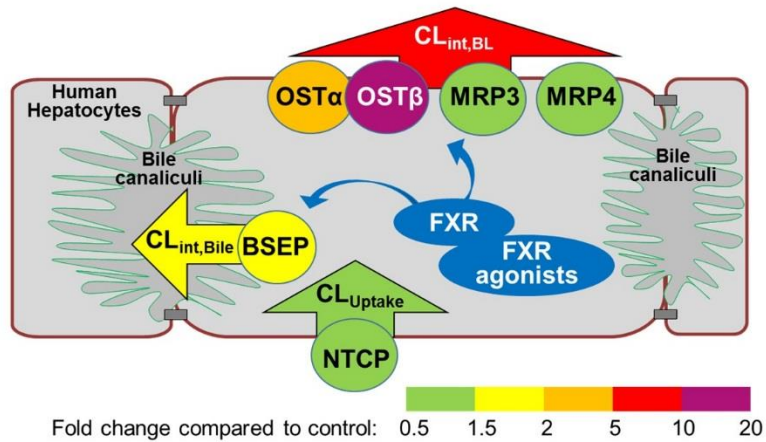
REFERENCES

Adorini L, Pruzanski M and Shapiro D (2012) Farnesoid X receptor targeting to treat nonalcoholic steatohepatitis. *Drug Discov Today* **17**:988-997.

Ananthanarayanan M, Balasubramanian N, Makishima M, Mangelsdorf DJ and Suchy FJ (2001) Human bile salt export pump promoter is transactivated by the farnesoid X receptor/bile acid receptor. *J Biol Chem* **276**:28857-28865.

Ahlin G, Hilgendorf C, Karlsson J, Szigyarto CA, Uhlen M and Artursson P (2009) Endogenous gene and protein expression of drug-transporting proteins in cell lines routinely used in drug discovery programs. *Drug Metab Dispos* **37**:2275-2283.

Allen K, Jaeschke H and Copple BL (2011) Bile acids induce inflammatory genes in hepatocytes: a novel mechanism of inflammation during obstructive cholestasis. *Am J Pathol* **178**:175-186.

Assem M, Schuetz EG, Leggas M, Sun D, Yasuda K, Reid G, Zelcer N, Adachi M, Strom S, Evans RM, Moore DD, Borst P and Schuetz JD (2004) Interactions between hepatic Mrp4 and Sult2a as revealed by the constitutive androstane receptor and Mrp4 knockout mice. *J Biol Chem* **279**:22250-22257.

Ballatori N, Christian WV, Lee JY, Dawson PA, Soroka CJ, Boyer JL, Madejczyk MS and Li N (2005) OSTalpha-OSTbeta: a major basolateral bile acid and steroid transporter in human intestinal, renal, and biliary epithelia. *Hepatology (Baltimore, Md)* **42**:1270-1279.

Ballatori N, Fang F, Christian WV, Li N and Hammond CL (2008) Ostalpha-Ostbeta is required for bile acid and conjugated steroid disposition in the intestine, kidney, and liver. *Am J Physiol Gastrointest Liver Physiol* **295**:G179-g186.

Ballatori N, Li N, Fang F, Boyer JL, Christian WV and Hammond CL (2009) OST alpha-OST beta: a key membrane transporter of bile acids and conjugated steroids. *Front Biosci (Landmark Ed)* **14**:2829-2844.

Boyer JL, Trauner M, Mennone A, Soroka CJ, Cai SY, Moustafa T, Zollner G, Lee JY and Ballatori N (2006) Upregulation of a basolateral FXR-dependent bile acid efflux transporter OSTalpha-OSTbeta in cholestasis in humans and rodents. *Am J Physiol Gastrointest Liver Physiol* **290**:G1124-1130.

Chandra P, Zhang P and Brouwer KLR (2005) Short-term regulation of multidrug resistance-associated protein 3 in rat and human hepatocytes. *Am J Physiol Gastrointest Liver Physiol.* **288**:G1252-1258.

Chai J, He Y, Cai SY, Jiang Z, Wang H, Li Q, Chen L, Peng Z, He X, Wu X, Xiao T, Wang R, Boyer JL and Chen W (2012) Elevated hepatic multidrug resistance-associated protein 3/ATP-binding cassette subfamily C 3 expression in human obstructive cholestasis is mediated through

tumor necrosis factor alpha and c-Jun NH2-terminal kinase/stress-activated protein kinase-signaling pathway. *Hepatology (Baltimore, Md)* **55**:1485-1494.

Chen W, Cai SY, Xu S, Denson LA, Soroka CJ and Boyer JL (2007) Nuclear receptors RXRalpha:RARalpha are repressors for human MRP3 expression. *Am J Physiol Gastrointest Liver Physiol* **292**:G1221-1227.

Dawson PA, Lan T and Rao A (2009) Bile acid transporters. *J Lipid Res* **50**:2340-2357.

Dawson PA, Hubbert ML and Rao A (2010) Getting the mOST from OST: Role of organic solute transporter, OSTalpha-OSTbeta, in bile acid and steroid metabolism. *Biochim Biophys Acta* **1801**:994-1004.

Denson LA, Sturm E, Echevarria W, Zimmerman TL, Makishima M, Mangelsdorf DJ, Karpen SJ (2001) The orphan nuclear receptor, shp, mediates bile acid-induced inhibition of the rat bile acid transporter, ntcp. *Gastroenterology.* **121**: 140-147.

Edwards JE, LaCerte C, Peyret T, Gosselin NH, Marier JF, Hofmann AF and Shapiro D (2016) Modeling and experimental studies of obeticholic acid exposure and the impact of cirrhosis stage. *Clin Transl Sci* **9**:328-336.

Fiorucci S, Rizzo G, Donini A, Distrutti E and Santucci L (2007) Targeting farnesoid X receptor for liver and metabolic disorders. *Trends Mol Med* **13**:298-309.

Geier A, Wagner M, Dietrich CG and Trauner M (2007) Principles of hepatic organic anion transporter regulation during cholestasis, inflammation and liver regeneration. *Biochim Biophys Acta* **1773**:283-308.

Gu X and Manautou JE (2010) Regulation of hepatic ABCC transporters by xenobiotics and in disease states. *Drug Metab Rev* **42**:482-538.

Guo C, Yang K, Brouwer KR, St Claire RL, 3rd and Brouwer KLR (2016) Prediction of altered bile acid disposition due to inhibition of multiple transporters: an integrated approach using sandwich-cultured hepatocytes, mechanistic modeling, and simulation. *J Pharmacol Exp Ther* **358**:324-333.

Inokuchi A, Hinoshita E, Iwamoto Y, Kohno K, Kuwano M and Uchiumi T (2001) Enhanced expression of the human multidrug resistance protein 3 by bile salt in human enterocytes. A transcriptional control of a plausible bile acid transporter. *J Biol Chem* **276**:46822-46829.

Jackson JP, Freeman KM, Friley WW, St Claire RL, 3rd and Brouwer KR (2016) Basolateral efflux transporters: a potentially important pathway for the prevention of cholestatic hepatotoxicity. *Appl In Vitro Toxicol* **2**:207-216.

Jiang T, Wang XX, Scherzer P, Wilson P, Tallman J, Takahashi H, Li J, Iwahashi M, Sutherland E, Arend L and Levi M (2007) Farnesoid X receptor modulates renal lipid metabolism, fibrosis, and diabetic nephropathy. *Diabetes* **56**:2485-2493.

Jung D, Elferink MG, Stellaard F and Groothuis GM (2007) Analysis of bile acid-induced regulation of FXR target genes in human liver slices. *Liver Int* **27**:137-144.

Landrier JF, Eloranta JJ, Vavricka SR and Kullak-Ublick GA (2006) The nuclear receptor for bile acids, FXR, transactivates human organic solute transporter-alpha and -beta genes. *Am J Physiol Gastrointest Liver Physiol* **290**:G476-485.

LeCluyse E, Madan A, Hamilton G, Carroll K, DeHaan R and Parkinson A (2000) Expression and regulation of cytochrome P450 enzymes in primary cultures of human hepatocytes. *J Biochem Mol Toxicol* **14**:177-188.

Lee H, Zhang Y, Lee FY, Nelson SF, Gonzalez FJ and Edwards PA (2006) FXR regulates organic solute transporters alpha and beta in the adrenal gland, kidney, and intestine. *J Lipid Res* **47**:201-214.

Lee JK, Marion TL, Abe K, Lim C, Pollock GM and Brouwer KLR (2010) Hepatobiliary disposition of troglitazone and metabolites in rat and human sandwich-cultured hepatocytes: use of Monte Carlo simulations to assess the impact of changes in biliary excretion on troglitazone sulfate accumulation. *J Pharmacol Exp Ther* **332**:26-34.

Lefebvre P, Cariou B, Lien F, Kuipers F and Staels B (2009) Role of bile acids and bile acid receptors in metabolic regulation. *Physiol Rev* **89**:147-191.

Liu J, Lu H, Lu YF, Lei X, Cui JY, Ellis E, Strom SC and Klaassen CD (2014) Potency of individual bile acids to regulate bile acid synthesis and transport genes in primary human hepatocyte cultures. *Toxicol Sci* **141**:538-546.

Liu X, LeCluyse EL, Brouwer KR, Lightfoot RM, Lee JI and Brouwer KLR (1999) Use of Ca^{2+} modulation to evaluate biliary excretion in sandwich-cultured rat hepatocytes. *J Pharmacol Exp Ther* **289**:1592-1599.

Markham A and Keam SJ (2016) Obeticholic Acid: first global approval. *Drugs* **76**:1221-1226.

Modica S, Gadaleta RM and Moschetta A (2010) Deciphering the nuclear bile acid receptor FXR paradigm. *Nucl Recept Signal* **8**:e005.

Ohtsuki S, Schaefer O, Kawakami H, Inoue T, Liehner S, Saito A, Ishiguro N, Kishimoto W, Ludwig-Schwellinger E, Ebner T and Terasaki T (2012) Simultaneous absolute protein quantification of transporters, cytochromes P450, and UDP-glucuronosyltransferases as a novel approach for the characterization of individual human liver: comparison with mRNA levels and activities. *Drug Metab Dispos* **40**:83-92.

Orntoft NW, Munk OL, Frisch K, Ott P, Keiding S and Sorensen M (2017) Hepatobiliary transport kinetics of the conjugated bile acid tracer 11C-CSar quantified in healthy humans and patients by positron emission tomography. *J Hepatol* **67**:321-327.

Oshio C and Phillips MJ (1981) Contractility of bile canaliculi: implications for liver function. *Science (New York, NY)* **212**:1041-1042.

Pfeifer ND, Yang K and Brouwer KLR (2013) Hepatic basolateral efflux contributes significantly to rosuvastatin disposition I: characterization of basolateral versus biliary clearance using a novel protocol in sandwich-cultured hepatocytes. *J Pharmacol Exp Ther* **347**:727-736.

Rius M, Hummel-Eisenbeiss J, Hofmann AF and Keppler D (2006) Substrate specificity of human ABCC4 (MRP4)-mediated cotransport of bile acids and reduced glutathione. *Am J Physiol Gastrointest Liver Physiol* **290**:G640-649.

Schonhoff CM, Webster CR and Anwer MS (2013) Taurolithocholate-induced MRP2 retrieval involves MARCKS phosphorylation by protein kinase C in HUH-NTCP Cells. *Hepatology (Baltimore, Md)* 58:284-292.

Seward DJ, Koh AS, Boyer JL and Ballatori N (2003) Functional complementation between a novel mammalian polygenic transport complex and an evolutionarily ancient organic solute transporter, OSTalpha-OSTbeta. *J Biol Chem* **278**:27473-27482.

Soisson SM, Parthasarathy G, Adams AD, Sahoo S, Sitlani A, Sparrow C, Cui J and Becker JW (2008) Identification of a potent synthetic FXR agonist with an unexpected mode of binding and activation. *Proc Natl Acad Sci USA* **105**:5337-5342.

Soroka CJ, Ballatori N and Boyer JL (2010) Organic solute transporter, OSTalpha-OSTbeta: its role in bile acid transport and cholestasis. *Semin Liver Dis* **30**:178-185.

Staels B and Kuipers F (2007) Bile acid sequestrants and the treatment of type 2 diabetes mellitus. *Drugs* **67**:1383-1392.

Sultan M, Rao A, Elpeleg O, Vaz FM, Abu Libdeh BY, Karpen SJ and Dawson PA (2017) Organic Solute Transporter-beta (SLC51B) Deficiency in Two Brothers with Congenital Diarrhea and Features of Cholestasis. *Hepatology.* [Epub ahead of print]

Swift B, Pfeifer ND, Brouwer KLR 2010. Sandwich-cultured hepatocytes: an in vitro model to evaluate hepatobiliary transporter-based drug interactions and hepatotoxicity. *Drug Metab Rev* 42(3):446-471.

Teng S, Jekerle V and Piquette-Miller M (2003) Induction of ABCC3 (MRP3) by pregnane X receptor activators. *Drug Metab Dispos* **31**:1296-1299.

Thomas C, Pellicciari R, Pruzanski M, Auwerx J and Schoonjans K (2008) Targeting bile-acid signalling for metabolic diseases. *Nat Rev Drug Discov* **7**:678-693.

Thompson CG, Fallon JK, Mathews M, Charlins P, Remling-Mulder L, Kovarova M, Adamson L, Srinivas N, Schauer A, Sykes C, Luciw P, Garcia JV, Akkina R, Smith PC and Kashuba ADM (2017) Multimodal analysis of drug transporter expression in gastrointestinal tissue. *AIDS (London, England)* **31**:1669-1678.

Trivedi PJ, Hirschfield GM and Gershwin ME (2016) Obeticholic acid for the treatment of primary biliary cirrhosis. *Expert Rev Clin Pharmacol* **9**:13-26.

Wang L, Soroka CJ and Boyer JL (2002) The role of bile salt export pump mutations in progressive familial intrahepatic cholestasis type II. *J Clin Invest* **110**:965-972.

Wagner M, Zollner G and Trauner M (2011) Nuclear receptors in liver disease. *Hepatology (Baltimore, Md)* **53**:1023-1034.

Watanabe S, Smith CR and Phillips MJ (1985) Coordination of the contractile activity of bile canaliculi. Evidence from calcium microinjection of triplet hepatocytes. *Lab Invest* **53**:275-279.

Wolf KK, Brouwer KR, Pollack GM and Brouwer KLR (2008) Effect of albumin on the biliary clearance of compounds in sandwich-cultured rat hepatocytes. *Drug Metab Dispos* **36**:2086-2092.

Yang K, Guo C, Woodhead JL, St Claire RL, 3rd, Watkins PB, Siler SQ, Howell BA and Brouwer KLR (2016) Sandwich-cultured hepatocytes as a tool to study drug disposition and drug-induced liver injury. *J Pharm Sci* **105**:443-459.

Yang K, Pfeifer ND, Kock K and Brouwer KLR (2015) Species differences in hepatobiliary disposition of taurocholic acid in human and rat sandwich-cultured hepatocytes: implications for drug-induced liver injury. *J Pharmacol Exp Ther* **353**:415-423.

Yu J, Lo JL, Huang L, Zhao A, Metzger E, Adams A, Meinke PT, Wright SD and Cui J (2002) Lithocholic acid decreases expression of bile salt export pump through farnesoid X receptor antagonist activity. *J Biol Chem* **277**:31441-31447.

Zhang DW, Gu HM, Vasa M, Muredda M, Cole SP and Deeley RG (2003) Characterization of the role of polar amino acid residues within predicted transmembrane helix 17 in determining the substrate specificity of multidrug resistance protein 3. *Biochemistry* **42**:9989-10000.

Zhang P, Tian X, Chandra P and Brouwer KLR (2005) Role of glycosylation in trafficking of Mrp2 in sandwich-cultured rat hepatocytes. *Mol Pharmacol* **67**:1334-1341.

Zhang Y, Jackson JP, St Claire RL, 3rd, Freeman KM, Brouwer KR and Edwards JE (2017) Obeticholic acid, a selective farnesoid X receptor agonist, regulates bile acid homeostasis in sandwich-cultured human hepatocytes. *Pharmacol Res Perspect* **5**: 1-11.

Zollner G, Fickert P, Silbert D, Fuchsbichler A, Marschall HU, Zatloukal K, Denk H and Trauner M (2003) Adaptive changes in hepatobiliary transporter expression in primary biliary cirrhosis. *J Hepatol* **38**:717-727

CHAPTER 6. Summary and Future Directions

This dissertation research has focused on developing methods to improve the understanding and prediction of drug interactions with hepatic bile acid transporters. Inhibition or induction of bile acid transporters can lead to altered hepatic bile acid disposition, and therefore, may exert hepatotoxic or hepatoprotective effects. The effect of a drug on bile acid transporters is often multifactorial, including simultaneous inhibition and/or induction of uptake and efflux transporters, and may involve transport mechanisms that are poorly characterized. Therefore, the linkage between the function of individual bile acid transporters in the presence of a drug, and the overall impact on bile acid disposition in hepatocytes, remains to be studied. To better understand this linkage, "bottom-up" and "top-down" modeling approaches were used (**Figure 6.1**). A series of studies was conducted utilizing in vitro systems, primarily rat and human sandwich-cultured hepatocytes (SCH), as well as in silico tools, including mechanistic pharmacokinetic (PK) modeling and simulation. Aims #1 and #2 focused on inhibitory interactions, and Aim #3 studied induction-type interactions. Taurocholic acid (TCA) was used as the model bile acid substrate to evaluate bile acid transporter function due to the wealth of data generated using TCA as the substrate. A number of model transporter inhibitors and inducers were used. Bosentan, telmisartan, and troglitazone sulfate (TS) were selected as inhibitors of multiple bile acid transporters. Obeticholic acid (OCA) and chenodeoxycholic acid (CDCA), which are strong Farnesoid X Receptor (FXR) agonists, were used to induce efflux transporters.

In **Aim #1**, a framework was developed to predict the net effect of inhibiting multiple transporters on bile acid disposition in human SCH. Individual transporter inhibition data [e.g., half maximal inhibition concentration (IC_{50})] and relevant inhibitor concentrations were integrated by using mechanistic PK modeling. The applicability of this framework was demonstrated by predicting the effect of bosentan and telmisartan on TCA disposition using unbound inhibitor concentrations (**Chapter 2**). To further assess the relevant inhibitor concentration in predicting the effect of hepatic efflux transporter inhibition, a method to determine the benefit of using the unbound versus total intracellular inhibitor concentration was proposed. This method was developed based on simulation results and evaluated with experimental data from human SCH (**Chapter 3**). In this Aim, a "bottom-up" approach was used to predict the overall bile acid disposition in hepatocytes using individual transporter inhibition data.

The translation of inhibition data generated in systems transfected with individual transporters to drug-bile acid interactions in the whole cells has its limitations, as discussed in Chapter 1 and 2. Therefore, it may be useful to derive the inhibition constant (K_i) for a clearance pathway (e.g., biliary or basolateral efflux), which is a composite K_i for multiple transporters in the same clearance pathway. In **Aim #2**, options for optimal study design in rat SCH were evaluated to provide a dataset for estimating K_i values for TS against the biliary and basolateral efflux clearance values of TCA simultaneously using a "top-down" PK modeling approach (**Chapter 4**).

In **Aim #3**, the induction of bile acid efflux transporters by FXR agonists, OCA and CDCA, was studied in human SCH. Basolateral efflux and biliary clearance values of TCA, determined by mechanistic PK modeling, were increased by FXR agonists, which provided

direct functional evidence of transporter induction. Immunoblot analysis suggested that organic solute transporter α/β (OSTα/β) may be the main transporter responsible for the increase in the basolateral efflux clearance of TCA (**Chapter 5**). In this Aim, a "top-down" approach was used to deconvolute the changes in each clearance pathway using the overall bile acid disposition data.

This dissertation has made a number of contributions in advancing the prediction and evaluation of drug interactions mediated by hepatic bile acid transporters. An overview of the experimental findings, the implications, and future directions for each chapter are discussed in the following sections.

Prediction of Altered Bile Acid Disposition Due to Inhibition of Multiple Transporters: An Integrated Approach Using Sandwich-Cultured Hepatocytes, Mechanistic Modeling and Simulation (Chapter 2)

Inhibition of bile acid efflux transporters may increase the hepatic accumulation of toxic bile acids, leading to liver toxicity (Morgan et al., 2010; Kock et al., 2014). However, translating inhibitory potency data to clinical risks is challenging (Dawson et al., 2012). The simultaneous inhibition of multiple transporters (Aleo et al., 2017) and the relevant inhibitor concentration need to be considered. The purpose of Chapter 2 was to develop a framework to predict altered bile acid disposition in the context of transporter interplay and relevant inhibitor concentrations. The kinetic parameters for deuterium-labeled TCA (d_8-TCA) in the presence of albumin in human SCH were characterized by PK modeling (**Table 2.2**). Based on kinetic parameters of d_8-TCA and the inhibition potency of telmisartan and bosentan, the effect of these inhibitors on the disposition of d_8-TCA was predicted and compared with experimental observations (**Table 2.4**).

The prediction accuracy using different measures of inhibitor concentrations, including cellular total ($[I]_{total,cell}$) or unbound concentrations ($[I]_{unbound,cell}$), and cytosolic total ($[I]_{total,cyt}$) or unbound concentrations ($[I]_{unbound,cyt}$) (**Table 2.3**), was assessed. Finally, a framework was proposed to predict bile acid disposition in human hepatocytes by integrating transporter inhibition data and PK parameters of the bile acid (**Figure 2.5**).

A previously published protocol was adopted to estimate kinetic parameters for TCA and a few modifications were made to better represent the in vivo scenario. First, instead of ^{3}H-TCA, d_8-TCA was used due to the high specificity of mass spectrometry-based quantification without interference from potential TCA metabolites, though the metabolism of TCA has been reported to be negligible (Hofmann and Hagey, 2008). In addition, 4% bovine serum albumin (BSA), approximating the plasma albumin concentration in humans, was added into the uptake buffer to represent the physiologically relevant condition. The impact of protein on the uptake process was mimicked, including the availability of unbound drug, the equilibrium between binding with the albumin and uptake transporters for TCA, and the potential interaction between albumin and transporters at the functional level (albumin-facilitated uptake) (Poulin and Haddad, 2013). In addition, the presence of albumin could limit the uncertainty arising from TCA binding to the experimental apparatus. Because of these benefits, the addition of protein in transport assays has gained more popularity in recent years (Riccardi et al., 2016; Kikuchi et al., 2017; Mao et al., 2018).

A strength of Chapter 2 was to leverage modeling and simulation to assist in the selection of sensitive model output and critical model input, and to explore the underlying rules for experimental findings. Sensitivity analysis of the model output showed that the total TCA concentration in Cells ($C_{t,Cells}$) was the most sensitive experimental readout to the impairment in

both uptake and efflux clearance values **(Figure. 2.2)**. Without this quantitative analysis, TCA amount in Cells+Bile could have been selected since it is most commonly measured. However, the amount in Cells+Bile was sensitive only to inhibition of uptake clearance; if one were relying solely on this value, the inhibitory effect of efflux clearance values might have been overlooked. Theoretically, the cytosolic unbound concentration of inhibitors is most relevant for the inhibition of efflux transporters and therefore, intracellular unbound fraction ($f_{u,cell,inhibitor}$) might be an important model input and worth collecting. Accordingly, the comparison between simulated and experimental observations indicated that the measurement of $f_{u,cell,inhibitor}$ for telmisartan was critical for accurately predicting its effect on TCA disposition, while it was less critical for bosentan (**Table 2.4**). Accordingly, sensitivity analysis was used to explore the underlying rules. Sensitivity analysis revealed that $f_{u,cell,inhibitor}$ was a critical input only for inhibitors with higher ($[I]_{total,cell}/IC_{50}$) values, such as telmisartan (**Figure 2.3, Figure 2.4**). In the case of inhibitors with lower ($[I]_{total,cell}/IC_{50}$) values, resources needed for the measurement of $f_{u,cell,inhibitor}$ could be better allocated elsewhere.

An advantage of the framework shown in **Figure 2.5** is the ability to integrate information readily available for many inhibitors and interpret this information together with TCA kinetics characterized in this study. Inhibition potency against individual bile acid transporters can be accessed through public databases (e.g. UCSF transportal, TP-search) and published studies (Morgan et al., 2010; Dong et al., 2013; Morgan et al., 2013; Dong et al., 2015; Aleo et al., 2017). Intracellular inhibitor concentrations can be estimated using partition coefficient values.

Some model assumptions were necessary due to the lack of knowledge regarding the transport characteristics of the substrate and inhibitors. Since the relative contribution of each

basolateral efflux transporter to the overall basolateral efflux clearance of TCA was unknown, two extreme scenarios were simulated assuming 100% contribution of either MRP3 or MRP4. Although the simulation results were similar in this study, this assumption could become an issue in certain populations in which OSTα/β plays a more important role in the basolateral efflux of TCA, as shown in Chapter 5. This limitation could be addressed by a novel approach to obtain K_i estimates against biliary and basolateral efflux clearance pathways proposed in Chapter 4. If it is necessary to characterize the contribution of each transporter towards the total clearance, RNA interference (RNAi) or Clustered Regularly Interspaced Short Palindromic Repeats (CRISPR)/CRISPR-associated 9 (Cas9) could be used to modulate gene expression in the human SCH (Yue et al., 2009; Dorr et al., 2017; Sosicka et al., 2017), although optimization of these techniques in human SCH would be needed.

In the process of predicting the inhibitor effect, the intracellular concentration of inhibitors was assumed to be static. Although this assumption is reasonable for screening purposes and is possible to achieve in vitro, the portal vein and hepatic concentration of drugs in vivo are rarely static. If a better representation of the in vivo scenario is critical, dynamic models of inhibitors could be incorporated in the simulation process. The kinetic parameters for some commonly used inhibitors are already available in the literature, including bosentan and telmisartan, which were published after the work described in Chapter 2 had been completed (Li et al., 2014; Matsunaga et al., 2016). For other inhibitors, the kinetic parameters need to be obtained through a PK modeling approach.

The small change in TCA $C_{t,Cells}$ observed in this study (**Table 2.4**) was due primarily to the short uptake period (10 min) and the simultaneous inhibition of uptake and efflux transporters. These results suggest that the current standard protocol may not be optimal to detect

the effect of dual inhibition of both uptake and efflux transporters. A simulation-based study design, such as that shown in Chapter 4, would be helpful to develop a dosing scheme that may lead to more extensive alterations in TCA $C_{t,Cells}$. Alternatively, compounds that caused a more extensive increase in TCA $C_{t,Cells}$ in human SCH could be used as model inhibitors, such as glyburide or cyclosporine A (Ansede et al., 2010). In addition, experimental data from additional hepatocyte donors would be helpful to evaluate the simulation results more thoroughly, and to characterize the inter-individual variability, which will be helpful for Monte Carlo simulations.

Outcomes of the research detailed in Chapter 2 serve as the basis for some ideas regarding additional studies. From a practical perspective, the cost of human hepatocytes required to generate time-course data is not trivial. To maximize the use of human hepatocytes, imaging techniques could be used to quantify drug disposition in vitro. Studies by De Bruyn et al. showed that a bile acid derivative N-(24-[7-(4-N,N-dimethylaminosulfonyl-2,1,3-benzoxadiazole)]amino-3α,7α,12α-trihydroxy-27-nor-5β-cholestan-26-oyl)-2'-aminoethanesulfonate (tauro-nor-THCA-24-DBD) was a useful fluorescent probe to study NTCP/Ntcp-, OATP1B1/1B3- and BSEP/Bsep-mediated transport. In addition, they demonstrated that the fluorescence of tauro-nor-THCA-24-DBD in different compartments (i.e., intracellular and bile canaliculi) of rat and human SCH could be quantified by real-time confocal imaging (De Bruyn et al., 2014) without destruction of hepatocytes at each time point. Since at least eight time points are needed for PK modeling, this real-time imaging technique could result in a significant cost savings (at least eight times fewer hepatocytes consumed). However, this approach assumes that the probe is metabolically stable.

The modeling approach developed in Chapter 2 could be applied to characterize the kinetic properties of other endogenous transporter substrates, or in other cellular models. Toxic

bile acids could be studied as substrates, since the disposition of these bile acid species may be more directly relevant to hepatotoxicity and the PK characteristics of various bile acids is likely different. One example is the differential effect of troglitazone on the disposition of TCA and CDCA species in rat SCH (Marion et al., 2011). Differences in PK properties among various bile acid species using transfected cell lines has been published (Notenboom et al., 2018). In addition to bile acids, the mechanistic PK modeling approach could be applied to coproporphyrin (CP) I and III, the endogenous probes for organic anion transporting polypeptide 1B and multidrug resistance-associated protein 2. Current PK models for CP I did not include basolateral efflux clearance due to the lack of knowledge about this clearance pathway (Barnett et al., 2017; Guo et al., 2018). In addition, the framework to predict bile acid disposition in human SCH developed in Chapter 2 could be applied to other holistic cell systems, such as HepaRG cells or the HepatoPac model. However, the cellular models must be polarized and the functionality of transporters and other proteins involved in hepatobiliary drug disposition (e.g., metabolic enzymes, nuclear receptors, trafficking proteins) must be well maintained in order to recover physiologically-relevant parameter estimates.

The prediction of bile acid disposition in human SCH would be of higher impact if the results could be scaled to in vivo. In vitro-in vivo extrapolation of bile acids has been limited by the unknown scaling factors discussed in Chapter 1. Scaling factors may be compound-specific and can be estimated accurately when in vivo data are available (Jones et al., 2012). Clinical PK studies of bile acids, albeit limited, may be useful for the extrapolation of in vitro data, such as the PK profile of [N-methyl-11C]cholylsarcosine (11C-CSar), a bile acid tracer similar to glycocholic acid (Orntoft et al., 2017), and OCA, an analogue of the endogenous bile acid CDCA (Edwards et al., 2016). Alternatively, scaling factors can be generated based on the

abundance of individual bile acid transporters determined by mass spectrometry in human SCH and human liver tissues. This approach has been used to predict the in vivo PK of nine groups of bile acids, such as CDCA and its conjugates (Notenboom et al., 2018).

Prediction of Hepatic Efflux Transporter-Mediated Drug Interactions: When Is It Optimal to Measure Intracellular Unbound Fraction of Inhibitors? (Chapter 3)

Studies in Chapter 2 showed that the impact of using $[I]_{unbound,cell}$ instead of $[I]_{total,cell}$ to predict the transporter inhibitor effect varies depending on the characteristics of the inhibitor, specifically the $([I]_{total,cell}/IC_{50})$ value. As an extension of Chapter 2, the objective of Chapter 3 was to determine when it is optimal to measure $f_{u,cell,inhibitor}$ to accurately predict the effect of efflux transporter inhibitors on the disposition of TCA. These inhibitors were referred to as "risk" inhibitors in Chapter 3. Based on simulation results (**Figure 3.1**), an approach was proposed to classify "risk" inhibitors determined by the plasma unbound fraction ($f_{u,plasma,inhibitor}$) and ($[I]_{total,cell}/IC_{50}$) values of the inhibitors was proposed. The cut-off value of ($[I]_{total,cell}/IC_{50}$) was greater for compounds with higher $f_{u,plasma,inhibitor}$ values (**Figure 3.2**). Experimental data were provided to demonstrate the utility of this approach (**Table 3.2**). For "low-risk" inhibitors, the simulations based on $[I]_{total,cell}$ and $[I]_{unbound,cell}$ were similarly close to experimental observations, which was not the case for "risk inhibitors".

Compared to simulations using $[I]_{unbound,cell}$, the TCA $C_{t,Cells}$ was over-predicted using $[I]_{total,cell}$, which may lead to false-positive predictions of drug-drug interactions (DDIs). The extent of over-prediction increased at first and then decreased as the ($[I]_{total,cell}/IC_{50}$) value became larger. Thus, for extremely strong or weak inhibitors, the differentiating power of using $[I]_{unbound,cell}$ versus $[I]_{total,cell}$ was smaller compared to inhibitors with moderate inhibition potency.

In addition, the benefit of using $[I]_{unbound,cell}$ was bigger for inhibitors with greater intracellular binding, which generally also show higher plasma protein binding. For compounds with lower protein binding, the difference between $[I]_{total,cell}$ and $[I]_{unbound,cell}$ would be smaller, resulting in a smaller difference in the prediction results using these two types of inhibitor concentrations.

The value of understanding the importance of using $[I]_{unbound,cell}$ is to avoid unnecessary collection of $f_{u,cell,inhibitor}$ data. Out of the fifteen experimental compounds, seven compounds were classified as "low-risk" inhibitors. For these compounds, the resources necessary for the measurement of $f_{u,cell,inhibitor}$ could be better allocated elsewhere. Accurate measurement of $f_{u,cell,inhibitor}$ may be labor- and resource-intensive. Although the measurement of $f_{u,cell,inhibitor}$ is higher-throughput using the homogenization method (Riccardi et al., 2018), $f_{u,cell,inhibitor}$ values measured using the homogenization method were generally lower than those obtained using other methods that are less efficient, such as the steady-state accumulation at 4 °C (temperature method)(Riede et al., 2017) and the "cytosol isolation" method that was used in Chapter 2 (Pfeifer et al., 2013). In the "cytosol isolation" method, human SCH are first incubated with the inhibitors, and then homogenized gently to avoid breaking the subcellular organelles. Following that, the cytosol of human SCH homogenate is isolated by differential centrifugation and the unbound fraction in the cytosol is measured.

Some necessary assumptions were made for the simulations. First, a quantitative relationship between intracellular and plasma protein binding was assumed based on the equation reported by Jones et al. (Jones et al., 2012). This assumption was needed since $f_{u,plasma,inhibitor}$ values are more readily available than $f_{u,cell,inhibitor}$ values. The determining factors for classifying "risk" inhibitors need to be easily accessible so this classification approach will be a useful predictive method and can save experimental resources a priori. If this assumed relationship is

inaccurate, the cut-off values might be slightly different. It would be ideal if a quantitative relationship can be established between $f_{u,cell,inhibitor}$ and other easier-to-measure parameters, such as physicochemical properties, chemical structures, etc. Other assumptions have been addressed by additional simulations shown in the Supplement of Chapter 3, including equal biliary IC_{50} and basolateral IC_{50} and the percentage of uptake inhibition.

In Chapter 3, it was assumed that a 2-fold difference between the simulation results is a reasonable criterion to determine that the $[I]_{unbound,cell}$-based simulations are superior to the $[I]_{total,cell}$-based simulations. Although an AUC ratio of 2 is generally used as an indicator of moderate clinical DDIs (FDA/CDER, 2012), this 2-fold criteria is arbitrary. For future studies, more experimental data will be needed to validate the simulation results, and to optimize this criterion by using a receiver operating characteristic (ROC) curve. In a ROC curve, the specificity (false positive rate) and sensitivity (true positive rate) are plotted on the x- and y-axis. The best cut-off value should provide the highest area under the ROC curve (Maiuri et al., 2017). The tolerance for risk should be considered as well.

One question that came up during the peer review process was whether the medium concentration of inhibitors could be used as a substitute for the cellular concentration. This approach is acceptable if the cell membrane does not present a diffusional barrier. Alternatively, the intracellular concentration could be estimated from the medium concentration using the partition coefficient values. Currently, it is still challenging to predict hepatocyte accumulation without experimentation.

Even though more experimental data are needed, Chapter 3 provides a first step towards bridging the gaps to determine the relevant inhibitor concentration a priori. In addition, the

experimental paradigm developed in Chapter 3 could be applied to additional substrates, such as drugs and toxic bile acids.

Modeling and Simulation-Guided Study Design for K_i Estimations against Bile Acid Efflux Clearance Values in Hepatocytes (Chapter 4)

As discussed in Chapter 1 and 2, the utility of individual transporter K_i values will be compromised if the transport mechanism of the substrate is not well characterized. Therefore, the concept of the K_i or IC_{50} against a clearance pathway instead of a specific transporter was proposed in Chapter 4. Traditional methods to estimate K_i values using transfected systems require several concentrations of the inhibitor and the substrate. A more efficient model-based approach to enable K_i estimations against biliary and basolateral efflux clearance values simultaneously using a physiologically-relevant system would be advantageous. Chapter 4 evaluated options for an optimal study design in rat SCH based on modeling and simulation, and used TS and TCA as the model inhibitor and substrate, respectively (**Figures 4.1, 4.5**). A PK model describing the interaction between TS and TCA was evaluated by experimental data (**Figure 4.4**) and used for the simulation. Using the proposed study design, the generated data were suitable for moderately accurate estimation of TS K_i values against biliary and basolateral efflux clearance, which were within 2-fold of the reference values, in different hepatocyte lots (**Figure 4.8, Table 4.7**).

This is the first time the concept of a K_i against a clearance pathway in SCH was proposed using intracellular unbound inhibitor concentration and modeling-based analysis. Compared to conventional methods and individual transporter K_i values, there are several advantages of the approach developed in Chapter 4. The K_i values can be used directly in whole-

body mechanistic models to predict the inhibitor-substrate interactions, even if the transporters involved in the substrate disposition are not fully characterized. In conventional methods, five concentrations for the substrate and inhibitor are added into the incubation buffer to create a dynamic range of concentrations for both compounds at the site of interaction. Similarly, a concentration range for both compounds was achieved in the proposed protocol by allowing the substrate and inhibitor to accumulate in the cells over time. Additionally, the proposed method requires measuring the intracellular unbound concentration of TS to account for the intracellular binding, which is relevant to in vivo conditions. Chapter 4 also demonstrated the advantages of using modeling and simulation to optimize the experimental design so that data input for the PK model is sufficient for reliable parameter estimation.

A similar concept was reported previously; the IC_{50} values of cyclosporine A were estimated against the uptake and efflux clearance of the phenylglucuronide metabolite of mycophenolic acid (Matsunaga et al., 2015). However, this study used the medium concentration of the inhibitor and did not measure the intracellular unbound concentration, which is crucial to obtain an accurate estimate of the K_i or IC_{50} against the efflux clearance, and to translate these values to in vivo.

Future experiments using this optimized study design will be helpful to assess the utility of this protocol, especially in the presence of experimental error. Several practical issues should be considered including the potential cytotoxicity of the inhibitor and the lowest limit for quantification for the substrate (i.e., TCA) and the inhibitor (i.e., TS). In Chapter 4, maximum velocity values for TCA efflux were estimated using data from a published study where TCA was dosed at 1 μM. This was not the ideal experimental condition to estimate nonlinear PK parameters, since the intracellular concentration of TCA was <1 μM, which is much lower than

the Michaelis-Menten constants for TCA efflux clearance. In future studies, TCA should be dosed at 5 μM, which would generate higher intracellular concentrations and provide more accurate estimates of the maximum velocity.

The framework proposed in Chapter 4 could be applied to design experiments for other inhibitors, in addition to TS. The necessary prior information and modifications in this study design are shown in **Figure 4.11**. This approach could be extended to estimate K_i for both the parent drug and metabolites. Transporter inhibition assays by metabolite(s) may not be evaluated routinely. However, some metabolites are potent inhibitors of BSEP, such as TS (Funk et al., 2001) and DM-4103, a metabolite of tolvaptan (Slizgi et al., 2016). In the present study, troglitazone was metabolized to TS rapidly, which made quantification of the troglitazone K_i challenging. The K_i information for metabolites could be especially useful in the early stages of drug discovery and development, when large amounts of pure metabolites are generally unavailable for traditional transporter assays.

Finally, the utility of the overall K_i for the clearance value can be evaluated against the "individual transporter IC_{50}" values by incorporating inhibition potency data into mechanistic models, including physiologically-based PK models and systems pharmacology models, such as DILIsym®, to predict troglitazone-mediated hepatotoxicity. The K_i value and inhibition mechanism of TS against TCA biliary clearance is an important model input for the prediction of troglitazone-mediated hepatotoxicity using DILIsym® (Yang et al., 2014).

FXR Agonists Obeticholic Acid and Chenodeoxycholic Acid Increase Bile Acid Efflux in Sandwich-Cultured Human Hepatocytes: Functional Evidence and Mechanisms (Chapter 5)

FXR is a nuclear receptor that is expressed at high levels in the liver and intestine and regulates bile acid homeostasis (Lefebvre et al., 2009). That mechanism contributed to the therapeutic rationale for FXR agonists being developed to treat cholestatic liver disease, such as primary sclerosing cholangitis, and chronic liver disease, such as non-alcoholic steatohepatitis (NASH) (Fiorucci et al., 2007; Wagner et al., 2011; Nevens et al., 2016). FXR agonists, OCA and CDCA, increased mRNA expression of bile acid efflux transporters in human SCH after 72 hr treatment (Jackson et al., 2016; Zhang et al., 2017). The purpose of Chapter 5 was to characterize the effects of OCA and CDCA treatment on the function and protein expression of bile acid transporters in human SCH. PK modeling of d_8-TCA data showed that the intrinsic basolateral efflux clearance ($CL_{int,BL}$) and intrinsic biliary clearance ($CL_{int,Bile}$) of TCA were significantly increased by OCA (1 µM) and CDCA (100 µM) treatment for 72 hr, with minimal change in the uptake clearance (CL_{Uptake}) (**Figure 5.3**, **Table 5.1**). Immunoblotting was performed to assess protein expression of individual transporters. Results showed that the expression of OSTα and OSTβ in FXR agonist-treated human SCH was significantly induced, with only modest changes in other TCA transporters (**Figure 5.4**). Therefore, OSTα/β appeared to be the major transporter responsible for the increase in $CL_{int,BL}$ of d_8-TCA.

It is challenging to study transporter induction, as suggested by the limited number of publications on transporter induction. With the assistance of PK modeling, **Chapter 5** addressed some of these challenges and provided, for the first time, clear functional evidence for bile acid efflux transporter induction in human SCH. Furthermore, quantifying the function of efflux

transporters, especially those on the basolateral membrane, is challenging due to the concurrent uptake processes. PK modeling can deconvolute these processes, and also provide high granularity in the quantification; even modest changes can be detected. Without time-course data and the assistance of mathematical/PK modeling, such changes could have been overlooked, as shown by the minor changes in model-independent parameters calculated from data at a single time point (e.g. biliary excretion index and buffer recovery index). Most of the published literature reporting transporter induction is at the mRNA level. However, changes in gene expression of transporters may not translate to changes in protein expression (Ahlin et al., 2009; Thompson et al., 2017) and/or function (Ohtsuki et al., 2012). Clinical evidence for drug-mediated transporter induction is very limited, although there are reports of disease-related up-regulation of transporters. For example, the mRNA and protein level of OSTβ were increased in the livers of NASH and PBC patients (Malinen et al., 2018), which may be due to increased bile acids in the liver (Lake et al., 2013). This is consistent with increased OSTβ protein levels in human SCH after exposure to CDCA reported in Chapter 5. The protein expression (Hardwick et al., 2011) and function of MRP3 were increased in NASH patients (Ferslew et al., 2015). Findings in Chapter 5 bridged the gap between mRNA and function data for the FXR agonist-mediated induction of bile acid efflux transporters.

The quantification of functional changes in transporters shown in this study can be helpful to predict clinical outcomes and optimize pharmacotherapy. For example, the changes in transporter function can be used as key data input for whole-body mechanistic PK models to predict clinical liabilities for DDIs or drug-induced liver injury as a result of induction of OSTα/β. OSTα/β transports various endogenous and exogenous substrates such as digoxin (Soroka et al., 2010; Malinen et al., 2018) and rosuvastatin (Schwarz, 2012). Digoxin has a

narrow therapeutic window (Ehle et al., 2011) and rosuvastatin is a potential co-medication with

OCA in NASH patients (Kargiotis et al., 2014). A recent clinical study showed a modest increase

in the systemic exposure of rosuvastatin in healthy subjects taking oral daily doses of 25 mg

OCA (1.3-fold increase compared to control) (Edwards et al., 2017), which may be related to the

induction of OSTα/β and increased hepatic basolateral efflux of rosuvastatin. In this clinical

study, no obvious changes in digoxin systematic exposure were observed (1.1-fold increase

compared to control). If these functional data were unavailable and gene data (43-fold increase

in OSTβ) were used instead to predict DDI liability, the DDI risk might be overpredicted.

This study was designed to mimic the in vivo scenario. There was no wash-out phase

between the FXR agonist treatment and the uptake of TCA. Thus, a caveat of this study design

was that the induction of transporters may be masked by the concurrent inhibition of transporters

by OCA and/or CDCA. Although the actual induction in transport might be higher than what was

observed, the study design was deemed most relevant to the in vivo situation, where induction

and inhibition may occur simultaneously.

Although $CL_{int,Bile}$ was increased by ~1.5 fold after OCA and CDCA treatment, there

were no significant changes in the total level of BSEP protein. This apparent discrepancy

between function and protein data could be explained by the localization and trafficking of

BSEP. Transporters must be expressed on the plasma membrane to be functional (Wang et al.,

2002; Chandra et al., 2005; Zhang et al., 2005). After being synthesized in the Golgi, BSEP is

transiently sequestered in an intracellular vesicle pool en route to the canalicular membrane

(Kipp and Arias, 2000; Van et al., 2000). As a mechanism of short-term regulation, BSEP can be

cycled between the membrane and the intracellular pools of vesicles (Kipp et al., 2001; Wustner

et al., 2001; Hoekstra et al., 2004). Therefore, although there was no change in the total protein

level, the amount of BSEP expressed on the plasma membrane might be increased. To prove this hypothesis, isolation of plasma membrane (Lee et al., 2008; Kweon et al., 2016) followed by immunoblotting analysis could be considered for future investigations. In addition, it would be ideal to use the same hepatocyte lots for the functional study and protein quantification. However, due to the limited availability of quality human hepatocytes, one of the three hepatocyte lots used for the functional study, HUM4199C, was no longer available when the immunoblotting studies were conducted.

The OCA- and CDCA-associated changes in d_8-TCA disposition were believed to be a result of FXR activation, since multiple FXR target genes were altered (Jackson et al., 2016; Zhang et al., 2017). To provide more definitive evidence for this cause effect relationship, additional studies could be considered. For example, if co-exposure of an FXR antagonist or FXR knockdown in human SCH (through RNAi or CRISPR) decreased the effect of OCA or CDCA on increasing the efflux of d_8-TCA, this would establish the FXR-dependence of the observed changes.

In the implementation of PK modeling, the rate constant describing the flux of compound from bile canaliculi to the medium (K_{Flux}) was fixed at the value from control human SCH to avoid over-parameterization. In addition, the effect of OCA and CDCA on K_{Flux} was unknown. A recent publication showed that the cholestatic drugs cyclosporine A and chlorpromazine changed the bile canalicular volume in HepaRG cells (Kaschek et al., 2018), indicating that K_{Flux} could be altered by some compounds.

The findings of Chapter 5 laid the foundation for some future studies that could expand the impact of this research. In vivo evidence is needed to prove transporter induction in response to FXR agonists. Biomarkers for OSTα/β, such as plasma bile acids, could be informative.

However, the bile acid profile is affected by bile acid synthesis and metabolism rates, which are regulated by FXR. Since OSTα/β is also expressed in the intestine, which is another important organ that governs bile acid disposition, the overall impact of OSTα/β induction on systemic bile acid exposure in vivo needs to be assessed by a whole-body physiologically-based PK model. Due to the challenges in quantifying bile acid kinetics in humans, quantitative intravital microscopy of fluorescent bile salts, such as cholylglycyl amidofluorescein and cholyl-lysyl-fluorescein, in rats could provide an estimate of bile acid transport clearance values (Ryan et al., 2018). However, the species difference needs be considered when interpreting bile acid data from rodents.

There are many other FXR agonists under development for the treatment of chronic liver diseases, including synthetic FXR agonists and herbal medicines (Gao et al., 2017; Kong et al., 2018). The paradigm used in Chapter 5 can serve as an in vitro tool to prioritize FXR agonists based on their induction effect on bile acid transporters, which is part of the therapeutic rationale for FXR agonists to treat cholestatic liver diseases. In addition to FXR, other nuclear receptors are exploited as drug targets and may regulate transporter function. For example, liver X receptor (LXR) is being developed as a potential therapeutic target for neurodegenerative diseases, such as Alzheimer's disease (Xu et al., 2013). A recent study using human SCH showed that an LXR agonist increased the protein level of P-glycoprotein and decreased the protein level of organic cation transporter 1 and organic anion transporter 2 (Ito and Brouwer, 2018) Alterations in the function of these transporters can be proven using the PK modeling approach in Chapter 5.

Concluding Remarks

The field of drug metabolism and transport research has generated abundant experimental data over the past few decades. This field is evolving towards an era when in silico tools will be

205

leveraged to integrate and interpret available in vitro and in vivo data, to predict untested scenarios, to facilitate the optimization of study designs, and to identify knowledge gaps. This dissertation research showcased these diverse applications by combining a physiologically-relevant cellular model and PK modeling, with a focus on bile acid transporter-mediated drug interactions. It is of great interest to obtain quality in vitro data in an effective and efficient fashion. The approaches developed in this research can be added into a toolbox that can be used by laboratory scientists and pharmacometricians to facilitate drug development using in vitro data.

Figure 6.1. Summary of the in vitro and in silico tools used in this dissertation research and the connection between each aims. The effect of inhibitors and inducers is shown in blue and orange, respectively.
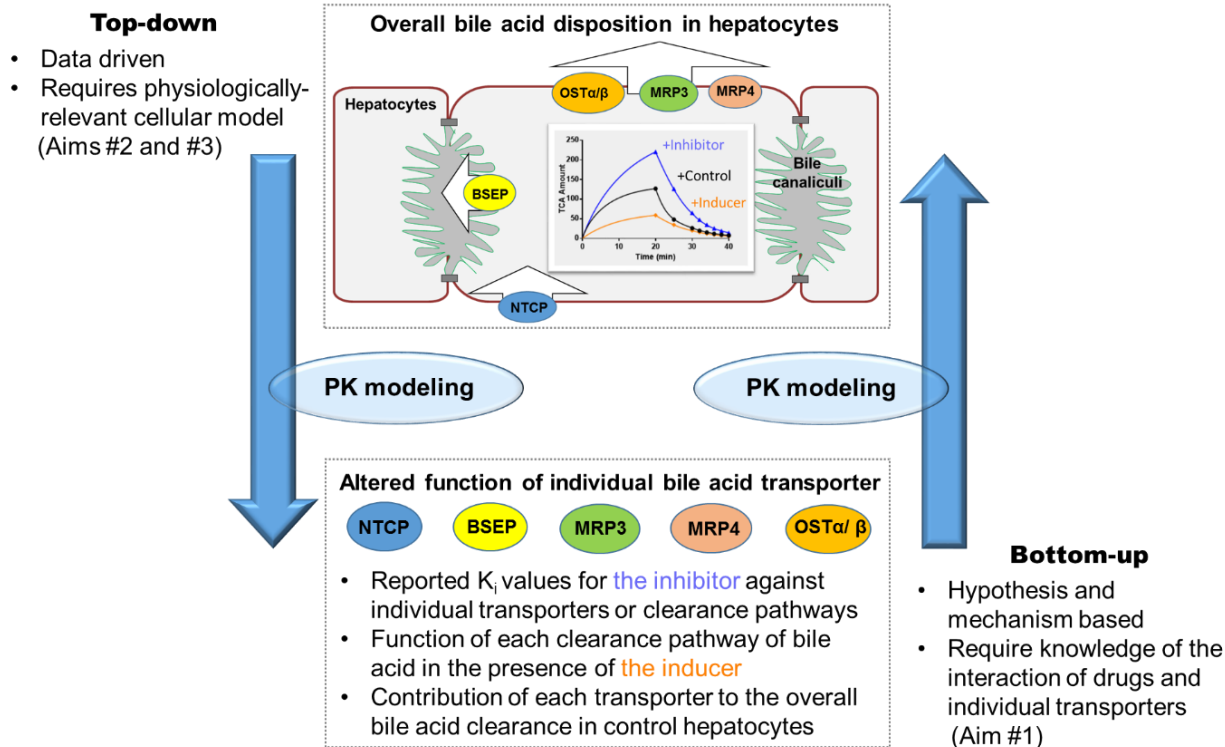
REFERENCES

Ahlin G, Hilgendorf C, Karlsson J, Szigyarto CA, Uhlen M and Artursson P (2009) Endogenous gene and protein expression of drug-transporting proteins in cell lines routinely used in drug discovery programs. *Drug Metab Dispos* **37**:2275-2283.

Aleo MD, Shah F, He K, Bonin PD and Rodrigues AD (2017) Evaluating the Role of Multidrug Resistance Protein 3 (MDR3) Inhibition in Predicting Drug-Induced Liver Injury Using 125 Pharmaceuticals. *Chem Res Toxicol* **30**:1219-1229.

Ansede JH, Smith WR, Perry CH, St Claire RL, 3rd and Brouwer KR (2010) An in vitro assay to assess transporter-based cholestatic hepatotoxicity using sandwich-cultured rat hepatocytes. *Drug Metab Dispos* **38**:276-280.

Barnett S, Ogungbenro K, Menochet K, Shen H, Lai Y, Humphreys WG and Galetin A (2017) Gaining Mechanistic Insight Into Coproporphyrin I as Endogenous Biomarker for OATP1B-Mediated Drug-Drug Interactions Using Population Pharmacokinetic Modeling and Simulation. *Clin Pharmacol Ther*.

Chandra P, Zhang P and Brouwer KL (2005) Short-term regulation of multidrug resistance-associated protein 3 in rat and human hepatocytes. *Am J Physiol Gastrointest Liver Physiol* **288**:G1252-1258.

Dawson S, Stahl S, Paul N, Barber J and Kenna JG (2012) In vitro inhibition of the bile salt export pump correlates with risk of cholestatic drug-induced liver injury in humans. *Drug Metab Dispos* **40**:130-138.

De Bruyn T, Sempels W, Snoeys J, Holmstock N, Chatterjee S, Stieger B, Augustijns P, Hofkens J, Mizuno H and Annaert P (2014) Confocal imaging with a fluorescent bile acid analogue closely mimicking hepatic taurocholate disposition. *J Pharm Sci* **103**:1872-1881.

Dong Z, Ekins S and Polli JE (2013) Structure-activity relationship for FDA approved drugs as inhibitors of the human sodium taurocholate cotransporting polypeptide (NTCP). *Mol Pharm* **10**:1008-1019.

Dong Z, Ekins S and Polli JE (2015) Quantitative NTCP pharmacophore and lack of association between DILI and NTCP Inhibition. *Eur J Pharm Sci* **66**:1-9.

Dorr CR, Remmel RP, Muthusamy A, Fisher J, Moriarity BS, Yasuda K, Wu B, Guan W, Schuetz EG, Oetting WS, Jacobson PA and Israni AK (2017) CRISPR/Cas9 Genetic Modification of CYP3A5 *3 in HuH-7 Human Hepatocyte Cell Line Leads to Cell Lines with Increased Midazolam and Tacrolimus Metabolism. *Drug Metab Dispos* **45**:957-965.

Edwards JE, LaCerte C, Peyret T, Gosselin NH, Marier JF, Hofmann AF and Shapiro D (2016) Modeling and Experimental Studies of Obeticholic Acid Exposure and the Impact of Cirrhosis Stage. *Clin Transl Sci* **9**:328-336.

Edwards JE, Eliot L, Parkinson A, Karan S and MacConell L (2017) Assessment of Pharmacokinetic Interactions Between Obeticholic Acid and Caffeine, Midazolam, Warfarin, Dextromethorphan, Omeprazole, Rosuvastatin, and Digoxin in Phase 1 Studies in Healthy Subjects. *Adv Ther* **34**:2120-2138.

Ehle M, Patel C and Giugliano RP (2011) Digoxin: clinical highlights: a review of digoxin and its use in contemporary medicine. *Crit Pathw Cardiol* **10**:93-98.

FDA/CDER US (2012) Drug interaction studies - study design, data analysis, and implications for dosing and labeling recommendations, DRAFT GUIDANCE.

Ferslew BC, Johnston CK, Tsakalozou E, Bridges AS, Paine MF, Jia W, Stewart PW, Barritt ASt and Brouwer KL (2015) Altered morphine glucuronide and bile acid disposition in patients with nonalcoholic steatohepatitis. *Clin Pharmacol Ther* **97**:419-427.

Fiorucci S, Rizzo G, Donini A, Distrutti E and Santucci L (2007) Targeting farnesoid X receptor for liver and metabolic disorders. *Trends Mol Med* **13**:298-309.

Funk C, Ponelle C, Scheuermann G and Pantze M (2001) Cholestatic potential of troglitazone as a possible factor contributing to troglitazone-induced hepatotoxicity: in vivo and in vitro interaction at the canalicular bile salt export pump (Bsep) in the rat. *Mol Pharmacol* **59**:627-635.

Gao X, Fu T, Wang C, Ning C, Kong Y, Liu Z, Sun H, Ma X, Liu K and Meng Q (2017) Computational discovery and experimental verification of farnesoid X receptor agonist auraptene to protect against cholestatic liver injury. *Biochem Pharmacol* **146**:127-138.

Guo C, Sane R, Liu L, Chen Y and Yoshida K (2018) Model-based evaluation of coproporphyrin I (CP-I) as a biomarker for organic anion transporting polypeptides (OATP) to Predict Clinical Drug-drug Interactions (DDIs). *ASCPT*.

Hardwick RN, Fisher CD, Canet MJ, Scheffer GL and Cherrington NJ (2011) Variations in ATP-binding cassette transporter regulation during the progression of human nonalcoholic fatty liver disease. *Drug Metab Dispos* **39**:2395-2402.

Hoekstra D, Tyteca D and van ISC (2004) The subapical compartment: a traffic center in membrane polarity development. *J Cell Sci* **117**:2183-2192.

Hofmann AF and Hagey LR (2008) Bile acids: chemistry, pathochemistry, biology, pathobiology, and therapeutics. *Cell Mol Life Sci* **65**:2461-2483.

Ito K and Brouwer KLR (2018) LXR/FXR agonist alters transporter expression in sandwich-cultured human hepatocytes; proteomics-driven PBPK modeling implicates a drug–drug interaction with metformin. *Drug Metab Pharmacokinet* **33**:S88.

Jackson JP, Freeman KM, Friley WW, St Claire RL, 3rd and Brouwer KR (2016) Basolateral Efflux Transporters: A Potentially Important Pathway for the Prevention of Cholestatic Hepatotoxicity. *Appl In Vitro Toxicol* **2**:207-216.

Jones HM, Barton HA, Lai Y, Bi YA, Kimoto E, Kempshall S, Tate SC, El-Kattan A, Houston JB, Galetin A and Fenner KS (2012) Mechanistic pharmacokinetic modeling for the prediction of transporter-mediated disposition in humans from sandwich culture human hepatocyte data. *Drug Metab Dispos* **40**:1007-1017.

Kargiotis K, Katsiki N, Athyros VG, Giouleme O, Patsiaoura K, Katsiki E, Mikhailidis DP and Karagiannis A (2014) Effect of rosuvastatin on non-alcoholic steatohepatitis in patients with metabolic syndrome and hypercholesterolaemia: a preliminary report. *Curr Vasc Pharmacol* **12**:505-511.

Kaschek D, Sharanek A, Guillouzo A, Timmer J and Weaver RJ (2018) A Dynamic Mathematical Model of Bile Acid Clearance in HepaRG Cells. *Toxicol Sci* **161**:48-57.

Kikuchi R, Peterkin VC, Chiou WJ, de Morais SM and Bow DAJ (2017) Validation of a total IC50 method which enables in vitro assessment of transporter inhibition under semi-physiological conditions. *Xenobiotica* **47**:825-832.

Kipp H and Arias IM (2000) Newly synthesized canalicular ABC transporters are directly targeted from the Golgi to the hepatocyte apical domain in rat liver. *J Biol Chem* **275**:15917-15925.

Kipp H, Pichetshote N and Arias IM (2001) Transporters on demand: intrahepatic pools of canalicular ATP binding cassette transporters in rat liver. *J Biol Chem* **276**:7218-7224.

Kock K, Ferslew BC, Netterberg I, Yang K, Urban TJ, Swaan PW, Stewart PW and Brouwer KL (2014) Risk factors for development of cholestatic drug-induced liver injury: inhibition of hepatic basolateral bile acid transporters multidrug resistance-associated proteins 3 and 4. *Drug Metab Dispos* **42**:665-674.

Kong Y, Gao X, Wang C, Ning C, Liu K, Liu Z, Sun H, Ma X, Sun P and Meng Q (2018) Protective effects of yangonin from an edible botanical Kava against lithocholic acid-induced cholestasis and hepatotoxicity. *Eur J Pharmacol* **824**:64-71.

Kweon HJ, Kim DI, Bae Y, Park JY and Suh BC (2016) Acid-Sensing Ion Channel 2a (ASIC2a) Promotes Surface Trafficking of ASIC2b via Heteromeric Assembly. *Sci Rep* **6**:30684.

Lake AD, Novak P, Shipkova P, Aranibar N, Robertson D, Reily MD, Lu Z, Lehman-McKeeman LD and Cherrington NJ (2013) Decreased hepatotoxic bile acid composition and altered synthesis in progressive human nonalcoholic fatty liver disease. *Toxicol Appl Pharmacol* **268**:132-140.

Lee YC, Block G, Chen H, Folch-Puy E, Foronjy R, Jalili R, Jendresen CB, Kimura M, Kraft E, Lindemose S, Lu J, McLain T, Nutt L, Ramon-Garcia S, Smith J, Spivak A, Wang ML, Zanic M and Lin SH (2008) One-step isolation of plasma membrane proteins using magnetic beads with immobilized concanavalin A. *Protein Expr Purif* **62**:223-229.

Lefebvre P, Cariou B, Lien F, Kuipers F and Staels B (2009) Role of bile acids and bile acid receptors in metabolic regulation. *Physiol Rev* **89**:147-191.

Li R, Ghosh A, Maurer TS, Kimoto E and Barton HA (2014) Physiologically based pharmacokinetic prediction of telmisartan in human. *Drug Metab Dispos* **42**:1646-1655.

Maiuri AR, Wassink B, Turkus JD, Breier AB, Lansdell T, Kaur G, Hession SL, Ganey PE and Roth RA (2017) Synergistic Cytotoxicity from Drugs and Cytokines In Vitro as an Approach to Classify Drugs According to Their Potential to Cause Idiosyncratic Hepatotoxicity: A Proof-of-Concept Study. *J Pharmacol Exp Ther* **362**:459-473.

Malinen MM, Ali I, Bezencon J, Beaudoin JJ and Brouwer KLR (2018) Organic Solute Transporter OSTalpha/ss is Over-Expressed in Nonalcoholic Steatohepatitis and Modulated by Drugs Associated with Liver Injury. *Am J Physiol Gastrointest Liver Physiol*.

Mao J, Doshi U, Wright M, Hop C, Li AP and Chen Y (2018) Prediction of the Pharmacokinetics of Pravastatin as an OATP Substrate using Plateable Human Hepatocytes with Human Plasma Data and PBPK Modeling. *CPT: pharmacometrics & systems pharmacology*.

Marion TL, Perry CH, St Claire RL, 3rd, Yue W and Brouwer KL (2011) Differential disposition of chenodeoxycholic acid versus taurocholic acid in response to acute troglitazone exposure in rat hepatocytes. *Toxicol Sci* **120**:371-380.

Matsunaga N, Kaneko N, Staub AY, Nakanishi T, Nunoya K, Imawaka H and Tamai I (2016) Analysis of the Metabolic Pathway of Bosentan and of the Cytotoxicity of Bosentan Metabolites Based on a Quantitative Modeling of Metabolism and Transport in Sandwich-Cultured Human Hepatocytes. *Drug Metab Dispos* **44**:16-27.

Matsunaga N, Suzuki K, Nakanishi T, Ogawa M, Imawaka H and Tamai I (2015) Modeling approach for multiple transporters-mediated drug-drug interactions in sandwich-cultured human hepatocytes: effect of cyclosporin A on hepatic disposition of mycophenolic acid phenyl-glucuronide. *Drug Metab Pharmacokinet* **30**:142-148.

Mohamed LA and Kaddoumi A (2013) In vitro investigation of amyloid-beta hepatobiliary disposition in sandwich-cultured primary rat hepatocytes. *Drug Metab Dispos* **41**:1787-1796.

Morgan RE, Trauner M, van Staden CJ, Lee PH, Ramachandran B, Eschenberg M, Afshari CA, Qualls CW, Jr., Lightfoot-Dunn R and Hamadeh HK (2010) Interference with bile salt export pump function is a susceptibility factor for human liver injury in drug development. *Toxicol Sci* **118**:485-500.

Morgan RE, van Staden CJ, Chen Y, Kalyanaraman N, Kalanzi J, Dunn RT, 2nd, Afshari CA and Hamadeh HK (2013) A multifactorial approach to hepatobiliary transporter assessment enables improved therapeutic compound development. *Toxicol Sci* **136**:216-241.

Nevens F, Andreone P, Mazzella G, Strasser SI, Bowlus C, Invernizzi P, Drenth JP, Pockros PJ, Regula J, Beuers U, Trauner M, Jones DE, Floreani A, Hohenester S, Luketic V, Shiffman M, van Erpecum KJ, Vargas V, Vincent C, Hirschfield GM, Shah H, Hansen B, Lindor KD, Marschall HU, Kowdley KV, Hooshmand-Rad R, Marmon T, Sheeron S, Pencek R, MacConell L, Pruzanski M and Shapiro D (2016) A Placebo-Controlled Trial of Obeticholic Acid in Primary Biliary Cholangitis. *N Engl J Med* **375**:631-643.

Notenboom S, Weigand KM, Proost JH, van Lipzig MM, van de Steeg E, van den Broek PHH, Greupink R, Russel FGM and Groothuis GMM (2018) Development of a mechanistic biokinetic model for hepatic bile acid handling to predict possible cholestatic effects of drugs. *Eur J Pharm Sci*.

Ohtsuki S, Schaefer O, Kawakami H, Inoue T, Liehner S, Saito A, Ishiguro N, Kishimoto W, Ludwig-Schwellinger E, Ebner T and Terasaki T (2012) Simultaneous absolute protein quantification of transporters, cytochromes P450, and UDP-glucuronosyltransferases as a novel approach for the characterization of individual human liver: comparison with mRNA levels and activities. *Drug Metab Dispos* **40**:83-92.

Orntoft NW, Munk OL, Frisch K, Ott P, Keiding S and Sorensen M (2017) Hepatobiliary transport kinetics of the conjugated bile acid tracer (11)C-CSar quantified in healthy humans and patients by positron emission tomography. *J Hepatol* **67**:321-327.

Pereira CD, Martins F, Wiltfang J, da Cruz ESOAB and Rebelo S (2018) ABC Transporters Are Key Players in Alzheimer's Disease. *J Alzheimers Dis* **61**:463-485.

Pfeifer ND, Harris KB, Yan GZ and Brouwer KL (2013) Determination of intracellular unbound concentrations and subcellular localization of drugs in rat sandwich-cultured hepatocytes compared with liver tissue. *Drug Metab Dispos* **41**:1949-1956.

Poulin P and Haddad S (2013) Toward a new paradigm for the efficient in vitro-in vivo extrapolation of metabolic clearance in humans from hepatocyte data. *J Pharm Sci* **102**:3239-3251.

Riccardi K, Li Z, Brown JA, Gorgoglione MF, Niosi M, Gosset J, Huard K, Erion DM and Di L (2016) Determination of Unbound Partition Coefficient and in Vitro-in Vivo Extrapolation for SLC13A Transporter-Mediated Uptake. *Drug Metab Dispos* **44**:1633-1642.

Riccardi KA, Ryu S, Lin J, Yates P, Tess DA, Li R, Singh D, Holder BR, Kapinos B, Chang G and Di L (2018) Comparison of Species and Cell-Type Differences in Fraction Unbound of Liver Tissues, Hepatocytes and Cell-Lines. *Drug Metab Dispos*.

Riede J, Camenisch G, Huwyler J and Poller B (2017) Current in vitro Methods to Determine Hepatic Kpuu: a Comparison of Their Usefulness and Limitations. *J Pharm Sci* **106**:2805-2814.

Ryan J, Morgan RE, Chen Y, Volak L, Dunn RT and Dunn KW (2018) Intravital multiphoton microscopy with fluorescent bile salts in rats as an in vivo biomarker for hepatobiliary transport inhibition. *Drug Metab Dispos*.

Schwarz UI (2012) Intestinal and hepatic drug transporters and their role in the disposition of lipid-lowering drugs. *Electronic Thesis and Dissertation Repository 817 https://irlibuwoca/etd/817*.

Slizgi JR, Lu Y, Brouwer KR, St Claire RL, Freeman KM, Pan M, Brock WJ and Brouwer KL (2016) Inhibition of Human Hepatic Bile Acid Transporters by Tolvaptan and Metabolites: Contributing Factors to Drug-Induced Liver Injury? *Toxicol Sci* **149**:237-250.

Soroka CJ, Ballatori N and Boyer JL (2010) Organic solute transporter, OSTalpha-OSTbeta: its role in bile acid transport and cholestasis. *Semin Liver Dis* **30**:178-185.

Sosicka P, Maszczak-Seneczko D, Bazan B, Shauchuk Y, Kaczmarek B and Olczak M (2017) An insight into the orphan nucleotide sugar transporter SLC35A4. *Biochim Biophys Acta* **1864**:825-838.

Thompson CG, Fallon JK, Mathews M, Charlins P, Remling-Mulder L, Kovarova M, Adamson L, Srinivas N, Schauer A, Sykes C, Luciw P, Garcia JV, Akkina R, Smith PC and Kashuba ADM (2017) Multimodal analysis of drug transporter expression in gastrointestinal tissue. *AIDS* **31**:1669-1678.

Ubhi K and Masliah E (2013) Alzheimer's disease: recent advances and future perspectives. *J Alzheimers Dis* **33 Suppl 1**:S185-194.

Van ISC, Maier O, Van Der Wouden JM and Hoekstra D (2000) The subapical compartment and its role in intracellular trafficking and cell polarity. *J Cell Physiol* **184**:151-160.

Wagner M, Zollner G and Trauner M (2011) Nuclear receptors in liver disease. *Hepatology* **53**:1023-1034.

Wang L, Soroka CJ and Boyer JL (2002) The role of bile salt export pump mutations in progressive familial intrahepatic cholestasis type II. *J Clin Invest* **110**:965-972.

Wustner D, Mukherjee S, Maxfield FR, Muller P and Herrmann A (2001) Vesicular and nonvesicular transport of phosphatidylcholine in polarized HepG2 cells. *Traffic (Copenhagen, Denmark)* **2**:277-296.

Xu P, Li D, Tang X, Bao X, Huang J, Tang Y, Yang Y, Xu H and Fan X (2013) LXR agonists: new potential therapeutic drug for neurodegenerative diseases. *Mol Neurobiol* **48**:715-728.

Yang K, Woodhead JL, Watkins PB, Howell BA and Brouwer KL (2014) Systems pharmacology modeling predicts delayed presentation and species differences in bile acid-mediated troglitazone hepatotoxicity. *Clin Pharmacol Ther* **96**:589-598.

Yue W, Abe K and Brouwer KL (2009) Knocking down breast cancer resistance protein (Bcrp) by adenoviral vector-mediated RNA interference (RNAi) in sandwich-cultured rat hepatocytes: a novel tool to assess the contribution of Bcrp to drug biliary excretion. *Mol Pharm* **6**:134-143.

Zhang P, Tian X, Chandra P and Brouwer KL (2005) Role of glycosylation in trafficking of Mrp2 in sandwich-cultured rat hepatocytes. *Mol Pharmacol* **67**:1334-1341.

Zhang Y, Jackson JP, St Claire RL, 3rd, Freeman K, Brouwer KR and Edwards JE (2017) Obeticholic acid, a selective farnesoid X receptor agonist, regulates bile acid homeostasis in sandwich-cultured human hepatocytes. *Pharmacol Res Perspect* *5: 1-11.*

Figure 2.1. d_8-TCA mass vs. time data in SCHH lysate and incubation buffer

	Amount in Cells+Bile (pmol/mg pro)					
Time (min)	Donor 1	Donor 2	Donor 3	Mean	CV%	S.E.M.
2	13	20	14	16	25	2
5	31	43	43	39	18	4
10	63	73	66	67	8	3
20	95	120	106	107	12	7
23	103	99	73	92	18	10
26	90	60	68	73	21	9
31	100	70	65	65	24	11
36	81	52	48	60	30	10
	Amount in Cells (pmol/mg pro)					
Time (min)	Donor 1	Donor 2	Donor 3	Mean	CV%	S.E.M.
2	5.3	3.6	2.8	3.9	33	1
5	10	13	15	13	19	1
10	23	16	30	23	29	4
20	33	47	48	42	20	5
23	30	27	23	26	14	2
26	23	12	22	19	31	4
31	13	28	23	18	35	4
36	5.4	7.2	7.6	6.7	18	1
	Amount in Standard HBSS (pmol/mg pro)					
Time (min)	Donor 1	Donor 2	Donor 3	Mean	CV%	S.E.M.
23	10	13	13	12	15	1
26	17	13	11	14	24	2
31	22	22	21	21	3	0
36	28	24	23	25	12	2
	Amount in Ca^{2+}-free HBSS (pmol/mg pro)					
Time (min)	Donor 1	Donor 2	Donor 3	Mean	CV%	S.E.M.
23	12	19	10	14	34	3

26	23	22	12	19	31	3
31	26	36	17	27	35	5
36	32	33	18	28	30	5

Figure 2.4. The sensitivity of the predicted TCA $C_{t,Cells}$ to changes in $f_{u,cell,inhibitor}$ as a function of $([I]_{t,cell}/IC_{50})$ values

$[I]_{t,cell}/IC_{50}$	$f_{u,cell,inhibitor}=0.02$	$f_{u,cell,inhibitor}=1$
0.5	1	1.5
1	1	2
2	1	2.9
4	1.1	4.5
8	1.2	7
20	1.4	11
40	1.8	13
60	2.1	14

Table 2.3. Measured unbound fraction (f_u) and unbound concentrations ($[I]_u$) of telmisartan and bosentan in the medium, cell lysate, and cytosol. Data were from triplicate measurements except that measurements from the medium were duplicates.

			Medium		Cell lysate			Cytosol		
	Inhibitor	$[I]_{t,med}$ (µM)	1	2	1	2	3	1	2	3
f_u	Telmisartan	1	0.014	0.0098	0.15	0.16	0.099	0.056	0.050	0.053
		10	0.022	0.018	0.068	N/A	0.12	0.098	0.090	0.052
	Bosentan	0.8	0.029	0.048	0.34	0.48	N/A	0.12	N/A	0.12
		8	0.058	0.055	0.18	0.26	N/A	N/A	N/A	N/A
$[I]_u$ (µM)	Telmisartan	1	0.014	0.0098	2.4	2.5	1.6	0.90	0.80	0.85
		10	0.22	0.18	2.7	N/A	4.8	3.4	3.1	1.8
	Bosentan	0.8	0.023	0.039	0.66	0.93	N/A	0.21	N/A	0.21
		8	0.47	0.44	3.1	4.5	N/A	N/A	N/A	N/A

[a]N/A: not available

Table 2.4. Experimentally observed TCA $C_{t,Cells}$ in the presence and absence of telmisartan and bosentan. Data were from duplicate measurements.

Inhibitor	Dosing concentration (μM)	TCA $C_{t,Cells}$ (pmol/mg protein)	
Bosentan	0	22.0	23.6
	0.8	19.0	21.0
	8	18.8	18.2
Telmisartan	0	28.8	28.1
	1	26.9	24.6
	10	30.7	29.1

Figure 4.3. Observed TCA amount vs. time in control rat SCH, provided by Yang et al. (Yang et al., J Pharmacol Exp Ther, 2015).

	Amount in Cells+Bile (pmol/well)				
Time (min)	Lot=1	Lot=2	Lot=3	Mean	S.E.M.
2	21.3	18.7	13.4	17.8	4.0
5	34.8	34.6	23.2	30.9	6.6
10	51.1	46.6	36.2	44.6	7.6
15	63.1	63.4	45.7	57.4	10.1
20	77.5	75.1	55.0	69.2	12.4
23	55.2	54.5	55.9	55.2	0.7
24.5	45.6	52.1	49.6	49.1	3.3
26	38.1	40.1	42.4	40.2	2.2
31	28.2	33.3	33.7	31.7	3.1
36	27.3	28.2	28.5	28.0	0.6
protein (mg/well)	1	0.73	0.8	0.8	
Vcell (µL/well)	7.59	5.54	6.07	6.40	
	Amount in Cells (pmol/well)				
Time (min)	Lot=1	Lot=2	Lot=3	Mean	S.E.M.
2	4.7	4.0	3.2	4.0	0.8
5	4.5	6.1	3.4	4.7	1.4
10	7.9	10	6.9	8.3	1.6
15	8.9	9.5	9.4	9.3	0.3
20	11.6	9.5	10.4	10.5	1.1
23	3.1	4.2	3.2	3.5	0.6
24.5	2.0	4.4	3.0	3.1	1.2
26	1.0	1.7	1.9	1.5	0.5
31	0.7	1.5	0.9	1.0	0.4
36	0.4	0.5	0.4	0.4	0.1
	Amount in standard HBSS (pmol/well)				
Time (min)	Lot=1	Lot=2	Lot=3	Mean	S.E.M.
23	18.4	16.2	10.3	15.0	4.2

Time	Lot=1	Lot=2	Lot=3	Mean	S.E.M.
24.5	23.3	26.0	16.2	21.8	5.1
26	28.3	29.2	19.7	25.7	5.2
31	39.9	43.5	24.8	36.1	9.9
36	49.0	51.3	33.3	44.5	9.8
Amount in Ca^{2+}-free standard HBSS (pmol/well)					
Time (min)	Lot=1	Lot=2	Lot=3	Mean	S.E.M.
23	7.3	9.7	4.5	7.2	2.6
24.5	7.7	9.8	4.9	7.5	2.5
26	6.6	8.4	6.0	7.0	1.2
31	10.8	13.0	6.7	10.2	3.2
36	11.0	9.0	8.2	9.4	1.4

Figure 4.4. Observed TCA amount vs. time in rat SCH after 30-min pre-incubation with TGZ, provided by Yang et al. (Yang et al., J Pharmacol Exp Ther, 2015).

	Amount in Cells+Bile (pmol/well)				
Time (min)	Lot=1	Lot=2	Lot=3	Mean	S.E.M.
2	6.6	3.3	3.3	4.4	1.9
5	7.2	5.6	6.4	6.4	0.8
10	10.9	7.1	7.6	8.5	2.1
15	11.7	8.9	9.4	10.0	1.5
20	15.0	10.1	11.9	12.3	2.5
23	8.5	4.3	4.2	5.7	2.5
24.5	4.1	3.6	4.2	4.0	0.3
26	5.6	2.6	3.6	3.9	1.5
31	4.0	1.5	2.0	2.5	1.3
36	2.0	1.1	1.3	1.5	0.5
Protein (mg/well)	1	0.73	0.8	0.8	
Vcell (µL/well)	7.6	5.5	6.1	6.4	
	Amount in Cells (pmol/well)				
Time (min)	Lot=1	Lot=2	Lot=3	mean	SEM
2	3.3	1.9	1.7	2.3	0.9
5	2.9	1.4	2.9	2.4	0.9
10	3.3	1.8	3.4	2.8	0.9
15	4.5	3.0	3.7	3.7	0.8
20	5.5	3.0	4.8	4.4	1.3
23	1.0	0.6	0.7	0.8	0.2
24.5	0.6	0.4	0.7	0.6	0.2
26	0.9	0.2	0.4	0.5	0.4
31	0.3	0.1	0.1	0.2	0.1
36	0.2	0	0	0.1	0.1
	Amount in standard HBSS (pmol/well)				
Time (min)	Lot=1	Lot=2	Lot=3	Mean	S.E.M.
23	5.0	3.5	3.5	4.0	0.9

24.5	6.7	4.4	4.7	5.3	1.3
26	9.0	6.1	6.0	7.0	1.7
31	11.3	6.5	6.7	8.2	2.7
36	10.6	7.1	7.1	8.3	2.0
	Amount in Ca^{2+}-free standard HBSS (pmol/well)				
Time (min)	Lot=1	Lot=2	Lot=3	Mean	S.E.M.
23	3.1	2.0	2.4	2.5	0.6
24.5	4.1	2.0	4.5	3.5	1.3
26	4.8	3.0	4.0	3.9	0.9
31	4.4	2.6	5.7	4.2	1.6
36	4.5	2.7	6.2	4.5	1.8

Figure 4.7. Observed amount of TCA in different compartments generated by using the optimal study design.

Time (min)	Amount in Cells+Bile (pmol/well)				Amount in Cells (pmol/well)		
	Lot=1	Lot=2	Lot=3		Lot=1	Lot=2	Lot=3
20	127	170	98		65	118	50
25	48	97	58		4.9	53	20
30	26	50	33		1.8	21	10
32	20	37	26		0.45	13	7.0
34	15	27	20		0.11	7.5	4.9
36	12	20	16		0.028	4.2	3.4
38	9.4	15	12		0.0076	2.4	2.4
40	7.4	11	10		0.0024	1.3	1.7
48	2.8	4.0	3.6		0.00059	0.14	0.44
50	2.2	3.1	2.8		0.00059	0.089	0.32
Time (min)	Amount in standard HBSS (pmol/well)				Amount in Ca^{2+}-free standard HBSS (pmol/well)		
32	3.0	6.5	3.6		0.48	3.9	1.4
34	7.4	16	9.3		0.82	9.3	3.5
36	11	23	14		0.90	12	5.0
38	13	28	17		0.92	14	6.0
40	15	32	20		0.93	15	6.8
48	20	39	26		0.93	17	8.0
50	20	40	27		0.93	17	8.1

Figure 5.2. Observed amount of TCA in different matrices from three different SCHH donors. The protein content for HUM4119C, HUM4122C, and HC3-26 was 0.14, 0.173, and 0.185 mg protein/well, respectively.

In control SCHH

| Time (min) | Amount in Cells+Bile (pmol/mg pro) | | | | |
	HUM4119C	HUM4122C	HC3-26	Mean	S.D.
2	11.5	9.37	14.4	11.8	2.5
5	23	17.6	23.8	21.5	3.4
10	40.7	27.5	47.3	38.5	10.1
20	63.4	35.7	72.2	57.1	19.0
23	48.7	28.8	55.7	44.4	14.0
26	40.3	26.1	54.1	40.2	14.0
31	35.1	18.7	45.1	33.0	13.3
36	31	16.8	41.6	29.8	12.4
	Amount in Cells (pmol/mg pro)				
2	6.17	3.8	5.56	5.2	1.2
5	9.34	5.72	8.67	7.9	1.9
10	14.7	10.1	13.6	12.8	2.4
20	25	15.8	22.9	21.2	4.8
23	16.7	12	17.4	15.4	2.9
26	14.2	11.2	15	13.5	2.0
31	11.1	5.23	8.51	8.3	2.9
36	7.74	3.73	4.92	5.5	2.1
	Amount in Standard HBSS (pmol/mg pro)				
23	8.97	6.42	6.2	7.2	1.5
26	12.9	9.79	10.2	11.0	1.7
31	15	11.9	13.9	13.6	1.6
36	20.5	14.4	17.6	17.5	3.1
	Amount in Ca^{2+}-free HBSS (pmol/mg pro)				
23	5.81	3.37	4.65	4.6	1.2
26	9.74	6.92	10.1	8.9	1.7
31	13.9	7.49	10.2	10.5	3.2

36	17.3	10.6	12.4	13.4	3.5

In OCA-treated SCHH

	Amount in Cells+Bile (pmol/mg pro)				
Time (min)	HUM4119C	HUM4122C	HC3-26	Mean	S.D.
2	14.4	7.37	12.3	11.4	3.6
5	23.1	11	19.4	17.8	6.2
10	34.1	15.6	26.1	25.3	9.3
20	45.6	26	39.3	37.0	10.0
23	29.5	16.2	26.1	23.9	6.9
26	28.1	21	27.8	25.6	4.0
31	25.2	13	24.1	20.8	6.7
36	19.2	9.24	18.2	15.5	5.5
	Amount in Cells (pmol/mg pro)				
2	11.5	5.31	6.78	7.86	3.2
5	11.2	5.7	6.65	7.85	2.9
10	11.3	5.82	6.68	7.93	2.9
20	14.4	8.32	9.54	10.8	3.2
23	5.08	2.7	2.71	3.5	1.4
26	3.51	2.35	2.39	2.8	0.7
31	1.95	1.19	1.14	1.4	0.5
36	1.26	0.729	0.757	0.9	0.3
	Amount in Standard HBSS (pmol/mg pro)				
23	7.67	4.2	4.76	5.5	1.9
26	10.7	6.69	10.3	9.2	2.2
31	16.9	7.35	12.7	12.3	4.8
36	18.7	9.77	14.9	14.5	4.5
	Amount in Ca^{2+}-free HBSS (pmol/mg pro)				
23	4.99	2.81	3.58	3.8	1.1
26	6.39	3.88	5.55	5.3	1.3
31	9	4.73	6	6.6	2.2
36	9.69	4.46	6.91	7.0	2.6

In CDCA-treated SCHH

Time (min)	Amount in Cells+Bile (pmol/mg pro)				
	HUM4119C	HUM4122C	HC3-26	Mean	S.D.
2	7.01	3.0	5.56	5.19	2.0
5	10.7	4.68	9.27	8.22	3.1
10	15.1	5.87	15.5	12.2	5.4
20	21.5	9.75	23.5	18.3	7.4
23	12.5	6.50	15.9	11.6	4.8
26	9.44	5.48	13.8	9.57	4.2
31	8.46	3.67	9.61	7.25	3.2
36	6.97	2.79	7.63	5.80	2.6
	Amount in Cells (pmol/mg pro)				
2	4.65	2.29	2.62	3.19	1.3
5	6.06	2.82	3.65	4.18	1.7
10	6.15	3.14	4.03	4.44	1.5
20	8.51	4.36	5.65	6.17	2.1
23	3.59	1.82	2.15	2.52	0.9
26	2.23	1.69	1.57	1.83	0.4
31	1.63	0.86	0.869	1.12	0.4
36	0.89	1.2	0.644	0.91	0.3
	Amount in Standard HBSS (pmol/mg pro)				
23	4.24	2.04	4.39	3.56	1.3
26	6.92	3.02	8.3	6.08	2.7
31	9.74	3.92	10.3	7.99	3.5
36	13.5	4.9	12	10.1	4.6
	Amount in Ca^{2+}-free HBSS				
23	2.7	1.38	1.97	2.02	0.7
26	4.6	2.02	2.86	3.16	1.3
31	4.66	2.54	3.41	3.54	1.1
36	7.05	2.78	3.35	4.39	2.3

Figure 5.3. Fold change in $CL_{int,BL}$, $CL_{int,Bile}$ and CL_{Uptake} in OCA- and CDCA-treated SCHH compared to control.

	Treatment	HUM4119C	HUM4122C	HC3-26
$CL_{int,BL}$	Control	1.2	1.0	0.77
	OCA	7.1	6.8	5.7
	CDCA	7.1	6.8	5.4
$CL_{int,Bile}$	Control	1.0	1.0	0.91
	OCA	1.7	1.7	2.0
	CDCA	1.4	1.8	1.9
CL_{Uptake}	Control	1.2	0.73	1.0
	OCA	1.5	0.79	1.2
	CDCA	0.78	0.41	0.60

Figure 5.4. Effect of OCA and CDCA treatment of SCHH on the protein expression of OSTα, OSTβ, MRP3, MRP4, BSEP, and NTCP. The absolute quantity was normalized by the quantity of ATPase.

OSTα (approximate M.W. 37 kD)						
Treatment	Control		OCA		CDCA	
Donor	Absolute value	% of control	Absolute value	% of control	Absolute value	% of control
Hu 8246	0.703	84	2.24	269	3.04	365
HUM4122D	1.01	122	1.91	229	2.10	252
HC3-26	0.783	94	2.44	293	2.08	250
OSTβ (approximate M.W. 19kD)						
Treatment	Control		OCA		CDCA	
Donor	Absolute value	% of control	Absolute value	% of control	Absolute value	% of control
Hu 8246	1.46	80	19.4	1058	25.5	1392
HUM4122D	1.83	100	17.7	967	18.9	1031
HC3-26	2.20	120	25.5	1390	29.6	1617
MRP3 (approximate M.W. 140kD)						
Treatment	Control		OCA		CDCA	
Donor	Absolute value	% of control	Absolute value	% of control	Absolute value	% of control
Hu 8246	1.57	104	1.63	108	1.96	130
HUM4122D	0.92	61	1.48	98	1.43	95
HC3-26	2.05	136	1.54	102	1.61	107
MRP4 (approximate M.W. 150kD)						
Treatment	Control		OCA		CDCA	
Donor	Absolute value	% of control	Absolute value	% of control	Absolute value	% of control
Hu 8246	0.853	89	1.31	136	1.05	109
HUM4122D	0.609	63	0.96	100	0.963	100
HC3-26	1.42	148	0.95	99	0.937	98
BSEP (approximate M.W. 146kD)						
Treatment	Control		OCA		CDCA	

Donor	Absolute value	% of control	Absolute value	% of control	Absolute value	% of control
Hu 8246	0.186	35	0.393	74	0.46	87
HUM4122D	0.563	107	0.88	167	0.575	109
HC3-26	0.834	158	1.68	318	1.58	300
NTCP (approximate M.W. 38kD)						
Treatment	Control		OCA		CDCA	
Donor	Absolute value	% of control	Absolute value	% of control	Absolute value	% of control
Hu 8246	0.204	94	0.268	123	0.240	111
HUM4122D	0.172	79	0.232	107	0.259	119
HC3-26	0.275	127	0.303	140	0.331	152